



Forming Miniature Ceramic Components Using Micro-forming and a Field Activated Sintering Technique (Micro-FAST)

Hasan Hamza Hijji

This thesis is submitted to

The Department of Design, Manufacturing and Engineering Management

Faculty of Engineering

University of Strathclyde

for the degree of

Doctor of Philosophy (PhD)

Glasgow, 2021

DECLARATIONS OF AUTHENTICITY AND AUTHOR'S RIGHTS

'This thesis is the result of the author's original research. It has been composed by the author and has not been previously submitted for examination which has led to the award of a degree.'

'The copyright of this thesis belongs to the author under the terms of the United Kingdom Copyright Acts as qualified by University of Strathclyde Regulation 3.50. Due acknowledgement must always be made of the use of any material contained in, or derived from, this thesis.'



Signed: _____

Date: Feb 2022

*In the name of Allah
Almighty, the most beneficent,
most gracious and most merciful,
who blessed me with the strength,
knowledge and wisdom to
accomplish my work and my goals*

DEDICATIONS

Dedicated to my great and lovely Mother and to my great Father, for their continuous prayers, endless love, unconditional support through thick and thin, better or worse and in sickness and health who wanted to see me here where I am today. May Allah bless them with health and blessing life.

I would like to dedicate this also to my wife, Afnan, for her patience and understanding throughout our marriage time. I would like to express deep love to my children, Hamza, Jamila and Abdulrahman, whose smiles, hugs and cuddles always give me relaxation, inspiration and happiness in this life.

I would like also to dedicate this to my brothers (Hassan and Wesam) for their help and support when I needed them all the time

ACKNOWLEDGEMENT

I would like to express and convey my sincere gratitude to Professor Yi Qin for his phenomenal supervision, unlimited support during my difficult circumstances, advice on the future research as well on the career, valuable guidance, and inspiration during the course of this research work. Their advice and comments have been valuable and have made a significant difference to the completion of this research work.

I would highly acknowledge the Government of Saudi Arabia for the scholarship under Ministry of Education and Umm Al-Qura University.

Moreover, I would like to thank the people who helped me to gain this scholarship especially Dr. Hamza Ghulman, Prof. Mohammed Alhazmi, Prof. Muhammad Alsoufi and Prof. Abdulmajeed Alghamdi.

Furthermore, I would like to appreciate the funding support from European Commission through FP7 FOF Micro-FAST Project and the project partners for supplying the powder materials for the experiments.

The work reported was carried out at the Department of Design, Manufacturing and Engineering Management and Advanced Materials Research Laboratories of the University of Strathclyde. Therefore, I would like to thank all the technician and colleagues in the department of DMED who helped me and gave the valuable advice, especially Dr. Quanren Zeng and Dr Kunlan Haung.

I would like especially thank Prof. Jianguo Lin and his colleagues at Department of Mechanical Engineering of the Imperial College London for providing the Gleeble® 3800 machine for conducting the experiments and for their kind support.

Many thanks to my friend Abdulrahman Al-Jifri for his valuable time, support and guidance in using the Inventor software.

I would like to thank my friend Dr. Abdulrahman Al-Ghamdi for his valuable time, support and guidance in using the ABAQUS software.

I would like to take this opportunity to thank all of my friends for their memorable company in Glasgow, especially to Yazeed, Sultan, Abdulmajeed, Omair, Albaraa, Osama, Ayeth, Mohammed, Eyad and Ahmad.

Special thanks to all my siblings, my family and my friends for their support all the time during my study.

ABSTRACT

The demand for miniature products has recently significantly increased as has the need for these products to be produced rapidly, flexibly and in a cost efficient manner. The application of electrical sintering shows significant potential to produce these components by using powder materials. However, previous research has shown that there are still challenges that need to be considered in order to achieve increased densification of products and simplification of the processes. The process concept utilised in this study is called Micro-FAST, which comprises the combination of an electrical-field activated sintering technique (FAST) and micro-forming processes.

The aim of the work was to develop the process concept for the manufacture of miniature components, and to develop the necessary die sets along with other tooling for experimental work to enable the forming of ceramic micro components from powder materials and to also develop a new tool design for mass production.

A comprehensive literature review is given on micro-manufacturing processes, challenges, key issues, micro forming, micro scale size effects, sintering processes and the electrical field activated sintering processes and their application. The concept of the Micro-FAST process was explained, and development of the die sets and materials selection justification for the process is described.

The finite element (FE) analysis of the effect of the coupled thermal-electrical characteristics of the die sets during the heating and cooling process was carried out. This was done in order to study the heating flows of the die sets using the material properties chosen for this research, the materials were zirconia, alumina and piezoceramic. The simulation analysis was focused on the heating distribution process resulting from the die set design. An experimental study has also been conducted in this work to validate the results from finite element (FE) analysis.

The experiment was conducted using a Gleeble[®] 3800 testing system, a Scanning Electron Microscope from HITACHI S-3700N, Energy Dispersive Spectroscopy and Nano Test Vantage system (Nano-indentation). The material powders that have been used for this

experiment were three different types of zirconia, alumina (Al_2O_3), and piezoceramics (PZT). The first zirconia powder was yttria partially stabilized zirconia (3Y-ZrO₂), the second powder is magnesia partially stabilized zirconia (MSZ) and the third powder was magnesia partially stabilized zirconia with 5 wt% organic additives or organic binders (MSZ(#)) to improve the forming process.

Based on the results, the development of a new tool die-design concept has been introduced which can potentially be used for mass production to produce miniature ceramic components. The new alternative design is going to be validated and examined using the finite element (FE) analysis of the new tool design sets effect on the coupled thermal-electrical characteristics during the heating and cooling process using ABAQUS/CAE software. In conclusion, improvements and promising results have been presented regarding a reduced process time for the manufacture of miniature components with a variety of ceramic powder materials. Recommendations for future work have been suggested and explained at the end of this work in order to make further improvements to the process.

LIST OF PUBLISHED RESEARCH PAPERS AND POSTERS

a) Research Papers:

- Dragut, D. V., Badilita, V., Motoc, A. M., Piticescu, R. R., Zhao, J., **Hijji, H.**, & Conte, L. (2017). Thermal stability and field assisted sintering of cerium-doped YSZ ceramic nanoparticles obtained via a hydrothermal process. *Manufacturing Review*, 4, 11.
- **Hijji, H.**, Qin, Y., Haung, K., Zulkipli, M. B., & Zhao, J. (2018). Fabrication of Miniature Components from ZrO₂ Powder by Combining Electrical-field Activated Sintering Technique and Micro-forming. In *MATEC Web of Conferences* (Vol. 190, p. 10007). EDP Sciences.
- Zhao, J., Qin, Y., Huang, K., Zulkipli, M. B., & **Hijji, H.** (2015). Forming of micro-components by electrical-field activated sintering. In *MATEC Web of Conferences* (Vol. 21, p. 10001). EDP Sciences.
- **Hijji, H.**, Qin, Y., Huang, K., Zulkipli, M. B., Yang, S., & Zhao, J. (2016). Forming alumina (Al₂O₃) by micro-FAST. In *Advances in Manufacturing Technology XXX*, (pp. 61-66). IOS Press.
- **Hijji, H.**, Qin, Y., Huang, K., Yang, S., Zulkipli, M. B., & Zhao, J. (2016). Fabrication of micro components with MSZ material using electrical-field activated powder sintering technology. In *Advances in Manufacturing Technology XXX* (pp. 55-60). IOS Press.
- Zulkipli, M., Qin, Y., Huang, K., **Hijji, H.**, Zhao, Y., & Zhao, J. (2015). Forming of titanium and titanium alloy miniature-cylinders by electrical-field activated powder sintering and forming. In *MATEC Web of Conferences* (Vol. 21, p. 10006). EDP Sciences.

- Huang, K., Qin, Y., Zhao, J., Zulkipli, M. B., & **Hijji, H.** (2015). Fabrication of NiTi shape memory alloy by Micro-FAST. In *MATEC Web of Conferences* (Vol. 21, p. 10003). EDP Sciences.
- Qin, Y., Zhao, J., Huang, K., Zulkipli, M., **Hijji, H.**, Yang, Y & Yin, D. (2017). Forming of miniature components from powders by combining field-activated sintering and micro-forming. *Procedia engineering*, 207, 1212-1217.

b) Posters:

- **Hasan Hijji**, Muhammad Bin Zulkipli & Yi Qin (31st January 2014), “*Development of a New Process for the Manufacture of Micro Parts by Using a Combination of Micro Forming and Fast Technology*”. Poster presentation. 8th Saudi Student Conference – Imperial College London, UK.
- **Hasan Hijj** & Yi Qin (13th - 14th February 2016), “*Forming Micro Components using Micro-FAST technology*”. Poster presentation. 9th Saudi Student Conference – University of Birmingham, UK.
- **Hasan Hijji** & Yi Qin (12th - 16th November 2017) “*Forming micro components from ceramics materials by using FAST process*”. Poster presentation. INTERNATIONAL CONFERENCE ON SINTERING 2017. SAN DIEGO, CALIFORNIA, USA

- **Hasan Hijji & Yi Qin** (7th - 8th November 2017) "*Forming ceramics components using Micro-FAST*". Poster presentation Special Interest Group: Micro/Nano Manufacturing. University of Strathclyde, Scotland, Glasgow, UK
- **Hasan Hijji & Yi Qin** (20th – 22nd November 2017) "*Forming micro components from ceramics materials by using FAST process*". Poster presentation SMART SPECIALIZATION AND ADVANCED MATERIALS FOR EXTREME CONDITIONS. Bucharest, Romania.
- **Hasan Hijji & Yi Qin** (March 2015) "*Development of a New Process for the Forming of Micro-Components*". Poster presentation. Faculty Engineering Research Presentation Day (RPD 2015) – University of Strathclyde Glasgow, Scotland, United Kingdom.

LIST OF CONTENTS

Declarations of Authenticity and Author's Rights	i
Dedications	iii
Acknowledgement	iv
Abstract	vi
List of Published Research Papers and Posters	viii
List of Contents	xi
List of Figures	xv
List of Tables	xx
1 Introduction	1
1.1 Research Background.....	1
1.2 Aims and Objectives.....	3
1.3 The Project Methodology and Approach.....	5
1.4 The Thesis Layout.....	6
2 Literature Review	9
2.1 Micro-Manufacturing.....	9
2.1.1 Micro Manufacturing Processes.....	12
2.1.2 Challenges and Key issues in Micro-Manufacturing.....	13
2.1.3 Micro Forming.....	15
2.1.4 Size Effect in a Micro Scale Forming Process.....	19
2.2 Conventional Sintering and Electrical-Field Activated Sintering.....	26
2.2.1 Overview.....	26
2.2.2 Densification.....	31
2.2.3 Heat Transfer.....	32
2.2.4 Grain Growth.....	34

2.2.5	Electrical-Field Activated Sintering	35
2.2.6	Application of Electrical-Field Activated Sintering	41
2.3	Summary of the chapter	46
3	Micro-FAST of Ceramics and Composites	50
3.1	Overview of Micro-FAST	50
3.2	Process Configuration.....	50
3.3	Die sets Improvement for Micro-FAST	57
3.4	Temperature Measurement	60
3.5	Material Selection for Micro-FAST Die Set	62
3.5.1	Thermal Expansion Coefficient.....	63
3.5.2	Maximum Sintering Temperature of the Die Sets and Sample Materials ...	67
3.6	Process Improvement for Sintering Ceramics and Composites	69
3.6.1	Heat Transfer During Electrical Field Sintering Process	69
3.7	Summary of the Chapter	73
4	Finite Element Analysis (FEA) of Heating and Cooling Process in The Micro-FAST	76
4.1	Introduction.....	76
4.2	Theory of Coupled Thermal-Electrical Analysis.....	76
4.3	Procedure	78
4.4	Results and Discussion	82
4.4.1	Zirconia.....	82
4.4.2	Alumina	85
4.4.3	Piezoceramic (PZT).....	88
4.5	Summary of the Chapter	91
5	Results and Discussion	94
5.1	Introduction.....	94

5.2	Powder Materials and Equipment.....	95
5.2.1	Gleeble® 3800 Machine.....	96
5.2.2	Relative Density	98
5.2.3	Scanning Electron Microscope (SEM)	100
5.2.4	Hardness Test	101
5.2.5	Powder Materials	102
5.3	Parameters of Experiments	105
5.3.1	Zirconia.....	105
5.3.2	Alumina	109
5.3.3	Piezoceramic (PZT).....	110
5.4	Procedures of The Experiment	111
5.4.1	Preparation of Powder Materials	111
5.4.2	Preparation of Gleeble® 3800 Operating System	111
5.4.3	The Ejection Process	113
5.5	Results and Discussions.....	114
5.5.1	Samples Relative Density and Dimensions	114
5.5.2	Samples Microstructures	137
5.5.3	Samples Hardness.....	151
5.6	Summary of the Chapter	156
6	New Tooling Concept For Micro-FAST of Ceramic Components	160
6.1	Tool Concept and Detail Design.....	160
6.2	Thermal-Electrical Finite Element Analysis of The Tool	166
6.3	Analysis Procedure	167
6.4	Results and Discussion	170
6.5	Summary of The Chapter.....	177
7	Conclusions and Recommendations	178

7.1	Conclusions.....	178
7.2	Contributions to Knowledge.....	180
7.3	Recommendation and Future Work.....	181
	References.....	183
	Appendices.....	194
	Appendix 1: New tool design for Micro-FAST process with full details	194
	Appendix 2: Base plate.....	195
	Appendix 3: Guide Pillar	195
	Appendix 4: Mandrel Holder.....	197
	Appendix 5: Contact spacer.....	198
	Appendix 6: Mandrel.....	199
	Appendix 7: Guide Plate.....	200
	Appendix 8: Isolating Ring.....	201
	Appendix 9: Lower conducting ring.....	202
	Appendix 10: The Die	203
	Appendix 11: Lower Strengthen Ring.....	204
	Appendix 12: Upper Punch	205
	Appendix 13: Upper Conducting Ring.....	206
	Appendix 14: Upper Strengthen Ring	207
	Appendix 15: Punch Holder	208
	Appendix 16: Spring.....	209
	Appendix 17: Protector.....	210

LIST OF FIGURES

Figure 2-1: The revolutionary of industrial towards productions of complex parts [21]	10
Figure 2-2: Example of some formed micro parts [30, 31]	12
Figure 2-3: The components of the micro-forming system [43, 46].....	17
Figure 2-4: Basic elements of a micro-forming system [27]	17
Figure 2-5: Illustration of grain siz and feature/specimen size effects	20
Figure 2-6: Effect of N on material flow stress under different testing conditions [27].	23
Figure 2-7: Grain and specimen size effect as function on N against the flow stress of the components [27].....	24
Figure 2-8: Surface layer model in bulk metal [43, 46].....	25
Figure 2-9: Powder particle shapes [62]	27
Figure 2-10: Sintering Stages [54, 64]	28
Figure 2-11: Sequence of the sintering process consist of preheat or burn off, high-temperature and cooling stage [3].....	29
Figure 2-12: Classification of sintering processes	30
Figure 2-13: Calssification of Sintering process according to sintering temperAture [62, 65]	30
Figure 2-14: Consolidation methods [62]	31
Figure 2-15: The six different mechanisms that could act during sintering of solid grains [67]	32
Figure 2-16: Heat transfer in a conventional convection furnace illustrating the three active mechanisms [68, 69]	33
Figure 2-17: Number of ECAS patents per decade from 1900 to the first semester of 2008. The exploration (1900–1960), development (1960–1990) and exploitation (1990–2008) stages are defined in accordance with the worldwide industrialization and commercialization of ECAS [76].....	36
Figure 2-18: Schematic of sintering process: (1) hot pressing and (2) FAST/ecas [76].....	37

Figure 3-1: Micro-FAST process for the forming of miniature/micro- components [75, 113, 114]	52
Figure 3-2: The die-set with powder inside the machine (a) Gleeble 1500D (b) Gleeble 3800 [2, 72].....	52
Figure 3-3: Illustration of the distribution of the current in a compact	53
Figure 3-4: Temperature time curve of the compact during the sintering process: (a) constant temperature sintering; (b) electro-heating loops sintering [2]	54
Figure 3-5: Illustration of stages for Micr-FAST Process [2, 75].....	56
Figure 3-6: The die set inside the gleeble machine 3800.....	62
Figure 3-7: Schematic drawing of the Gleeble® 3800 machine tooling and current flows (red arrows) during the electrical-field sintering process [3, 75]	70
Figure 3-8: Pictures showing the applications of IR heating in daily life and industry [68] ..	72
Figure 3-9: Schematic drawing of the Gleeble ® 3800 Machine tooling and current flow during the Micro-FAST process for ceramic materials	73
Figure 4-1: Simplified parts used in the simulation of coupled thermal-electrical analysis....	79
Figure 4-2 : Simplified parts used in the simulation of coupled thermal-electrical analysis with the mesh	80
Figure 4-3 : Heating temperature distribution of Zirconia sample in Die Set A for step 1: electrical and thermal analysis and step 2: heat transfer analysis after the current switch off	83
Figure 4-4: Contour of Zirconia sample for heating temperature distribution at integration points of step one and two	85
Figure 4-5: Heating temperature distribution of Alumina sample in Die Set A for step 1: electrical and thermal analysis and step 2: heat transfer analysis after the current switch off	86
Figure 4-6: Contour of Alumina sample for heating temperature distribution at integration points of step one and two	88
Figure 4-7: Heating temperature distribution of piezoceramic sample in Die Set A for step 1: electrical and thermal analysis and step 2: heat transfer analysis after the current switch off	89
Figure 4-8: Contour of piezoceramic sample for heating temperature distribution at integration points of step one and two	90
Figure 4-9: Comparison heating temperature of zirconia, alumina and peizoceramic in die sets A for electrical analysis in step one	92

Figure 4-10: Comparison heating temperature of zirconia, alumina and peizoceramic in die sets A for electrical and thermal analysis in step 2	93
Figure 5-1: Die set with powder material inside it during the experiment using Gleeble 3800 machine.	95
Figure 5-2: Gleeble [®] 3800 machine.....	97
Figure 5-3: Density determination kit (Sartorius YDK03) and powder measuring scale (Sartorius Practum).	100
Figure 5-4: Scanning Electron Microscope (W-SEM) from HITACHI S-3700N [133]......	101
Figure 5-5: NanoTest Vantage System [134].	102
Figure 5-6: Small amount of the high-temperature specimen graphite lubricant (Thred Gard) and stickers was put at both the punches of the Gleeble [®] 3800 machine.....	112
Figure 5-7: QuickSim TM software used to operate the Gleeble [®] 3800 during Micr-FAST process.....	113
Figure 5-8: (A) Before experiment and (B) During experiment for the condition gap between upper and lower punches towards the die during The Micro-FAST process	115
Figure 5-9: Comparison of relative density with parameters of experiment for 3YZrO ₂ samples	117
Figure 5-10: The heating temperature and shrinkage of stroke punches of Gleeble [®] 3800 machine for 3YZrO ₂ samples.....	118
Figure 5-11: The 3YZrO ₂ samples	119
Figure 5-12: Comparison of relative density with parameters of experiment for MSZ samples	121
Figure 5-13: The heating temperature and shrinkage of stroke punches of Gleeble [®] 3800 machine for MSZ samples.	122
Figure 5-14: The MSZ samples	123
Figure 5-15 Comparison of relative density with parameters of experiment for MSZ samples	125
Figure 5-16: The heating temperature and shrinkage of stroke punches of Gleeble [®] 3800 machine for MSZ(#) samples.....	127
Figure 5-17: The MSZ(#) samples.....	128

Figure 5-18: Comparison of relative density with parameters of experiment for Alumina samples.....	130
Figure 5-19: The heating temperature and shrinkage of stroke punches of Gleeble® 3800 machine for Alumina samples.	131
Figure 5-20: The Alumina samples.....	132
Figure 5-21: Comparison of relative density with parameters of experiment for PZT samples	135
Figure 5-22: The heating temperature and shrinkage of stroke punches of Gleeble® 3800 machine for PZT samples.	136
Figure 5-23: The piezoceramic samples	137
Figure 5-24: SEM micrograph for 3YZrO ₂ sample at centre position (Magnification: 950 BSE)	139
Figure 5-25: SEM micrograph for 3YZrO ₂ sample at edge position (Magnification: 950 BSE)	141
Figure 5-26: SEM micrograph for MSZ sample at centre position (Magnification: : 1.20 k SE)	142
Figure 5-27: SEM micrograph for MSZ sample at edge position (Magnification: : 600 SE).....	144
Figure 5-28: SEM micrograph for MSZ (#) sample at centre position (Magnification: : 1.20 k SE).....	145
Figure 5-29: SEM micrograph for MSZ (#) sample at edge (Magnification: : 1.20 k SE) ...	146
Figure 5-30: SEM micrograph for Alumina sample at centre position	148
Figure 5-31: SEM micrograph for Alumina sample at edge position.....	149
Figure 5-32: SEM micrograph for piezoceramic sample at centre position	150
Figure 5-33: SEM micrograph for PZT sample at edge position.....	151
Figure 5-34: Positions of nano-hardness indentation of MSZ-3 sample by using NanoTest Vantage hardness tester.....	152
Figure 5-35: Large image FOR SOME Positions of nano-hardness indentation of MSZ-3 sample	153
Figure 5-36 : Distribution of nano-hardness and reduced Young Modulus (Er) value for MSZ-3.....	154

Figure 5-37: Positions of nano-hardness indentation of MSZ(#)-4 sample by using NanoTest Vantage hardness tester.....	155
Figure 5-38: Distribution of nano-hardness and reduced Young Modulus (E_r) value for MSZ(#)-4	156
Figure 6-1: The initial design for the alternative tool for Micro-FAST process	160
Figure 6-2: The first two design of the alternative tools for Micro-FAST	162
Figure 6-3: The new tool design for Micro-FAST process with full details	163
Figure 6-4: New tool design for Micro-FAST process (A) without the applied pressure (B) With the applied pressure.....	164
Figure 6-5: The lower parts of the new tool design and where the powder going to be filled	165
Figure 6-6: Simplified parts of the new tool design used in the simulation of coupled thermal-electrical analysis	167
Figure 6-7: Heating temperature distribution of new tool design and Alumina sample for step one: electrical and thermal analysis and step two: heat transfer analysis after the current is off	170

LIST OF TABLES

Table 2-1: Typical methods/processes in micro-manufacturing[1]	13
Table 2-2: Examples of classification of feature sizes and specimen sizes on several processes [3].....	21
Table 2-3: Types of size effects and characteristic parameters [27, 50].....	21
Table 3-1: The two die sets that used by Zulkipli [3]	58
Table 3-2: The improved die sets for Micro-FAST process	60
Table 3-3: The cross section die used in the Micro-FAST process	61
Table 3-4: Mechanical and thermal properties between graphite and tungsten carbide materials based on compressive strength, thermal expansion coefficient and maximum service temperature [120]	63
Table 3-5: Combination of the die sets materials of graphite and tungsten carbide by comparing thermal expansion coefficient among the materials for the punches and body of the die.	64
Table 3-6: Selection combination of die sets materials of graphite (C) and tungsten carbide (WC) with powder that need to been sintered which is Alumina, Zirconia and piezoceramic by comparing on their thermal expansion coefficient.....	66
Table 3-7: Selection combination of die sets materials of graphite and tungsten carbide with powder that need to be sintered which is Alumina, Zirconia and piezoceramic by comparing their maximum service temperature of the die sets and sintering temperature of the powder during the electrical-field activated sintering and forming process.	68
Table 4-1: properties of part materials used in the thermal-electrical analysis [120].....	81
Table 4-2: Global seeds used for meshing the simulation of thermal-electrical analysis.....	82
Table 4-3: Temperature data for contour of Zirconia sample as presented in Figure 4-3	84
Table 4-4: Temperature data for contour of Alumina sample as presented in Figure 4-5.....	87
Table 4-5: Temperature data for contour of Alumina sample as presented in Figure 4-7.....	90
Table 5-1: General specification of the thermal system for Gleeble® 3800 machine [132]. ...	97
Table 5-2: General specification of the mechanical systems for Gleeble® 3800 machine [132].	98

Table 5-3: The classification of for Zirconia, Alumina and piezoceramic POWDERs used in Micro-FAST PROCESS which performed by Gleeble [®] 3800 machine.....	104
Table 5-4: Experiment parameters for 3Y-ZrO ₂ powder material performed by Gleeble [®] 3800 machine for Micro-FAST process	106
Table 5-5: Experiment parameters for MSZ powder material performed by Gleeble [®] 3800 machine for Micro-FAST process	107
Table 5-6: Experiment parameters for MSZ (#) powder material performed by Gleeble [®] 3800 machine for Micro-FAST process	108
Table 5-7: Experiment parameters for Alumina powder material performed by Gleeble [®] 3800 machine for Micro-FAST process.	109
Table 5-8: Experiment parameters for piezoceramic powder material performed by Gleeble [®] 3800 machine for Micro-FAST process	110
Table 5-9: Results of the dimensions, weight and relative density for 3Y-ZrO ₂ samples using the die set A for the Micro-FAST process which performed by Gleeble [®] 3800 machine.....	116
Table 5-10: Results of the dimensions, weight and relative density for MSZ samples using the die sets A and B for the Micro-FAST process which performed by Gleeble [®] 3800 machine.	120
Table 5-11: Results of the dimensions, weight and relative density for MSZ (#) samples using the die set A for the Micro-FAST process which performed by Gleeble [®] 3800 machine.....	124
Table 5-12: Results of the dimensions, weight and relative density for Alumina samples using the die set B for the Micro-FAST process which performed by Gleeble [®] 3800 machine.....	129
Table 5-13: Results of the dimensions, weight and relative density for piezoceramic samples using the die set B and C for the Micro-FAST process which performed by Gleeble [®] 3800 machine.....	134
Table 5-14: Chemical element weight percentage of carbon (wt%) at the positions of centre and edge of 3YZrO ₂ samples.	140
Table 5-15: Chemical element weight percentage of carbon (wt%) at the positions of centre and edge of MSZ samples.....	143
Table 5-16: Chemical element weight percentage of carbon (wt%) at the positions of centre and edge of MSZ (#) samples	146
Table 5-17: Chemical element weight percentage of carbon (wt%) at the positions of centre and edge of Alumina samples	148

Table 5-18: Chemical element weight percentage of carbon (wt%) at the positions of centre and edge of piezoceramic samples.....	151
Table 5-19: Average values for nano-hardness test for MSZ-3 by using NanoTest Vantage hardness tester.....	153
Table 5-20: Average values for nano-hardness test for MSZ(#)-4 by using NanoTest Vantage hardness tester.....	155
Table 6-1: Properties of part materials used in the thermal-electrical analysis for the new tool design [120]	168
Table 6-2: The number of the mesh (nodes and elements) for each part in new tool design	169
Table 6-3: Temperature and time data for contour of the new tool design and Alumina sample for step one: electrical and thermal analysis	171
Table 6-4: The Figures of the new tool design and Alumina sample for heating temperature distribution at integration points of step one : electrical and thermal analysis.....	172
Table 6-5: Temperature and time data for contour of the new tool design and Alumina sample for step two: heat transfer analysis after the current is off.....	175
Table 6-6: The Figures of the new tool design of the Die, punch and Alumina sample for heating temperature distribution at integration points of step two: heat transfer analysis after the current is off	176

1 INTRODUCTION

1.1 RESEARCH BACKGROUND

Today there is a significant increase in the demand for micro and miniature products and micro-electromechanical systems (MEMS). This is due to the rapid growth that can be seen in the fields of medicine, telecommunications and the automotive industry. For example, the global industry association Semiconductor Equipment and Materials International (SEMI) has forecast that the sales for semiconductor equipment, which had a market value of \$37 billion in 2015, is going to grow globally by 1.4% [1-3]. With regard to classic MEMS manufacturing recent efforts have been made to scale down traditional methods and to develop new processes to produce micro- and nano-components [2, 4-6]. For example, the manufacturing of micro gears which are used widely in MEMS and micro-mechanical-systems (MMS), is often enabled through lithographic techniques especially LIGA processes (German acronym for Lithographie, Galvanoformung, Abformung (Lithography, Electroplating, and Molding) that describes a fabrication technology used to create high-aspect-ratio microstructures) or ultra-precision machining [3, 7, 8]. Moreover, Micro-forming plays an important role in the manufacture of millions of micro products, such as micro screws through upsetting and rolling. Furthermore, micro-extrusion has been well investigated where it is capable of extruding micro pins in the laboratory with a shaft diameter of 0.5 to 0.8 mm and a wall thickness of 50 to 125 μm . In addition, forming ceramic materials is a challenging matter and there are some processes that can be used to produce miniature products such as those made by slip casting, tape casting, injection moulding, dry pressing and hot isostatic pressing [2, 9-11]. Therefore, based on previous research and experimental results there is no question that it is possible to manufacture micro components with high precision and accuracy. However the cycle time and cost for high production remain problematic and improvements are still necessary.

In micro-forming, the limits of the process are influenced largely by the workpiece's geometry and dimensions and the type of materials. This occurrence is being described as the size effects. The size effects that exist in the materials can be described as grain and feature/specimen size effects grain size effect can be described by the Hall-Petch law which states that the material strengthens as the grain size decreases. The grain is a piece of a single crystal that can grow by absorbing atoms from neighboring grains. Grain growth is driven by a reduction in the total system energy and could lead into in reduction the grain boundary surface area. When some grains grow, the total number of grains in the material decrease, thus reducing the free energy of the system. The performances of polycrystalline materials are strongly affected by the formed microstructure inside, which is mostly controlled by grain growth behaviors. In the Meantime, when the flow stress declines due to the miniaturization of a part, the feature or specimen size effect appears. This effect can be considered an isotropic continuum if the volume of the part remains unaffected by the various tools used in the process. Moreover, It was found that by reducing the workpiece dimensions this could lead to an rise of friction factor by 20 times, when performing extrusion experiments on the brass alloy (CuZn15) [11-14].

Additionally, micro forming requires tools with overall sizes in a range of tens of microns. Electrical discharge machining (EDM) is one of the processes that has been used as the main process of producing the micro tools. The benefit of using the micro-wire EDM method is the capability to provide excellent results for producing micro tools with a high accuracy and good quality, but the process is lacking in geometrical flexibility. Other technologies for micro tools such as, grinding drilling, and milling were used for making tools such as tools for stamping and coining processes. However, micro-tooling is expensive to manufacture [15, 16]. Moreover, plasticity remains largely absent in most ceramic materials. It has been shown that fracture can be suppressed to some extent in a few ceramics at low temperatures, such as ZrO_2 and yttria-stabilized zirconia (YSZ) [17]. The development of micro forming technologies is facing big challenges that need to be addressed for producing micro-tooling. In addition, the cost issue is a key factor that needs to be considered. The fragility of tools can be a problem due to the forming force and tool wear at the micro and small scales. The micro scale process is regularly slower than at the macro scale process due to the size effect issues and

difficulties in fabricating micro parts with complex design. This was mainly the issue when a high strength material was used in the micro forming process.

Therefore, the development of a new high volume production and low-cost manufacturing process is required. The concept of this research comprises the combination of micro forming and Field Assisted Sintering Technology (FAST). It has a potential to address the problems and meet market needs in terms of reducing the influence of size effects, shortening the process time, improving the shape of the produced part, decreasing the required pressure for the forming process, providing options to use different material powders and improving the forming of micro parts with high strength materials. Among applications that uses electricity, electro-plasticity electrical sintering and (SPS) processes spark plasma sintering has successfully formed components in many types of materials. However, there are still considerable challenges to meet the requirements of achieving high relative densification of samples and simplification of the processes[18]. Moreover, using the conventional powder sintering process to consolidate or densify materials could produce a coarsening or neck growth, which is critical because it is needed to achieve densification caused by surface evaporation or diffusion [19]. Therefore, it is the reason why conventional methods take a long time to complete. Currently using the forming process and electrical-field activated sintering technology, the densification can be completed more promptly by powder particles deformation and breakage. It is not like the SPS method which uses spark discharge to generate the heating, because it requires the spark to ignite in the gaps, which means that the pressure used will not be too high to prevent the spark from vanishing [20]. However, by using the forming process and field activated sintering technology (FAST) by applying high pressure this will assist breakage and increase plastic deformation of the particles between interfaces. Based on that it is important for the process of the breakage and deformation of the material particles to occur in order to get a sufficient and quick densification of micro products and components.

1.2 AIMS AND OBJECTIVES

The aim of this project is to develop a new fast forming process configuration to manufacture miniature/micro components and corresponding tool-designs for machine setup enabling bulk-forming from powder materials. The project involves a combination of micro forming and Field Assisted Sintering Technology (FAST). The FAST process uses as low voltage and high current, pressure-assisted sintering and synthesis technique, which has been used recently in materials processing. This method can be used to densify materials and synthesize compounds, and it is similar to hot pressing, but the heating and powder densification mechanisms are different. Micro-FAST is a processing technology which scales down the conventional FAST process for small-length scale manufacturing which involves a different sintering mechanism and tooling technique, such as size-effect, electrical-thermo phenomena at micro-scale, and micro/nano-interfacial fusion bonding, etc. The specific objectives of the research were:

- a) Understanding the fundamentals of the densification process for micro forming and Field Assisted Sintering Technology (FAST).
- b) Developing the optimal parameters for the Micro-FAST process, die sets and other tooling for experiments and thermal-electrical FEA setup with the Gleeble[®] 3800 (vacuum) and the new tool design.
- c) Conducting Finite Element Analysis for the die sets and the samples for the Micro-FAST process.
- d) Conducting experiments by using three types of zirconia alumina and piezoceramic powder to produce high relative density cylindrical and cuboid samples with the Gleeble[®] 3800.
- e) Developing an alternative tool design for the Micro-FAST process.

- f) Conducting Finite Element Analysis alternative tool design for the Micro-FAST process.

1.3 THE PROJECT METHODOLOGY AND APPROACH

Fundamental studies have been done consisting of process concept evolution, a design of tools and process configurations for the experiments to achieve the aims and objectives as stated above.

It started with a comprehensive literature review in the subject areas such as micro manufacturing, issues in micro-manufacturing, micro forming and size effects, powder sintering and the electrical-field assisted sintering technology (FAST) application in the sintering process. Through the literature review, key development issues have been identified, and solutions for technology advances have been proposed.

After that, a development of Micro-FAST process parameter configurations, die sets and other tooling have been identified and explained in order to prepare an experiment.

Then an electrical-thermal finite element analysis has been conducted for the for Micro-FAST process for ceramics materials (zirconia, alumina and piezoceramic) to achieve the best parameter for the process and prepare it for the experiment using Gleeble[®] 3800 machine from Dynamic Systems Inc. The FEA has been used to show the heating characteristics of the die sets that are going to be used in the experiment. The information collected from the FE simulation is useful for understanding how the heating distribution happens to the die used in the experiments of the FAST process.

Then, a series of experiments using three kinds of powder were used as raw materials which were alumina, zirconia and piezoceramic powder materials. The experiment was conducted by using a Gleeble[®] 3800 machine from Dynamic Systems Inc. The experiments were conducted in London with the collaboration of Imperial College with die sets prepared by the Micro-FAST project partners.

After the experiments were conducted, the effects of parameters of the experiments such as pressure, heating rate, heating temperature, holding time and the die sets used were reviewed to see how they related to the densification, microstructures, and surface hardness of the produced samples. The results with high sample densification were compared with a previous electrical sintering process that had been used to see if the samples were achieving excellent results or not. Improvements of the experimental process parameters and tool design were performed to increase the process efficiency and improve product quality.

Finally, the issues and the problems encountered in the experiment have been stated that could lead to some difficulties in applications of the technology. These included difficulty with filling the powder, difficulty in controlling the volume of the powder feeding, difficulty in handling the die during the operation, difficulty in injecting the component outside the die, and the die-life being too short due to small sizes having fragility. These lead to the development of a new tool design concept with the die-set inside it which can hypothetically be used for mass production in the industry. The new tool design concept has a general design and a manufacturing methodology by using electrical-field activated sintering technology (FAST) and micro-forming to create micro-components from powder materials was established.

1.4 THE THESIS LAYOUT

Chapter 1 *Introduction*

This chapter consists of a description of the background of the project and the aims along with the objectives which this research intended to achieve. This was followed by detailed discussion of the project methodology to be used to complete the research. The layout of the thesis for all the development works carried out was shown.

Chapter 2 *Literature Review*

The second chapter provides a literature review of the subject areas such as micro manufacturing, issues in micro-manufacturing, micro forming and size effects, powder sintering and the electrical-field assisted sintering technology (FAST) application in the sintering process. Through the literature review, key development issues have been identified, and solutions for technology advances have been proposed.

Chapter 3 *Micro-FAST of Ceramics and Composites*

This chapter explains the process configuration and densification mechanism of the Micro-FAST process which mainly consists of four stages. In addition, the development works on the die sets used in the Gleeble® 3800. The discussion on consideration of tool geometric feature design and selection of the material for the die sets is explained. The improvement of the Micro-FAST process and the role of the heat transfer for this process is discussed.

Chapter 4 *Thermal-Electrical Finite Element Analysis (FEA) of The Micro-FAST with Ceramic Material*

In this chapter, the work by using ABAQUS/CAE software as a tool for coupled FE thermal-electrical analysis, the effect of heating distributions applied to the die sets during the electrical-field activated sintering and forming processes were achieved. Results and discussion from each of the die sets and materials have been analysed in detail.

Chapter 5 *Experiment of Micro-FAST of Ceramic Powder*

This chapter clarifies the experimental study of the Micro-FAST process. All the information regarding the equipment, ceramics and composite powder materials, parameters and procedures used in the experiment and analysis has been identified. The formed samples from the experiments were analysed and discussed to provide conclusive results of reliability of the Micro-FAST process. Moreover, the die sets produced excellent quality micro-components with a high process efficiency.

Chapter 6 *New Tooling Concept for Micro-fast of Ceramic Components*

In this chapter, the possible issues faced in the experiment have been stated which could lead to some difficulties in applications of using the technology. Therefore, a new tool design concept with the die-set inside it has been proposed which can potentially be used for mass production. The Micro-FAST concept going to be used with the new tool design concept to create micro-components from powder materials was established.

Chapter 7 *Conclusions and Recommendations*

This chapter concludes the thesis and makes recommendations for possible future work

2

LITERATURE REVIEW

2.1 MICRO-MANUFACTURING

The meaning of manufacturing is making products that have been designed for a certain purpose or application. It is a process for making an excellent output concerning quantity with the maximum possible utilisation of raw materials. The manufacturing process can produce either discrete or continuous process. However, in the last 20 years, the ‘manufacture’ meaning has changed. Due to the economic, social and even the political changes manufacturing has been influenced and became more organized and more implemented these days. Nowadays, there is an increase in demand for miniature products that have been designed and produced within small scales, such as MEMS, micro-mechanical devices, micro-medical components, etc. Moreover, nanotechnology is becoming more mature and influential and many nanotechnology-based products are being seen in the market such as nano-materials and coating surfaces, nano-devices for communication, sensors and medical treatments and these are produced in a volume production scale [1, 2, 21, 22].

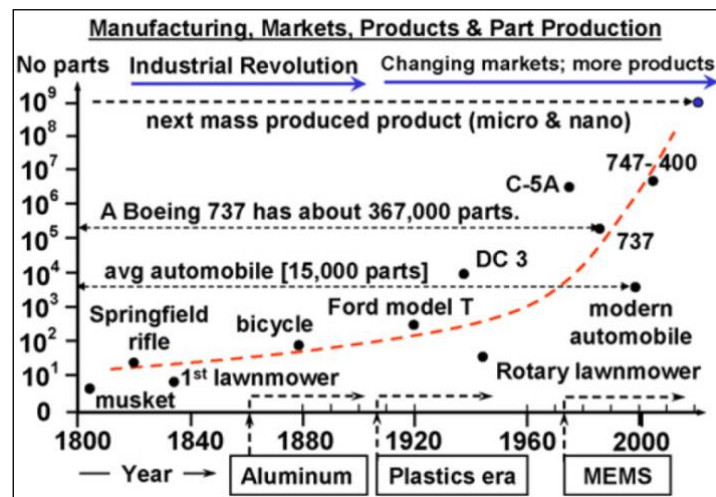


FIGURE 2-1: THE REVOLUTIONARY OF INDUSTRIAL TOWARDS PRODUCTIONS OF COMPLEX PARTS [21]

The development of manufacturing can be observed in the production of micro-products as applied in mechanical, MEMS and medical industries. It has been widely used in, telecommunications devices, vehicles, aircraft, household appliances, and information technology facilities as shown in Figure 2-1. Due to this trend for miniature products, there are challenges where the industries are trying to produce new products that integrate with a range of functions and expand the application area without increasing the weight or the overall size of the product [2, 23]

In industry, the concept of micro manufacturing can be understood within the context of a miniature of the factory and manufacturing system. This means that all devices and machines can be reduced to small scales. By decreasing the scale the energy will be reduced also which means a reduction in the cost and the pollution [24] [25].

According to Qin [2], the scope of micro-manufacturing might need to be redefined as follows:

- Micro-precision manufacturing of macro-sized components
- Micro-/nano-feature manufacturing over large and small areas
- Manufacturing of micro-sized components
- Manufacturing with micro-/nano-structured materials

- Manufacturing with controlled micro-structures of materials

The micro-manufacturing is the link between the macro- and nano-manufacturing. The micro-manufacturing engineering covers all aspects that have at least 2 dimensions within sub-millimeter ranges. These aspects include manufacturing methods, strategies, equipment, technologies and systems. The term of micro-manufacturing engineering concerns a series of relevant activities within the chain of manufacturing micro-products/features, including design, analysis, materials, processes, tools, machinery, operational management methods and systems, etc.. [1, 2]. There is a huge amount of research and literature about the manufacture of microsystems and MEMS. The technologies that include design and fabrication of micro-systems sometimes are referred to as MEMS or MST [1] [26] [23].

The micro-manufacturing techniques are often divided into 2 categories, MEMS manufacturing and non-MEMS manufacturing. The MEMS manufacturing includes many techniques, such as plating, photolithography, chemical etching, LIGA, laser ablation, etc. Meanwhile, the non-MEMS manufacturing includes some techniques, such as EDM, micro-mechanical cutting, laser cutting, laser patterning, laser drilling, micro-extrusion, micro-stamping, micro-embossing, micro-injection moulding, etc. On the other hand, sometimes the micro manufacturing cauterised regarding the use of materials into silicon-based manufacturing and non-silicone material manufacturing [1, 27]. Figure 2-2 shows the example of micro parts produced by using the micro-forming process (Micro-extruding process). It can produce products in near-net shape with less finishing operations. However, there are also some difficulties regarding the size and frictional effects in forming material. For the components in the range of 0.1 to 5 mm, the surface area per volume ratio is large and the forces on the surface play a major role. When the ratio of the grain and feature size becomes larger, deformation characteristics change in an unexpected way with significant variations in the response of the material [28-30]



FIGURE 2-2: EXAMPLE OF SOME FORMED MICRO PARTS [30, 31]

2.1.1 MICRO MANUFACTURING PROCESSES

Recently, the trend is to concentrate on miniaturizing or downscaling both conventional and non-conventional methods to produce micro-products. Therefore, there are several processes that have been applied which can be classified as conventional, non-conventional and hybrid micro-manufacturing. The conventional process involves changing the workpiece shape using a device made from hard material. Meanwhile, for non-conventional methods other forms of

energy are utilised which are not associated with the sharp cutting tools needed for conventional processes. Hybrid manufacturing is the combination of two or more processes to manufacture the micro-products [3, 32]. According to Qin [1, 2] manufacturing processes can be classified according to the energy type that has been used in the process, such as mechanical, chemical, electrochemical, electrical and laser processes. The working principles behind each process include consideration of mechanical forces, thermal effects, ablation, dissolution, solidification, re-composition, polymerisation/lamination, and sintering. General production processes also can be categorised depending to the way in which the micro-products are to be made such as subtractive, additive, deforming, joining and hybrid processes as shown in Table 2-1 [1, 2].

TABLE 2-1: TYPICAL METHODS/PROCESSES IN MICRO-MANUFACTURING[1]

Processes	Subtractive	Micro-mechanical cutting (milling, turning, grinding and polishing), micro-EDM, micro-ECM, laser beam machining, electro-beam machining and photo-chemical-machining.
	Additive	Surface coating (CVD and PVD), direct writing (ink-jet and laser-guided), micro-casting, micro-injection moulding, sintering, photo-electro-forming, chemical deposition, polymer deposition and stereolithography.
	Deforming	Micro-forming (stamping, extrusion, forging, bending, deep drawing, incremental forming, superplastic forming and hydro-forming), hot-embossing and micro/nano-imprinting.
	Joining	Micro-mechanical-assembly, laser-welding, resistance, laser, vacuum soldering, bonding and glueing.
	Hybrid	Micro-laser-ECM, LIGA combined with laser-machining, micro-EDM and laser assembly, shape deposition and laser machining, laser-assisted-micro-forming, micro assembly injection moulding and combined micro-machining with casting.

2.1.2 CHALLENGES AND KEY ISSUES IN MICRO-MANUFACTURING

The manufacturing of micro-products needs to address production issues extensively to be able to succeed compared to the situation with prototype-products based on micro-technologies. The high-volume and low cost production of micro-components should be the

main aim for the design of micro-manufacturing. The primary difficulties that relate to the manufacture of micro-products are negligible when the work is done conventionally. When these products are designed, not only will functional requirements need to be considered, but also micro-manufacturing-related factors will have to be taken into account. This is because manufacturing these products produces more significant challenges, compared to those for the manufacture of macro-products. In the macro-scale manufacturing, the limit is how far it can be scaled down, and factors that were insignificant at the macro-scale become more important in influencing the manufacturing process for a micro-product. The essential factors in micro-manufacturing that are negligible or ignored in the conventional machining are chip removal, vibration, tool-offset, the rigidity of the tools and temperature [2, 6, 24, 33].

Another issue to be addressed at the design stage of micro-manufacturing is volume production and automation. Most of the processes such as pressing, milling, turning etc, and handling processes such as material loading and unloading, tool positioning and aligning; were all manually configured and controlled by separate dedicated controllers to obtain precise and accurate motion and alignment. It is different from prototyping in a lab scale compared to products that are manufactured in volume production. The materials selection for manufacturing and design of the component with their features will have an influence on achievable production yield, which is mainly relevant by the capability of the machinery, tools, processes and auxiliary equipment. It can be noticed that the micro-process technology is time consuming and only suitable for low yield-rates. Moreover, the micro-process technology does not have the potential yet for conventional processes due to the manual adjustments in every aspect of the process [3, 33]

Unwanted external forces involved in physical contact are another issue that needs to be removed. The precise positioning is a main problem encountered in the handling of micro-parts. These external forces involved in physical contact are the electrostatic, sticking or adhesion effect, and Van Der Waals forces. These are key issues and numerous studies have been undertaken to recognize the situation and determine the strategy necessary to eliminate these forces using mathematical simulation [34-39]

Dimensional factors are also challenging when dealing with micro-manufacturing. The development of micro-tooling started a long time ago, but there is still a limitation on the tooling applicability [40, 41]. For example, in the process of drilling, the suitable aspect ratio which is the tool diameter to the drilling depth is from 5-10 and sometimes can be lower than five. However, deeper plunging and drilling could cause breakage in the tooling and that could make the tooling unsuitable for aerospace and automotive industries [42]. Moreover, the sensor dimensions need to be taken into account, because using the appropriate tooling in the micro-manufacturing also deals with the sensors dimension. Recently, the available sensors are bulky in size and that affects the performance and the precision of the work. Due to their large size, the sensors are difficult to be placed accurately on a small workspace. While this level of precision is not feasible for micro parts application as they require at least sub-micron precision and accuracy. Additionally most current machines have less precision and accuracy than that required in micro-handling [6, 24].

The limitations on the shape and the capability of the materials in producing micro-products are important issues that face the manufacturer. For example, most of the processes are only dealing with 2D/2.5D compared to 3D shapes, since to create 3D shapes needs significant efforts such as development new processes and expensive equipment. The material capability plays an important role in the micro-manufacturing process. It can be shown from previous research that certain materials, such as brass, copper and aluminium used as test materials due to their flexible and soft characteristics with low mechanical strength properties will tend to deform easily under a low applied force. Only simple micro-features were generated successfully by the efforts made [2, 13, 25, 43-45]

2.1.3 MICRO FORMING

Micro-forming can be defined as the technology of forming materials with at least two part dimensions in the submillimeter range. For forming micro components from conventional scale to smaller scale range, some aspects of the workpiece remain unchanged, such as the micro

structure and the surface topology. This causes a change in the relation between the dimension and of the component and the parameter of the surface or the micro-structure to be changed, and that refers to the size effect. Micro-forming can be considered as a forming technology processed in the so-called micro-factory [2, 27, 46] . A micro-factory is a downscaled manufacturing system that represents a method to produce miniaturised products with less space and operational costs, and as well as reduced consumption of energy and resources. It has been established that in the case of 1/10 size reduction of production machines, the total energy consumption in the factory could be reduced to nearly 1/100 of that of the conventional factory [1, 25].

In conventional forming processes, the theories and technologies in macroscale have been well established and widely used to manufacture high quality parts with highly sophisticated tools, making the forming of several geometrical features possible. The conventional forming process has been the appropriate choice for the economic and reliable manufacturing of a variety of components in large-scale production. However, forming theories and technologies for the macro scale cannot be scaled down to the micro scale easily, because it is impossible to scale down all parameters in the micro-forming process according to the theory of similarity due to the size effects [27, 43, 46]

According to several publications [43, 46], a micro- forming system can be split into four groups as shown in Figure 2-3 the components of the micro-forming system [43, 46] :
Material, Processes, Tools and Machines/equipment.

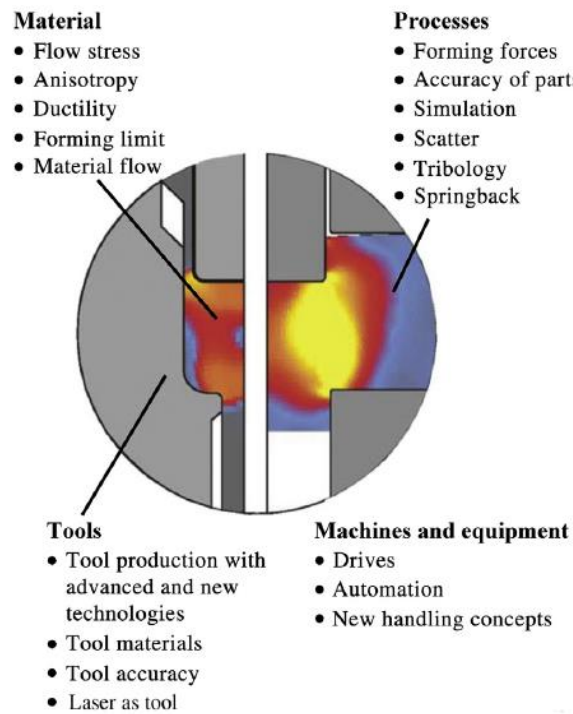


FIGURE 2-3: THE COMPONENTS OF THE MICRO-FORMING SYSTEM [43, 46]

Another author [27] classified the forming process to five elements as seen in Figure 2-4

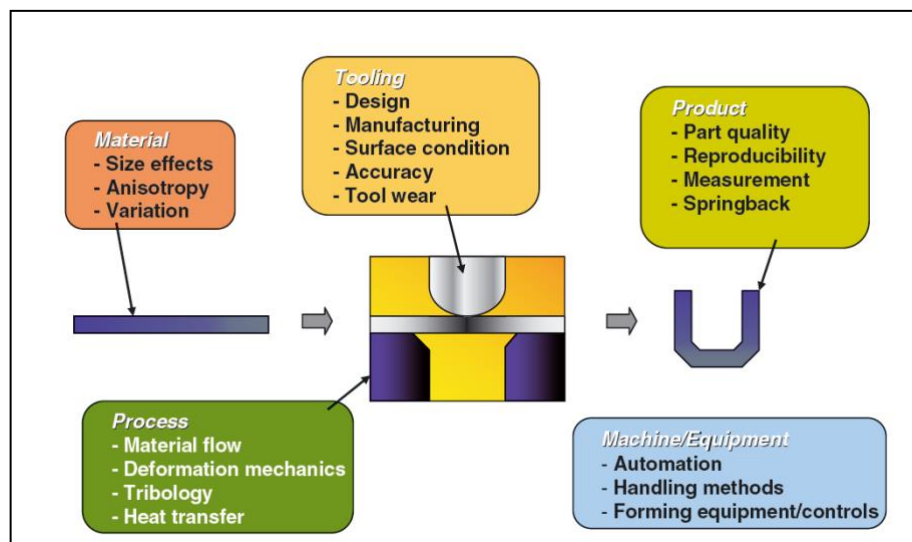


FIGURE 2-4: BASIC ELEMENTS OF A MICRO-FORMING SYSTEM [27]

For the materials, when scaling down the forming process to micro-scale, the deformed material will not be considered as a continuum because of the large share of volume that has been occupied by an individual grain. Differently from the conventional forming process, only restricted grains are placed in the forming area during micro-forming. Grain and grain boundaries will have a significant impact on the mechanical behaviour with the micro-scale dimensions. Compared to macroscale compression where there is less impact on the material's mechanical behaviour [27, 43, 46].

In conventional forming, appropriate design of forming processes is essential for economical and reliable manufacturing of high-quality products. Recently it has become possible to form complex-shaped components with different geometrical features by combining optimised forming processes with appropriate tools and equipment within the macro-scale in the industry. However, the conventional forming methods and strategies are not suitable for reliable forming processes in micro-scale. Micro-forming scaling down or modifying the conventional processes or normally uses non-conventional processes to fully address the issues and other factors of forming the micro component, such as forming forces, tribology, spring-back, scatter of the results, and accuracy of formed parts, simulation models and improved and optimized design [27, 43, 46]

Forming tools are main parts of the forming processes. In conventional forming, the manufacturing process of the tools is not as complex as that for micro-scale tools. Due to the micro-scale, the demands for specific tools with high surface quality and close tolerance will increase. The complexity of micro-forming tools comes from the difficulties in the creation of very small shapes with high accuracy which are necessary for micro-forming. Therefore, development of advanced and new manufacturing technologies of micro-forming tools is essential. In the manufacturing of micro-forming tools, there are two main factors to be considered, the tool materials and tool accuracy. The materials should have higher performance so that the service life of tools can be long. Moreover, flexibility of tools is also a very important factor that should be taken into account for the development of tooling system in order to reach efficient micro-forming processes. Nowadays, with the trend toward miniaturisation, forming of micro products with more complex shapes will become more common, and advanced technologies involving innovative manufacturing methods are expected [27, 43, 46].

Many problems occur in micro-forming processes related to miniaturisation. In conventional forming processes, the clearance between machine parts can be negligible. However, the detrimental influence on the accuracy of the produced products in the range of a few 100 μm . Therefore, it is necessary to develop machines and equipment that are particularly suitable for the micro-forming processes. Currently, the trend in the machines and equipment development in micro-forming is to decrease the scale in order to decrease the energy consumption, pollution, and cost, due to the use of fewer materials for the miniaturised system. Also, due to the reduction in scale of machines and equipment, the weight of the parts will be reduced. As a result of that, the speed of the forming tools and the rate of production could be increased. Moreover, the handling and measurement systems should also be considered in the development of machines and equipment in order to achieve a high productivity [27, 43, 46].

2.1.4 SIZE EFFECT IN A MICRO SCALE FORMING PROCESS

In micro-forming processes, to reach an accurate design and analysis, a proper modelling for the material behaviour is required by taking into the account the size effects. The issues associated with the size effects occur when the sizes/features are reduced from a conventional (macro-scale) process to micro-scale process. This causes the ratio between dimensions of the part like height, length width, and thickness with the microstructure of grain size to change. Due to that, the size effects will change almost all aspects of the forming process, for example, behaviour of material, heat transfer, friction and handling. Therefore, the conventional methods of metals and materials forming technology cannot be applied to micro-scale processes. Several conventional forming machine designs with micro-tools that have been scaled down from conventional to micro-forming have been used. However, considerations merged with machine design have to meet the requirements of the process for higher quality and efficiency concerning positional precision and handling of micro-parts/materials [1, 27, 43, 47-49]

According to Koc *et al* [27] There are two size effects existing in metallic materials, these are grain and feature/specimen size effect as shown in Figure 2-5. The grain size effect is represented by the Hall-Petch equation, which illustrate that the material strengthens as the grain size decreases. Grain size effect is dependent on the average size of the grains which dominate an effect on the material response at the macro-level. Meanwhile a feature/specimen size effect that has been observed, when the miniaturisation of the part happens, is a decline of the flow stress [27].

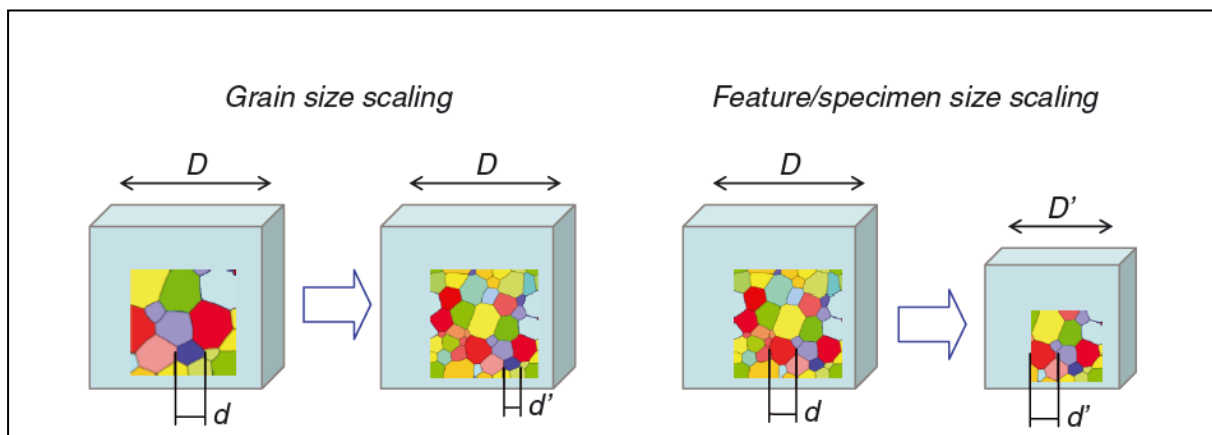


FIGURE 2-5: ILLUSTRATION OF GRAIN SIZE AND FEATURE/SPECIMEN SIZE EFFECTS

Depending on the testing methods of the material and forming process, the feature/specimen size effect could be divided into two distinctive effects: the feature size effect and the specimen size effect. The specimen size effect can be referred to as the diameter of a billet/rod to the thickness of the blank/sheet to be formed or tested. Meanwhile, the feature size effect can be referred to as the smallest feature such as channels, radius or protrusions of which the final part will be formed. **Table 2-2** shows several processes used as an example to define and differentiate between feature and specimen size [3, 27].

TABLE 2-2: EXAMPLES OF CLASSIFICATION OF FEATURE SIZES AND SPECIMEN SIZES ON SEVERAL PROCESSES [3].

Example Processes	Feature Size	Specimen Size
Extrusion process of micro-pins.	Diameter of the reduced section.	Initial diameter of the rod
Micro-channels formed on an initially flat thin sheet blank.	Micro-channel with their dimensions.	Thickness of the blank.
Bulge test of thin sheet blank.	Bulge diameter.	Thickness of the blank.

According to several authors [27, 50] as the grain, specimen and feature size get smaller into micro-scales, their effects are coupled and therefore should be considered together. The authors proposed the use of two characteristic parameters N and M to couple and represent the interactive effects. Where N is defined as the ratio between the specimen and the grain sizes, and M can be defined as the ratio between the feature and specimen sizes. By defining N and M , all combinations of the interactive effects (feature to grain size) can be represented and qualified using N , M and $N \times M$ as shown in Table 2-3.

TABLE 2-3: TYPES OF SIZE EFFECTS AND CHARACTERISTIC PARAMETERS [27, 50].

Processes Description	Size Effects		
	Grain Size	Feature Size	Specimen Size
Tensile Test	d		t_o, D_o
Bulge Test	d	D_c	t_o
Stamping Process	d	D_c	t_o
Extrusion Process	d	D_c	D_o

Characteristic Parameter	$N = t_o/d \text{ or } D_o/d$ $M = D_c/t_o \text{ or } D_c/D_o$ $N \times M = D_c/d$
-------------------------------------	--

Where:

d - Grain size of the materials.

t_o - Specimen thickness.

D_o - Specimen diameter.

D_c - Die cavity.

N - Ratio between the specimen and grain sizes.

M - Ratio between the feature and the specimen sizes.

Figure 2-6 shows a variety of materials such as Aluminium CuNi18Zn20, CuZn36, CuZn15 and CuAl alloy that were observed on the curve of material flow under various tensile testing conditions as shown in order to measure the material response on specimen size [3, 27]. Based on the tests that have been done, it has been established that the trend of decreasing flow stress with a decreasing of N value was rather consistent. In the meantime the grain size effect shows a strong influence on the material response at all scales until the N value is around 10 to 15 when the size effect of specimen starts to affect the materials response [3, 27].

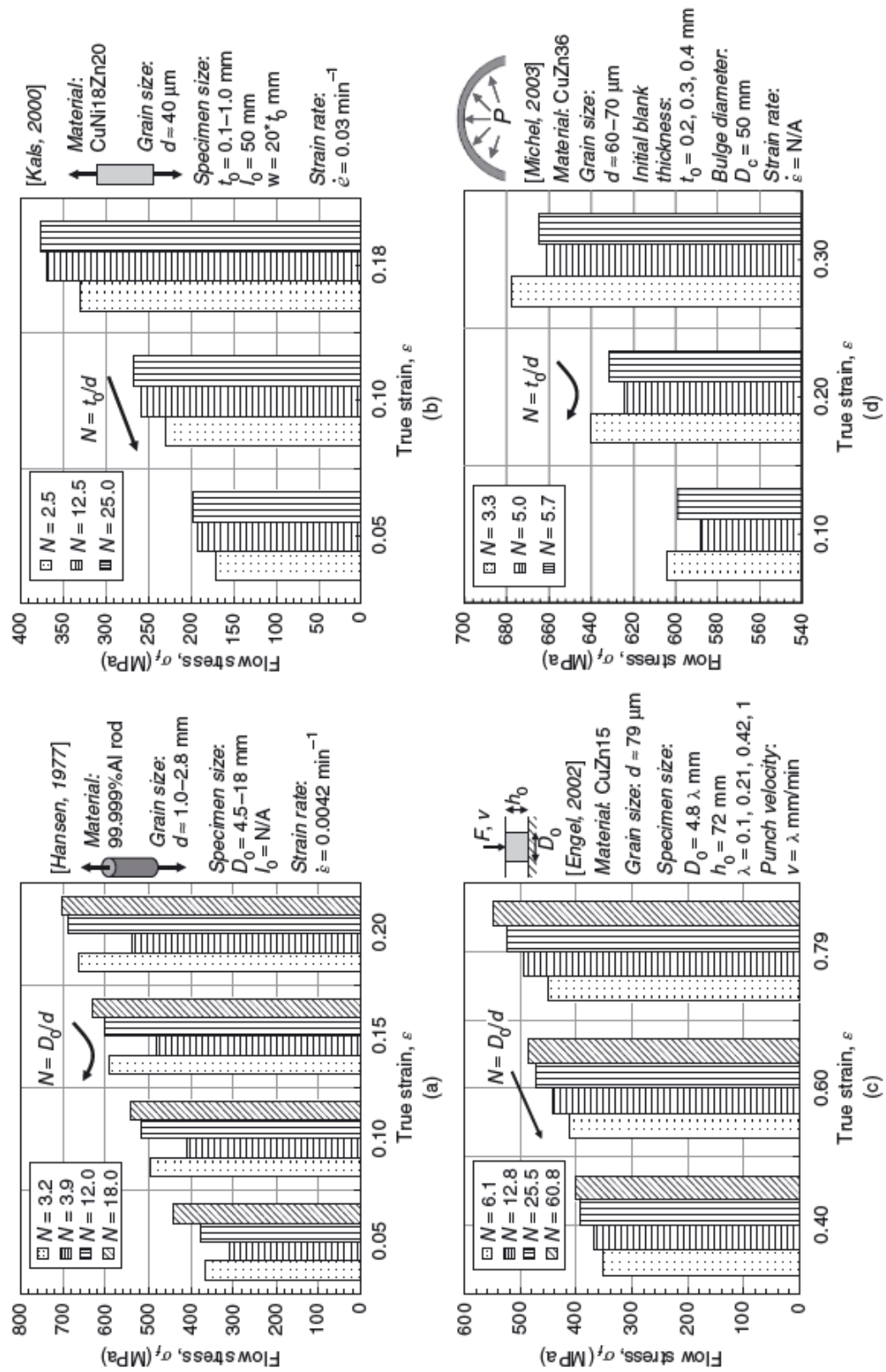


FIGURE 2-6: EFFECT OF N ON MATERIAL FLOW STRESS UNDER DIFFERENT TESTING CONDITIONS [27].

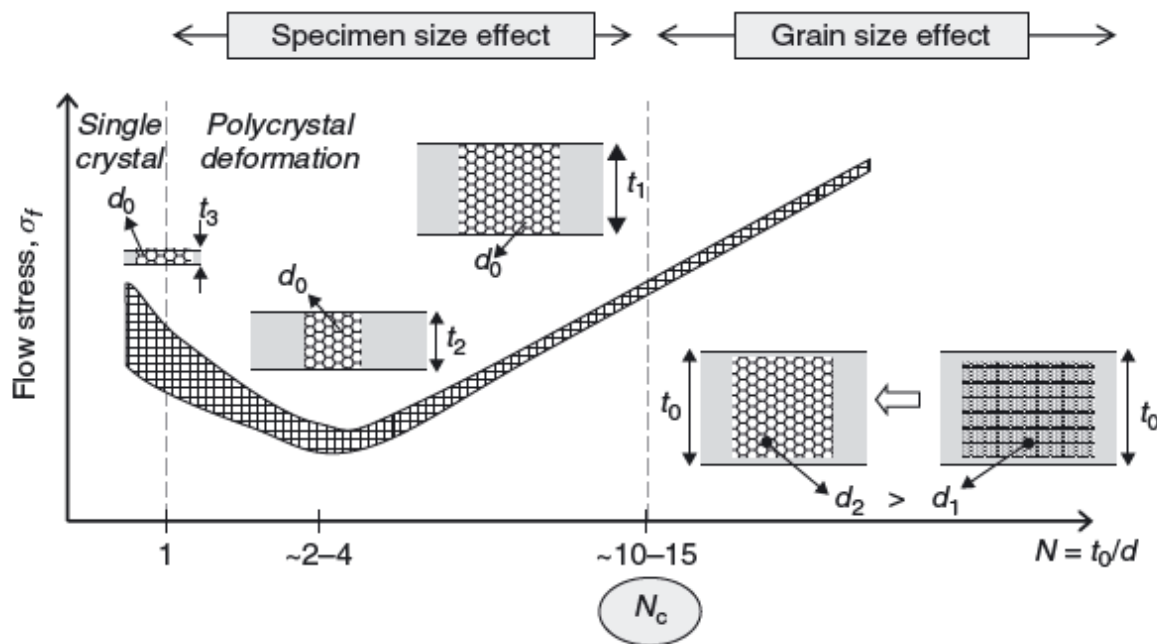


FIGURE 2-7: GRAIN AND SPECIMEN SIZE EFFECT AS FUNCTION ON N AGAINST THE FLOW STRESS OF THE COMPONENTS [27].

Nevertheless, based on the testing reported, an increase in flow stress N was reduced close to the range of 2 to 4. As an example, in a conducted tensile test of 99.999% Aluminium rods, the results showed an increase in flow stress as N decreased from 3.9 to 3.2 as illustrated in Figure 2-6 (a). Moreover, a hydraulic bulge testing of thin CuZn36 blanks showed similar results, where there was an increase in flow stress as N value decreased from 5 to 3.3 as shown in Figure 2-6 (d). An observation of increase in flow stress continued to occur as N value was reduced close to 1 (single crystal deformation) as reported in the bending test of CuZn15 and Aluminium 99.0 to 99.5%. Figure 2-7 shows the summary of the effect of N against the flow stress of the components tested. However, in the results of the tensile test of the CuNi18Zn20 specimen a continuous reduction in the flow stress was reported as N decreased from 25 to 2.5 as shown in Figure 2-6 (b) [27].

In contrast, the studies on feature size effect were still lacking a comprehensive understanding. As an example, a thin blanks of CuZn36 with the initial thickness of 0.25 mm were bulged by using two different bulged diameters of 20 and 50 mm. As the result when

using a diameter of 20 mm the value for M was recorded as 80, while using 50 mm the value for M was equal to 200. It has been observed that there was a decrease in the material flow stress when a smaller bulge diameter was used. This indicated the effect of the featured size on the response of the material. However, there was no discussion provided regarding the effect of feature size [27].

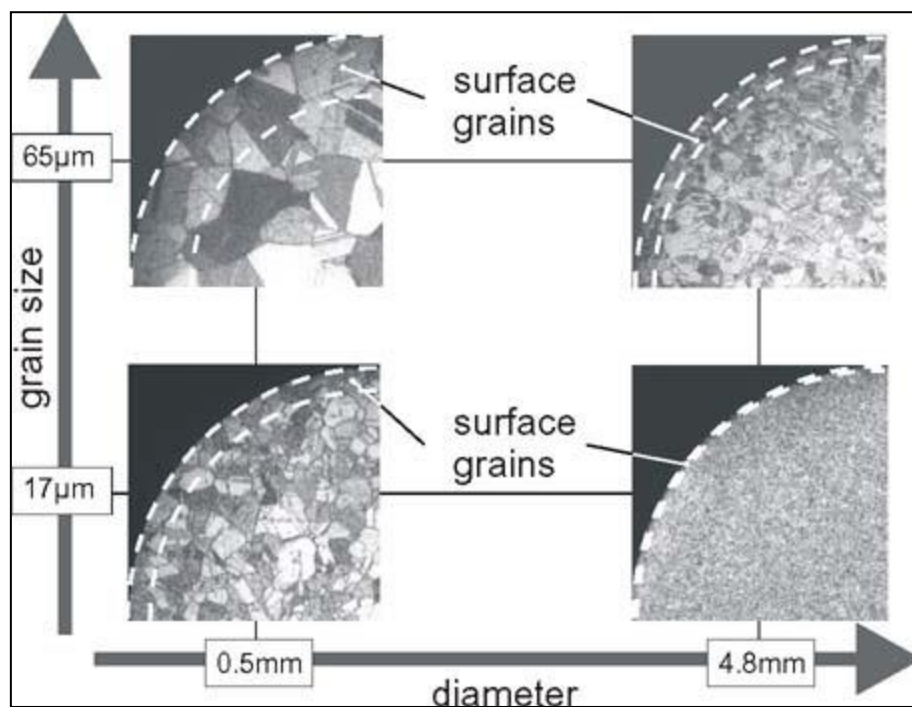


FIGURE 2-8: SURFACE LAYER MODEL IN BULK METAL [43, 46]

Figure 2-8 shows the explanation of variations in the material flow curve due to the size effects can be described by using a surface layer model. The dislocation movements in the grains located at the surface are less restricted than grains inside the material. Therefore, these surface grains show less hardening [30, 43, 46, 51]. The diameter of the components has been decreased, but the grain size is still the same, the surface grain's area becomes larger as shown in Figure 2-8. Therefore, the movements of grains located at the surface are more active compared to the inside of the material and show less hardening. Therefore, the flow stress is going to be decreased. Meanwhile, when the grain size is reduced and the diameter of the components remains the same, the surface grains area becomes smaller. As a result, the

movements of grains that located at the surface are limited compared to the inside of the material and show more hardening. Therefore, the flow stress will be increased [3, 43, 46, 51].

According to Li, Jin, et al. [52] it is challenging to get or maintaining a small grain size during the processing or sintering ceramics materials.. To produce or form advanced ceramic materials with low porosity and small grains, various techniques have been extensively investigated. One of these techniques is the conventional sintering technique and it requires high temperatures and long sintering times and thus often leads to substantial grain coarsening.

2.2 CONVENTIONAL SINTERING AND ELECTRICAL-FIELD ACTIVATED SINTERING

2.2.1 OVERVIEW

Sintering is a process that is used to bond contacting particles to produce solid components and densified materials from powder by using pressure and/or thermal energy without reaching the melting point. The material atoms diffuse across the boundaries of the particles, fusing the particles together and creating one solid piece. The bonding leads to improved strength and lowers the energy system. The process of sintering leads to elevated mechanical, thermal, and electrical properties. Sintering is one of the oldest human technologies and has been studied significantly since the 1940's and has been developed remarkably since then. One of the most beneficial and important uses of the sintering is the fabrication of sintered parts, including powder-metallurgical and bulk ceramics parts [53-55]. In general, sintering aims to produce sintered parts or components with reproducible microstructures. That happens through the control of sintering variables, which means microstructure control or grain size control, sintered density and size and other phases distribution including pores. The final purpose of the control of the microstructure is to prepare a fully dense form with good grain structure [53-55]. According to Lakshmanan [56], the result of a sintering process is affected by several points which can be divided into two basic categories. The first one called the "process variables" and that contains all parameters that could be affected by the change of sintering process (sintering temperature and holding time, sintering pressure, furnace atmosphere etc.). The other category is known as "material variables" (geometrical structure of particles, their size and size distribution) [57]. The sintering processes can be affected by the particles structure and particles size

distribution. It has been established that particle size affects the sintering kinetics, especially at the neck forming areas among the grains [58, 59]

In the sintering process, many mathematical models usually assume that the particles are spherical or based on the joining of two spherical particles [60-62]. However, the powder particles in industrial use have many shapes as seen in Figure 2-9. Most shapes used comes in the form of angular, spongy and flaky particles depending on the types of the materials and properties. The process of spherical or rounded particle production is mostly used for creating material particles. A pulsated orifice ejection method has been developed for mass-production of monosized micro particles [62, 63].

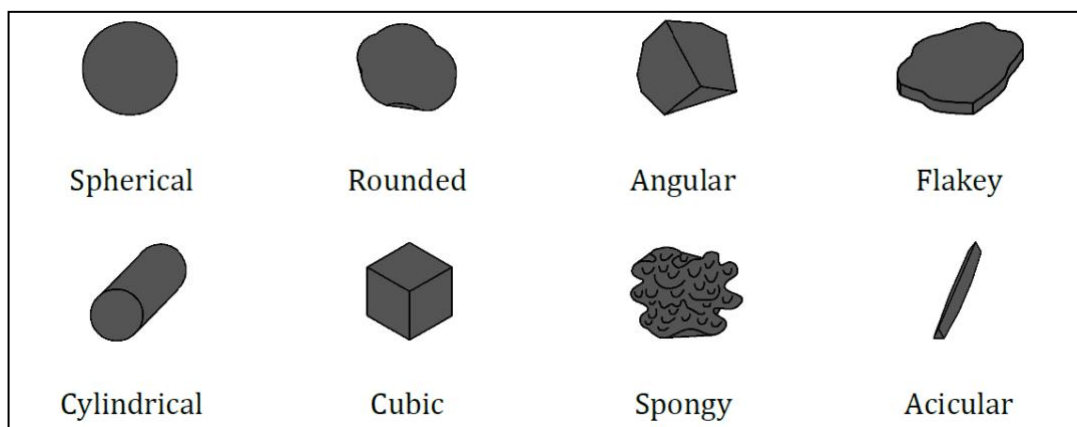


FIGURE 2-9: POWDER PARTICLE SHAPES [62]

The sintering process can be divided into four stages (loose powder and three subsequently sintering stages), as illustrated in Figure 2-10, based on the geometrical transformations the grains undergo during the densification process. The densification process using the conventional sintering process involves a coarsening or neck growth that is a critical mechanism needed to achieve densification caused by surface diffusion or evaporation/condensation as shown in Figure 2-10. Therefore, the conventional powder sintering takes a long time to be finished [3, 53, 54].

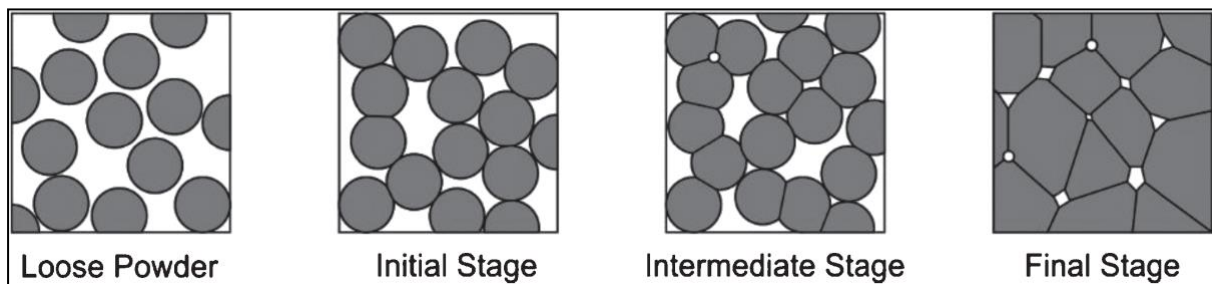


FIGURE 2-10: SINTERING STAGES [54, 64]

The initial stage is considered as the growth of the sintered bond from the initial single point contact. In the intermediate stage, the pores start to decrease and the major densification of the compact takes place. Moreover, this stage is also characterised by pore rounding and an increase in grain size. The final stage of sintering is categorised by the closing of pores, pore isolation, and pore migration [54, 64].

However, the three sintering stages after the loose powder can be explained as illustrated in Figure 2-11, which is preheat or burn off stage, high-temperature and cooling period. The first stage is to combust any air and remove lubricants. Then, during the high-temperature period, solid-state diffusion and bonding between powder particles from mechanical to materials bonding occurs. Finally, during the last period, controlled cooling atmosphere happens to prevent oxidation and possible thermal shock. Additionally, processing of the sintered component is needed such as hot isostatic pressing, forging, heat treatment, impregnation, coating, plating and de-burring to ensure the high quality of the final product [3].

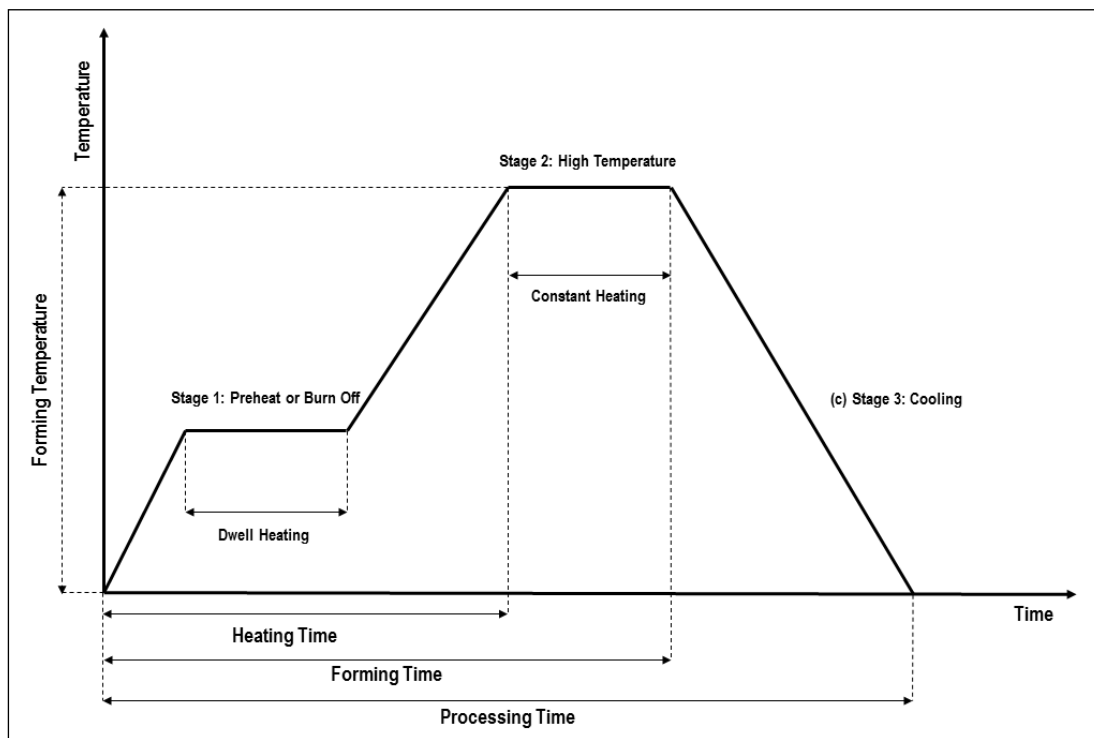


FIGURE 2-11: SEQUENCE OF THE SINTERING PROCESS CONSIST OF PREHEAT OR BURN OFF, HIGH-TEMPERATURE AND COOLING STAGE [3]

According to German [54], The sintering processes can be classified into pressure-less and pressure assisted sintering as seen in Figure 2-12. Solid state sintering and liquid phase sintering are the most commonly used techniques in pressure-less sintering. The pressure assisted sintering techniques can be categorised into low stress and high stress processes based on the magnitude of the pressure applied during the process.

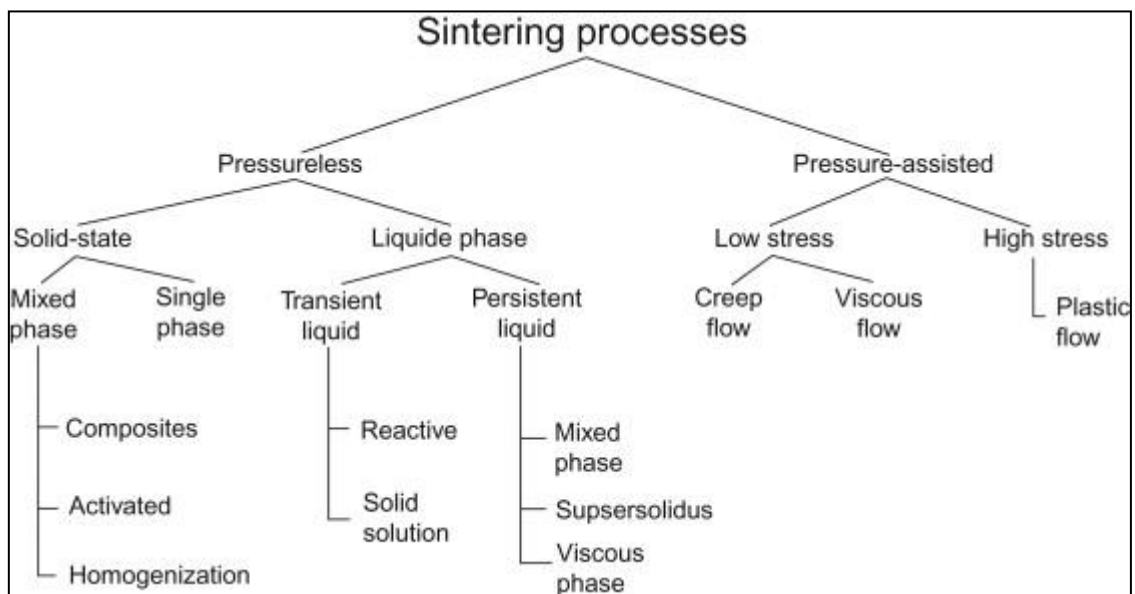


FIGURE 2-12: CLASSIFICATION OF SINTERING PROCESSES

However, Cinert [62] uses the same classification for the sintering processes which is pressureless and pressure assisted sintering, but he claims that the two categories can be divided according to the sintering temperature as shown in Figure 2-13.

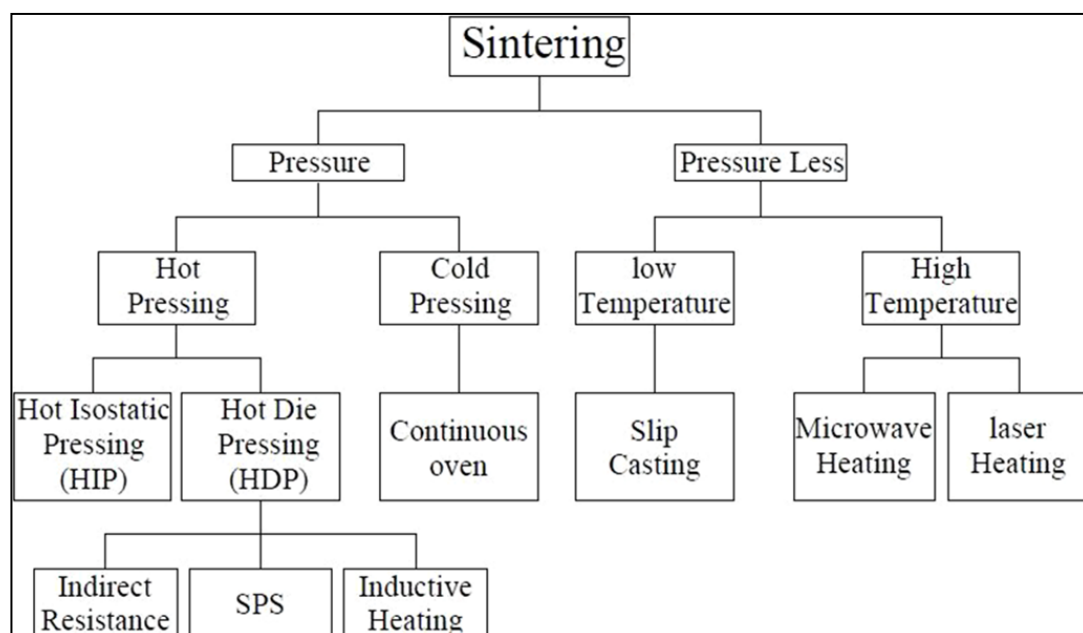


FIGURE 2-13: CALSSIFICATION OF SINTERING PROCESS ACCORDING TO SINTERING TEMPERATURE [62, 65]

According to Cinert [62] in pressure-less-sintering the compacting process is done without pressure (except gravity). High component density can be obtained by using a fine-grained starting powder ($<3\mu\text{m}$) and different additives. Two basic processes have been developed up to recent time. The main difference is whether the final product needs to be burned by high temperature. In pressure-assisted sintering, compact ceramic or metal parts are mostly done from nano or micro powder pressed and heated by a pressure-assisted process. The powder material is filled into the die and pressured between two or more punches. The high sintering temperature and relatively long sintering time often results in extreme grain growth. Two main types of pressure-assisted sintering methods are shown in Figure 2-14. There are many heating techniques according to German [54], such as Induction heating, Microwave Heating, Plasma Heating, Electrical Discharge Heating, ..etc.

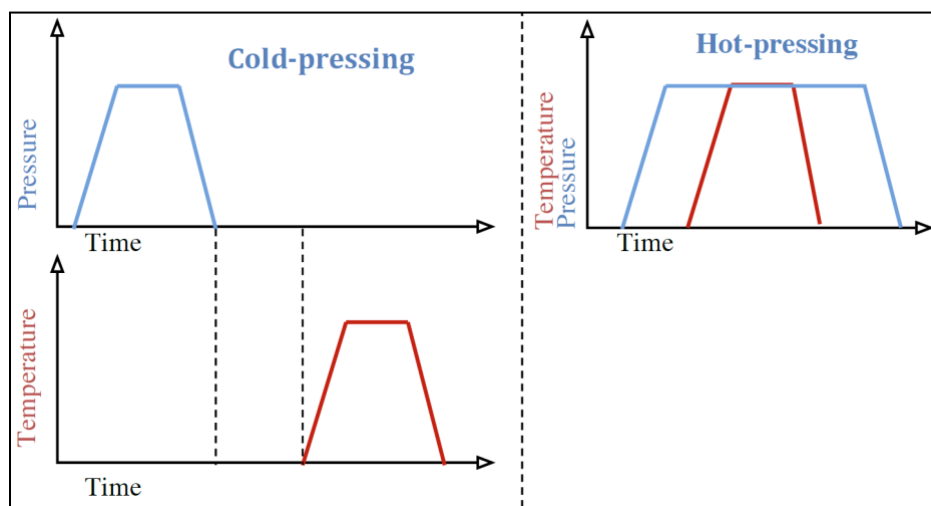


FIGURE 2-14: CONSOLIDATION METHODS [62]

2.2.2 DENSIFICATION

Heat transfer and mass transport are essential in the sintering process, contributing to densification and thermodynamics, respectively. In crystalline ceramics, mass transport happens mainly from regions of higher chemical potential to that of lower

potential by diffusion of atoms, ions, molecules, or other species via different mechanisms. Mainly, there are six mechanisms that could lead to the bonding and growth of necks between particles; these are: grain boundary diffusion, lattice diffusion from the grain boundary to the pore, plastic flow, surface diffusion, lattice diffusion from the particle surfaces to the neck, and vapour transport as seen in Figure 2-15 . The first three are recognised as densifying mechanisms which directly contribute to shrinkage. The second three mechanisms cause only neck growth without densification and are referred to as non-densifying mechanisms. For polycrystalline ceramics, grain boundary diffusion and lattice diffusion from the grain boundary to the pore are very critical [54, 55, 66, 67].

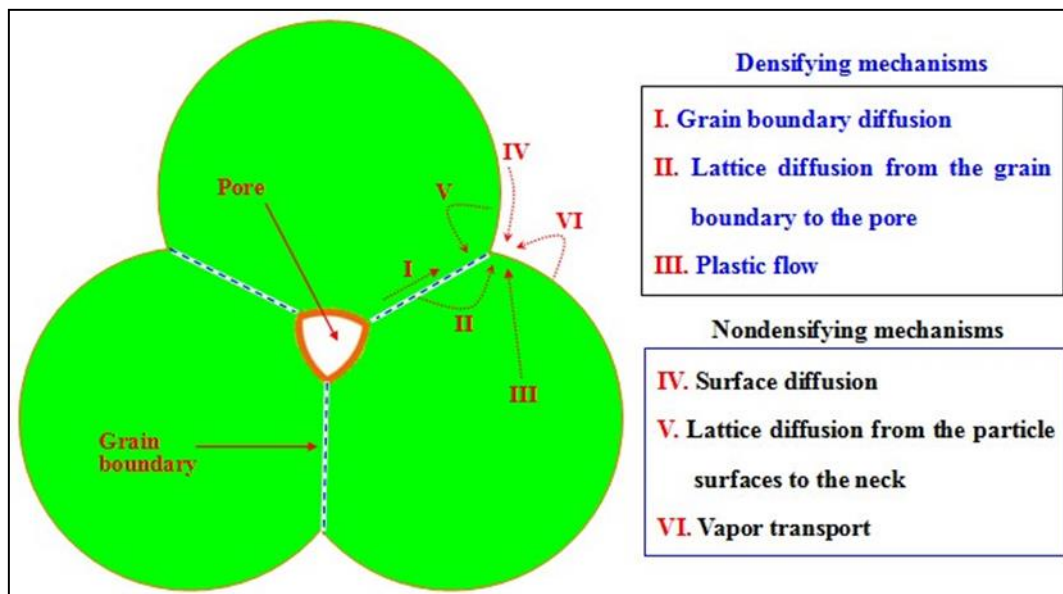


FIGURE 2-15: THE SIX DIFFERENT MECHANISMS THAT COULD ACT DURING SINTERING OF SOLID GRAINS [67]

2.2.3 HEAT TRANSFER

Heat transfer plays a significant role during a sintering process. An adequate sintering requires a perfect heat transfer that enables a rise in temperature of the precursor material high enough for the densification process to occur [67-69] . The three

types of heat transfer are conduction; convection and thermal radiation (see Figure 2-16). Conduction heat transfer relies on direct thermal contact within solid objects. Heat conduction basically occurs via rapidly moving or vibrating atoms and molecules interacting with their neighbours with an energy transfer. Moreover, convection heat transfer occurs through the motion of a hot fluid (liquid or gas) which acts as a carrier. Thermal radiation can take place between two distant bodies without the need of any medium. In conduction and convection cases, the energy transfer between two objects depends approximately on the temperature difference between them [68-70]. Thermal radiation transfer relies on the difference between the fourth power of their absolute temperatures, according to the well-known Stefan-Boltzmann's law. Consequently, the importance of radiation transfer is significantly enhanced at high temperatures [69-71].

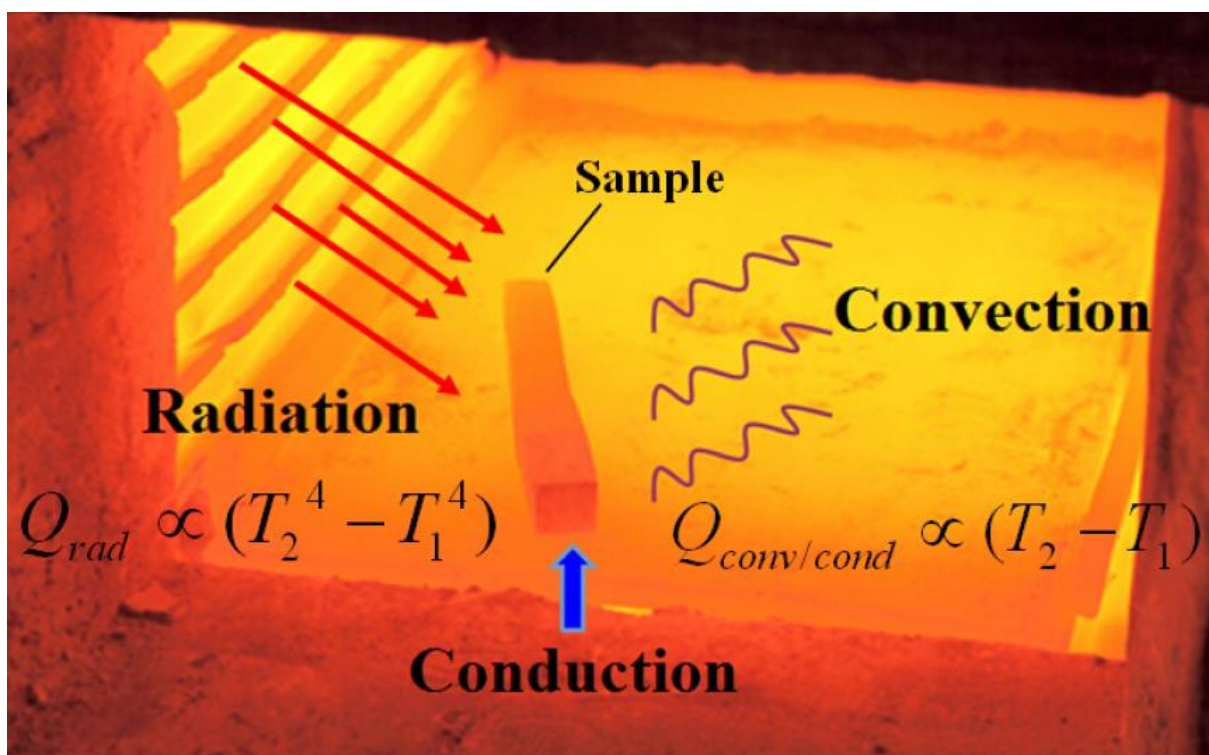


FIGURE 2-16: HEAT TRANSFER IN A CONVENTIONAL CONVECTION FURNACE ILLUSTRATING THE THREE ACTIVE MECHANISMS [68, 69]

2.2.4 GRAIN GROWTH

Grain growth, or coarsening, takes place when the atoms diffuse from the convex grains to the concave grains so that the grain boundaries move to the centre of curvature [54, 66]. Grain growth decreases the driving force of sintering and increases the mass diffusion path, and that leads to the reducing of the densification rate. A direct observation is the increase in the average grain size, which is generally divided into two types: (i) normal grain growth and (ii) abnormal grain growth [54, 66].

In the normal grain growth, the average grain size increases with the time, but the distribution of grain size remains similar (invariant by time) [66]. For a typical single-phase polycrystalline model, the grain growth can be described by a kinetic equation:

$$\bar{G}_t^2 - \bar{G}_{t_0}^2 = Kt \quad (2.2-1)$$

$$K = \frac{4D_b^\perp \gamma_b V_m}{\beta RT \omega} \quad (2.2-2)$$

Where, D_b^\perp , γ_b , V_m , β , R , ω are atom diffusion coefficient across the grain boundary, grain boundary energy, molar volume, a constant including the proportionality constant, ideal gas constant, and grain boundary thickness, respectively [54, 55, 66].

On the other hand, abnormal grain growth is a coarsening process during which a few large grains grow quickly at the expense of the fine grains having a very slow growth rate. This leads to a bimodal grain size distribution [54, 55, 66]. The corresponding kinetic equation is described as:

$$\bar{G}_{a,t}^2 - \bar{G}_{a,t_0}^2 = Kt \quad (2.2-3)$$

$$K = \frac{2D_b^+ \gamma_b V_m}{\beta RT \bar{G}_m \omega} \quad (2.2-4)$$

Where \bar{G}_m is the average size of the matrix (fine) grains.

In practice, abnormal grain growth can be classified into three types [1-3]: (i) materials containing second-phase precipitates or impurities of high concentrations; (ii) materials with a high anisotropy in interfacial energy, (*e.g.* solid/liquid interfacial energy, grain boundary energy in the bulk or surface energy in thin films); and (iii) materials in high chemical non-equilibrium. Therefore, abnormal grain growth is a result of very high local rates of interfacial migration.

2.2.5 ELECTRICAL-FIELD ACTIVATED SINTERING

The Electric Current Assisted Sintering (ECAS) or Field Assisted Sintering Technique (FAST) is one of the promising technologies that have been used widely recently. The FAST technology is a general term for a class of consolidation methods which combine external electric field/currents with mechanical pressure for powder sintering. Currently this is divided mainly into two categories: Resistance Sintering (RS) and Electric Discharge Sintering (EDS). The first category is a low-voltage and a high current with a characteristic waveform, such as (direct current (DC), alternate current (AC), rectified current (RC), pulsed, etc.). The other category depends on the sudden electrical energy that discharged from a capacitor bank through a column of the powder of the workpiece contained within an electrically non-conducting tube. ECAS/FAST was rarely achieved until 1990 when significant research interests and industrial applications were identified from many countries, especially Japan, China and USA. Many papers have been published and efforts have been made on tools and machines development for industrial-scale production for this technology. Several technologies, such as, Pulsed Electric Current Sintering (PECS), and Spark Plasma Sintering (SPS) and Plasma Assisted Sintering (PAS) have been developed, introduced and registered as patents. The SPS is being one of the most recognised and widely used technology for sintering many types of materials [19, 72-76].

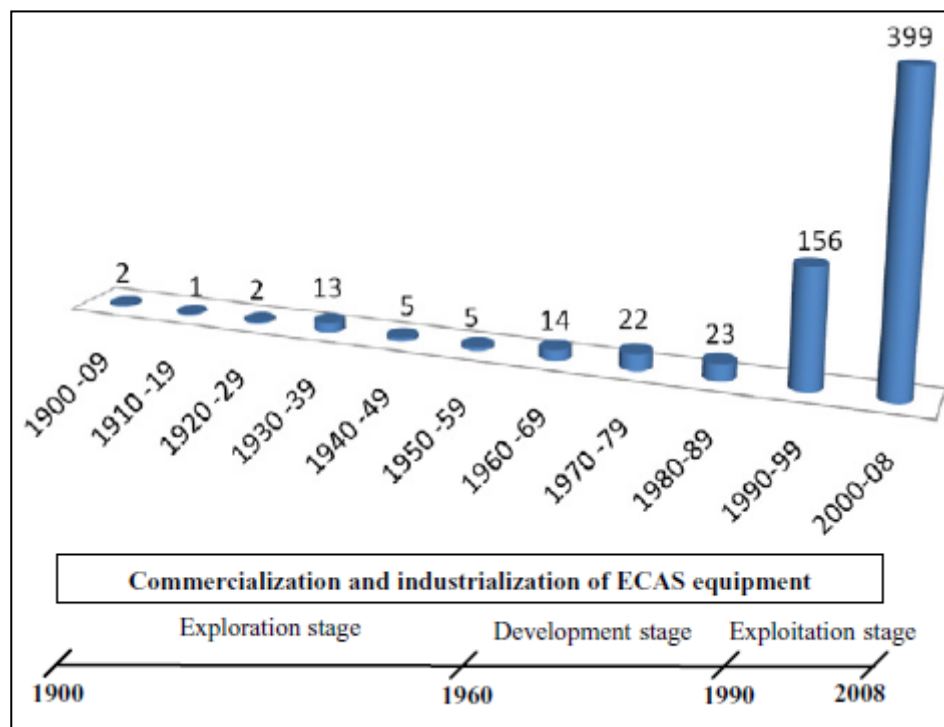


FIGURE 2-17: NUMBER OF ECAS PATENTS PER DECADE FROM 1900 TO THE FIRST SEMESTER OF 2008. THE EXPLORATION (1900–1960), DEVELOPMENT (1960–1990) AND EXPLOITATION (1990–2008) STAGES ARE DEFINED IN ACCORDANCE WITH THE WORLDWIDE INDUSTRIALIZATION AND COMMERCIALIZATION OF ECAS [76]

Figure 2-17 shows the number of published ECAS patents per decade from 1900 to the first semester of 2008. Most of them were taken from the worldwide patent office. Only a few countries as mentioned before (especially China, Japan and United States) have actively contributed to ECAS technology development. The rapid growth in the number of patents in the last two decades resulted from the worldwide spread of the technology in the industrial sector and the scientific community [76].

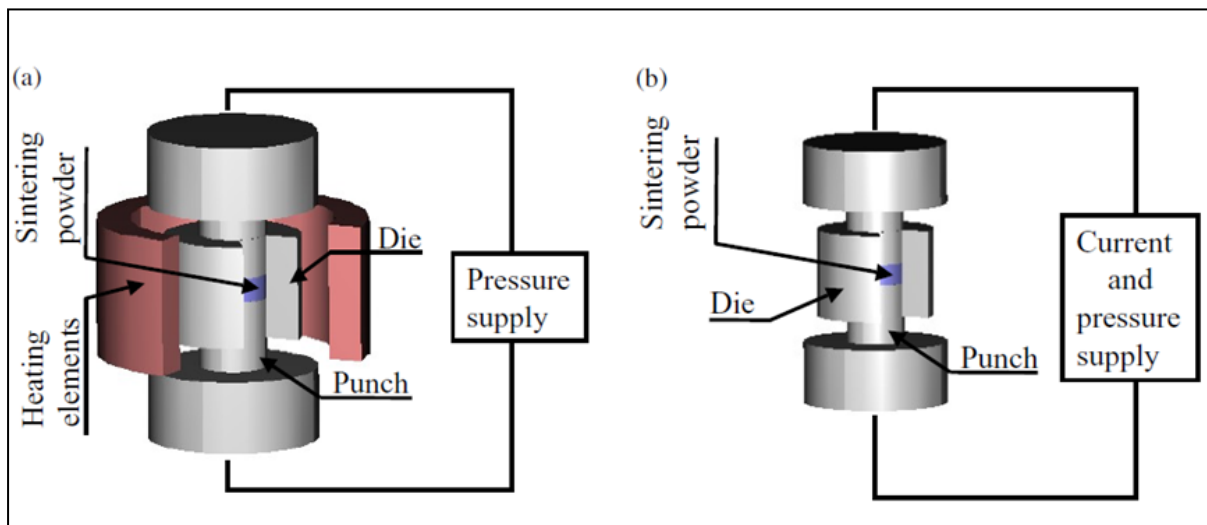


FIGURE 2-18: SCHEMATIC OF SINTERING PROCESS: (1) HOT PRESSING AND (2) FAST/ECAS [76]

Compared with other sintering processes, such as pressure sintering or hot pressing, the FAST process has many advantages. The *FAST/ECAS* has faster heating rate, lower sintering temperature, shorter holding time, the consolidation of difficult-to-sinter-powders, the elimination of the need of sintering aids, no need of cold compaction, less sensitivity to the characteristics of the initial powders, and marked comparative improvements in the properties of the consolidated materials [74-76]

Figure 2-18 shows the difference in the heating mode between the ECAS and Hot Pressing. In Hot Pressing an array of heating elements indirectly heats the punch/powder/die assembly by radiation (convection /conduction). The powder heating rate is controlled by the rate of radiation (convection /conduction). On the other hand, in *ECAS* the punches transfer the electricity and Joule heat directly to the powder. As the supplied current density can be very large, the heating rate in the powder can approach 10^6 Ks^{-1} . This heating rate is much higher than $80^\circ\text{C min}^{-1}$ for the HP process. Therefore, the *ECAS* sintering time can be lowered and the production rate increased [76]

According to Lange [19], the densification process using the conventional powder-sintering method involves a coarsening or neck growth, which is a critical mechanism needed in order to achieve densification. This is caused by surface diffusion or evaporation/condensation and that is the reason why conventional powder sintering is taking a long time to be completed [72, 73].

2.2.5.1 MECHANICAL AND THERMAL EFFECTS

Sintered powders are heated by floating current and higher densification is also achieved by uniaxial applied pressure simultaneously to the heating. The applied pressure enhances densification and reduces grain growth. The pressure has a direct mechanical effect on particle rearrangement and destruction of agglomerates. The compressive stress from the applied pressure results in more contact between the powder particles. This causes an enhancement of free sintering densification mechanisms such as grain boundary diffusion and lattice diffusion, while potentially triggering other densification mechanisms such as grain boundary sliding or plastic deformation. Moreover, the pressure is a driving force for sintering which might lead to a decrease in sintering temperature and a limitation of grain growth. Validation of the effect of applied pressure was provided in many of the recent filed sintering processes investigations [62, 66, 77, 78]. According to Cinert [62] the density increased with the pressure and a 100 % density was achieved for 255 MPa and 363 MPa for sintering TaC. The reason for observed densities higher than true density is the reaction between B₄C and TaC leading to formation of new products with higher density than TaC. Samples sintered at 255 MPa and 363 MPa were without any porosity. In general, it was found that higher pressurising conditions can decrease the sintering temperatures [62].

The thermal effects from the high heating rates are similar to the effects from the applied pressure. High heating rates could enhance and improve densification while reducing grain growth. However, this could occur only if the activation energy for the coarsening mechanism is less than the activation energy for the densification mechanism. If these conditions are met, high heating rates will increase the rate of densification and limit the rate of coarsening leading to enhanced densification with reduced grain growth [62, 66, 77, 78] .

However, Cinert [62] claims that some research showed that it is not necessary that high heating rates could enhance the densification. Some of these experiments showed some conflicts and the heating rate could have some influence on some materials and not on others.

High heating rate is one of the dominant parameters of electrical filed sintering which make it different from other conventional sintering techniques. Three different mechanisms, surface

diffusion, grain boundary diffusion and power-law creep, heating rate influence the grain boundary diffusion which increases the ability of the sintering. One of the biggest differences between conventional hot pressing and SPS method is a very rapid heating rate of 1000 °C/min that can be achieved by using the SPS method [79, 80].

2.2.5.2 ELECTRO-PLASTICITY AND ELECTRICAL EFFECTS

Plasticity is the deformation the materials undergoing non-reversible changes of shape in response to applied forces [81]. In the electrical current sintering, the powder is heated by Joule heating from the applied current, which means high heating rates are a result of the applied electric field. Therefore, the thermal and electrical effects are very difficult to separate. However, the majority of the literature claims that an electric field enhances densification while limiting grain growth, similar to the effects from the high heating rates and the applied pressure [80, 82]. However, the electro-plasticity can be referred as a phenomenon that involves using high electric current density pulses through the part during the forming process. By applying the current or the electrical field to the materials (metals, ceramics, superconductors and powder materials) has shown significant improvements in the material plasticity [83-86]. Many researchers claim that the electro-plasticity can improve the surface quality and reduce the defects on the formed components and eliminate the annealing and the acid-pickling processing in the traditional processing methods [84, 87]. The hot forming process is a traditional method that has been used to decrease the flow stress. However, there are limitations of hot forming in micro-scale processes. The hot forming process has a complex and bigger apparatus as an overall machine due to the heating needed. As a result, it has low efficiency and high energy consumption. Moreover, using the hot forming process at high temperature could cause oxidation and poor surface quality of the workpiece. Furthermore, it takes some time to soften the workpiece. Therefore, the electro-plasticity is more appropriate for selection because it provides more reduction in the flow stress and the electro-plasticity effect happens immediately when the current flows through the part [3, 86, 88, 89].

In ceramic materials, plasticity remains largely absent. It has been shown that fractures can be suppressed to some extent some ceramics at low temperatures, such as ZrO₂ and yttria-stabilized zirconia (YSZ) [52]. Ceramic materials have been widely used in many applications.

However, most ceramics have rather limited plasticity at low temperatures and fracture well before the onset of plastic yielding [52]. In ceramic materials, the electro-plasticity enhances glide mobility of dislocations in halide single crystals at room temperature resulting from an enhancement of cross slip by the field [86, 90, 91]. The electro-plasticity process is efficient for materials with more dislocation barriers during the plastic deformation. The dislocations are created due to applied stress and interaction with the impurity particles. During deformation, dislocations move through the lattice structure until their motion is stalled by the grain boundaries or the impurity [3, 91, 92]. When applying cold work to the materials in the compacting process, the dislocation density increases and as a result enhances the strength of the material. Therefore, when the electrical current is used, it will lead to a higher dislocation, and this gives the most significant decrease in flow stress. This is due to the increase in current that increases energy in the lattice. As a result, the metal atoms increase their vibration that acts as a force on the dislocation and accelerates the movement. Hence, the friction resistance can be reduced in the deforming and the plasticity of the metal can be improved to make the forming process easier.[3, 86, 93-95].

According to Li, Jin, et al. [52] applying an electric field, or “flash,” significantly accelerates the sintering process that forms zirconia and other ceramics, and at much lower furnace temperatures than conventional sintering and improves the deformation of the ceramics to be similar to metals. Flash-sintered ceramics also have little porosity, which makes them denser and therefore easier to deform. Improved plasticity means more stability during process at relatively low temperatures. The sample could survive almost as much compression strain as some metals do before cracks started to appear.

2.2.5.3 TEMPERATURE EFFECT

Temperature plays an important role in powder densification. The mass transfer is required and is consequently estimated by temperature dependant. In the electrical field sintering, the

heat comes from the current in the form of Joule heat. The Joule heating is a form of resistive heating; it is the process by which the passage of an electric current through a conductor releases heat [62, 80, 96]. The amount of heat Q is given by Equation (2.2-1)

$$Q = I^2 R t \quad (2.2-5)$$

Where:

Q is Heat generated by current passing through the compact.

I is Current.

R is Resistance of the particle or contact resistance.

t is Time.

The resistance between two particles depends on their geometry. The resistance is indirectly related to the contact area size of two particles and to the cross-section of particles. If the contact size of both particles is smaller than the cross-section, more heat is generated on the border of the particles. It might be one mechanism of neck growing in an early sintering step [62, 80, 96].

2.2.6 APPLICATION OF ELECTRICAL-FIELD ACTIVATED SINTERING

The application of electrical-field activated sintering technology shows a significant potential to produce the micro-component by using powder as a raw material. However, there are still major challenges to the manufacture of micro-scale components associated with long processing times to achieve high densification of micro-parts. In this review, it has focused more on Zirconia and Alumina samples that have been conducted by the previous of electrical-field activated sintering processes. Based on the review that has been made below, experiments on electrical-field activated sintering on piezoceramic, zirconia and alumina show there are

still significant challenges to manufacture miniature and micro-components to in short production times with higher densification of formed samples.

2.2.6.1 ZIRCONIA

Zirconia (ZrO_2) is one of the most favourable materials for a new generation of ceramics due to excellent mechanical properties. When compared to other ceramic materials, zirconia has unique strength at room temperature. Moreover, Zirconia has high fracture toughness, high density, high hardness and wear resistance, good frictional behaviour, high-temperature capability, non-magnetic, low thermal conductivity, electrical insulation, a coefficient of thermal expansion similar to iron, and modulus of elasticity similar to steel. Zirconia is being used widely in the production of many products, such as such as structural ceramics, dentistry, wear parts, ceramic bearings, etc.... [75]

According to the literature [97], several sintering conditions of SPS were investigated to obtain high-density yttria-stabilized-zirconia (YSZ). Specifically, nano-sized YSZ raw powder (50 nm) was densified to a relative density of 99.1% at 1400 °C, with an applied pressure of 23 MPa, and a total of four consecutive sintering cycles at 30 min per cycle. Moreover, for conventional sintering, the green pellets were formed at 50 MPa and heated up at 1450 °C in an electrical resistance furnace for 2 h. The relative density of the workpiece was 97%.

Furthermore, SPS (2080, SPS Syntex Inc., Japan) was recently used to consolidate commercially available granulated ZrO_2 at temperatures in the range 950–1200 °C and the heating rate was 50 °C/min with sintering time of 180 min average, under a pressure of 100 MPa. Porous materials, exhibiting open porosity, average grain size of 80 nm and with a relative density in the range 61–90% were achieved at temperature below 1050 °C. However, dense materials characterized by closed porosity, average grain size of 80 nm and high relative density (90–98%) were gained when sintering at 1125–1200 °C or when the temperature was set to 1050 °C with a holding time of 60 min. Finally, fully dense samples with submicron grain sizes (160 nm) were fabricated at a temperature of 1200 °C and a holding time of 3 hours [98].

SPS (Dr. Sinter 1020 Sumitomo Coal Mining Co.) used in sintering ZrO_2 –3 mol% Y_2O_3 (ZrO_2 –3Y) nano-powders synthesised by a co-precipitation approach at 1050–1500 °C and a heating rate of 600 °C/min, under a applied pressure of 40 MPa for holding time of 1–10 min.

High relative density exceeding 98% was achieved when sintering at 1300 °C for 3 min, while the full density was achieved at 1400 °C. It was also found that a higher density (99%) was generally achieved by SPS at lower temperature (1180 °C) and in a shorter time (9 min dwelling time) as compared to hot pressing (96% relative density, $T = 1250$ °C, 30 min dwelling time) under similar pressure levels [99].

Additionally, a high relative density and a high Vickers hardness were obtained for magnesia stabilised zirconia sintered at 1100 °C for more than 5 min under 40 MPa of pressure. The formed samples exhibited a final density of 99.8% of the theoretical value with the microstructure showing an average grain size of 100 nm by using SPS. No surface cracks were observed and the nano-crystalline structure was retained [100].

However, adding binders to the ceramic or other materials will improve the forming and sintering process, but it will increase the time of the total process because it will need more steps to any process [101, 102]. According to Wang, J., Li, S.H.P. and Stevens [103], adding binders for sintering zirconia has improved the density and the quality of the formed samples. However, in this process, a higher calcination temperature and a longer calcination dwell time may be required to eliminate the organic residuals in the isostatically pressed ceramic powder compacts than in the conventional die-pressed samples. Wang, J., Li, S.H.P. and Stevens [103] have sintered the zirconia with binders under several pressures from 80 MPa to 300 MPa and the total time was 2 hours at 1500 °C.

2.2.6.2 ALUMINA

Alumina (Aluminium Oxide), Al_2O_3 is a major engineering material. It offers good mechanical properties and electrical properties which leads to a wide range of industrial applications

According to Gao, L., et al [104] Al_2O_3 ceramics were densified quickly by using SPS (Dr. Sinter 1020, Sumitomo Coal Mining Co.) at temperatures ranging between 1350 and 1700 °C (600 °C/min heating rate) at 40 MPa pressure, without selecting an exact holding time.

Moreover, Alumina powders with four different particle sizes were densified by SPS (1050 Sumitomo Coal Mining) at 1550 °C, with the heating rate changing from 20 to 300 °C/min for 30

min and at pressures of 20 to 40 MPa. It was found that particle size of the starting powders played an important role in the SPS process, since relative density increased with reducing particle size under unchanged sintering conditions. The relative density was also found to increase with increasing holding time. In general, when sintering at 1550 °C (200 °C/min heating rate) under an applied pressure of 30 MPa, without holding time, relative density increased from 92 to 99% of the theoretical value. Additionally, relative density of the samples increased from 92 to 98.7 and 99.4% as the holding time was increased from 0 to 10 and 30 min. After observing the microstructure, it has been found that the edge is more dense than the inside of the samples sintered at 1550 °C for a shorter holding time (10 min) [105].

In order to investigate the effect of sintering parameters (temperature, pressure and heating rate) on the properties of porous Al₂O₃, several PECS (Pulse Electric Current Sintering) experiments were conducted starting from a mixture of submicron Al₂O₃ (0.23 μm) and 10 wt.% carbon black (20 nm), under several sintering conditions. The vacuum sintered compacts were then post-heat treated in air at different temperatures between 800 and 1300 °C, for more than 10 hours.

At temperature 1400 °C, soaking time 5 min, pressure 5.5 MPa and heating rate 100 °C/min, it was observed that the relative density was 75%. The same parameters used again with an increase in the temperature to 1500 °C but the density remained the same. However, the relative density improved to 83% with a soaking time of 5 min, pressure 15 MPa and heating rate 100 °C/min. The relative density also increased from 83% to 86% of the theoretical value with the pressure and heating rate varying from 5 to 15 MPa and from 100 to 200 °C/min. It was observed that when the applied pressure was as low as 5.5 MPa, an increase in temperature from 1400 to 1500 °C did not enhance the densification of Al₂O₃-C ceramics, and their relative density (75% of the theoretical density) remained the same. In addition, an increase in either pressure and/or heating rate, did not affect significantly the densification and the relative density of the Al₂O₃-C ceramics which changed from 83% to 86% of the theoretical value with pressure and heating rate varying from 5 to 15 MPa and from 100 to 200 °C/min [106]

A systematic study of various SPS parameters (temperature, holding time, heating rate, pressure, and pulse sequence) was also carried out to investigate their effect on the densification, grain growth kinetics, hardness and fracture toughness of a commercially available sub

micrometer sized ($0.4 \mu\text{m}$) alumina powder. It has been found that the SPS enhances the densification and grain growth. Fully dense samples with a density of 99.3% were obtained by SPS (2050 Sumitomo Coal Mining Co.) at $1250 \text{ }^\circ\text{C}$ (heating rate $150\text{--}200 \text{ }^\circ\text{C}/\text{min}$), with a holding time of 30 min, under a pressure of 50 MPa. For a sintering temperature lower than $1250 \text{ }^\circ\text{C}$ a limited grain growth occurred ($0.8\text{--}1 \mu\text{m}$), while at higher temperature grain size significantly increased from 1 to $27.5 \mu\text{m}$ [107].

Furthermore, PECS apparatus (SPS-1050 Sumitomo Coal Mining Co.) was used to densify two kinds of Al_2O_3 powders with average particles size of 0.15 and $0.7 \mu\text{m}$. Consolidation was conducted at 1200 and $1400 \text{ }^\circ\text{C}$, under a 40 MPa pressure, with a heating rate of 50 or $300 \text{ }^\circ\text{C}/\text{min}$, without holding time. It was found that, when $0.15 \mu\text{m}$ powders were sintered at $1200 \text{ }^\circ\text{C}$ with $50 \text{ }^\circ\text{C}/\text{min}$ heating rate, the density was 98.7% and grain sizes were found to be four times larger than that of the starting powders. At faster heating rate, ($300 \text{ }^\circ\text{C}/\text{min}$) a lower density is achieved (96.3%) and grain size were smaller. In contrast, for the powders ($0.7 \mu\text{m}$), increasing the temperature to $1200 \text{ }^\circ\text{C}$ resulted in a density lower than 75% and almost no grain growth ($0.74\text{--}0.72 \mu\text{m}$). The fast heated specimens exhibited density of 74.4% which is higher than the slow heated ones (72.8%). When sintering was performed at $1400 \text{ }^\circ\text{C}$ fine Al_2O_3 powders led to fully dense compacts (99.4 and 99.3%, respectively) for both slow and fast heating processes [108].

2.2.6.3 PIEZOCERAMIC (PZT)

Piezoceramic, or lead zirconate titanate, is one of the most widely used piezoelectric ceramic materials around the world. In general, piezoceramic materials, and piezoelectric materials show a unique range of properties. Basically, if a piezoelectric material is deformed, an electric charge is generated in what is known as the piezoelectric effect. Moreover, the opposite happens, if an electric field is applied to a piezoelectric material, deformation occurs and that is known as the inverse piezoelectric effect. Recently, there are various properties that encourage the use of piezoelectric materials for certain applications. The material constants most commonly referred to are electromechanical coupling factor, mechanical quality factor,

and piezoelectric charge/voltage coefficient. The application of piezoelectric materials is usually categorised into four fields, actuators, transducers, sensors, and generators [109-111].

According to Chinen, Fausto Kenzo, et al. [111], SPS consolidation was conducted using a SPS-1050 system, (SPS Syntex Inc). The heating rate for the experiment was 100 °C/min under pressure of 50MPa and they examined that in several holding times. The results showed a 97.35% relative density of the theoretical value for up to 40 min holding times and 98.98% has been achieved for 20 min holding time.

Furthermore, Orru, Roberto, et al. [18] claims that piezoceramic was fabricated at different temperatures ranging from 900 to 1050 °C and pressure levels between 50 and 100 MPa. A relative density of 98% was achieved when the sintering temperature was 950 °C.

Moreover, Su, Xinghua, et al. [112] used the Flash Sintering method to fabricate the piezoceramic, the furnace temperature was raised up to a maximum of 1200 °C at a heating rate of 10 °C/min. The holding time was 30 min and they achieved relative densities from 83.7% to 94.3%.

2.3 SUMMARY OF THE CHAPTER

Based on the previous studies in this chapter, it has been conclusively shown that there are needs to produce micro- components using fast cycle time and high quality taking into consideration the reduction of the cost. The micro-manufacturing showed how it is important in recent days and it has received significant attention regarding its processes. The micro manufacturing processes can be classified according to the energy type that has been used in the process, such as mechanical, chemical, electrochemical, electrical and laser processes. The working principles behind each process include consideration of mechanical forces, thermal effects, ablation, dissolution, solidification, re-composition, polymerisation/lamination, and sintering.

Regarding the challenges of micro manufacturing, high volume and low-cost production are not only essential, but the challenges with the design of micro-products need to be taken

into full consideration. The limitation on the shape and the capability of the materials in producing micro-products are important issues that need to be faced. The micro-forming process has many advantages and this drives the micro-component manufacturers to attempt to produce parts and components with complex geometries and features that are suitable for replacing many of the costly conventional micro-manufacturing processes. However, it is not easy to achieve the desirable shape of a product or a component using conventional processes. This is because complicated details of some products require the use of the specific processes to achieve the accuracy in shape and dimensions of the final product. Other than that, the issues and challenges for manufacturing micro-products need to be handled such as tolerance and surface quality capability, overall dimension of parts, tooling dimensions and unwanted external forces. The issues have been discussed widely in this chapter. It can be summarised that the manufacture of miniature products is still challenging and improvement needs to be made due to lack of sufficient standards, design/manufacturing rules and understanding of the manufacturing processes. Micro-forming is one of the most important processes known that can fulfil the demands of mass production with minimal waste. In this chapter, the micro forming processes and systems have been explained as has the difference between the micro forming and the conventional forming processes.

Moreover, the size effect is an important matter that needs to be considered and in this chapter the size effect in micro forming has been shown in order to understand the need for a new technique for forming miniature parts. Using a combination of micro forming and electrical field sintering processing can be considered as a promising new forming technique with high efficiency and low consumption of energy. This method was suitable for the materials that are difficult to be formed and especially for the bulk-form of micro components. This phenomenon happened due to the grain size effect as the Hall-Petch law stated that the finer the grains of the material, the higher the strength of the material.

An overview of the sintering technique was explained in the literature review. This section showed the definition of sintering and how particles of the material powder densify together. Moreover, the types of the sintering processes showed, and the electrical methodology has been explained. The electrical field assisted sintering or Field Assisted Sintering Technique (FAST) was explained and can be seen in the sintering technology which shows a significant potential to produce micro-components by using powder as a raw material. Moreover, by using Field

Assisted Sintering Technique (FAST), the microstructure of the material and its plastic flow could be controlled more efficiently and as a result improves surface quality, reduces the number of defects compared to conventional micro-forming processes and extends tools life due to lower forming forces.

The application of electrical field assisted sintering shows a significant potential to produce micro-components by using ceramic powder. Based on the research review as stated above, it has shown that there are still significant challenges to manufacturing micro-components to fulfil the requirement of the process which can be handled in the short time and achieve a higher relative densification of the product. The reviews showed that several researchers have made developments using mainly the SPS process on several Zirconia (ZrO_2) powders. The total time to achieve sample densification above 90% was approximately in the range of 30 to 120 minutes. The sintering temperatures were between 1100 and 1400 °C. Moreover, some of the operations used (PECS and SPS) in the Alumina materials achieved relative a density from 83 to 99% and to have formed the samples in about 5 to 30 minutes at range of 1,200 °C to 1500 °C. In addition, SPS and Flash sintering were used for to sinter piezoceramic powder materials. The total time to achieve piezoceramic samples were in range of 20 to 40 minutes and the densification was from 83 to 98%.

From the previous studies, it would be beneficial to have improvements of the reviewed processes for the manufacture of miniature components through reduced cycle times and good densification quality. Therefore, the Micro-FAST process has been developed to save time compared to the conventional process. In the Micro-FAST, the loose powders were directly fed into the die set without the need to prepare a green compact and hence small size components could be made based on the design of the die set. Moreover, forming the component without using lubricants reduces the impact on the environment. Additionally, the Micro-FAST process makes it easy to manage the microstructure of the part formed which could decrease the required forming pressure, and it could also increase the tooling life. This is due to the induced heating from the high-efficiency of the alternating current. It is also feasible to form miniature components with high strength materials through reducing the influence of the grain size effect in the micro forming process. In addition, there is also the option to use different powder material combinations.

To sum up, there are needs to produce micro-components using fast cycle time and high quality taking into consideration the reduction of the cost. The micro-manufacturing showed how it is important in recent days and it has received significant attention regarding its processes. The application of electrical field assisted sintering showed a significant potential to produce micro-products by using the powder ceramic materials. However, there are some challenges in the manufacturing of micro-components to fulfil the requirement of the process which can be handled in the short time and achieve a higher relative densification of the components. Therefore, the Micro-FAST process has been developed to save time compared to the conventional process.

3

MICRO-FAST OF CERAMICS AND COMPOSITES

3.1 OVERVIEW OF MICRO-FAST

Micro-FAST is a novel process used to produce miniature/micro-parts directly from loose powder by combining the Field- Activated Sintering Technique (FAST/ECAS) and micro-forming to manufacture miniature/micro parts under coupled multi-field actions and achieve high-density, near-net-shaped components with high efficiency [2, 18, 113]. The powders are pressed when an external electric field is applied to them while the powders are joined together through fusion bonding under high temperatures created either by resistance heating at the powder interfaces and/or by the mould due to the high current flowing through it. It has been demonstrated that the process is particularly suitable for forming micro/miniature components due to using very high heating and cooling rates and is of high flexibility for processing different powder-materials [2, 3, 73, 113]

According to Qin [2] and Zulkipli [3] , the Micro-FAST process is an efficient process for manufacturing miniature-sized components because the entire process takes less time than other conventional processes while still obtaining a high relative density. The parameters of the Micro-FAST process such as the temperature, heating rate and mechanical pressure have significant effects on the densification of the parts. Moreover, there is no significant coarsening of grains during the densification process due to the continued high pressure used during the short forming time [3].

3.2 PROCESS CONFIGURATION

Micro-FAST is a promising and energy-efficient technique that uses electricity to quickly raise the compact's temperature and exert pressure simultaneously, which can be turned off immediately after the preset sintering time. Figure 3-1 shows the principle of the micro-FAST process. By applying Joule heating as the main heat source during the electrical-field activated sintering, plus the pressure, plus possible electric plasticity in the powder material, densification can be achieved within a short time [2, 3, 113]

In the Micro-FAST process, the powder is sintered under the simultaneous effect of the high temperature from the current flow through the die set and the applied forming pressure as illustrated in Figure 3-1. In this process the loose powder is being placed directly into a small die and the punch assembly is placed between the machine electrodes. The heating was achieved by passing an AC current through the die to generate the necessary temperature within the die sets and powder inside. Then pressure was applied onto the powder to enable the consolidation of the powder that made a significant contribution in forming miniature components with complex geometries. The electrical-field that has been used in the Micro-FAST process is produced using a thermal simulation machine (Gleeble-3800 and Gleeble-1500D) from Dynamic System Inc., USA. It has a low voltage (3 to 10 volt), high current (3,000 to 30,000 A), large current density (200 to 400 kA/cm²) and the operation is done in a vacuum atmosphere (4.6×10^{-1} Torr) see Figure 3-2 [2, 3, 72].

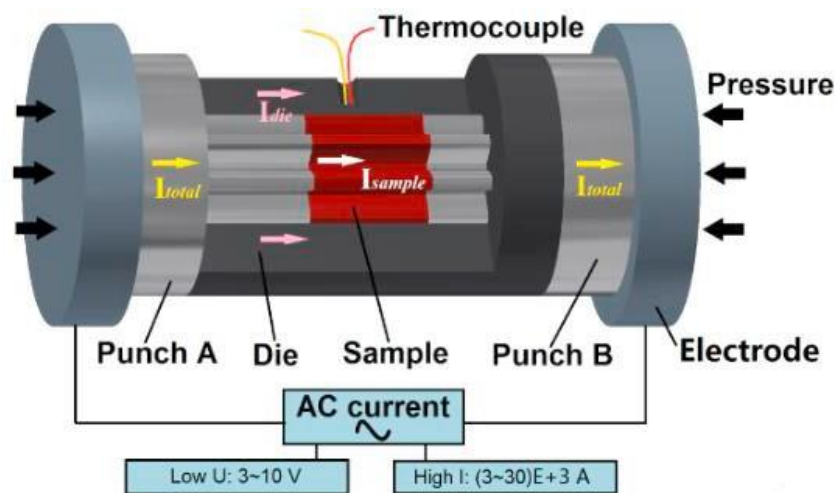


FIGURE 3-1: MICRO-FAST PROCESS FOR THE FORMING OF MINIATURE/MICRO- COMPONENTS [75, 113, 114]

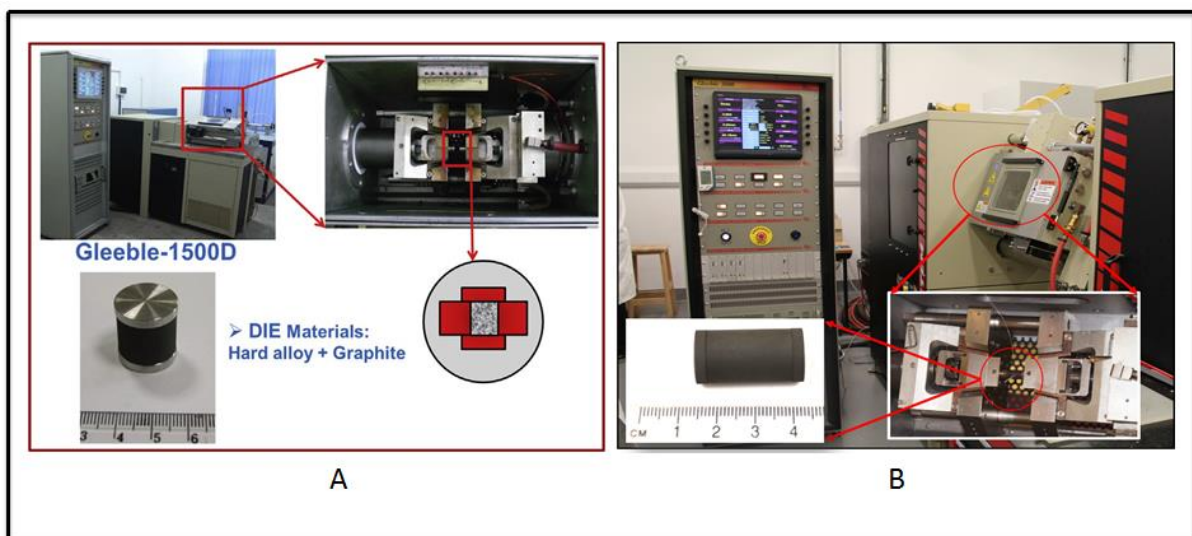


FIGURE 3-2: THE DIE-SET WITH POWDER INSIDE THE MACHINE (A) GLEBLEE 1500D (B) GLEBLEE 3800 [2, 72]

According to Lang [19], in the conventional powder sintering process, neck and grain growth are the critical mechanisms needed to achieve densification. Grain growth was caused coarsening which is associated with surface diffusion or evaporation/condensation. Therefore,

the process takes a long time to be completed, due to the high temperature and longer time processing needed that leads to unwanted grain growth in the sintered body [3, 115]. In the meantime, by using the Micro-FAST process, there was no neck growth or coarsening with a short sintering time. The densification can be done rapidly by the deformation and breakage of the powder particles. The rise and the disappearance of the interface area between particles were the results of the densification of the samples being formed. Based on that, it was critical for the particle to be present under multi-fields (pressure and electrical-field activation) to reach quick densification and high quality micro-parts [2, 3, 73].

By using the AC current Joule heat will be generated at the interfaces due contact resistance between powders and the resistance of the powder itself. The temperature will rise quickly when a large current passes through the powders. According to the Joule-Lenz's law, the heat created by the current that passes through the compact as presented in literature review in equation 2.2-1, which is $Q = I^2 R t$

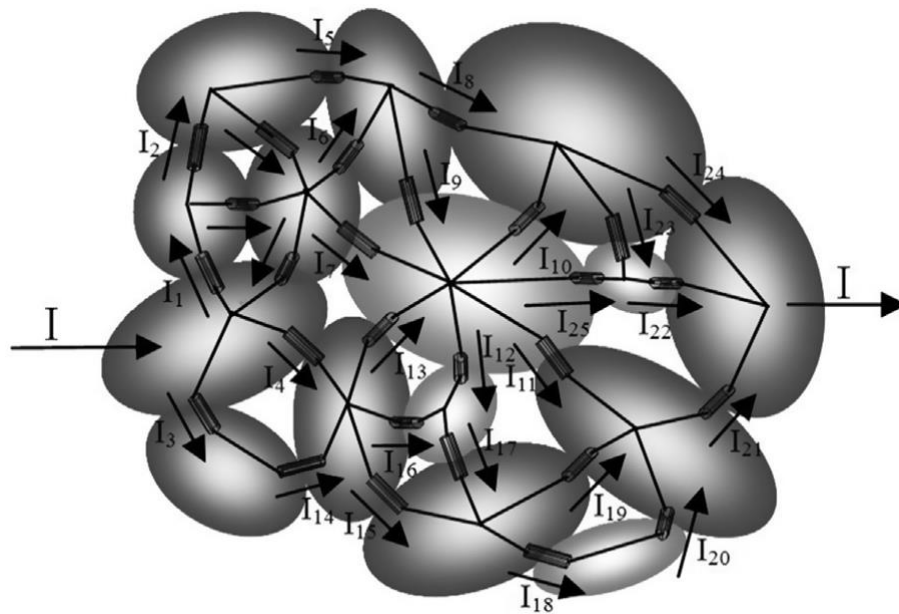


FIGURE 3-3: ILLUSTRATION OF THE DISTRIBUTION OF THE CURRENT IN A COMPACT

Figure 3-3 shows the distribution of the current in the compacts. In the Micro-FAST process, some important matters need to be recognised due to small contact-areas and high-

temperature, which play significant roles during the densification of the powders. As shown, when the temperature and electric current density is high, the Joule heat and emission current intensity is high. The collision of emission current with the particles due to the transfer of the emission current's kinetic energy to internal energy speeded atomic diffusion at a lower temperature under the electric field. The powders that have been used in the experiments were discontinuous, catching a lot of gas among the powder particles. During the heating process, the gas inside the sintered powder system was moved out and a liquid phase formed. Simultaneously, the liquid phase flow was accelerated at high pressure because of the extra pressure that has been applied to the powder and parts of the liquid phase filled into the pores by plastic flow. It should be taken into the account that the pressure field influences the temperature formation field and electrical field. Moreover, the increased temperature and Joule heat change the distribution of the pressure field. As a consequences, the coupled multi-field activation causes intensive densification of the powders [2].

In the Micro-FAST process, there are two types of sintering process. The first one is the constant temperature sintering. The other type is the electro heating loop sintering as illustrated in **Figure 3-4** [2].

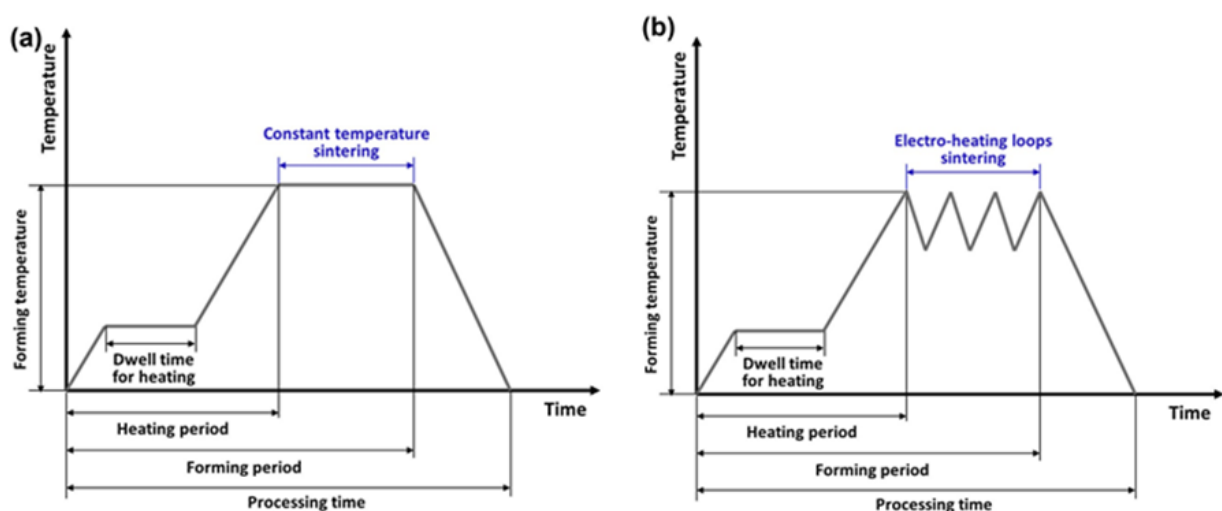


FIGURE 3-4: TEMPERATURE TIME CURVE OF THE COMPACT DURING THE SINTERING PROCESS: (A) CONSTANT TEMPERATURE SINTERING; (B) ELECTRO-HEATING LOOPS SINTERING [2]

According to Qin [2], the densification mechanism of the Micro-FAST process from the two types can generally be described as shown in **Figure 3-5** into four stages. This figure is just to explain the stages and it is not from the experiments that have been conducted in this work.

Stage 1: the preheating period

After the powder material had been prepared and placed into the die set, it was distributed loosely inside the die set cavity. During the preheating process the powder was heated using electric current in a vacuum chamber (4.6×10^{-1} Torr) to a low temperature (usually 200 to 400 °C) and then held for a certain time, during which dwell time at the low temperature the gas trapped inside the sintered powder system is forced out [2, 3, 116]

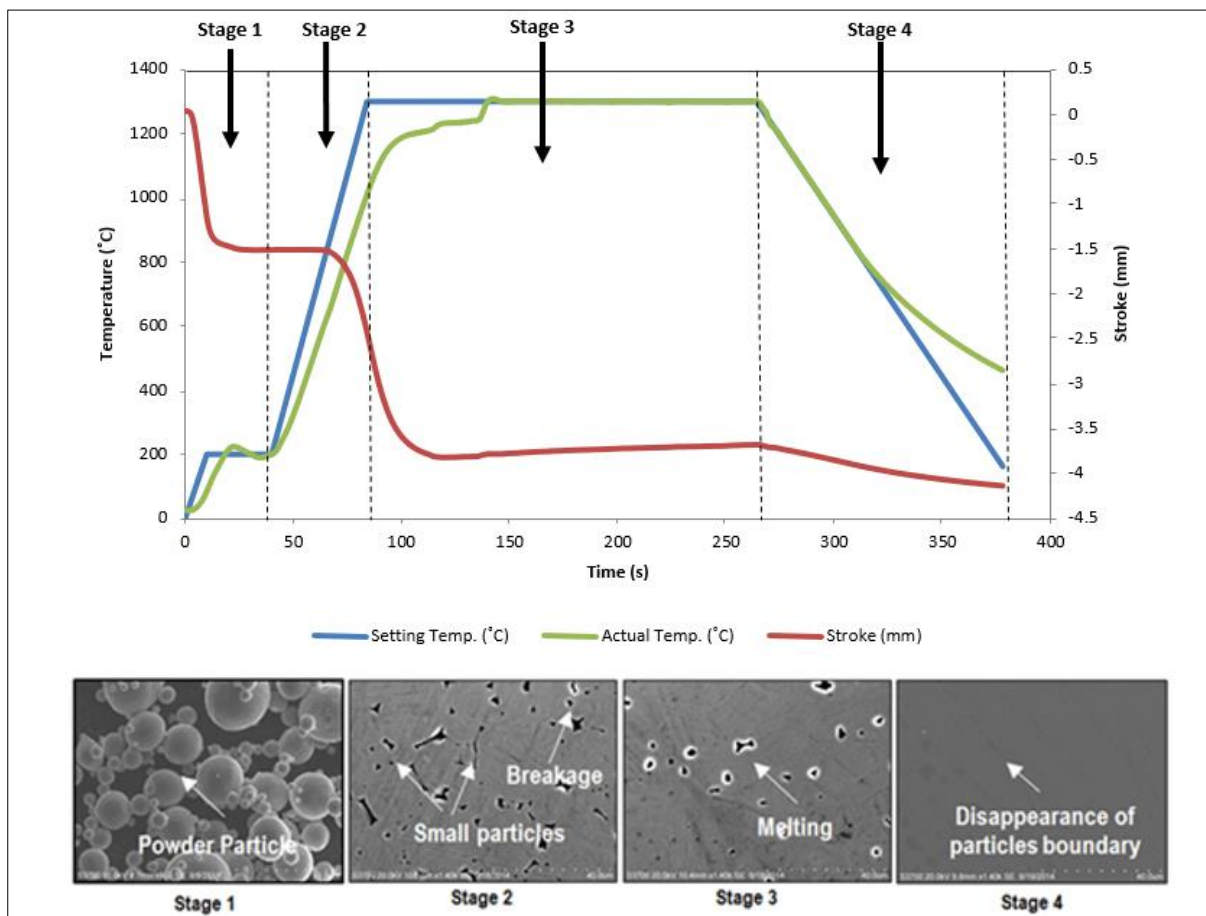


FIGURE 3-5: ILLUSTRATION OF STAGES FOR MICR-FAST PROCESS [2, 75]

Stage 2: the calefactive period or the high-temperature pressing.

During this process the compacts are heated to the pre-set sintering temperature from the dwell temperature. Starting from the end-point of the first stage, the temperature continues to rise upon the setting sintering temperature while the pressure was maintained. The transmitted stress to the pores of the low-density body and the contact area between particles is larger compared to the macroscopic applied stress. Moreover, the ability of the plastic deformation for the powder materials at high temperature was one of the excellent properties for this process [2, 3, 116]

Stage 3: The sintering period

This stage is when the compact of the powder and punches is held for a certain time at the sintering temperature which is fluctuating and cycles for a fixed number of times. During this stage, while keeping the pressure towards the die set, the sintering temperature will be constant for some time. Significant heating was produced towards the interface particles, where the melting point of fine powder particles is likely to be achieved at the points, this will cause the generation of a liquid phase at local areas. When the liquid phase was formed, that would lead to the fusing of the contact surface between particles. Meanwhile, with the help of the applied pressure to the compact, the liquid phase fills into the nearby pores due to the viscous flow and capillary force that causes the disappearance of the interface between particles and fast densification of the compact [2, 3, 116]





Stage 4: The Cooling Period

The final stage of the process was the cooling period where the electric current is reduced then switched off and the compacts were cooled to room temperature. According to the results of the present experiments, different material powders should be sintered by different sintering processes [2, 3]

3.3 DIE SETS IMPROVEMENT FOR MICRO-FAST

There are many dies that have been used in previous studies that can be used for the experiment of Micro-FAST. Zulkipli [3] used two designs of die sets with some differences to sinter titanium and titanium alloy powder materials. The two dies designs had been made for the development of electrical-field activated sintering and forming processes (Micro-FAST) See Table 3-1.


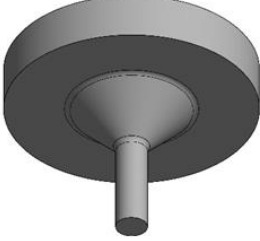
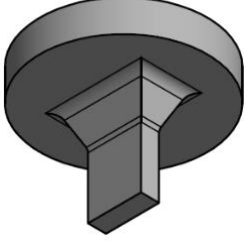


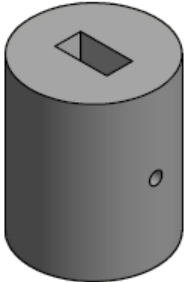
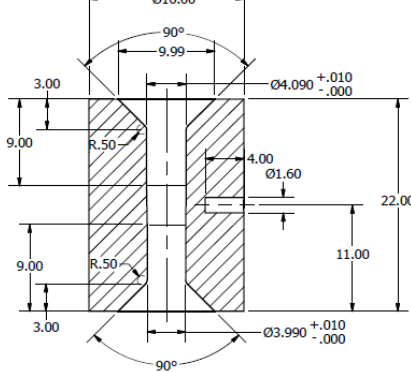
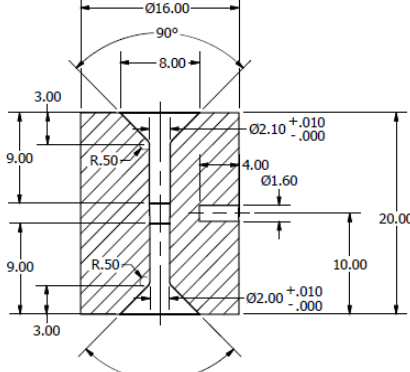
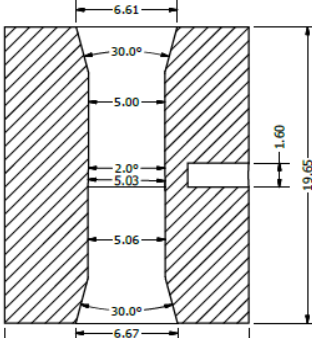
TABLE 3-1: THE TWO DIE SETS THAT USED BY ZULKIPLI [3]

Part	The First Die Set	The Second Die Set
Punches		
Die		

As for the first one, it was used for the initial testing to examine the efficiency and robustness of the die under the applied experiment parameter, which required a high pressure and temperature. Meanwhile, the second die set is an improvement and an optimisation after using the first die set in some experiments and proved its more efficient use in the electrical-field sintering processes. The two die sets were designed to fabricate cylindrical shapes samples with the diameter of 4 mm and height of 4 mm. In the first die, the total dimensions were 16 mm in diameter, 14 mm in die height and 6 mm in the thickness wall of the die set. The punch nose has the diameter and height of four and five millimetres respectively. In the meantime, in the second die set, the overall dimension was 16 mm in diameter, 22 mm in die height and 6 mm in the thickness wall of the die set. The punch nose still has the same diameter as the first design which is four millimetres, but the height of nine millimetres has been added to new die set due to the new large transition. The shape design on large transitions at the second die set was made to decrease the thermal stress concentration in the punch. Moreover, the concentrated heating at the punch nose during the process whereas more uniform temperature distribution occurred in the die's middle section and that is making the second die set more reliable [3, 75]. Therefore, the second die set will be considered to be used in the Micro-FAST experiment for the ceramic materials. However, due to some difficulties in the ejecting process and avoiding

any jammed samples, an improvement has been made for the suggested die sets. Table 3-2 shows the improved die set that have been used in the Micro-FAST process. For the die set A, the hole diameters have been increased by 0.10 mm from one side and decreased by 0.10mm from the other side. The reason for that is to make the samples more easily ejected during the ejection process. Moreover, another die has been produced with the same design of the die set A, but with smaller size in the shape (die set B). The new design was made to produce cylindrical shapes samples with the diameter of 2 mm and height of 2 mm. The same thing has been used in the die set B, which is an increase in the hole diameter by 0.10 mm from one side and decreased by 0.10mm from the other side. Furthermore, another die set (C) has been manufactured to produce cuboid samples. The dimensions of the samples were Width= 1.65 mm, Length= 5mm and the Height= 1.65 mm.

TABLE 3-2: THE IMPROVED DIE SETS FOR MICRO-FAST PROCESS

Die set A	Die set B	Die set C
		
		
 <p>Technical drawing of Die set A punch and die. The punch has a diameter of $\varnothing 16.00$ and a length of 22.00. It features a 90° chamfered top edge with a radius of R.50. The die has a diameter of $\varnothing 16.00$ and a length of 11.00. The punch diameter is specified as $\varnothing 4.090^{+0.010}_{-0.000}$ and the die diameter as $\varnothing 3.990^{+0.010}_{-0.000}$. Other dimensions include 3.00, 9.00, 9.99, 4.00, and $\varnothing 1.60$.</p>	 <p>Technical drawing of Die set B punch and die. The punch has a diameter of $\varnothing 16.00$ and a length of 20.00. It features a 90° chamfered top edge with a radius of R.50. The die has a diameter of $\varnothing 16.00$ and a length of 10.00. The punch diameter is specified as $\varnothing 2.10^{+0.010}_{-0.000}$ and the die diameter as $\varnothing 2.00^{+0.010}_{-0.000}$. Other dimensions include 3.00, 9.00, 8.00, 4.00, and $\varnothing 1.60$.</p>	 <p>Technical drawing of Die set C punch and die. The punch has a diameter of $\varnothing 16.00$ and a length of 19.65. It features a 90° chamfered top edge with a radius of R.50. The die has a diameter of $\varnothing 16.00$ and a length of 19.65. The punch diameter is specified as $\varnothing 6.61$ and the die diameter as $\varnothing 6.67$. Other dimensions include 3.00, 9.00, 5.00, 2.00, 5.03, 5.06, and 1.60.</p>

3.4 TEMPERATURE MEASUREMENT

Based on the previous research that has been done, it was shown that the thermocouple was the best way to measure the temperature by attaching it to the surface the die during the

process [75, 114, 116, 117]. Because the thermocouple is planted on the surface of the die during the experiment, the nominal temperature of the sample was slightly lower than the actual temperature inside the sample. Therefore, there are temperature gradients for the real temperature of the sample. A placement for the thermocouple has been made by drilling a small cylindrical cavity on the body of die as seen in Table 3-4. The depth of the hole was set 4 mm to secure the attachment of the thermocouple inside the tight cavities and prevent any fill out. Moreover, the position of the tip of the thermocouple could get near to the sample's wall. Therefore, it could help to achieve an accurate temperature reading during the Micro-FAST process compared to the previous research.

TABLE 3-3: THE CROSS SECTION DIE USED IN THE MICRO-FAST PROCESS

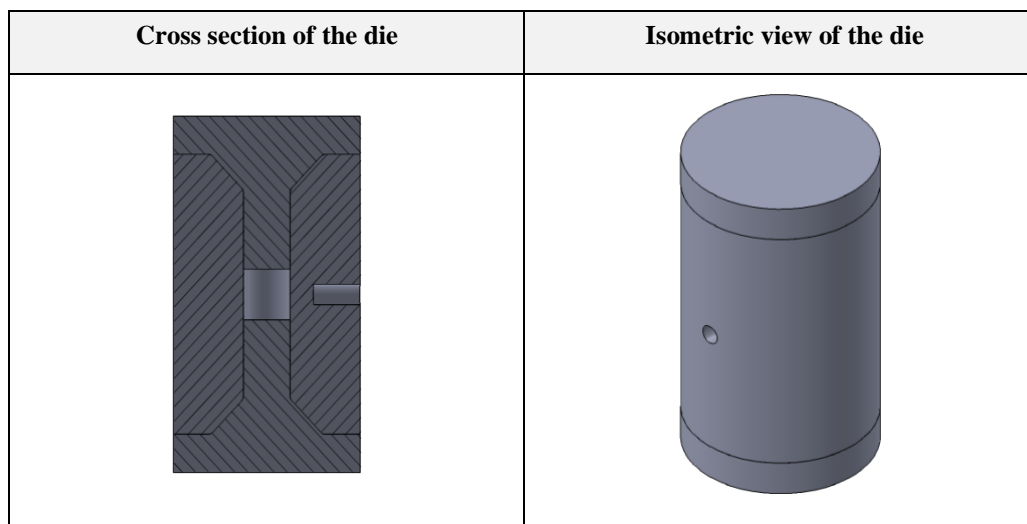


Figure 3-6 shows the positioning the die that set in the Gleeble 3800 machine. It can be seen that the die set needs to fit the punch tooling perfectly to get the required efficiency of heating and pressure during the Micro-FAST process.

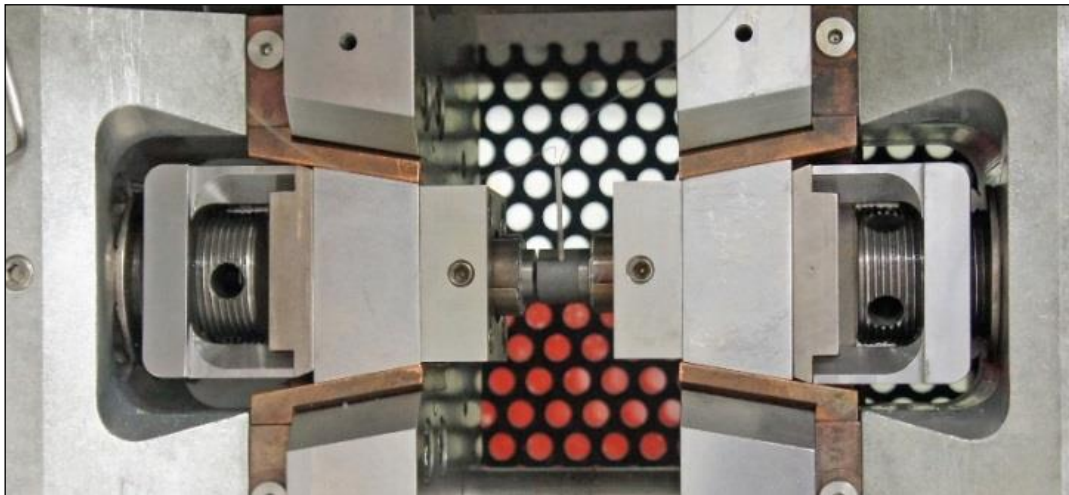


FIGURE 3-6: THE DIE SET INSIDE THE GLEEBLE MACHINE 3800

3.5 MATERIAL SELECTION FOR MICRO-FAST DIE SET

Based on the previous studies, most conventional electrical sintering applications used tungsten carbide and graphite as die set materials, which shows an excellent choice concerning its capability working at high temperatures from 700 °C to 2,700 °C respectively [118-120]. The graphite and tungsten carbide dies were used to produce cylindrical samples with dimensions of 20 to 42 mm in diameter and 5 to 15 mm in height with different materials [18, 99, 111, 121-123]. Therefore, the materials selection for dies used in the Micro-FAST experiment has been made which involved two possible materials which were graphite and tungsten carbide. The graphite had positive reviews on previous research as mentioned before. The Tungsten carbide has excellent compressive strength compared to other materials which would make the die set more convenient when dealing with the high pressure and temperature environment during the Micro-FAST process. Moreover, the thermal expansion coefficient (TECoE) needs to be considered besides maximum service temperature (T_{max}) and compressive strength. The reason behind that is due to the fraction of the expanded die set material per degree of temperature increase during the process needs to be small between the thermal expansion coefficient for punches, the body of die and the sintered powder. Table 3-4 shows

the mechanical and thermal properties of the graphite and tungsten carbide materials used. Further details regarding the guidelines on how to choose the suitable combination of die sets with powder being sintered by comparing the compressive strength, thermal expansion coefficient and maximum service temperature of selected materials have been shown in the section below. By using the guidelines, all the possible combinations for the die set with particularly sintered powder can be managed and known whether it is a good combination or not based on the fulfilment of requirement.

TABLE 3-4: MECHANICAL AND THERMAL PROPERTIES BETWEEN GRAPHITE AND TUNGSTEN CARBIDE MATERIALS BASED ON COMPRESSIVE STRENGTH, THERMAL EXPANSION COEFFICIENT AND MAXIMUM SERVICE TEMPERATURE [120].

Materials	Compressive Strength	Thermal Expansion Coefficient	Maximum Service Temperature
	(MPa)	(μ strain/ $^{\circ}$ C)	($^{\circ}$ C)
Graphite	43 to 350	0.3 – 8.63	1,300 - 2,700
Tungsten Carbide	4,250 to 6,830	4.5 to 7.1	727 - 777

3.5.1 THERMAL EXPANSION COEFFICIENT

As mentioned, two materials have been selected for the die set. There are the graphite and tungsten carbide. These should make an excellent contribution towards the Micro-FAST process experiment due to the applied pressure required which is in the range of 75 to 125 MPa. However, a comparison of selected combinations of the die set of the thermal expansion coefficient between the punches and body of die will be required to be done. It has been suggested that the value of the thermal expansion coefficient for the die must be less than the punches (TECoE die < TECoE punches) when using different materials to avoid any jamming inside the die during the ejection process of the sample. The reason behind that is when the thermal expansion coefficient of the die is higher than the punch; the fraction of used material

in the die is likely to be expanding more quickly per degree of temperature compared to the punches. Due to that, the punches would be stuck inside the die wall. Moreover, the punches would break during the opening if excessive forces were applied. The appropriate condition for the die and the punches was to have a similar material for both of them to have the same thermal expansion coefficient value for uniform heating and cooling during the Micro-FAST process.

TABLE 3-5: COMBINATION OF THE DIE SETS MATERIALS OF GRAPHITE AND TUNGSTEN CARBIDE BY COMPARING THERMAL EXPANSION COEFFICIENT AMONG THE MATERIALS FOR THE PUNCHES AND BODY OF THE DIE.

Die Materials	Punches Materials	Graphite	Tungsten Carbide
	TECoE ($\mu\text{strain}/^{\circ}\text{C}$)	0.3 – 8.63	4.5 - 7.1
Graphite	0.3 – 8.63	Acceptable	Acceptable
Tungsten Carbide	4.5 - 7.1	In Range	Acceptable

As shown in Table 3-5, four possible combinations scenarios can be made for the material of die and punches. The first one is both of the die and the punches using graphite as their material. This choice is acceptable due to the value of thermal expansion coefficient being the same. The second choice showed the punches would be utilising the tungsten carbide material. The die would use the graphite. The combination was also an acceptable one due to the range of thermal expansion coefficient of the die (graphite) was less than the punches (tungsten carbide). The third choice is to make the tungsten carbide as the die, and graphite as the punches. The third choice was in range, and acceptable with reservation due to die (tungsten carbide) thermal expansion coefficient range value could be exceeding the punches (graphite). The fourth combination is making the tungsten carbide for both die and punches. Same effect as the first option would happen, this was acceptable due to the value of thermal expansion being the same. Therefore, it can be shown that three combinations can be chosen for the Micro-FAST process. However, another comparison will be examined with the powder materials and the three best combinations for the die sets to choose the best material for the die that is going to be used in the Micro-FAST process.

Based on the selection of the combination materials for the die set criteria from Table 3-4 the three possible materials for the die set can be used for the Micro-FAST process. The same approach has been used for the three materials combination of the die set and the sample materials (alumina, zirconia and piezoceramic) which were by comparison of its thermal expansion coefficient value. Furthermore, the criteria of the temperature related expansion behaviour of materials for the die and the punches need to be determined. Then, the ability to eject the sintered sample out easily from the die also needs to be considered. It was a precautionary step not to use a higher force during the ejection process that could break the die set and sintered samples. Therefore, it was suggested that the thermal expansion coefficient for the die and the punches must be less than the sintered sample material (TECoE punch and die < TECoE sintered sample). The purpose was to avoid any trap for the punch inside the die due to the expansion of materials used by the die and the punch with the increasing temperature which would push the wall of the sintered sample to the die and the punches. As a result, it would obstruct the movement of the ejection process.

TABLE 3-6: SELECTION COMBINATION OF DIE SETS MATERIALS OF GRAPHITE (C) AND TUNGSTEN CARBIDE (WC) WITH POWDER THAT NEED TO BEEN SINTERED WHICH IS ALUMINA, ZIRCONIA AND PIEZOCERAMIC BY COMPARING ON THEIR THERMAL EXPANSION COEFFICIENT.

Combination of Die Set	Die Set		Sample Materials	Alumina	Zirconia	Piezoceramic
	Section	Materials	TECoE ($\mu\text{strain}/^{\circ}\text{C}$)	4.5-10.9	2.3-12.2	0.002- 0.6
First	Punches	Graphite	0.3 – 8.63	In Range	In Range	In Range
	Die	Graphite	0.3 – 8.63	In Range	In Range	In Range
Output Results				Acceptable	Acceptable	Acceptable
Second	Punches	Tungsten Carbide	4.5 to 7.1	In Range	In Range	Not Acceptable
	Die	Graphite	0.3 – 8.63	In Range	In Range	In Range
Output Results				Acceptable	Acceptable	Not Acceptable
Third	Punches	Tungsten Carbide	4.5 to 7.1	In Range	In Range	Not Acceptable
	Die	Tungsten Carbide	4.5 to 7.1	In Range	In Range	Not Acceptable
Output Results				Acceptable	Acceptable	Not Acceptable

Based on the output results from Table 3-6, the first combination of the die set which consists of graphite punches and the die with alumina, zirconia and piezoceramic powder that needs to be sintered has no problem and can be accepted because the thermal expansion coefficient was in the range of all three materials. It needs to be borne in mind that thermal expansion coefficient of the die and the punches must be less than the sintered sample material (TECoE punch and die < TECoE sintered sample). The second combination of the die set which

consists of a graphite die and tungsten carbide punch was accepted for testing Alumina and Zirconia samples. This is because the comparison range of thermal expansion coefficients of the tungsten carbide and Graphite were near to the tested sample materials. However, for the piezoceramic materials tungsten carbide was not accepted because the TECoE of the punch choice was not in the range of TECoE of the piezoceramic. This would create some difficulties with the opening of the punches which might be tighter due to the sample and punches being expanded towards each other as the temperature increases. However, if the punches have been opened, the ejection process would have no problem and be easily done due to the graphite die which could have a lower thermal expansion coefficient compared to the tested material. Therefore, the second could be accepted with reservation and concerns for the Tungsten Carbide punches. Lastly for the third combination where all the die and punches were made from tungsten carbide was accepted for Alumina and Zirconia, but was not accepted for the piezoceramic due to both of thermal expansion coefficients being out of the range of sintered samples. Therefore, the same approach will be used in the next comparison for material combinations of die sets which is the maximum service temperature of the material die sets and sintered materials.

3.5.2 MAXIMUM SINTERING TEMPERATURE OF THE DIE SETS AND SAMPLE MATERIALS

The maximum service temperature of the material used by die sets during the sintering heating applied to the sample needs to be considered. It is important to know the highest temperature at which die set material can be used for an extended period without significant change in the property or any problems such as oxidation, excessive creep, chemical change, and material strength. The reason behind this was to ensure that the die set performs with excellent efficiency even if the higher sintering temperature ($T_{\text{sintering}}$) of the sample was used. Therefore, it was advised that the maximum service temperature for the materials of the die and the punch must be greater than the temperature of the sintered sample ($T_{\text{max}} \text{ punch and Die} > T_{\text{sintering sample}}$).

TABLE 3-7: SELECTION COMBINATION OF DIE SETS MATERIALS OF GRAPHITE AND TUNGSTEN CARBIDE WITH POWDER THAT NEED TO BE SINTERED WHICH IS ALUMINA, ZIRCONIA AND PIEZOCERAMIC BY COMPARING THEIR MAXIMUM SERVICE TEMPERATURE OF THE DIE SETS AND SINTERING TEMPERATURE OF THE POWDER DURING THE ELECTRICAL-FIELD ACTIVATED SINTERING AND FORMING PROCESS.

Combination of Die Set	Die Set		Sample Materials	Alumina	Zirconia	Piezoceramic
	Section	Materials	Max. Service Temp. (°C)	1,100 - 1,700	1300 - 1700	900-1200
First	Punches	Graphite	1,300- 2,700	Acceptable	Acceptable	Acceptable
	Die	Graphite	1,300 - 2,700	Acceptable	Acceptable	Acceptable
Output Results				Acceptable	Acceptable	Acceptable
Second	Punches	Tungsten Carbide	727 to 777	Not Acceptable	Not Acceptable	Not Acceptable
	Die	Tungsten Carbide	727 to 777	Not Acceptable	Not Acceptable	Not Acceptable
Output Results				Not Acceptable	Not Acceptable	Not Acceptable

Based on Table 3-7, the first combination of the die set by using graphite as the material for the die and the punches was acceptable for all samples (alumina, zirconia and Piezoceramic) due to the maximum service temperature for graphite being higher compared to the sintering temperature used by the samples. On the other hand, the second combination of the die set which used graphite as a material for the die and tungsten carbide for the punch was not acceptable due to the maximum service temperature of the tungsten carbide punches being much lower (727 to 777 °C) compared to the alumina, zirconia and Piezoceramic sintering temperature. Therefore, based on the previous investigation, graphite was the most suitable materials for the die set for the Micro-FAST process experiment.

3.6 PROCESS IMPROVEMENT FOR SINTERING CERAMICS AND COMPOSITES

Heat transfer plays a very important role during any sintering process. A sufficient sintering requires an ideal heat transfer that allows the temperature increase of the precursor material to get high enough for the densification process to happen [67-69]. As mentioned before, the three types of heat transfer are conduction; convection and thermal radiation (see Figure 2-16). Conduction heat transfer relies on the direct thermal contact within solid objects. The convection heat transfer occurs through the motion of a hot fluid (liquid or gas) which acts as a carrier. Thermal radiation can take place between two distant bodies without the need of any medium. In conduction and convection cases, the energy transfer between two objects depends approximately on the temperature difference between them [68-70]. Thermal radiation transfer relies on the difference between the fourth power of their absolute temperatures, according to the well-known Stefan-Boltzmann's law. [69-71]. Sintering metals is different from sintering ceramics due the differences in the thermal and electrical properties. Metals have a very good thermal conductivity due to a relatively high concentration of free conduction electrons, and these can transfer heat as they move through the lattice. Most metal powders can be sintered and give a very high level of purity. Sintering metals is considered as a part of powder metallurgy and categorised as a combination of processing consolidation to make a solid metal from fine particles. Most ceramic materials have low thermal and electrical conductivity, therefore they require high temperatures to sinter and form their powders [54, 55].

3.6.1 HEAT TRANSFER DURING ELECTRICAL FIELD SINTERING PROCESS

Electrical field sintering is a sintering process that uses electrical current to generate high temperatures to sinter the material powder into a solid piece. It is shown passing high density electric current pulses through the workpiece in Figure 3-7. By applying current pulses or electric fields to the metals, ceramics, superconductors and powder metallurgy products significant improvements in the material plasticity have been shown. The Micro-FAST process is a combination of heat transfer in the form of convection, radiation and conduction. However,

in ceramic materials it is challenging due to their low thermal and electrical conductivity [2, 3, 52, 54].

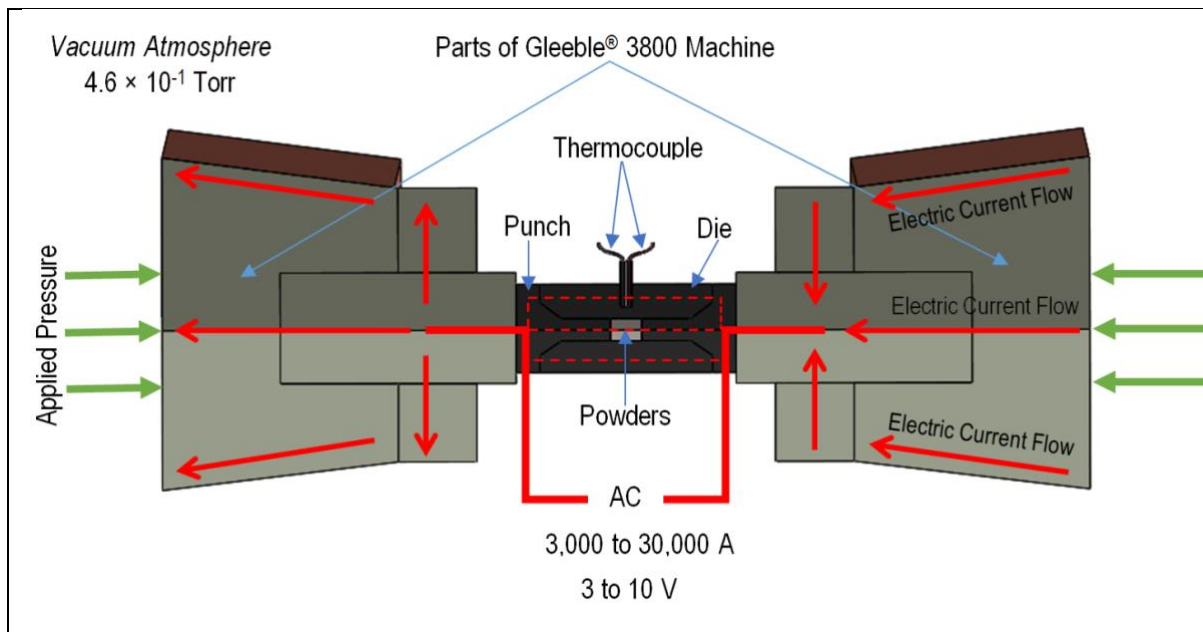


FIGURE 3-7: SCHEMATIC DRAWING OF THE GLEEBLE® 3800 MACHINE TOOLING AND CURRENT FLOWS (RED ARROWS) DURING THE ELECTRICAL-FIELD SINTERING PROCESS [3, 75]

In the Micro-FAST process, conduction heat transfer plays an important role in sintering despite the low thermal conductivity of the ceramics. Conduction heat transfer is the transfer of heat through anything that has mass (i.e., solids, liquids, or gases). Specifically, conduction is the transfer of energy from the more energetic to less energetic particles of a substance due to interaction between the particles. Conduction heat transfer in gases and liquids is due to the collisions and diffusion of the molecules during their random motion. The heat transfer in solids is due to the combination of lattice vibrations of the molecules and the energy transport by free electrons. Heat conduction can be found in everyday examples, such as when a fire started, and then moves around the burning logs with a poker. Heat is going to be conducted from the burning logs to the poker, making the end of the poker become red and hot if it is left there for too long. In the cars, when the engine is turned on, and the hood becomes warm, that is due to the conduction of heat from the engine to the hood of the car. In industry, electrical wires are good examples for heat conduction. The heat/electricity will move through the metal easily because it is a conductor of heat and quickly get to where it needs to go.

Heat convection is the motion of heat caused by the transfer of energy through gasses or liquids. In meteorology, convection is the transfer of heat and other atmospheric properties by the movement of masses of air, particularly in an upward direction. For example, when a fan, pump or device of suction is used to enable convection, the result is forced convection. Some examples are air conditioning, central heating, a car radiator using fluid, or a convection oven [68, 124].

Thermal radiation is electromagnetic radiation produced by thermal motion of charged particles in matter. On other words, it is radiation generated from a material that is due to the heat of the material, the characteristics of which depend on its temperature[124].

An example of thermal radiation is the infrared radiation emitted by common appliances like household radiators or electric heaters. People near a raging bonfire will feel the radiated heat of the fire, even if the weather was very cold. Thermal radiation is generated when heat from the movement of charges in the material (electrons and protons in common forms of matter) is converted to electromagnetic radiation. Sunshine, or solar radiation, is thermal radiation from the extremely hot gasses of the sun, and this radiation heats the earth [68, 124]. In industry, there are many examples of using infrared radiation heating or electric infrared radiation heating. Its history started over half a century ago when heat radiation produced by commercial lighting bulbs was used for curing car paint in “infrared tunnels”. In the following years, a lot of efforts were made to develop new types of heat sources to manufacture various products. With different electric infrared sources, heat is normally produced by passing a constant (or variable) current through a coiled resistive element giving different temperatures [68, 124]. For example, the tubular metal and grill elements on electric cookers operating at around 700 °C generate enough infrared radiation, while the latest quartz halogen infrared heaters used for cooking operate at a high temperature that can reach 2200 °C resulting in luminous emission. Due to that, many applications are being enabled, such as moisture evaporation, printing ink drying, moulded plastics forming, adhesives and metals bonding, and electronics printing [68, 124].



FIGURE 3-8: PICTURES SHOWING THE APPLICATIONS OF IR HEATING IN DAILY LIFE AND INDUSTRY [68]

Thermal radiation represents a conversion of thermal energy into electromagnetic energy. All matter with a temperature greater than absolute zero emits thermal radiation. If a radiation-emitting object meets the physical characteristics of a black body in thermodynamic equilibrium, the radiation is called blackbody radiation. Planck's law describes the spectrum of blackbody radiation, which depends only on the object's temperature. Wien's displacement law determines the most likely frequency of the emitted radiation and the Stefan-Boltzmann law gives the radiant intensity. As mentioned before, the successful applications of forming ceramics for industrial heating indicate its potential use in the sintering processes. There have been a few studies based on the electrical field sintering process and technique to create similar conditions to electric heating infrared radiation. The basic principle is: the current passes through the graphite die and heats it up due to the Joule heating effect; the heated-up graphite, which is considered to be a grey-body due to an emissivity value of ~ 0.90 , gives off strong thermal energy to the sample owing to a small heat transfer volume [68, 69, 71, 125].

Much work has been done a lot of experiment on ceramics materials and its composites such as Zirconia and Alumina which is going to be more focused on this work [18, 82, 111, 126, 127]. Ceramics can be defined as solid compounds made up of mixed elements that have been shaped and then hardened by heating to high temperatures or heating and pressure. In general, they are hard, corrosion-resistant and brittle [128]. In general, the powder is sintered by conduction, radiation and convection heating from external heating elements. However, most of the ceramics materials have low thermal conductivity such as Zirconia [128]. Therefore, the best way to achieve a high-quality formed sample for some ceramics materials is to use the

thermal radiation, the convection and the conductivity of the materials. Figure 3-9 shows how the schematic of the current and the thermal flow during sintering ceramic materials. The challenging part is how to make the ceramic powder particles heat up and be sintered together. As seen in Figure 3-9, the die is heated up and the current and the thermal flow go through the ceramic powder slowly due to the low thermal conductivity. Therefore, the process needs more holding time and a higher temperature. When the die is heated up and held for a certain time, the heat transfers to the ceramic powder and makes the particles start to sinter and after applying the required pressure, a solid sample is formed.

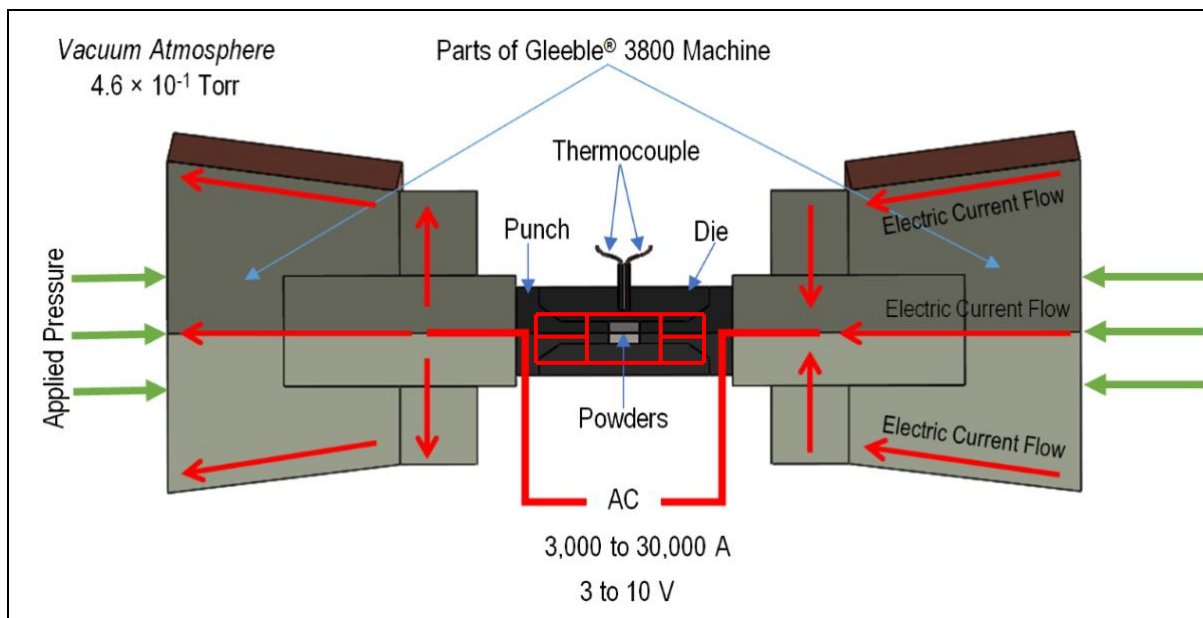


FIGURE 3-9: SCHEMATIC DRAWING OF THE GLEEBLE® 3800 MACHINE TOOLING AND CURRENT FLOW DURING THE MICRO-FAST PROCESS FOR CERAMIC MATERIALS

3.7 SUMMARY OF THE CHAPTER

In this chapter, the principles of the Micro-FAST process have been introduced and how this process has been improved for fabricating miniature parts from ceramic powder. In addition, the materials for the die sets that have been used for the experiment have been

described and the justification of using these materials. The conventional sintering processes are taking an excessive time to complete due to the densification process which involves a coarsening or neck growth which is a critical mechanism needed to achieve the densification of parts where it is caused by surface diffusion or evaporation. Although several researchers have made developments using the SPS process, the total time needed to achieve high densification of the samples still needs considerable time. This is due to SPS depending on gaps between the particles to simulate the spark discharge that has been made by the pulse current. Therefore, the applied pressure used for the sintering process cannot be too high as this would close the gap and could lead to the disappearance of the spark. By using a low sintering temperature and short sintering time this will inhibit the grain growth and permit the formation of materials with density and a fine crystalline structure. Therefore, using a higher heating rate in the Micro-FAST process can be a major factor that will contribute to making the process faster and complete in few minutes. Thus, after consideration, it can be concluded that the densification of the components by using the Micro-FAST process can be achieved by the involvement of the deformation, particle rearrangement, breakage and interface disappearance which was different from the conventional sintering process. The process could be finished within a short time due to it being a coupled process of the electrical field which generated the Joule heat and high pressure. There were 4 stages involved in the densification mechanism of the Micro-FAST process which were a preheating period, high-temperature pressing, a sintering period and a cooling period.

For the die sets, there were two designs of die sets suggested for the Micro-FAST process as shown in Table 3-1. However, based on the previous studies made by Zulkibli [3] the second die set introduced better results. The two die sets were designed to decrease the thermal stress concentration in the punches. Another positive contribution towards the punch modification was the concentrated heating at the punch nose, as more uniform temperature distributions in the middle section of the die occurred which could help to optimise the process of sintering. However, the design of the second die set showed more reduction in the thermal stress concentration in the punch. Based on these studies, 3 designs have been chosen for the Micro-FAST process. Some changes were introduced for the modification of the 3 die sets. The final output sample was in the cylindrical and cuboid shapes with different millimetre dimensions. The material selection for the die set needs to follow the standards on how to choose the suitable combination of die sets with powder being sintered by doing a comparison of the compressive

strength, thermal expansion coefficient and maximum service temperature of the selected materials. By doing the comparison, all the possible combinations for the die set with sintered powder can be managed and it can be determined whether the combination will meet and fulfil the process requirements or not. The purpose of this comparison is to prevent any conflict or trapping between punches and the sample after finishing the sintering process and starting the ejection process. Moreover, the die set needs to be robust due to the impact from a higher forming pressure. Based on previous studies for the die sets, all the punches and dies were made from graphite and used in the experiment for the zirconia, alumina and piezoceramic samples.

The heat transfer is an important matter that needs to be considered in the Micro-FAST process. A sufficient sintering requires an ideal heat transfer that allows the temperature increase of the precursor material to get high enough for the densification process to take place. Ceramic and composite materials have different thermal and electrical properties compared to metal materials. Metals have a very good thermal conductivity due to a relatively high concentration of free conduction electrons, and these can transfer heat as they move through the lattice. On the other hand, most ceramic materials have low thermal and electrical conductivity which make them difficult to sinter compared to metals. Therefore, the Micro-FAST process requires more holding time and higher temperatures to fabricate solid ceramics and composites.

4

FINITE ELEMENT ANALYSIS (FEA) OF HEATING AND COOLING PROCESS IN THE MICRO-FAST

4.1 INTRODUCTION

The Finite Element (FE) analysis of the effect of coupled thermal-electrical characteristics of the die sets during the heating and cooling process was examined by using ABAQUS/CAE software (Abaqus version 6.14). The information collected from the FE simulation was useful for the experimental process in order to gain information on how the heating distribution happened within the die sets used in the Micro-FAST process. The initial step of the analysis involved the electrical potential being exposed to the die sets that was calculated by using electrical boundary conditions. In the second step transient heat transfer analysis was conducted by the application of Joule heat generation to each finite element under a given thermal boundary condition. The temperature dependency of the electrical conductivity was used for the analysis where the electrical and thermal analyses are fully coupled. Below shows a brief summary of the theoretical background of coupled thermal-electrical analysis [129-131]

4.2 THEORY OF COUPLED THERMAL-ELECTRICAL ANALYSIS

The equation of conservation of charge was shown as in the equation (4.2-1).

$$\int_s J \cdot n \, dS = \int_v r_c \, dS \quad (4.2-1)$$

Where:

- v - Any control volume whose surface was.
- n - Outward normal to S .
- J - Electrical current density (current per unit area).
- r_c - Internal volumetric current source per unit volume.

By using the definition of an electrical field, Ohm's law can be written as shown in the equation (4.2-2). The constitutive relation was linear where it was assumed that the electrical conductivity was independent of the electrical field.

$$J = \sigma \cdot E = -\sigma \cdot \nabla \phi \quad (4.2-2)$$

Where:

- ϕ - Electrical potential field.
- E - Electrical potential.
- σ - Electrical conductivity.

Using Ohm's law in the equation (4.2-2) in a conservation equation, an electrical equation analysis was obtained in the equation (4.2-3). Joule's law describes the rate of electrical energy, P_{ec} , dissipated by current flowing through a conductor as in the equation (4.2-4).

$$\int \nabla \delta \phi \cdot (\sigma \cdot \nabla \phi) dV = \int_v \delta \phi r_c dV + \int_s \delta \phi \bar{J} dS \quad (4.2-3)$$

Where

- \bar{J} - Electrical current density towards a control volume V ($\bar{J} = J \cdot n$).

$$P_{ec} = J \cdot E = (E \cdot \sigma) \cdot E \quad (4.2-4)$$

Where

P_{ec} - The rate of electrical energy.

On the other hand, an equation for conductive thermal analysis was as shown in the equation (4.2-5).

$$\int_v \rho C_v \frac{\partial \theta}{\partial t} \delta \theta dV + \int_v \nabla \delta \theta \cdot (k \cdot \nabla \theta) dV = \int_v \delta \theta r dV + \int_s \delta \theta q dS \quad (4.2-5)$$

Where

θ - Temperature.

k - Thermal conductivity.

ρ - Density.

C_v - Specific heat.

q - Heat flux towards a control volume V .

r - Heat generation density.

4.3 PROCEDURE

In the coupled thermal-electrical analysis, both transient responses have been applied for electrical analysis in step one and thermal analysis in step two where they are sequentially conducted in each time increment. Consequently, the temperature at the integration points of each of the die sets can be obtained dependent on the step time to complete the process. The sample materials used in the simulation were zirconia, alumina and piezoceramic. The simulation analysis was only concentrated on the heating distribution process on the design of

die sets A. Figure 4-1 and Figure 4-2 show the simplified parts used in the Gleeble® 3800 machine for thermal-electrical analysis.

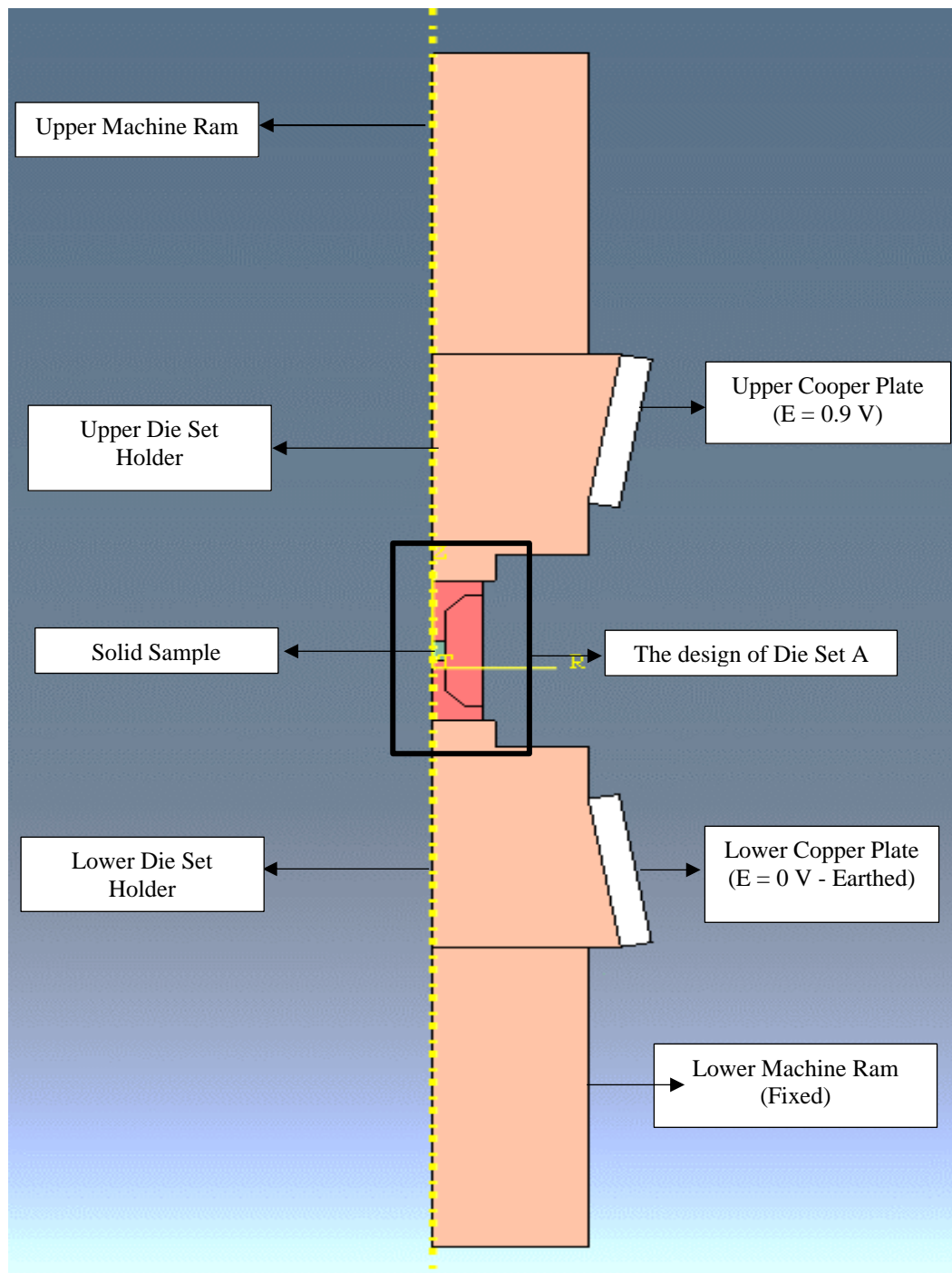


FIGURE 4-1: SIMPLIFIED PARTS USED IN THE SIMULATION OF COUPLED THERMAL-ELECTRICAL ANALYSIS.

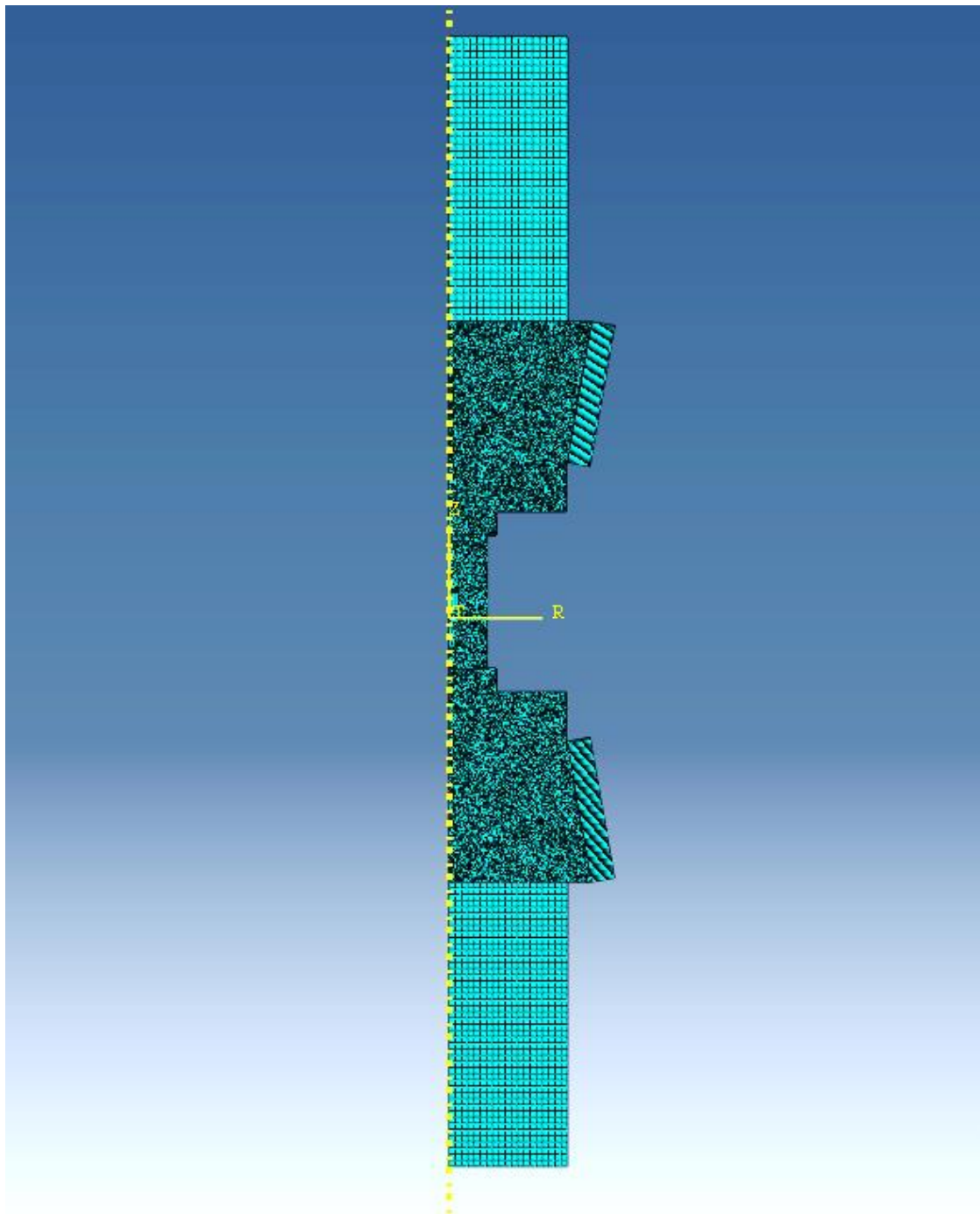


FIGURE 4-2 : SIMPLIFIED PARTS USED IN THE SIMULATION OF COUPLED THERMAL-ELECTRICAL ANALYSIS WITH THE MESH

Table 4-1, shows the physical, thermal and electrical properties of Tungsten carbide, Graphite, zirconia, alumina, piezoceramic and Copper-nickel-silver alloy material used to evaluate the coupled thermal-electrical analysis for the Micro-FAST process. Regarding the boundary conditions, the electrical potential at the first plate was set to 0.9 V and at the second

plate it was assumed to be zero because it was electrically grounded as seen in Figure 4-1. The displacement for the first and second machine ram is assumed to be zero, because the sample is already in the solid condition and the temperature for the cooling condition after the end of step one was set to 30 °C in the machine rams. The emissivity and the film coefficient used were 0.8 and 10 respectively and the ambient temperature was set to 20 °C. The initial in time increment was 1×10^{-5} s and the automatic time increments function provided from Abaqus software was used. After the first step of the electrical and thermal analysis, no electrical load will be exist. Therefore, general transient heat transfer analysis was conducted to save calculation time in the second step. Table 4-2 shows, the global seed of the part that has been used in the simulation of electrical-heat analysis for meshing. The thermal electric element type has been assigned for all the parts.

TABLE 4-1: PROPERTIES OF PART MATERIALS USED IN THE THERMAL-ELECTRICAL ANALYSIS [120].

Part Name	Materials	Density	Specific Heat	Thermal Conductivity	Electric Conductivity
		(kg/m ³)	(J/kg)	(W/m.K)	(S/m)
Upper and Lower Machine Ram	Tungsten Carbide	15,580	292	88	1×10^6
Upper and Lower Die Set Holder					
Die and Punches of Die Set A	Graphite	1,860	771	81	9.1×10^6
Samples	Zirconia	5,600	460	3	1×10^{-13}
	Alumina	3900	850	18	1×10^{-8}
	Piezoceramic	7400	350	1.1	0.0008
Upper and Lower Copper Plate	Copper-Nickel-Silver Alloy	8,720	383	30	2.63×10^6

TABLE 4-2: GLOBAL SEEDS USED FOR MESHING THE SIMULATION OF THERMAL-ELECTRICAL ANALYSIS.

Part Name	Global Seed
Upper and Lower Machine Ram	15×10^{-4}
Upper and Lower Die Sets Holder	3×10^{-4}
Upper and Lower Copper Plate	4×10^{-4}
Die and Punches of Die Sets A	2.5×10^{-4}
Sample	1×10^{-4}

4.4 RESULTS AND DISCUSSION

The section below shows the results and discussions of coupled thermal-electrical analysis for the design of die set A with zirconia, alumina and piezoceramic sample. It consists of two steps which were the electrical and thermal analysis for the first step and, the heat transfer analysis conducted in the second step.

4.4.1 ZIRCONIA

Figure 4-2 shows the heating temperature distribution of the die set A with the Zirconia sample for electrical and thermal analysis in step one and heat transfer analysis on step two. The material used for the punches and body of the die was graphite due to its high efficiency for transmitting heating to the samples. In the design of the die the large transition at the punches of die set A plays a significant role to ensure the high efficiency of the heating during the Micro-FAST process for powder material. It can be seen in Figure 4-3 in step one in the first row (No. 1) to (No. 5) from left to right, the heating started at the surface of the die punch continued to the whole die, but not in the sample. By setting the step time to 60 s, the heating temperature of the punches of the die set could reach 1428.11°C which is in the range of maximum working temperature for graphite. It can be seen from Figure 4-3 and Table 4-3 that

the temperature increased in the die and the punch to 193.785 °C and 175.012 °C respectively in the step time 1.06243 s. Meanwhile, the temperature in the core of the sample was 66.7469 °C due to low conductivity of the Zirconia. Therefore, the temperature of the sample will be increased slower than the die and the punch. By reaching the step time to 60 s, the heating temperature that was recorded at the core and surface of the Zirconia sample was 1346.15°C and 1363.18°C respectively. The illustration of its contour can be seen in Figure 4-3.

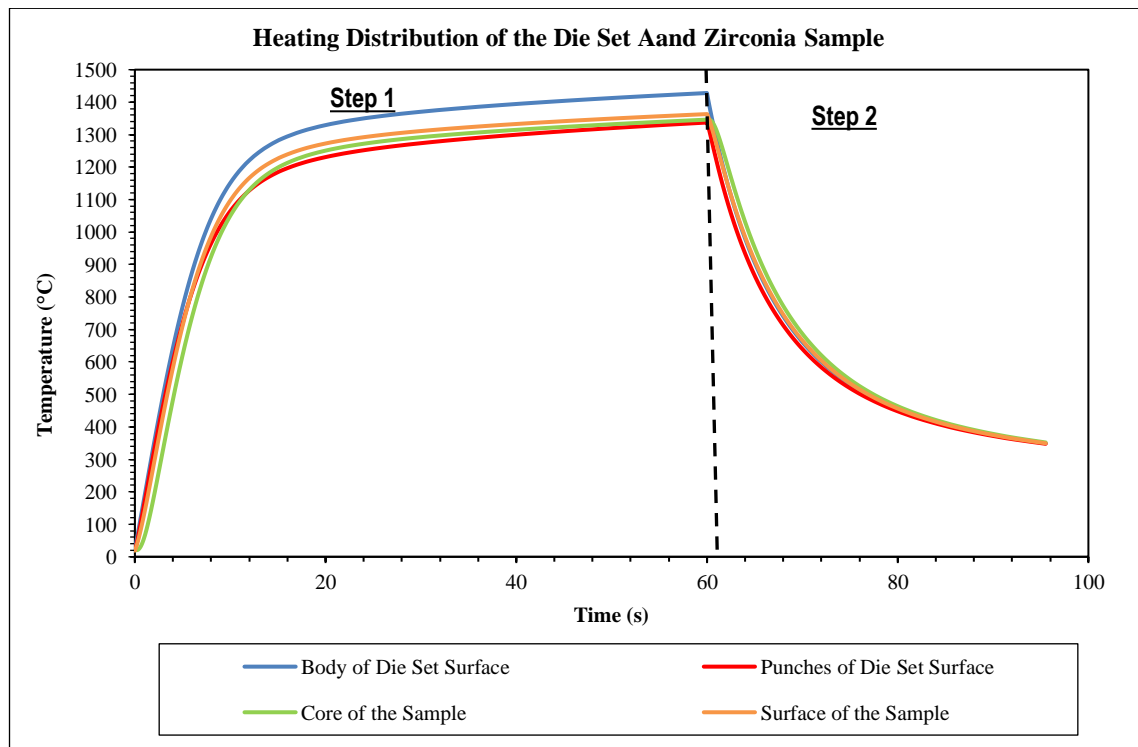


FIGURE 4-3 : HEATING TEMPERATURE DISTRIBUTION OF ZIRCONIA SAMPLE IN DIE SET A FOR STEP 1: ELECTRICAL AND THERMAL ANALYSIS AND STEP 2: HEAT TRANSFER ANALYSIS AFTER THE CURRENT SWITCH OFF

TABLE 4-3: TEMPERATURE DATA FOR CONTOUR OF ZIRCONIA SAMPLE AS PRESENTED IN FIGURE 4-3

Contour No.	Step Time (s)	Body of Die Set Surface (°C)	Punches of Die Set Surface (°C)	Core of the Samples (°C)	Surface of the Sample (°C)
1	0.04097	26.7762	22.8993	20	22.0391
2	1.06243	193.785	175.012	66.7469	144.161
3	2.38672	437.006	382.452	243.524	347.082
4	10.5926	1174.8	1085.96	1077.15	1120.83
5	60	1428.11	1337.22	1346.15	1363.18
6	63.7578	999.28	952.125	1051.87	1004.54
7	67.6833	754.771	726.019	788.095	760.67
8	71.2444	621.822	603.179	643.594	626.044
9	77.1318	494.207	484.594	505.564	496.244
10	95.5226	349.696	347.936	351.99	349.544

During step two of the heat transfer analysis, rapid cooling of the die set A and Zirconia sample has occurred. After consuming 7.6833s, the heating temperature can be dropped on average to 757.39 °C for all the parts of the die set and the Zirconia sample. At the total step time of 95.5226 s, the heat transfer analysis was stopped and the average temperature of the die set and the sample was 349.792 °C. The temperature data for the contour of the die set A and the Zirconia sample are presented in Figure 4-3. As mentioned before, it can clearly be shown that there was a low temperature in the workpiece due to no current going through the ceramic body, however, it is then heated up quickly through the heat transfer from the graphite die.

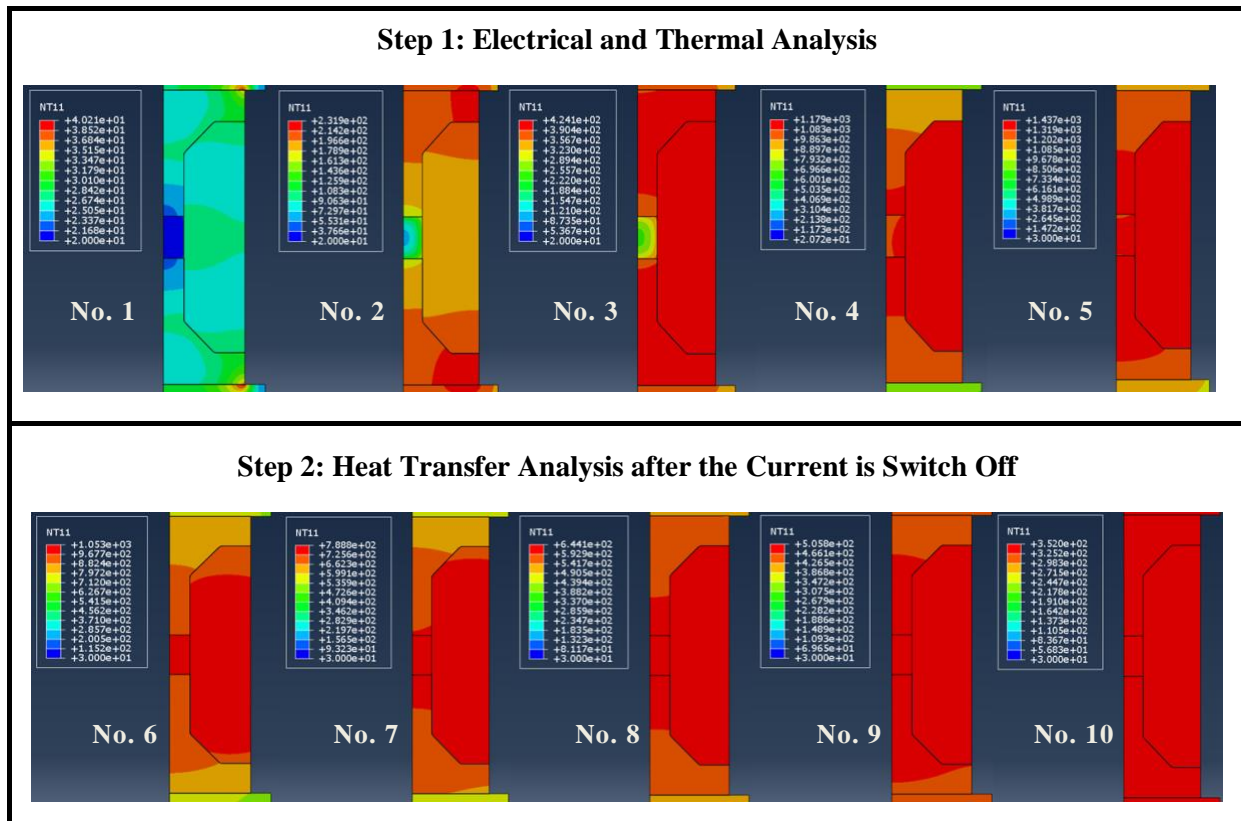


FIGURE 4-4: CONTOUR OF ZIRCONIA SAMPLE FOR HEATING TEMPERATURE DISTRIBUTION AT INTEGRATION POINTS OF STEP ONE AND TWO

4.4.2 ALUMINA

Figure 4-4 shows the heating temperature distribution of the die set A with the Alumina sample for electrical and thermal analysis in step one and heat transfer analysis in step two. The material used for the punches and body of the die was graphite similar to the one used with the Zirconia sample due to the high efficiency of heat transmission to the samples. Based on observation, Figure 4-5 shows that in step one from (No. 1) to (No. 5), the heating started at the surface of the die punch and continued to the whole die, but not in the sample. The temperature increased in the die and the punch to 193.049 °C and 171.882 °C respectively in

the step time 1.06286 s. The temperature in core of the sample was 109.023 °C and in the surface of the sample the temperature was 128.096 °C. It can be seen that the temperature of the Alumina sample is higher than the Zirconia at the same step time which is 1.06 s. This is because that the Alumina has better thermal conductivity than the Zirconia. After that, the temperature distributes steadily in all parts to reach around an average of 1100 °C. By setting the step time to 60 s, the heating temperature of the body of the die set could reach 1427.78°C and the punches of the die set reached 1341.26°C which is in the range of the maximum working temperature for graphite. The heating temperature recorded at the core and surface of the Alumina sample was 1345.71°C and 1352.38°C respectively.

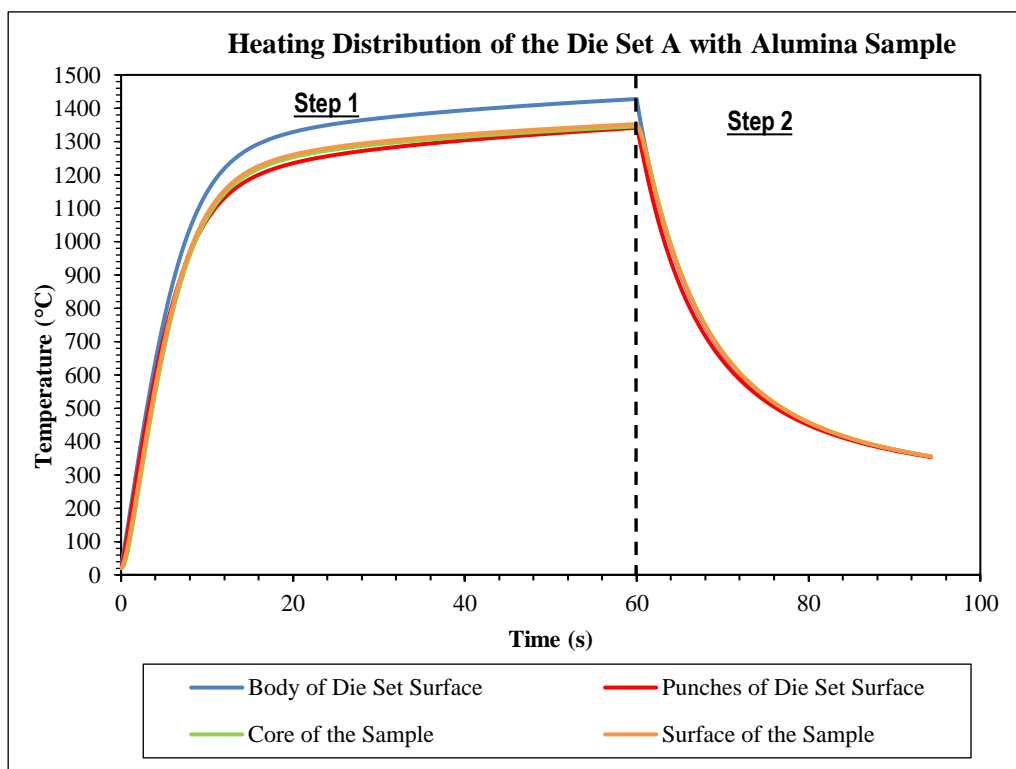


FIGURE 4-5: HEATING TEMPERATURE DISTRIBUTION OF ALUMINA SAMPLE IN DIE SET A FOR STEP 1: ELECTRICAL AND THERMAL ANALYSIS AND STEP 2: HEAT TRANSFER ANALYSIS AFTER THE CURRENT SWITCH OFF

TABLE 4-4: TEMPERATURE DATA FOR CONTOUR OF ALUMINA SAMPLE AS PRESENTED IN FIGURE 4-5

Contour No.	Step Time (s)	Body of Die Set Surface (°C)	Punches of Die Set Surface (°C)	Core of the Samples (°C)	Surface of the Sample (°C)
1	0.04097	26.776	22.8637	20.0233	20.9447
2	1.06286	193.049	171.882	109.023	128.096
3	2.39264	407.706	379.617	311.483	333.311
4	10.9845	1186.95	1101.13	1110.63	1121.67
5	60	1427.78	1341.26	1345.71	1352.38
6	63.7892	997.724	954.567	1008.14	1000.99
7	68.7407	710.157	686.979	717.976	714.404
8	73.2076	570.994	557.351	575.826	573.707
9	77.4032	491.064	482.468	494.039	492.646
10	94.2671	355.035	353.254	355.322	354.888

In the heat transfer analysis in step two, the cooling process of the die set and Alumina sample has occurred. As seen in Figure 4-5 and Table 4-4, after 8.7407s, the temperature was dropped to 710.157°C and 686.979 °C for the die set and the punches respectively. For the Alumina samples the temperature was dropped to an average of 716.19 °C in the core and surface of the sample. At the total step time of 94.2671s, the heat transfer analysis was stopped and the average temperature of the die set and the sample was decreased to 354.625 °C. Figure 4-5 shows the temperature data for the contour of the die set A and the Alumina sample.

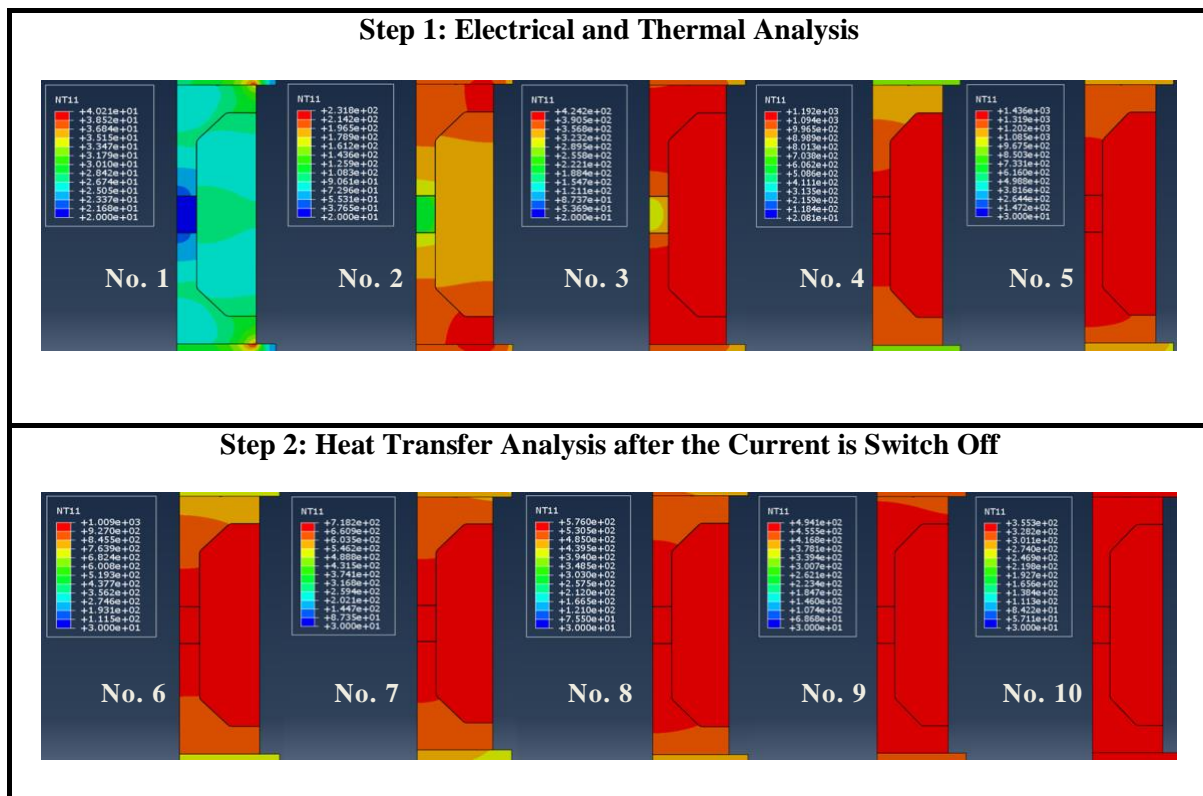


FIGURE 4-6: CONTOUR OF ALUMINA SAMPLE FOR HEATING TEMPERATURE DISTRIBUTION AT INTEGRATION POINTS OF STEP ONE AND TWO

4.4.3 PIEZOCERAMIC (PZT)

Figure 4-6 shows the illustration of the heating temperature distribution of the die set A with the piezoceramic sample for electrical and thermal analysis in first step and heat transfer analysis on the second step. The material used for the punches and body of the die was graphite due to its high efficiency transmitting heating to the samples as mentioned before. As seen in Figure 4-7, the heating in step one (from No. 1 to No. 5) started at the surface of the die punch and continued to the whole die, but not in the sample due to the low thermal conductivity of the piezoceramic. At step time of 1.807s, the temperature reached to 82.105 °C and 78.179 °C in the die and the punch respectively. Meanwhile, the temperature in core of the sample was 28.01°C and in the surface of the sample the temperature was 76.721°C. Compared with Alumina and Zirconia, it can be seen that the temperature of the piezoceramic sample is lower than the Alumina and Zirconia at the same step time which is nearly 1s. This is because the piezoceramic has very low thermal conductivity compared to the Zirconia and Alumina. After consuming 60 s in step time, it can be observed from Figure 4-7 and Table 4-5 that the heating

temperature of the body of the die set could reach $1105.0683^{\circ}\text{C}$. Additionally, the heating temperature of the punches has reached $1037.9744^{\circ}\text{C}$. Both the temperature of the punches and the body of the die sets are in the range of maximum working temperature for graphite. Moreover, the heating temperature at the core and surface of the piezoceramic sample was 1070.721°C and 1012.39°C respectively.

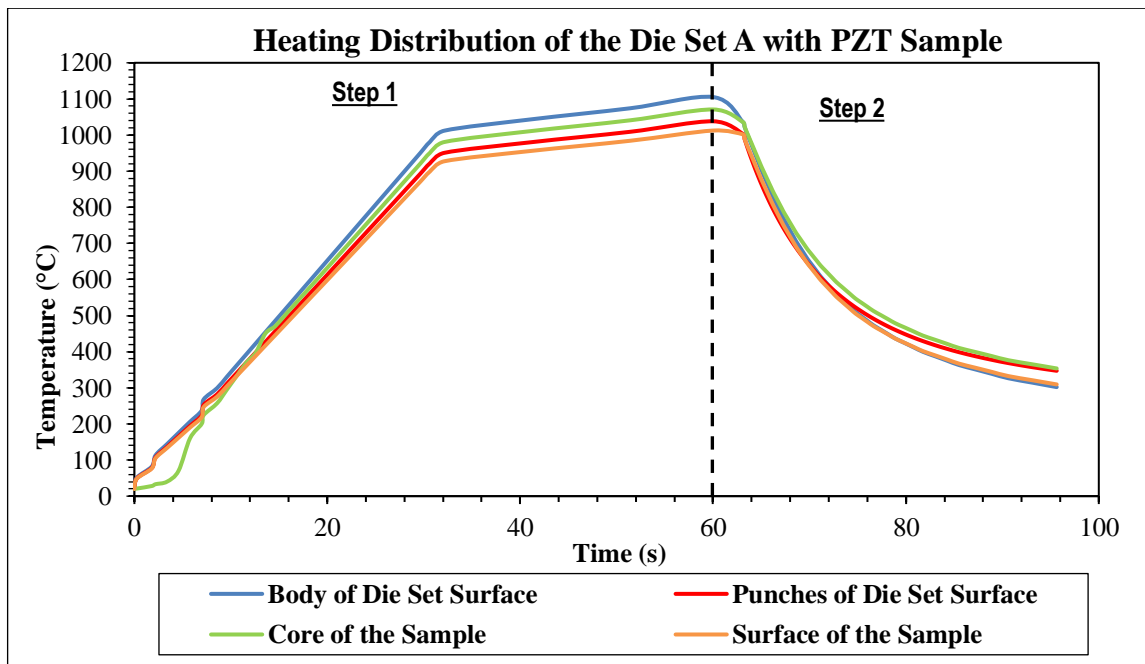


FIGURE 4-7: HEATING TEMPERATURE DISTRIBUTION OF PIEZOCERAMIC SAMPLE IN DIE SET A FOR STEP 1: ELECTRICAL AND THERMAL ANALYSIS AND STEP 2: HEAT TRANSFER ANALYSIS AFTER THE CURRENT SWITCH OFF

Through step two of the heat transfer analysis, the rapid cooling of the die set and piezoceramic sample has occurred. In the 67.8559s, the heating temperature dropped to 742.22°C for the die set. Furthermore, the temperature for the punch reached 717.948°C at the same step time. The temperature in the core of the sample was 762.93°C and the surface of the sample the temperature was 724.76°C . At the total step time of 95.6376 s, the heat transfer analysis was stopped and the average temperature of the die set was 324.528°C and on the surface of the sample, the temperature dropped to 309.32°C and the sample reached 353.61°C .

TABLE 4-5: TEMPERATURE DATA FOR CONTOUR OF ALUMINA SAMPLE AS PRESENTED IN FIGURE 4-7

Contour No.	Step Time (s)	Body of Die Set Surface (°C)	Punches of Die Set Surface (°C)	Core of the Samples (°C)	Surface of the Sample (°C)
1	0.04097	26.7764	22.9226	20	22.7621
2	1.807	82.105	78.179	28	76.721
3	3.38388	136.349	140.0824	40.0824	133.4282
4	12.58264	423.0925	398.111	410.2678	388.6115
5	60	1105.0683	1037.9744	1070.721	1012.3929
6	65.8401	791.14	760.572	808.41	770.9
7	67.8559	742.22	717.948	762.93	724.76
8	74.2825	522.08	532.013	558.27	517.04
9	79.8542	456.502	449.115	483.685	458.783
10	95.6376	301.94	347.116	353.61	309.32

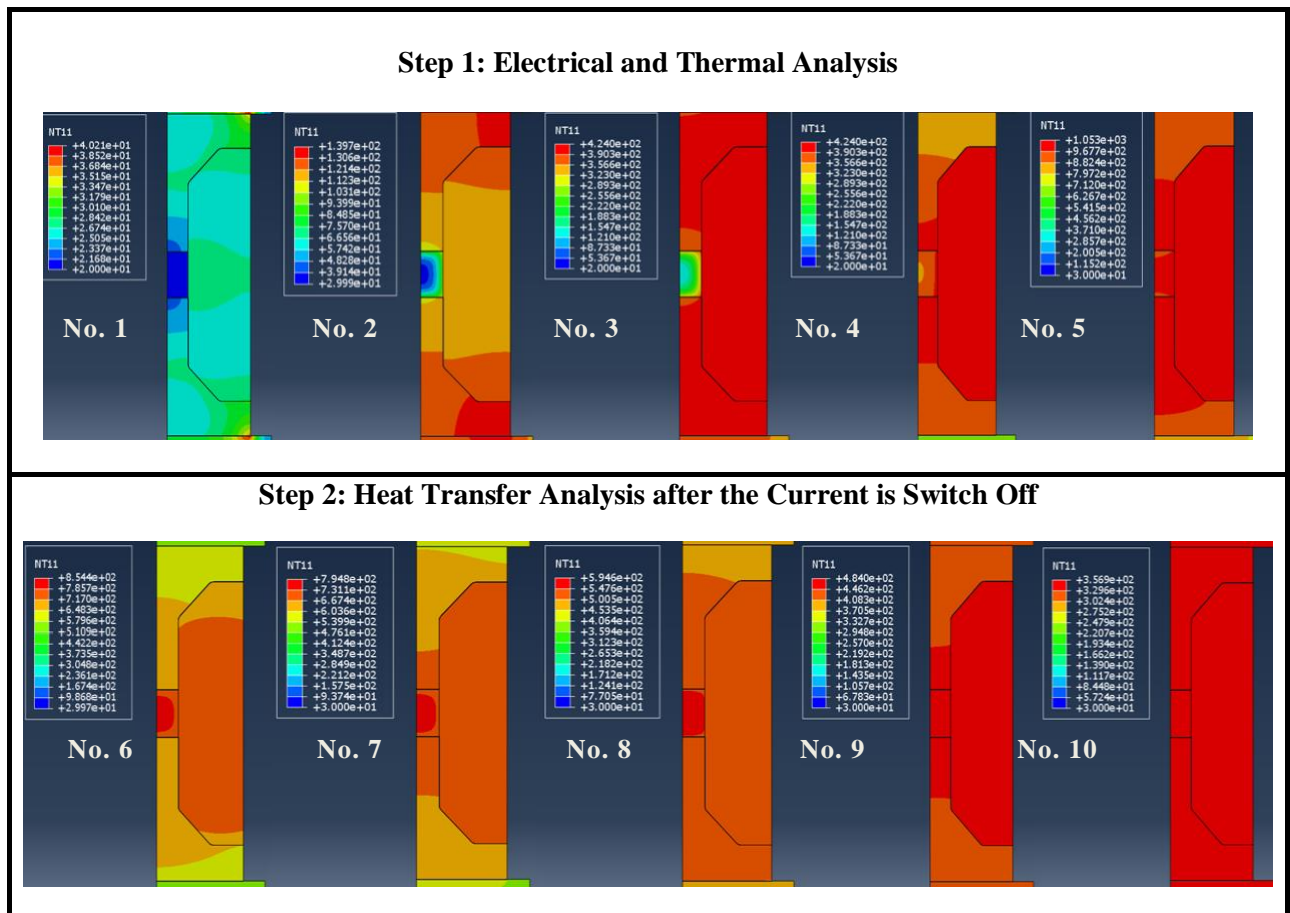


FIGURE 4-8: CONTOUR OF PIEZOCERAMIC SAMPLE FOR HEATING TEMPERATURE DISTRIBUTION AT INTEGRATION POINTS OF STEP ONE AND TWO

4.5 SUMMARY OF THE CHAPTER

In this chapter, a simulation of the electrical-heat analysis has been done on zirconia, alumina and piezoceramic. The simulation has been done using the design of die set A as shown in Table 3-2. It can be shown that the die set A has promising results concerning the heating distribution towards its parts. In step one which was electrical analysis involving the electrical potential, the die set A has shown good and rapid heating temperature distribution. The information collected from the FE simulation was useful for the experimental process in order to have the proper information on how the heating distribution happens in the die sets used in the Micro-FAST process and to create suitable parameters for the experiments.

Figure 4-9 shows the comparison of the results between the three materials (zirconia, alumina and piezoceramic) for the simulation of the electrical-heat analysis. It can be seen that all simulation worked properly and the results showed a promising heating distribution through all parts in step one at 60 seconds. However, the charts for the piezoceramic showed some slight differences when comparing them with the alumina and zirconia charts. The reason behind that is the differences in the properties of zirconia, alumina and piezoceramic. The thermal conductivity of the piezoceramic is very low compared to zirconia and alumina. That is why the piezoceramic reach nearly 1100 °C in 60 seconds.

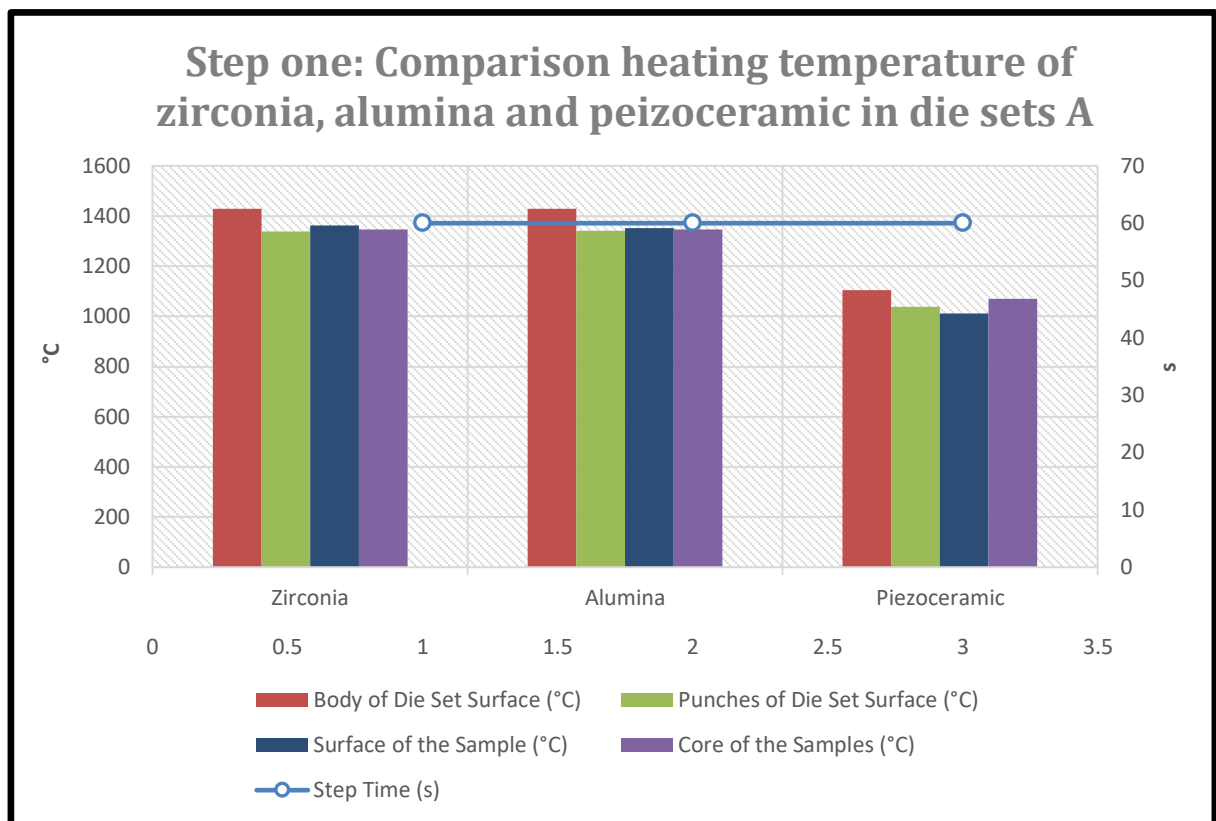


FIGURE 4-9: COMPARISON HEATING TEMPERATURE OF ZIRCONIA, ALUMINA AND PEIZOCERAMIC IN DIE SETS A FOR ELECTRICAL ANALYSIS IN STEP ONE

Meanwhile, in the step two of the thermal analysis which involved of the transient heat transfers shows that the alumina has the fastest cooling compared to the zirconia and piezoceramic as presented in Figure 4-10. The simulation shows that the alumina took 94 seconds to cool down, meanwhile the zirconia and the piezoceramic took nearly 96 seconds. The charts below shows that the piezoceramic has fluctuated results among all parts when during the cooling process. This is because of the material properties of the piezoceramic and one of these properties is the thermal conductivity.

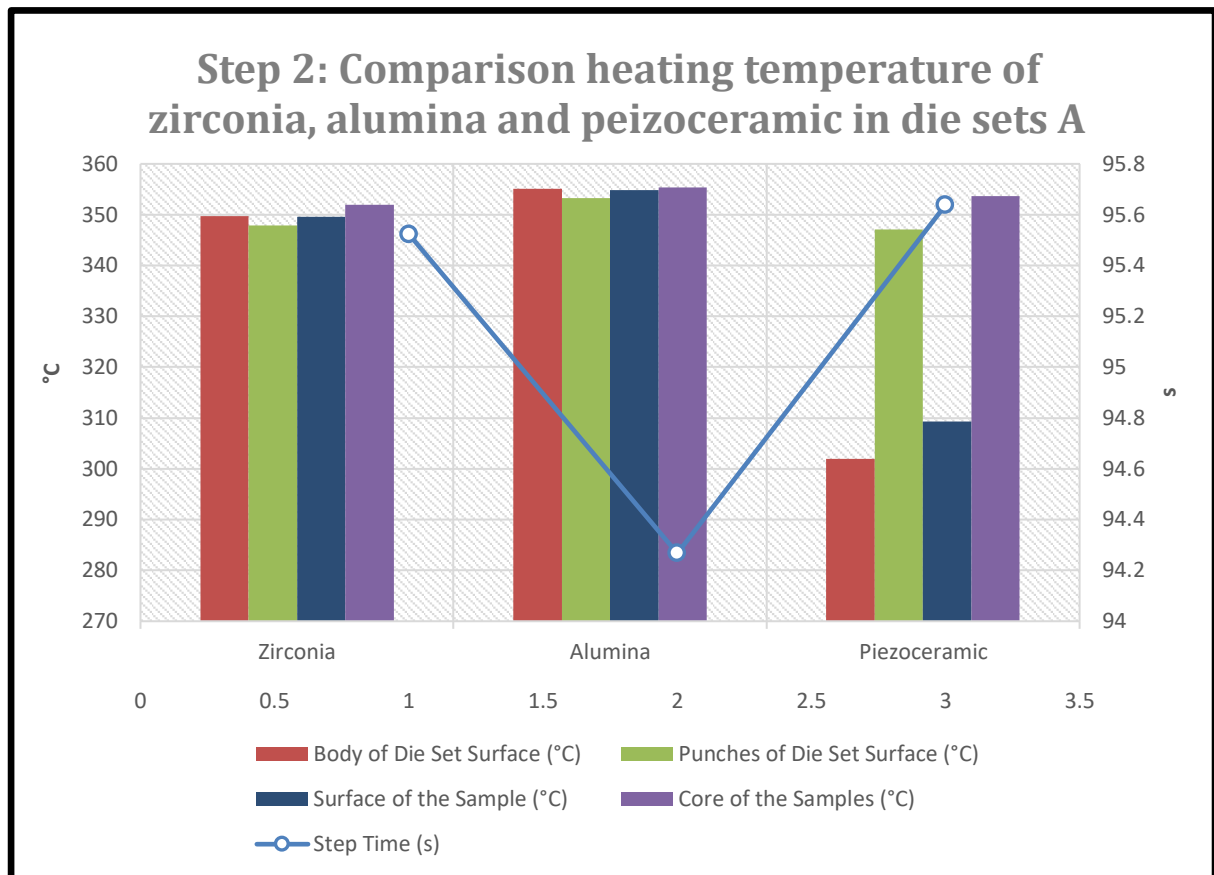


FIGURE 4-10: COMPARISON HEATING TEMPERATURE OF ZIRCONIA, ALUMINA AND PEIZOCERAMIC IN DIE SETS A FOR ELECTRICAL AND THERMAL ANALYSIS IN STEP 2

5

RESULTS AND DISCUSSION

5.1 INTRODUCTION

In the Micro-FAST process experiments, three kinds of powders were used as raw materials, these were alumina, zirconia and piezoceramic. The experiment was conducted using a Gleeble[®] 3800 which is a thermal mechanical machine from Dynamic Systems Inc. USA. The parameters that have been used in the experiments, such as pressure, heating temperature, heating rate and holding time were controlled automatically using a computer-controlled system (QuickSim[™] software). The electrical field produced by the Gleeble[®] 3800 machine has a high current (3000~30000 A) and low voltage (3~10 V). It was also capable of controlling the accuracy of the temperature up to ± 3 °C. The die sets used in the experiment were of the optimised design shown in the previous chapter and punches and dies were made from graphite (grade: Mersin 2333). The graphite material was selected because of the value of the thermal expansion coefficient of the punches and die must be less than the powder material being tested. This will prevent any traps and sticking between the punches, die and samples during the ejection process. Moreover, by using graphite for the die set material, a higher sintering temperature can be utilised up to its maximum service temperature of 2,700 °C.

After the powder material had been weighed, it was carefully poured into the die sets. Then, the die set with the powder material was placed into the chamber of Gleeble[®] 3800 machine with the thermocouple as in Figure 5-1. After that, the die set with the powder material was heated promptly to a specific sintering temperature in the vacuum. The electrical current was passed through the die set with powder material inside it and at the same time pressure

was applied to the upper and lower die punches. The sample was then ejected out from the die set. The formed samples from the experiments were analysed using several apparatus. For their relative density, Sartorius YDK03 apparatus was used, and for the surface of sample microstructure, the scanning electron microscope machine (SEM/EDS – HITACHI SU-6600) was used. Moreover, a chemical element weight percentage test has been performed at the centre and edge of the sample parts using an energy dispersive spectroscopy (EDS) facility. A nano-hardness (NanoTest Vantage) test was also done at the sintered neck of the zirconia sample. All the results and discussions regarding the experimental study have been described in detail to obtain conclusive findings of reliability for the overall processes and the die sets used for producing an excellent quality of micro-components. All pictures in this chapter has been taken by the main author of this work in the Imperial College London between 2014 and 2017.

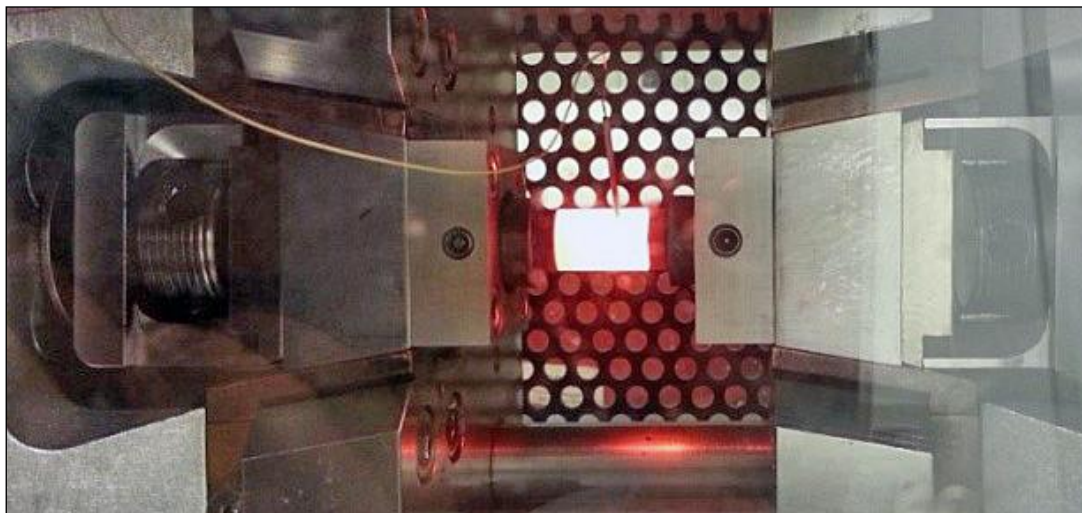


FIGURE 5-1: DIE SET WITH POWDER MATERIAL INSIDE IT DURING THE EXPERIMENT USING GLEEBLE 3800 MACHINE.

5.2 POWDER MATERIALS AND EQUIPMENT

In this section, a detailed description of equipment and powder materials used in the Micro-FAST process has been made. It consists of the Gleeble[®] 3800 machine, density determination

kit from Sartorius YDK03, Tungsten Filament Scanning Electron Microscope (W-SEM) from HITACHI S-3700 (2010), and NanoTest Vantage System hardness tester. Meanwhile, powder materials used in the experiment consisted of alumina, zirconia and piezoceramic.

5.2.1 GLEEBLE[®] 3800 MACHINE

Gleeble[®] 3800 from Dynamic Systems Inc. was designed specially to offer increased capabilities for thermal deformation and was equipped with a heavy-duty mechanical system and high-speed servo valves for quick response. See Figure 5-2. The Gleeble[®] 3800 is capable of applying as much as 20 tonnes of static force in compression and up to 10 tonnes of force in tension. Furthermore, the rates of stroke displacement can be programmed to reach 2,000 mm/s as illustrated in Table 5-2. Additionally, Gleeble[®] 3800 systems offer a high-speed thermal system for heating specimens. It has an ability to reproduce the broad range of thermal profiles that materials undergo in actual processes which were critical to the success of thermal-mechanical testing and physical simulation. Gleeble[®] 3800 systems have both high heating and cooling rates to accomplish the assigned task. The heating and quenching rate could operate up to 10,000 °C/s respectively as shown in Table 5-2 [132].

The Gleeble[®] 3800 machine also has an ability to control the temperature uniformity with the thermal gradients within the test specimen. In this condition, thermal gradients are dependent upon the material, thermal and electrical resistivity, surface-to-volume ratio, specimen length, total cross section, free span and grips. In the experiment of the Micro-FAST process, each of the parameters used such as pressure, heating temperature, heating rate and holding time, was controlled automatically using a computer-controlled system called QuickSim[™] software. In terms of the electrical-field produced by the Gleeble[®] 3800 machine, it has high current in the range of 3,000~30,000 A with a low voltage which was 3 and 10 voltage. Table 5-1 and Table 5-2 show the general specification of the thermal and mechanical system for the Gleeble[®] 3800 machine [132].

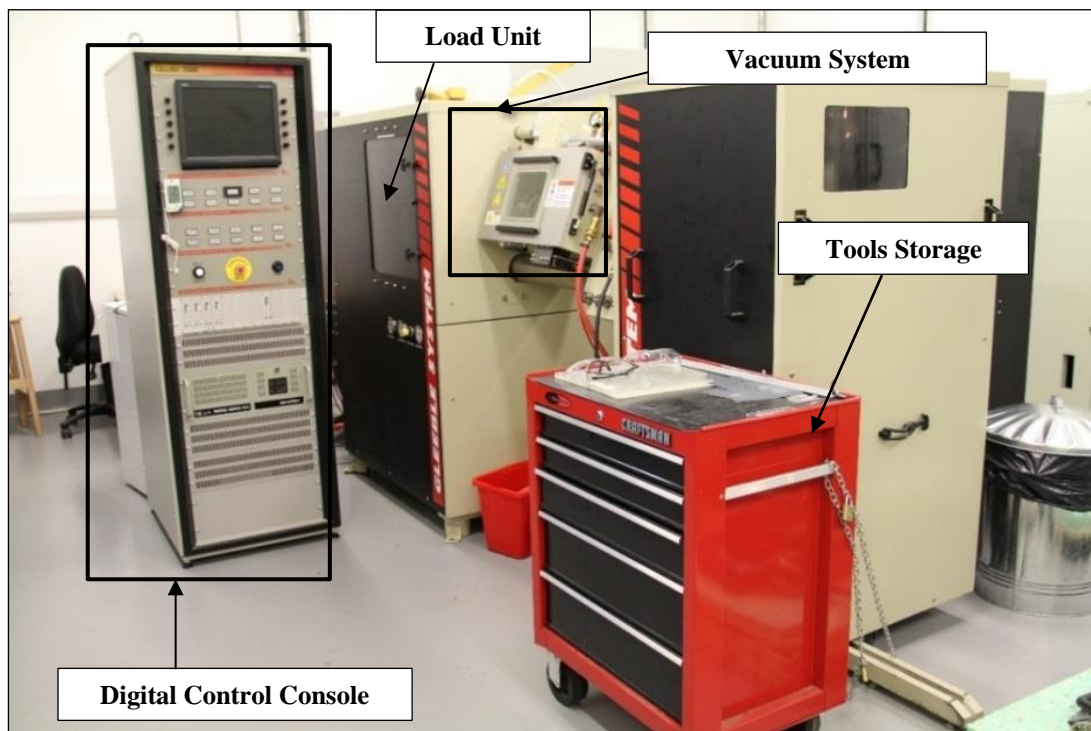


FIGURE 5-2: GLEEBLE® 3800 MACHINE.

:

TABLE 5-1: GENERAL SPECIFICATION OF THE THERMAL SYSTEM FOR GLEEBLE® 3800 MACHINE [132].

Type of Heating System	Direct resistance with closed-loop control.
Temperature Controller	Digital closed-loop control using 16-bit analog-to-digital converter and 16/32-bit digital signal processor.
Temperature Range	Room temperature up to 1700°C based on choice of thermocouples.
Response Rate	10,000°C/s.
Thermocouple Sampling Rate	120 times per second at 60 Hz (100 times per second at 50 Hz).
Resolution	One degree (°C or F).
Maximum Number of Simultaneous Thermal Channels	Four thermocouple channels or three thermocouple channels and one pyrometer channel. (Pyrometer system is optional).
Accuracy of Control	± One degree Celsius (in steady state).
Accuracy of Measurement	± One percent of temperature plus the accuracy of the thermocouple wire (steady state).

TABLE 5-2: GENERAL SPECIFICATION OF THE MECHANICAL SYSTEMS FOR GLEEBLE® 3800 MACHINE [132].

Test Frame	Horizontal type with dual 99 mm diameter columns.
Mechanical System	Closed-loop hydraulic servo control.
Maximum Static Force/Load in Compression	20,000 kg (~ 44,000 lbs.) (196 kN).
Maximum Static Force/Load in Tension	10,000 kg (~ 22,000 lbs.) (98 kN).
Maximum Stroke Rate (No Load)	2,000 mm/s in tension or compression.
Minimum Stroke Rate (Varies with Configuration)	0.001 mm/s in tension or compression.
Maximum Stroke Distance	125 mm.
Maximum Number of Compression Stroke	10 strokes (hits) over 20 mm distance.
Force Measurement Accuracy	± 1.0% of full scale.
Stroke Measurement Accuracy	± 0.5% of full scale.
Force Measurement Resolution	± 1 kg.
Stroke Measurement Resolution	0.002 mm.
C-Strain Measurement Resolution	0.002 mm (Standard).

5.2.2 RELATIVE DENSITY

The results obtained from the experiment were analysed for their relative density using a density determination kit (Sartorius YDK03). During the testing, the Archimedean principle was applied for determining the density of a sample with the Sartorius YDK03 measuring device. A sample immersed in a liquid was subjected to the force of buoyancy. The value of this force was the same as the weight of the liquid displaced by the volume of the sample. By using hydrostatic balance from a density determination kit (Sartorius YDK03) this enables a sample to be weighed in air as well as in water in order to determine its density if the density of the liquid causing buoyancy was known as presented in equation (5.2-1).

$$\rho = \frac{W(a) \cdot \rho(fl)}{W(a) - W(fl)} \quad (5.2-1)$$

Where:

ρ	-	Specific gravity of the sample.		$W(a)$	-	Weight of the solid in air.
$\rho(fl)$	-	Density of the liquid.		$W(fl)$	-	Weight of the solid in liquid.

Or determine the density of liquid if the volume of the immersed sample was known as presented in equation (5.2-2).

$$\rho(fl) = \frac{G}{V} \quad (5.2-2)$$

Where:

- G - Buoyancy of the immersed sample.
 V - Volume of the solid.

The relative density of the sample from the Mirco-FAST process was determined by making a ratio percentage of the calculated density of the sample from equation (5.2-1) to the reference theoretical density of the sample that been tested. Figure 5-3 shows the density determination kit (Sartorius YDK03)

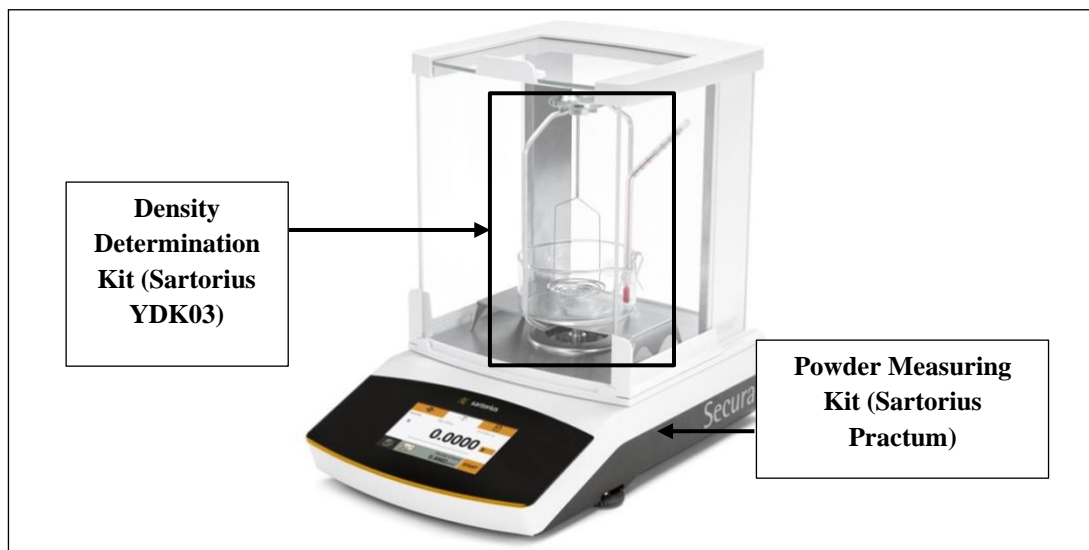


FIGURE 5-3: DENSITY DETERMINATION KIT (SARTORIUS YDK03) AND POWDER MEASURING SCALE (SARTORIUS PRACTUM).

5.2.3 SCANNING ELECTRON MICROSCOPE (SEM)

The Scanning Electron Microscope from HITACHI S-3700N as shown in Figure 5-4 is used to detect imaging microstructures of the sample's surface fracture. Using the microstructure images, will help to show the deformation and breakage of the powder material particle after the densification mechanism process ends during the Micro-FAST process. The Scanning Electron Microscope (W-SEM) is also suitable for imaging metallic, ceramics, polymers, ceramic matrix composites (CMC), metal matrix composites (MMC), carbon fibre composite (CFC) and fibrous materials [133].

A chemical element weight percentage test was also performed at the centre and the edge of the sample by using an Energy Dispersive Spectroscopy (EDS) facility (Oxford Inca 350 with 80 mm X-Max detector) which was built in a W-SEM machine to allow elemental analyses of materials. This process has been done to monitor the percentage of carbon element that was absent on the inside and the edge of the sample after a cleaning process due to the usage of the graphite die set [133].

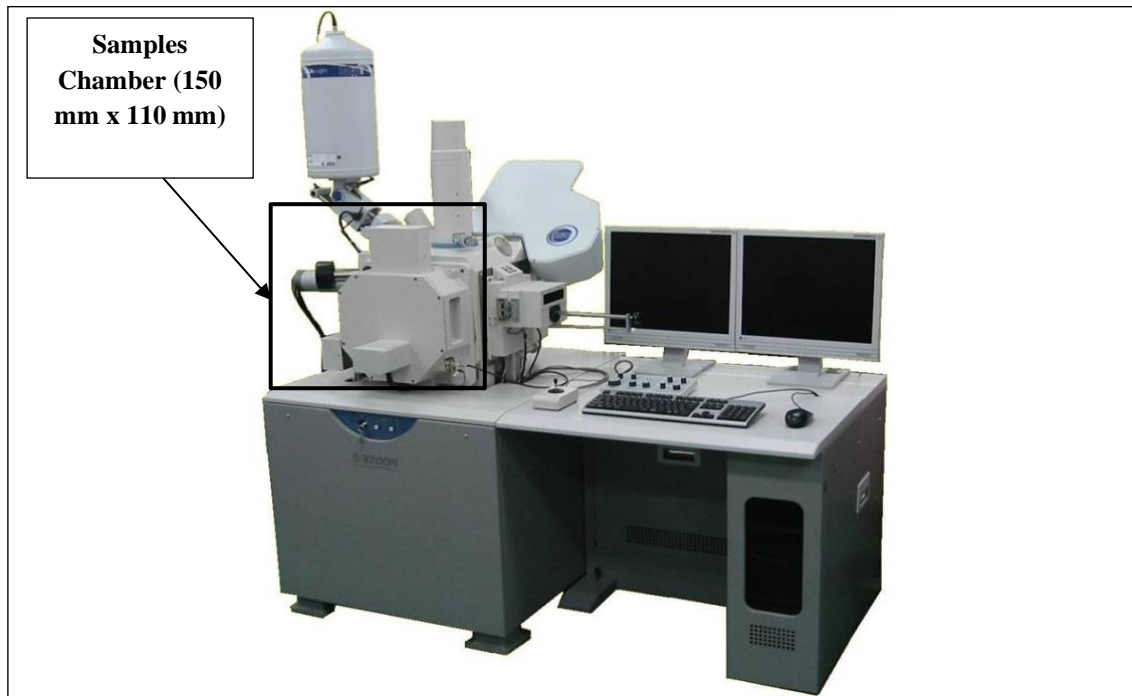


FIGURE 5-4: SCANNING ELECTRON MICROSCOPE (W-SEM) FROM HITACHI S-3700N [133].

5.2.4 HARDNESS TEST

The nano-hardness test for the Micro-FAST process was done by using the Nano Test Vantage system (Nano-indentation) as shown in Figure 5-5 which consists of a variety of nano-mechanical testing methods in one instrument. All relevant requirements for the nano-indentation standard including ISO14577 and ASTM E2546-07 have been fulfilled by the NanoTest Vantage. Regarding the operating principle of the NanoTest Vantage system for micro-samples, it uses the application of electromagnetic force and capacitive depth measurement to measure the elastic and plastic characteristics of materials at nano-scale. Based on this capability it fits with the micro-sample that has been produced in the electrical-field activated sintering and forming process where the interest area that needs to be indented can be targeted [134].

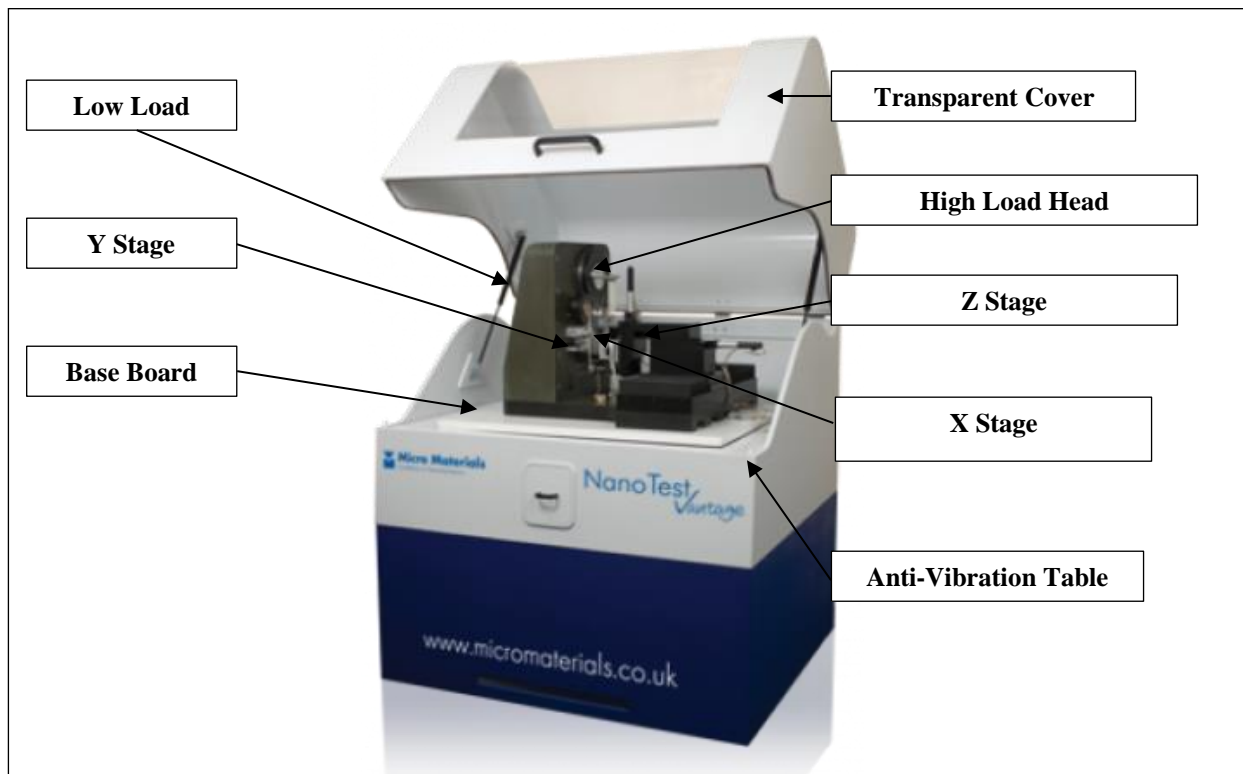


FIGURE 5-5: NANOTEST VANTAGE SYSTEM [134].

5.2.5 POWDER MATERIALS

Table 5-3 shows that three kinds of powder were used as raw materials which were zirconia, alumina and piezoceramic for Micro-FST process using Gleeble[®] 3800 machine. For Zirconia, three different types were examined. The first one is Ytria Partially Stabilized Zirconia ($ZrO_2 + 3 \text{ mol\% yttria}$) ($3Y-ZrO_2$) the average particle size of powder materials was $6.5 \mu\text{m}$ and has 5.285 g/cm^3 for theoretical density. The other type of Zirconia is the Magnesia Partially Stabilized Zirconia (MSZ) and the starting particle size was below $5 \mu\text{m}$ with spray dried granulates that were sieved to between $40\text{-}80 \mu\text{m}$ and a theoretical density of 5.82 g/cm^3 . The Third Zirconia powder was MSZ(#) with 5 wt% organic additives or organic binders to improve the forming process, and the theoretical density for this one was 5.72 g/cm . The

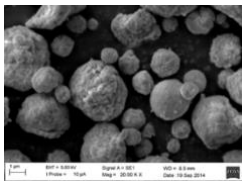
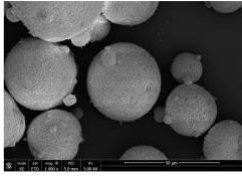
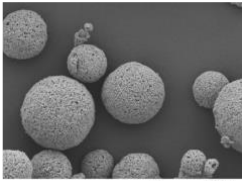
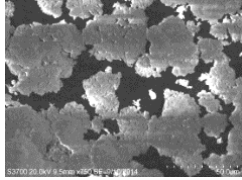
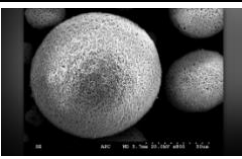
starting particle size for MSZ(#) was below 2 μm with spray dried granulates that were sieved between 40-80 μm . The organic materials burn out in two steps. Around 2.2 wt% organic material can be removed at 200°C and the other 2.6 wt% can removed around 380°C.

Meanwhile, for Alumina powder material Al_2O_3 powder with an average particle size of 0.18 μm and purity of 99.9% and the theoretical bulk density for the used powder is 3.95 g/cm^3 .

The piezoceramic used for this experiment has a particle size of 6.5 and the theoretical density for the used powder is 7.4 g/cm^3 .

For the experiment of the Micro-FAST process, a graphite die set was used due to the sintering temperature of the ceramic powders being in the range of 1000 to 1,400 °C. Since the melting temperature of graphite is around 3,800 °C it is suitable for the die and punches and of being used with the assigned sintering temperature.

TABLE 5-3: THE CLASSIFICATION OF FOR ZIRCONIA, ALUMINA AND PIEZOCERAMIC POWDERS USED IN MICRO-FAST PROCESS WHICH PERFORMED BY GLEEBLE® 3800 MACHINE.

Powder Materials	Average Particles Size (μm)	Theory Density (g/cm^3)	Image of Particles Agglomerates
3Y-ZrO ₂	6.5	5.285	
MSZ	40 and 80	5.82	
MSZ(#)	< 2 μm	5.72	
Al ₂ O ₃	0.18	3.95	
PZT	6.5	7.4	

5.3 PARAMETERS OF EXPERIMENTS

In this section the parameters of the experiments that have been used for the electrical-field Micro-FAST process have been described. The crucial parameters that needed to be configured during the experiment were the applied pressure, the heating temperature for the sintering stage, the heating rate and the holding time respectively. All the stated parameters contributed to the densification of the samples. The development of the experiment parameters were made by using the guideline parameters obtained from the literature review such as resistance heating and spark plasma sintering that has been performed concerning zirconia, alumina and piezoceramic materials. In addition to that, the development of the experiment parameters continued with the trial and error method. This has been implemented to find the optimum parameters to produce an excellent density of samples with high efficiency of the process.

5.3.1 ZIRCONIA

As has been mentioned in the literature review, the range of the temperature used during the experiment on previous electrical field sintering applications for the zirconia was in the range of 1050 to 1,500 °C with the sintering time of 6 to 180 minutes and a capability of producing the sample with the relative density of 90 to 99%. The heating rate of the process was also limited to 50 to 600 °C/min and the pressure that has been applied was in the range of 25 to 100 MPa. However, some previous studies suggested that organic binders will improve the sintering and the quality of the sintered samples. Zirconia has been sintered with binders at 1,500 °C for 2 hours under several pressures. Therefore, proposed experimental parameters for the Micro-FAST process for Ytria Partially Stabilized Zirconia and Magnesia Partially Stabilized Zirconia (MSZ) with and without additives have been illustrated in Table 5-4, Table 5-5 and Table 5-6.

TABLE 5-4: EXPERIMENT PARAMETERS FOR 3Y-ZRO2 POWDER MATERIAL PERFORMED BY GLEEBLE® 3800 MACHINE FOR MICRO-FAST PROCESS

Parameter No.	Units	3YZro2-1	3YZro2-2	3YZro2-3	3YZro2-4
Powder Weight	g	0.2657	0.2657	0.2657	0.2657
Pressure	MPa	75	75	125	125
Force	kN	0.9	0.9	1.6	1.6
Initial Temp. (Room Temp.)	°C	20	20	20	20
First Heating Rate	°C/s	20	20	20	20
First Heating Temp.	°C	200	200	200	200
First Heating Time	s	9.0	9.0	9.0	9.0
First Holding Time	s	30.0	30.0	30.0	30.0
Second Heating Rate	°C/s	50	50	50	25
Second Heating Temp.	°C	1200	1300	1300	1300
Second Heating Time	s	20.0	22.0	22.0	44.0
Second Holding Time	s	240.0	240.0	120.0	120.0
Cooling Rate	°C/s	10	10	10	10
Final Temp. (Room Temp.)	°C	20	20	20	20
Cooling Time	s	118.0	128.0	128.0	128.0
Process Total Time	s	417.0	429.0	309.0	331.0

TABLE 5-5: EXPERIMENT PARAMETERS FOR MSZ POWDER MATERIAL PERFORMED BY GLEEBLE® 3800 MACHINE FOR MICRO-FAST PROCESS

Parameter No.	Units	MSZ-1	MSZ- 2	MSZ- 3	MSZ- 4
Powder Weight	g	0.2915	0.2915	0.2915	0.0366
Pressure	MPa	125	125	125	125
Force	kN	1.6	1.6	1.6	0.4
Initial Temp. (Room Temp.)	°C	20	20	20	20
First Heating Rate	°C/s	20	20	20	20
First Heating Temp.	°C	200	200	200	200
First Heating Time	s	9.0	9.0	9.0	9.0
First Holding Time	s	30.0	30.0	30.0	30.0
Second Heating Rate	°C/s	100	25	50	25
Second Heating Temp.	°C	1300	1300	1300	1400
Second Heating Time	s	11.00	44.00	44.00	48.00
Second Holding Time	s	120.0	120.0	180.0	90.0
Cooling Rate	°C/s	10	10	10	10
Final Temp. (Room Temp.)	°C	20	20	20	20
Cooling Time	s	128.0	128.0	128.0	138.0
Process Total Time	s	298.0	331.0	391.0	315.0

TABLE 5-6: EXPERIMENT PARAMETERS FOR MSZ (#) POWDER MATERIAL PERFORMED BY GLEEBLE® 3800 MACHINE FOR MICRO-FAST PROCESS

Parameter No.	Units	MSZ(#)-1	MSZ(#)-2	MSZ(#)-3	MSZ(#)-4
Powder Weight	g	0.2875	0.2875	0.2875	0.2875
First Pressure	MPa	75	75	75	75
First Force	kN	0.9	0.9	0.9	0.9
Initial Temp. (Room Temp.)	°C	20	20	20	20
First Heating Rate	°C/s	20	20	20	20
First Heating Temp.	°C	200	200	200	200
First Heating Time	s	9.0	9.0	9.0	9.0
First Holding Time	s	100.0	100.0	100.0	100.0
Second Pressure	MPa	75	75	75	75
Second Force	kN	0.9	0.9	0.9	0.9
Second Heating Rate	°C/s	20	20	20	20
Second Heating Temp.	°C	380	380	380	380
Second Heating Time	s	9.0	9.0	9.0	9.0
Second Holding Time	s	100.0	100.0	100.0	100.0
Third Pressure	MPa	125	125	125	125
Third Force	kN	1.6	1.6	1.6	1.6
Third Heating Rate	°C/s	25	25	50	100
Third Heating Temp.	°C	1300	1300	1300	1300
Third Heating Time	s	36.80	36.80	18.40	9.20
Third Holding Time	s	5.0	60.0	120.0	120.0
Cooling Rate	°C/s	10	10	10	10
Final Temp. (Room Temp.)	°C	20	20	20	20
Cooling Time	s	138.0	128.0	128.0	128.0
Process Total Time	s	387.8	442.8	484.4	475.2

5.3.2 ALUMINA

Based on previous studies, which showed the range of the temperature used during the experiment on previous electrical field sintering application for Alumina 83 to 99% was in the range of 1200 to 1,500 °C using the slow heating rate of 20 °C/min. The holding time during the sintering was in the range of 30 minutes with the applied pressure of 30 to 40 MPa. Therefore, suggested parameters for the Micro-FAST process have been shown in Table 5-7.

TABLE 5-7: EXPERIMENT PARAMETERS FOR ALUMINA POWDER MATERIAL PERFORMED BY GLEEBLE® 3800 MACHINE FOR MICRO-FAST PROCESS.

Parameter No.	Units	Al ₂ O ₃ -1	Al ₂ O ₃ -2	Al ₂ O ₃ -3	Al ₂ O ₃ -4
Powder Weight	g	0.0248	0.0248	0.0248	0.0248
Pressure	MPa	75	75	75	125
Force	kN	0.2	0.2	0.2	0.4
Initial Temp. (Room Temp.)	°C	20	20	20	20
First Heating Rate	°C/s	20	20	20	20
First Heating Temp.	°C	200	200	200	200
First Heating Time	s	9.0	9.0	9.0	9.0
First Holding Time	s	30.0	30.0	30.0	30.0
Second Heating Rate	°C/s	50	50	50	50
Second Heating Temp.	°C	1200	1300	1200	1300
Second Heating Time	s	20.0	22.0	20.0	22.0
Second Holding Time	s	240.0	240.0	360.0	240.0
Cooling Rate	°C/s	10	10	10	10
Final Temp. (Room Temp.)	°C	20	20	20	20
Cooling Time	s	118.0	128.0	118.0	128.0
Process Total Time	s	417.0	429.0	537.0	429.0

5.3.3 PIEZOCERAMIC (PZT)

Based on previous studies the range of the temperature used during the experiment on previous electrical field sintering application for piezoceramic 83.7% to 99% was in the range of 950 to 1,200 °C using a heating rate of 100 °C/min. The holding time during the sintering was in the range up to 40 minutes with the applied pressure of 50 to 100 MPa. Table 5-8 shows the parameters used for forming the piezoceramic using the Micro-FAST process.

TABLE 5-8: EXPERIMENT PARAMETERS FOR PIEZOCERAMIC POWDER MATERIAL PERFORMED BY GLEEBLE® 3800 MACHINE FOR MICRO-FAST PROCESS

Parameter No.	Units	PZT-1	PZT-2	PZT-3	PZT-4
Powder Weight	g	0.3833	0.3833	0.1021	0.1021
Pressure	MPa	125	125	125	125
Force	kN	1.6	1.6	1.1	1.1
Initial Temp. (Room Temp.)	°C	20	20	20	20
First Heating Rate	°C/s	20	20	20	20
First Heating Temp.	°C	200	200	200	200
First Heating Time	s	9.0	9.0	9.0	9.0
First Holding Time	s	30.0	30.0	30.0	30.0
Second Heating Rate	°C/s	50	50	50	50
Second Heating Temp.	°C	1100	1000	1100	1100
Second Heating Time	s	18.0	16	18	18
Second Holding Time	s	60	60	60	60
Cooling Rate	°C/s	10	10	10	10
Final Temp. (Room Temp.)	°C	20	20	20	20
Cooling Time	s	108.0	98.0	108.0	108.0
Process Total Time	s	225.0	213.0	225.0	225.0

5.4 PROCEDURES OF THE EXPERIMENT

The experimental study for the Micro-FAST process using the Gleeble[®] 3800 machine was divided into three steps. The three steps are: the preparation of the powder materials, the preparation of the Gleeble[®] 3800 operating system and the preparation of the ejection after the Micro-FAST process ended.

5.4.1 PREPARATION OF POWDER MATERIALS

The required powder material for the Micro-FAST process was measured using a powder measuring scale (Sartorius Praxos) as in **Figure 5-3** with the equation **(5.4-1)**. The measured powder was carefully poured into the die set. After insertion of the powder into the die, the die was carefully checked to ensure it was fully closed and no powder had leaked.

$$m = V \times \rho \quad (5.4-1)$$

Where:

m - Mass of powder material required during the process (g).

V - Volume of the cavity die set (mm³).

ρ - Theoretical skeletal density of powder material required during the process (g/mm³).

5.4.2 PREPARATION OF GLEEBLE[®] 3800 OPERATING SYSTEM

Cooled water (17 °C) was used for the Gleeble[®] 3800 machine. This water was cooled by the fan in the machine. A graphite lubricant and stickers were put at both the punches of the Gleeble[®] 3800 machine as in **Figure 5-6**. The die set with the powder material was located in

the vacuum chamber and aligned with the punches of Gleeble[®] 3800 machine. The measurement of the heating temperature during the experiment process was made by using the thermocouple which was inserted into the centre hole of the die set and the other end of the thermocouple wire attached to the C-Strain connection of the Gleeble[®] 3800 machine. After this the door of the vacuum chamber was closed securely. The air inside the chamber was eliminated by shutting down the lever air intake. The vacuum 'on' button was pressed to start the process of taking out the air from the chamber. The best reading for the vacuum chamber was 4.5×10^{-1} Torr.

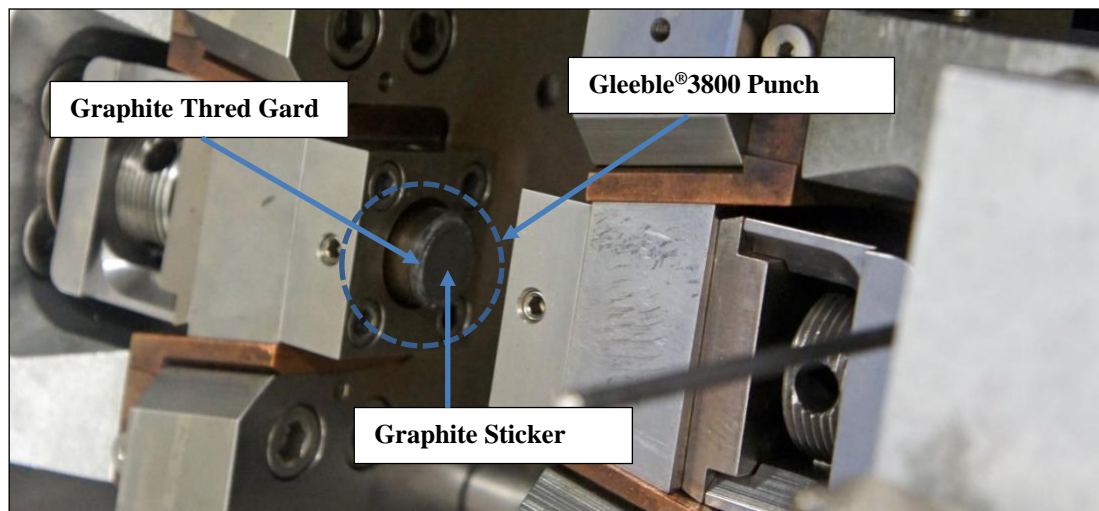


FIGURE 5-6: SMALL AMOUNT OF THE HIGH-TEMPERATURE SPECIMEN GRAPHITE LUBRICANT (THRED GARD) AND STICKERS WAS PUT AT BOTH THE PUNCHES OF THE GLEEBLE[®] 3800 MACHINE.

After that, all the parameters of the experiment were input using QuickSim[™] software as seen in Figure 5-7. The Micro-FAST process was started and in case of any emergency there is a stop button if something unpredictable happens during the experiment. All safety procedure must be followed including wearing eye protection during the experiment due to the extreme bright light that could be produced by the heating process. After the process finished, the vacuum chamber was checked to ensure that the temperature increased to at least 200 °C before the chamber door was open. The reason for this is to reduce the oxidation towards the die set and powder inside. After the temperature has reached at least 200 °C, the vacuum 'off' button was pressed with the air intake lever open to allow air inside the vacuum chamber. The release door button was pressed and vacuum chamber door was opened. The run and mechanical button

were pressed. The die set was carefully taken out from the chamber by tweaking the displacement button very slowly to release the die set. The punches of the Gleeble® 3800 machine were cleaned and the process started again until finished. After all the experiment were finished, the white start, water cooling and fan switch buttons were switched off.

#	L	Time	Axis 1	Axis 2	Axis 3	Comment
1		System	Setup	Limits: Compression=-13mm, Force=50000kgf, Heat=100%		
2		Stress/Strain	Axial strain using LGauge, l = 12.000mm, d = 8.000mm			
3		Acquire	Force force.line LGauge PowAngle Power PTemp Strain Stress Stroke TC1			
4		*				
5		*				
6		*				
7		Start	<input checked="" type="checkbox"/> Mechanical	<input type="checkbox"/> High	<input checked="" type="checkbox"/> Thermal	
8		Mode	Force(kN)	Wedge(cm)	TC1(C)	
9		Sample	10.0Hz			
10		GSL>	set strainki to -0.15pct			
11		GSL>				
12		GSL>	set tpcoef to 0.4			
13		GSL>	set ticoef to 0.4			
14		00:01.0000	-0.1	0	20	
15		00:09.0000	-0.9	0	200	
16		00:30.0000	-0.9	0	200	
17		00:20.0000	-0.9	0	1200	
18		02:00.0000	-0.9	0	1200	
19		01:58.0000	-0.9	0	20	
20		End	<input type="checkbox"/> Mechanical	<input type="checkbox"/> High	<input type="checkbox"/> Thermal	

FIGURE 5-7: QUICKSIM™ SOFTWARE USED TO OPERATE THE GLEEBLE® 3800 DURING MICR-FAST PROCESS

5.4.3 THE EJECTION PROCESS

After the die set has been taken out from the chamber, the die set was cooled to room temperature. The upper and lower punches were carefully opened by hand. After that, the die set was placed above the die ring and by using an ejector and hammer, the sample inside the die set was carefully knocked out. This action was made to prevent the sample from being damaged. The contamination of carbon from the punches and inside wall graphite die set will stick to the surface of the sample. To remove the carbon contamination sand paper was used from rough to fine grade (grade: 800, 1,200 and 2,000). After that, the clean sample was put into a labelled plastic bag for the analysis process.

5.5 RESULTS AND DISCUSSIONS

The results and discussion from the Micro-FAST samples using the Gleeble® 3800 machine are shown below.

5.5.1 SAMPLES RELATIVE DENSITY AND DIMENSIONS

The tables below show the results for dimensions, sample weights and relative density for the sintered samples. In the tables the condition of the gap existing after the experiment finished between the upper and lower punches within the die whether it was fully closed or not will be described. Figure 5-8 shows the gap in the die before and during the process. The ideal scenario is to have the die fully closed during and at the end of the process due to the need for the current to pass through the overall die set thus heat will be generated more efficiently to densify the powder materials in the die. The samples would then be made more precisely to the actual design. Therefore, the die set heating distribution during the Micro-FAST process has been observed to see the performance of die set design. Furthermore, the output of the actual sample size and the sample weight (before and after the cleaning process due to the sticking carbon) have been measured and calculated respectively for all samples. Lastly, the relative density of each sample has been calculated by using the density determination kit (Sartorius YDK03) (see Figure 5-3) and Archimedean principle.

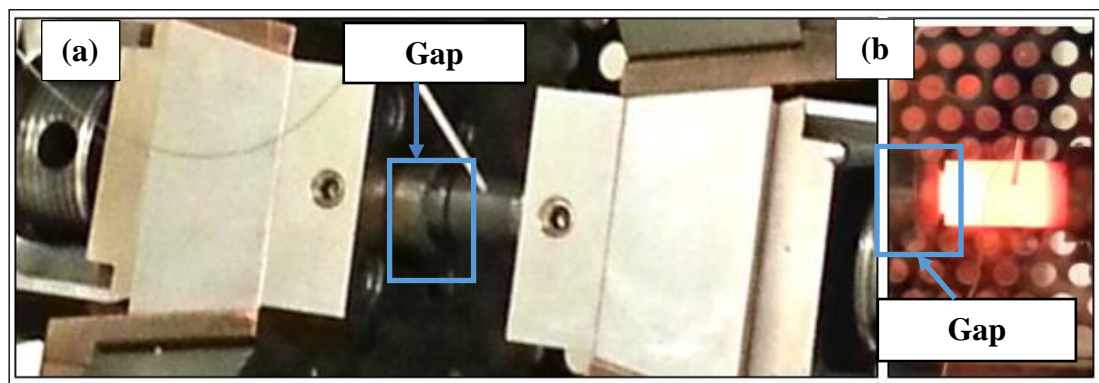


FIGURE 5-8: (A) BEFORE EXPERIMENT AND (B) DURING EXPERIMENT FOR THE CONDITION GAP BETWEEN UPPER AND LOWER PUNCHES TOWARDS THE DIE DURING THE MICRO-FAST PROCESS

5.5.1.1 ZIRCONIA

Three types of zirconia have been tested. The first one is Yttria Partially Stabilized Zirconia (3Y-ZrO₂). The second type of Zirconia is the Magnesia Partially Stabilized Zirconia (MSZ). The Third one is Magnesia Partially Stabilized Zirconia with with 5 wt% organic additives or organic binders MSZ(#).

5.5.1.1.1 3YZrO₂

Table 5-9 shows the results of the Micro-FAST experiment for 3YZrO₂ powder. The first two experiments showed very good results showing no gap between the punches and the die and the die set is fully closed. However, the 3YZrO₂-1 and 3YZrO₂-2 recorded 4.09 mm and 4.08mm of height respectively. Meanwhile the diameter was 4.03 mm for 3YZrO₂-1 and 4.02 mm for the 3YZrO₂-2. On the other hand, the samples 3YZrO₂-3 and 3YZrO₂-4 have produced the diameter dimension of 3.98 and 4.02 mm respectively and reported a decreasing height of 4.04 and 4.01 mm respectively. This difference was due to the increase to the applied pressure for the 3YZrO₂-3 and 3YZrO₂-4.

TABLE 5-9: RESULTS OF THE DIMENSIONS, WEIGHT AND RELATIVE DENSITY FOR 3Y-ZrO₂ SAMPLES USING THE DIE SET A FOR THE MICRO-FAST PROCESS WHICH PERFORMED BY GLEEBLE® 3800 MACHINE.

Parameters and Results	Units	3YZrO ₂ -1	3YZrO ₂ -2	3YZrO ₂ -3	3YZrO ₂ -4
Pressure	MPa	75	75	125	125
Second Heating Rate	°C/s	50	50	50	25
Second Heating Temp.	°C	1200	1300	1300	1300
Second Holding Time	s	240.0	240.0	120.0	120.0
Process Total Time	s	417.0	429.0	309.0	331.0
Gap Between Punches and Die		No	No	No	No
Die Set Heating Temp. Distribution		Uniform	Uniform	Uniform	Uniform
Diameter of the Sample	mm	4.03	4.02	3.98	4.02
Height of the Sample	mm	4.09	4.08	4.04	4.01
Sample Weight Before Cleaning (BC)	g	0.2532	0.2575	0.2564	0.2542
Sample Weight After Cleaning (AC)	g	0.2518	0.2544	0.2548	0.2521
Different Sample Weight (BC-AC)	g	0.0014	0.0031	0.0016	0.0021
Relative Density	%	89.17	91.67	97.60%	99.47%

As seen in Table 5-9, the die set heating distribution during the process for the 3YZrO₂ samples using the die set shows that the heating distribution was uniform for each of the samples. This is a good indicator for the overall heating of the die set during the Micro-FAST process. The fraction difference in sample weights before and after the cleaning process was in the range of 0.553 to 1.2% which shows that the amount of carbon sticking to the samples was very low.

Figure 5-9 and Table 5-9 show the incremental value of the relative density directly proportional to the applied pressure, second heating rate, second heating temperature and second holding time for 3YZrO₂ samples. For the relative density, there is an increase in the percentage from 89.17% to 99.47% for the last sample. For the 3YZrO₂-1 and the 3YZrO₂-2 samples the relative density was 89.17% and 91.67% respectively. The two samples have all the main parameters such as applied pressure and the second heating rate the same which

indicates the reading of 75 MPa and 50 °C/s individually. By increasing the second heating temperature and second holding time from 1,200 to 1,300 °C for 3YZrO₂-1 and the 3YZrO₂-2 samples respectively, the relative incremental density of 2 % has been achieved. The total time needed for 3YZrO₂-1 and the 3YZrO₂-2 samples to complete the process was 417 s and 429 s for each.

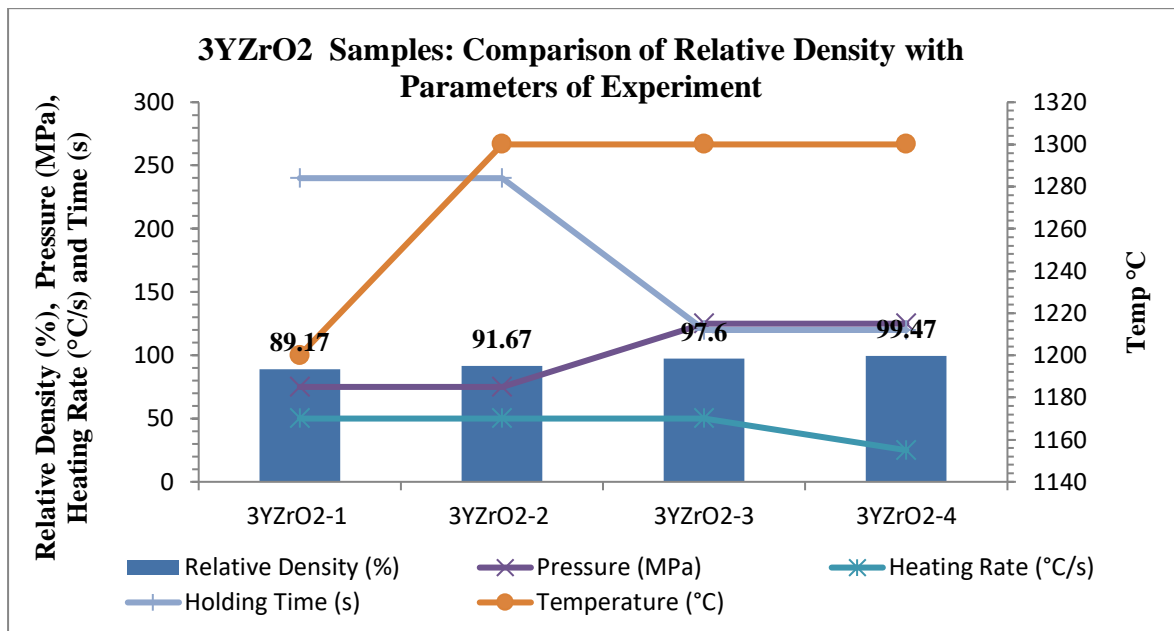


FIGURE 5-9: COMPARISON OF RELATIVE DENSITY WITH PARAMETERS OF EXPERIMENT FOR 3YZRO₂ SAMPLES

As seen in Figure 5-9 and Table 5-9, the 3YZrO₂-3 and 3YZrO₂-4 have achieved 97.31 and 99.47 % relative density and it is clear that the applied pressure played a significant role in increasing the relative density of the samples. The holding time for these samples has been increased to 120 seconds which is half of the previous time. This led to an increase in the total process time. However, the heating rate for the last sample 3YZrO₂-4 has been decreased to 25 °C/s and that increased the total time for the process to 331 second in total.

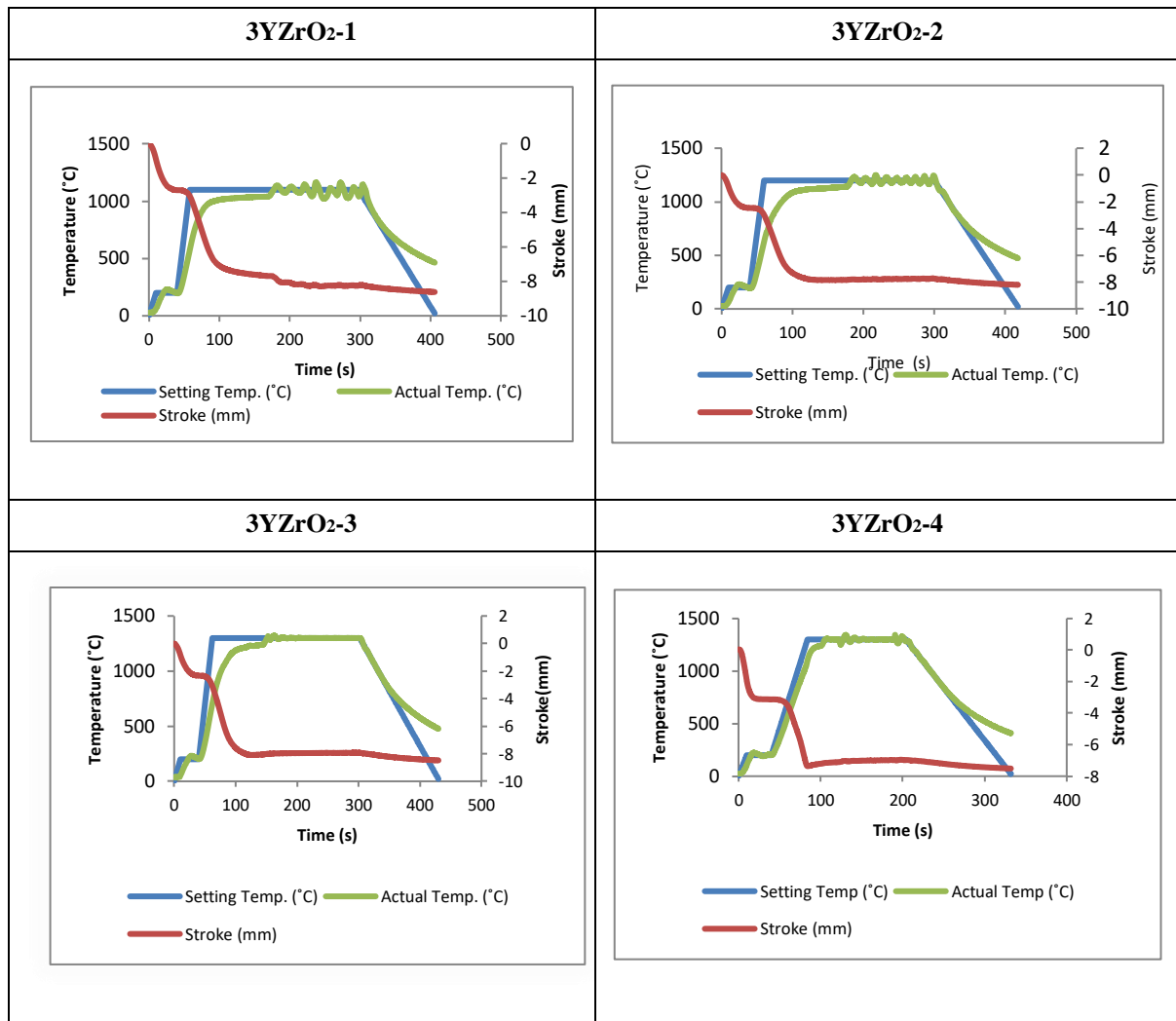


FIGURE 5-10: THE HEATING TEMPERATURE AND SHRINKAGE OF STROKE PUNCHES OF GLEEBLE® 3800 MACHINE FOR 3YZRO₂ SAMPLES.

Figure 5-10 illustrates the actual temperature that has been measured using the thermocouple and the temperature that has been set up in the software. The required temperature has been achieved for all samples in some points, however there are some fluctuation in the graphs possibly due to a problem with the thermocouples. The graphs show the stroke of the punches for the Gleeble Machine. When comparing the four samples 3YZrO₂-1, 3YZrO₂-2, 3YZrO₂-3 and 3YZrO₂-4, this can show some slight differences in the stroke distance. There was a small difference between the 3YZrO₂-1 and 3YZrO₂-2 due to increasing the heating temperature or sintering temperature that led to a slight increase in the relative density. For the comparison between 3YZrO₂-2 and 3YZrO₂-3, the difference was not that

obvious, but the increase in the applied pressure increases the relative density by nearly 6% to achieve 97.60% relative density. For the last sample 3YZrO₂-4, it was obvious that there is a difference in the stroke due to reduction in the heating rate, also the process time has been increased and the relative density has been improved and achieved 99.47 % relative density.

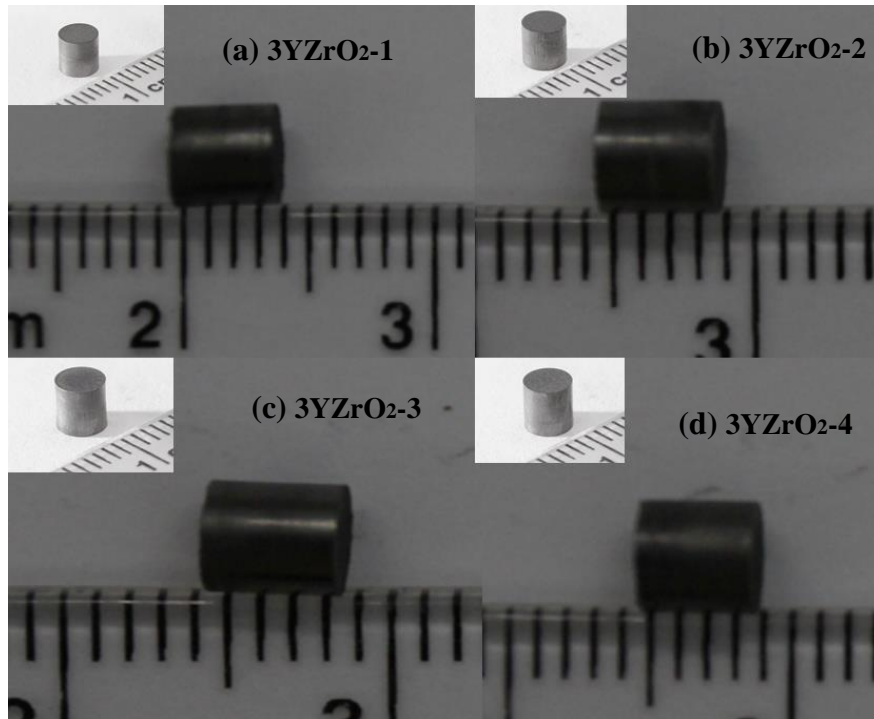


FIGURE 5-11: THE 3YZRO₂ SAMPLES

The 3YZrO₂-4 has reached the optimal parameter for the Micro-FAST process. It is clear that the applied pressure, second heating rate, second heating temperature and second holding time have a direct effect on the relative density of the samples. Figure 5-11 shows the formed sample after having been ejected from the die. The samples have very good relative density and have been produced in very good condition. As a result, the Micro-FAST process has a very good potential for producing miniature parts from 3YZrO₂ powder with less process time than previous experiments.

5.5.1.1.2 MSZ

Based on the Table 5-10 and Figure 5-12, the results showed very good relative densities and there was no gap between the die and the punches. The first two samples MSZ-1 and MSZ-

2 recorded 4.03 mm and 4.02 in diameter respectively. Meanwhile the height for MSZ-1 was 4.01 mm and MSZ-2 recorded 4.08 mm. For the MSZ-3, the diameter was 3.98 mm and the height was 4.03 mm. In the last sample, the die set B was used in this experiment. Therefore, the MSZ-4 sample was dimensionally different. The height for the MSZ-4 was 1.99 mm.

TABLE 5-10: RESULTS OF THE DIMENSIONS, WEIGHT AND RELATIVE DENSITY FOR MSZ SAMPLES USING THE DIE SETS A AND B FOR THE MICRO-FAST PROCESS WHICH PERFORMED BY GLEEBLE® 3800 MACHINE.

Parameters and Results	Units	MSZ-1	MSZ- 2	MSZ- 3	MSZ- 4
Pressure	MPa	125	125	125	125
Second Heating Rate	°C/s	100	25	50	25
Second Heating Temp.	°C	1300	1300	1300	1400
Second Holding Time	s	120.0	120.0	180.0	90.0
Process Total Time	s	298.0	331.0	391.0	315.0
Gap Between Punches and Die		No	No	No	No
Die Set Heating Temp. Distribution		Uniform	Uniform	Uniform	Uniform
Diameter of the Sample	mm	4.03	4.02	3.98	2.02
Height of the Sample	mm	4.01	4.08	4.03	1.99
Sample Weight Before Cleaning (BC)	g	0.2832	0.2825	0.2864	0.0342
Sample Weight After Cleaning (AC)	g	0.2820	0.2814	0.2848	0.0337
Different Sample Weight (BC-AC)	g	0.0012	0.0021	0.0016	0.0005
Relative Density	%	93.81%	96.36%	97.53%	99.49%

The heating distribution of the die set during the experiment was uniform for all the samples. This gives a good indication that the condition was good and higher relative densification will be achieved to obtain excellent dimensional features between the samples. The difference percentage of the sample weight before and after the cleaning process was in the range of 0.389% to 1.46%. This showed that the carbon sticking to the samples was still low.

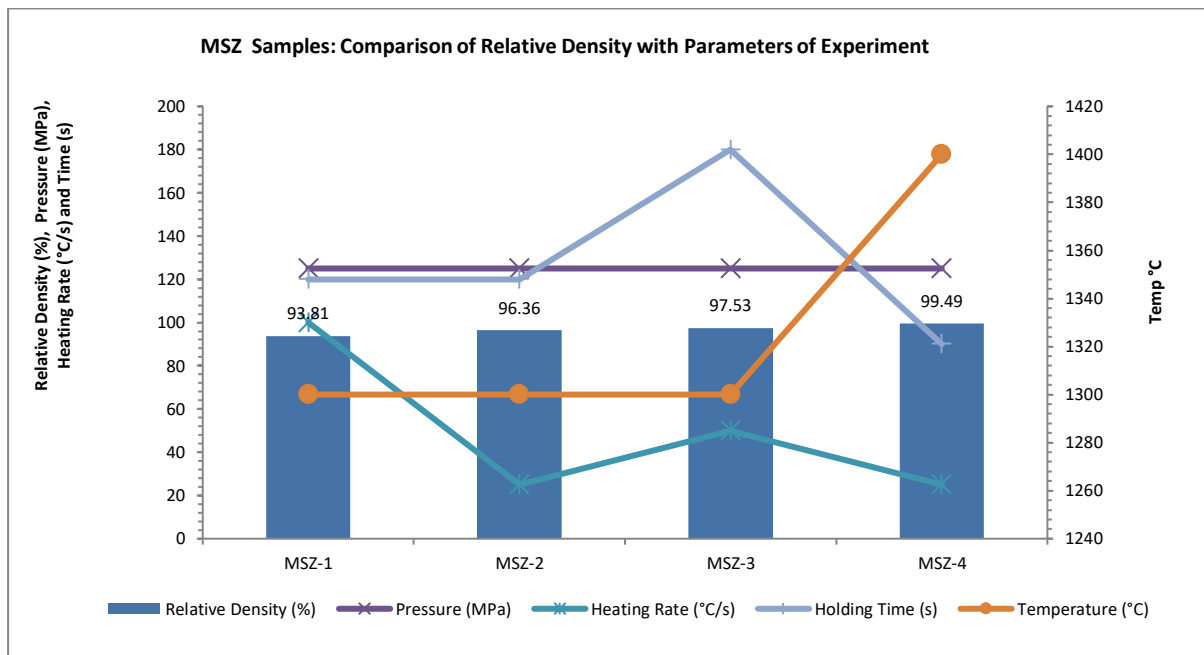


FIGURE 5-12: COMPARISON OF RELATIVE DENSITY WITH PARAMETERS OF EXPERIMENT FOR MSZ SAMPLES

According to the observed results shown in Table 5-10 and the comparisons that have been illustrated in Figure 5-12, the incremental value of the relative density of MSZ samples was directly proportional to the second heating temperature and second heating rate. The applied pressure was 125 MPa for all samples because it showed very good results from previous experiments. The four samples have recorded very good relative densities. The value of the relative densities for the four samples is from 93.81% to 99.49%. In the first two samples (MSZ-1 and MSZ-2), the same applied pressure, the heating temperature and the holding time have been used. However, the heating rate that has been used in the MSZ-1 was 100 °C/s and has been reduced to 25 °C/s for the MSZ-2 sample and that caused an increase for the total time process for MSZ-2. The MSZ-1 sample has achieved 93.81% relative density. Meanwhile the MSZ-2 has reached 96.36% due to a decrease of the heating rate. This gives an indication that the heating rate directly proportional to the relative density of the sample.

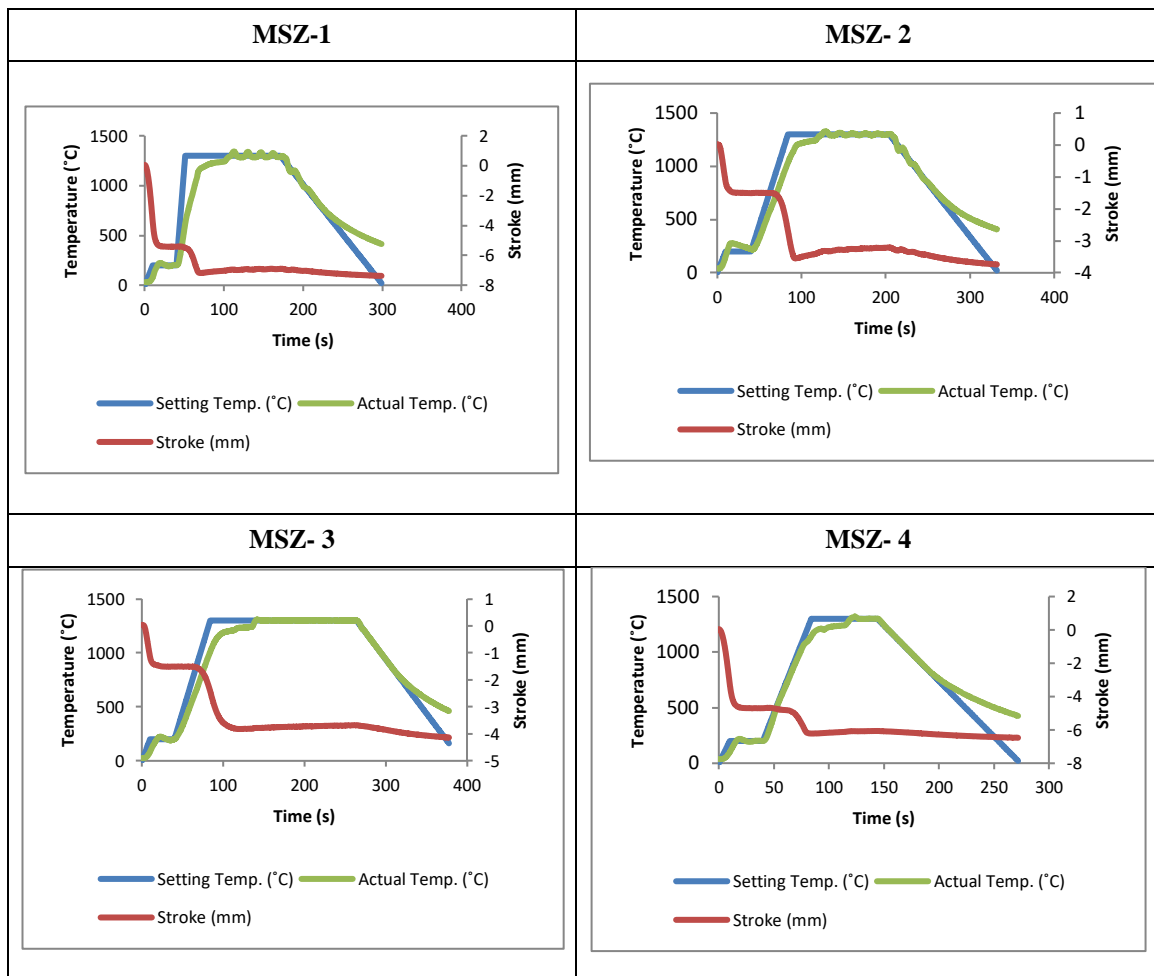


FIGURE 5-13: THE HEATING TEMPERATURE AND SHRINKAGE OF STROKE PUNCHES OF GLEEBLE® 3800 MACHINE FOR MSZ SAMPLES.

For the sample MSZ-3, the parameters that have been used are 125 MPa applied pressure, 1300°C sintering temperature, 50 °C/s heating rate and the holding time was 180 seconds. The MSZ-3 sample has recorded a 97.53% relative density and the total process time has increased to 391.0 seconds, which is good compared to the conventional sintering process. For sample MSZ-4, the applied pressure was maintained the same (125 MPa), but the sintering temperature increased to 1400 °C. Compared with MSZ-3 the heating rate holding time increased for MSZ-4 sample to 25 °C/s and 90 second respectively. The MSZ-4 has recorded a 99.49% relative density.

Figure 5-13 shows the actual temperature that was measured using the thermocouple and the temperature that was set up in the software. The required temperature has been mostly achieved for all samples but there were some fluctuations in the graphs due to a possible

problem with the thermocouples. The graphs show the stroke of the punches for the Gleeble Machine. When comparing the four samples MSZ-1, MSZ-2, MSZ-3 and MSZ-4, it can be seen that there are differences in the stroke distance due to the differences in the parameters and the die set used.

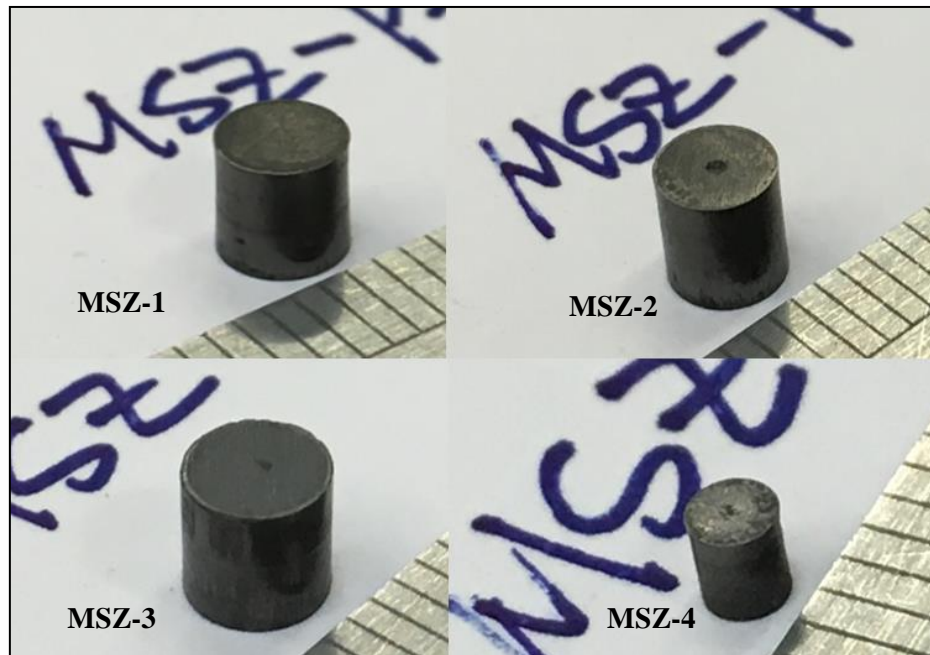


FIGURE 5-14: THE MSZ SAMPLES

The MSZ-4 has reached the ideal parameter for the Micro-FAST process. It is clear that the applied pressure, second heating rate, second heating temperature and second holding time have a direct effect on the relative density of the samples. Figure 5-14 shows the produced samples after the ejection process. The samples have very good relative density and have been produced in a very good condition. As a result the Micro-FAST process has a very good potential for making miniature parts from MSZ powder with less process time than previous experiments with conventional processes.

5.5.1.1.3 MSZ(#)

In this part the samples from using Magnesia Partially Stabilized Zirconia with 5 wt% organic additives (MSZ#). Table 5-11 shows the results of the Micro-FAST experiment for MSZ(#) powder. In this experiment, the process was different from the previous experiment

with other Zirconia powders. In this process three stages were required. The first and second stages are used for heating the additives and vapour, the third stage is the sintering process. The additives have been used to see if the sintering will be improved and if the nano-powder becomes stable at room temperature. The die set A has been used in this experiment.

TABLE 5-11: RESULTS OF THE DIMENSIONS, WEIGHT AND RELATIVE DENSITY FOR MSZ (#) SAMPLES USING THE DIE SET A FOR THE MICRO-FAST PROCESS WHICH PERFORMED BY GLEEBLE® 3800 MACHINE.

Parameters and Results	Units	MSZ(#)-1	MSZ(#)-2	MSZ(#)-3	MSZ(#)-4
Initial Pressure	MPa	75	75	75	75
Sintering Pressure	MPa	125	125	125	125
Third Heating Rate	°C/s	25	25	50	100
Third Heating Temp.	°C	1300	1300	1300	1300
Third Holding Time	s	5.0	60.0	120.0	120.0
Process Total Time	s	387.8	442.8	484.4	475.2
Gap Between Punches and Die		No	No	No	No
Die Set Heating Temp. Distribution		Uniform	Uniform	Uniform	Uniform
Diameter of the Sample	mm	3.98	4.01	4.03	3.99
Height of the Sample	mm	4.03	4.02	4.02	4.01
Sample Weight Before Cleaning (BC)	g	0.2797	0.2811	0.2781	0.2806
Sample Weight After Cleaning (AC)	g	0.2782	0.2795	0.2769	0.2783
Different Sample Weight (BC-AC)	g	0.0015	0.0016	0.0012	0.0023
Relative Density	%	89.55%	93.08%	95.51%	97.45%

The initial pressure used in the first and the second stage was 75 MPa, then the applied pressure increased to 125 MPa for all four MSZ(#) samples. The heating temperature was 1300 °C for all samples because it has been sufficient for all previous zirconia samples. The MSZ(#)-1 and MSZ(#)-2 sample recorded 4.03 mm and 4.02mm of height respectively. Meanwhile the

diameter was 3.98 mm for MSZ(#)-1 and 4.01 mm for the MSZ(#)-2. For the last two the samples (MSZ(#)-3 and MSZ(#)-4) the diameter dimension was 4.03 and 3.99 mm and a height of 4.02 and 4.01 mm respectively. The heating distribution of the die set during the experiment also has been uniform for each sample. This gives a good indicator for the overall heating of the die set A during the Micro-FAST process. The difference in sample weights before and after the cleaning process was in the range of 0.4315 to 0.82% which shows that the carbon sticking to the samples was very low.

As seen in Table 5-11 and Figure 5-15, the relative density for the all four samples was very good. The percentage of the relative density started from 89.55% and increased to reach 97.45% for MSZ(#)-4 sample. For the first sample MSZ(#)-1 as mentioned before, the applied pressure started from 75 MPa then increased to 125 MPa. The heating temperature was 1300 °C, but the heating rate was 25 °C/s. Due to the first two stages, the holding time was set up to 5 seconds in order to explore the possibility of sintering and forming the part in a short holding time. The sample has been sintered and formed successfully with a relative density of 89.55% and the total time for the process was 387.8 seconds.

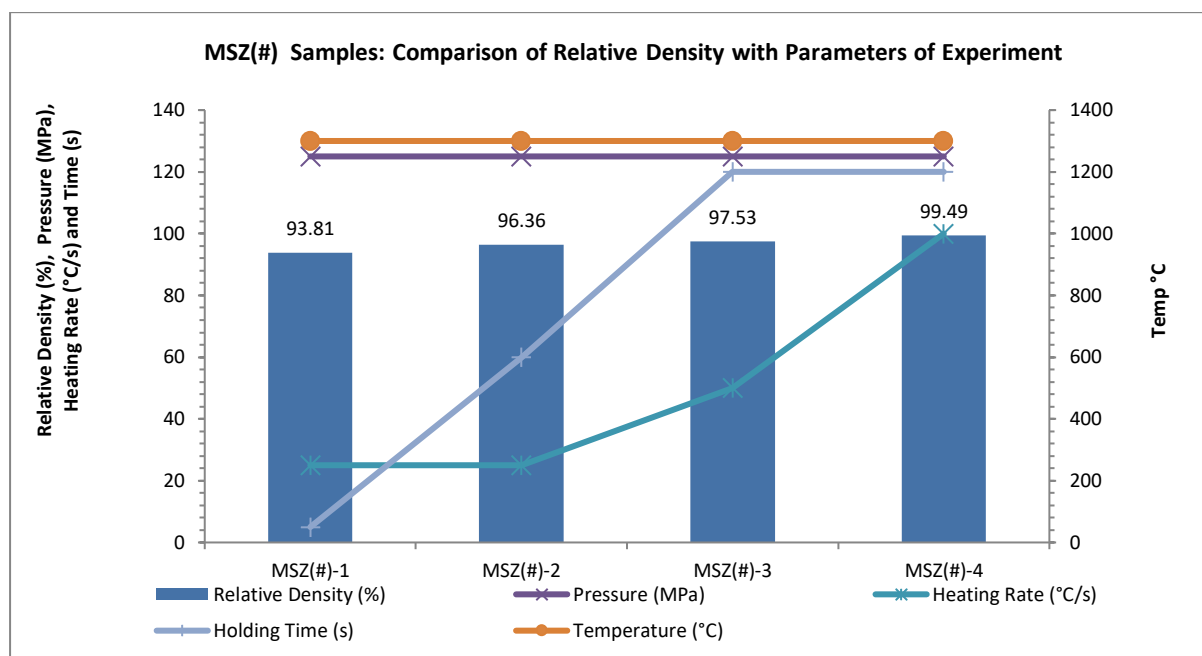


FIGURE 5-15 COMPARISON OF RELATIVE DENSITY WITH PARAMETERS OF EXPERIMENT FOR MSZ SAMPLES

For the MSZ(#)-2, the holding time has been increased to 60 seconds in order to investigate how this will affect the formed sample. The other parameters have been kept the same as for MSZ(#)-1 sample. The results showed that the MSZ(#)-2 has recorded an increase in the relative density by 3.53% and reached 93.08%. The total time for this process was 442.8 seconds. In investigating the MSZ(#)-3, the heating rate and the holding time have been increased. The holding time for MSZ(#)-3 was 120 seconds and the heating rate increased to 50 °C/s. The MSZ(#)-3 sample has achieved 95.51% density which is better than the MSZ(#)-2 sample, but the total time process increased to 484.4 seconds. In the last sample MSZ(#)-4, the holding time was the same as MSZ(#)-3 which is 120 seconds, but the heating rate was increased to reduce the total time process. The relative density for MSZ(#)-4 sample was 97.45% with a total process time of 475.2 seconds.

Figure 5-16 illustrates the setting and the actual temperature that has been measured using the thermocouple. The sintering temperature has been achieved for all samples in most points, but there was some wavering in the graphs again possibly due to some errors with the thermocouples. The graphs show the stroke of the punches for the Gleeble Machine. When comparing the four samples MSZ(#)-1, MSZ(#)-2, MSZ(#)-3 and MSZ(#)-4, it can be seen that there are differences in the stroke distance due to the differences in the parameters and the die set used.

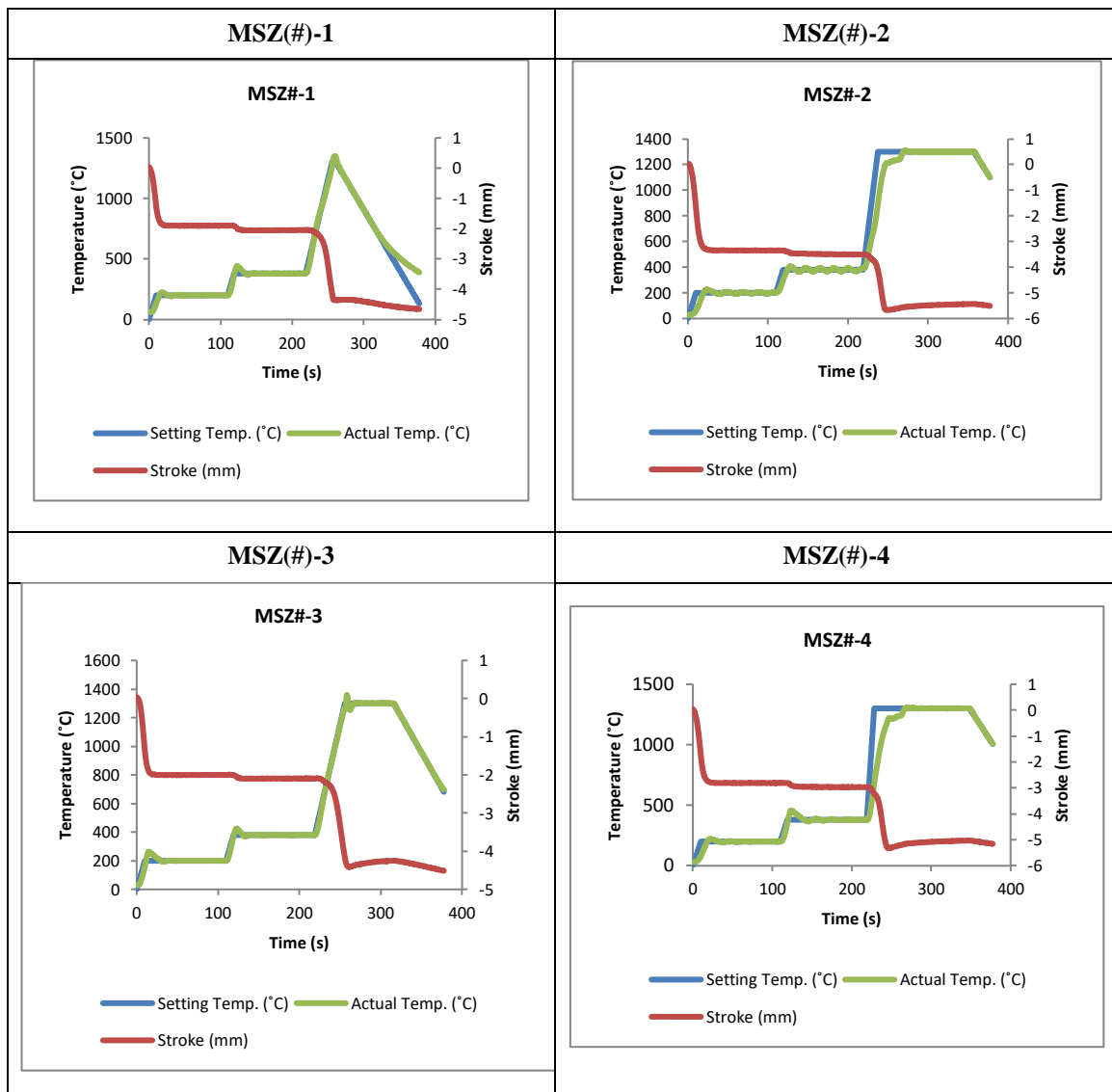


FIGURE 5-16: THE HEATING TEMPERATURE AND SHRINKAGE OF STROKE PUNCHES OF GLEEBLE® 3800 MACHINE FOR MSZ(#) SAMPLES.

The MSZ(#)-4 sample has reported the best parameters for the Micro-FAST process using the MSZ(#) powder. It is clear that the applied pressure, second heating rate, second heating temperature and second holding time have a direct effect on the relative density of the samples. The first two stages in the experiment helped to clear the additive which improved the sintering process.

Figure 5-17 below shows the formed samples from MSZ(#) powder. The samples were in very good condition and the relative density was very good. Therefore, the Micro-FAST

process has a very good potentiality for making miniature parts from MSZ(#) powder with less process time than previous experiments with conventional sintering processes.

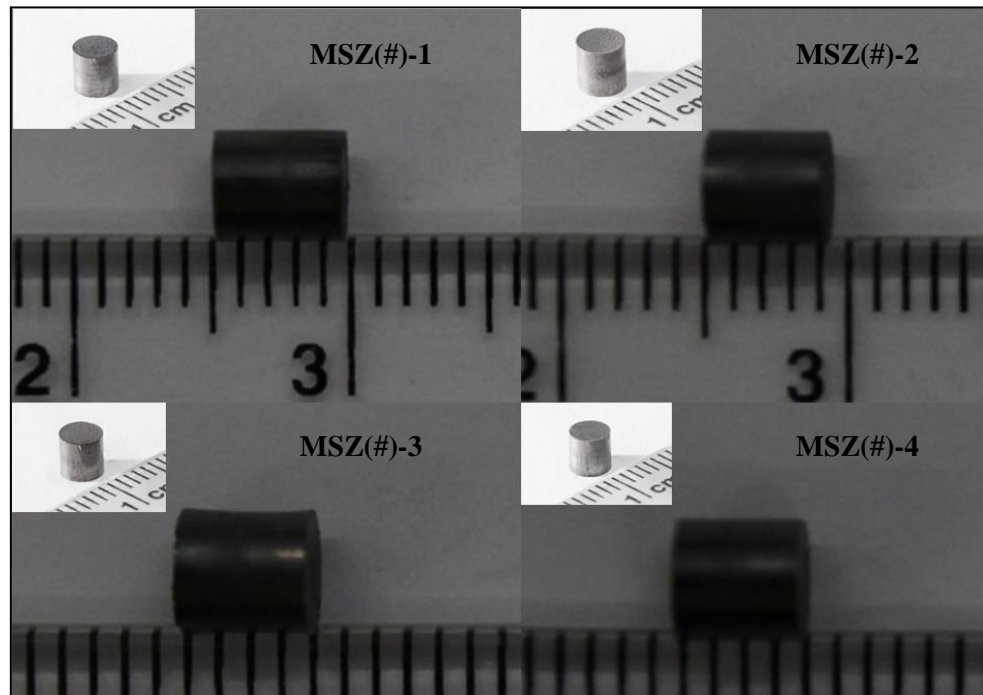


FIGURE 5-17: THE MSZ(#) SAMPLES

5.5.1.2 ALUMINA

In this part the results of using Alumina powder in the Micro-FAST process will be discussed. The die set B has been used in this experiment and the parts produced were of 2x2 mm cylindrical shape. Table 5-12 shows the detail of the results including dimensions, weights measurements and relative density. The samples have shown no gap between the die and the punch. The heating distribution of the die set during the experiment also has been uniform for all the samples.

TABLE 5-12: RESULTS OF THE DIMENSIONS, WEIGHT AND RELATIVE DENSITY FOR ALUMINA SAMPLES USING THE DIE SET B FOR THE MICRO-FAST PROCESS WHICH PERFORMED BY GLEEBLE® 3800 MACHINE

Parameters and Results	Units	Al ₂ O ₃ -1	Al ₂ O ₃ -2	Al ₂ O ₃ -3	Al ₂ O ₃ -4
Pressure	MPa	75	75	75	125
Second Heating Rate	°C/s	50	50	50	50
Second Heating Temp.	°C	1200	1200	1300	1300
Second Holding Time	s	240.0	360.0	240.0	240.0
Process Total Time	s	417.0	537.0	429.0	429.0
Gap Between Punches and Die		No	No	No	No
Die Set Heating Temp. Distribution		Unifrom	Unifrom	Unifrom	Unifrom
Diameter of the Sample	mm	2.02	2.02	2.00	1.99
Height of the Sample	mm	2.19	1.93	2.05	2.03
Sample Weight Before Cleaning (BC)	g	0.0237	0.0231	0.0239	0.0236
Sample Weight After Cleaning (AC)	g	0.0232	0.0225	0.0229	0.0231
Different Sample Weight (BC-AC)	g	0.0005	0.0016	0.0010	0.0005
Relative Density	%	72.91%	86.08%	87.09%	92.68%

The first sample Al₂O₃-1 has recorded 2.02 mm diameter and 2.19 mm height. The applied pressure used in this process for Al₂O₃-1 was 75 MPa. The heating temperature and the heating rate were 1200 °C and 50 °C/s respectively. The soaking time for this sample was 240 seconds. For samples Al₂O₃-2 and Al₂O₃-3, the same applied pressure and the heating rate have been used as the first sample Al₂O₃-1. However, in sample Al₂O₃-2 the holding time was increased to 360 seconds. The diameter of the produced sample Al₂O₃-2 was 2.02 mm and the height was 1.93 mm. In the third sample Al₂O₃-3, the same parameters have been used as the first sample, but the heating temperature was increased by 100 °C. The Al₂O₃-3 has recorded a diameter of 2 mm and 2.05 mm in height. The last sample, Al₂O₃-4, has recorded a diameter

of 1.99 mm and 2.03 mm in height. The parameters that have been used in this experiment are the same as Al_2O_3 -3, but with increasing the applied pressure to 125 MPa.

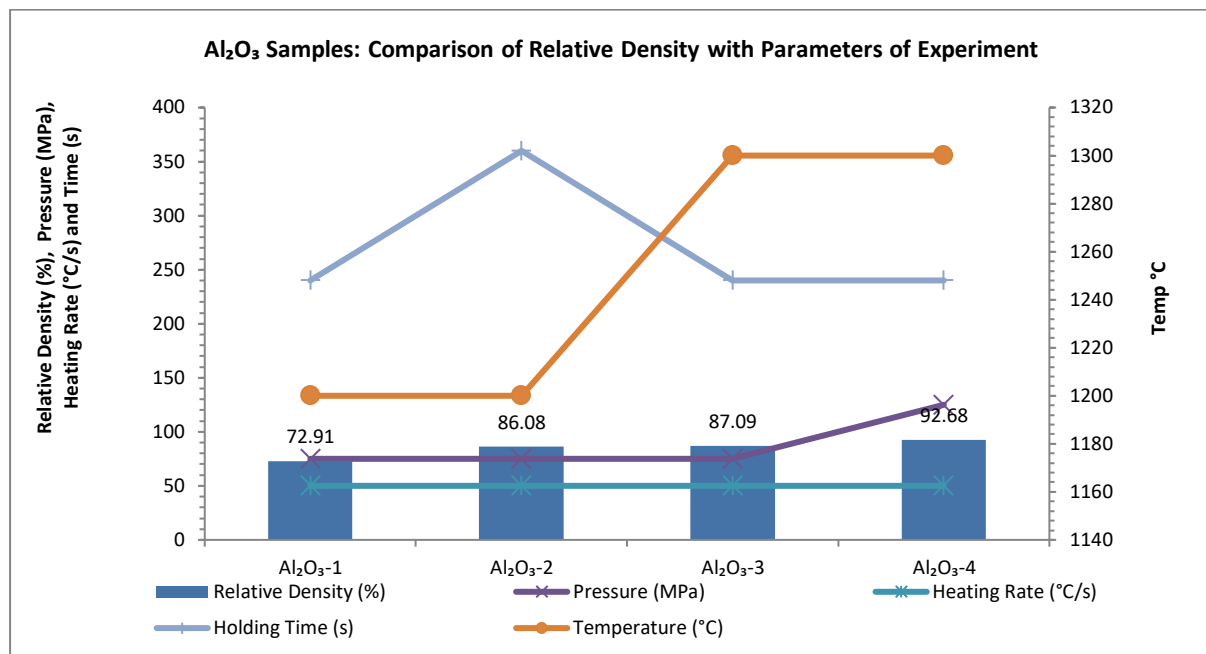


FIGURE 5-18: COMPARISON OF RELATIVE DENSITY WITH PARAMETERS OF EXPERIMENT FOR ALUMINA SAMPLES

The total process times for the first two samples (Al_2O_3 -2 and Al_2O_3 -1) were 417 and 537 seconds respectively. Meanwhile, the Al_2O_3 -3 and Al_2O_3 -4 samples recorded the same total time which is 429 seconds. The difference percentage of the sample weight before and after the cleaning process was in the range of 2.11% to 4.184%. This showing that there was carbon sticking to the samples. This carbon could play an important role in affecting the relative density of the formed samples.

As seen in Table 5-12 and Figure 5-18 the incremental value of the relative density of Alumina samples was directly proportional to the heating temperature, holding time and applied pressure. The relative density of all samples was in the range of 72.91% to 92.68%.

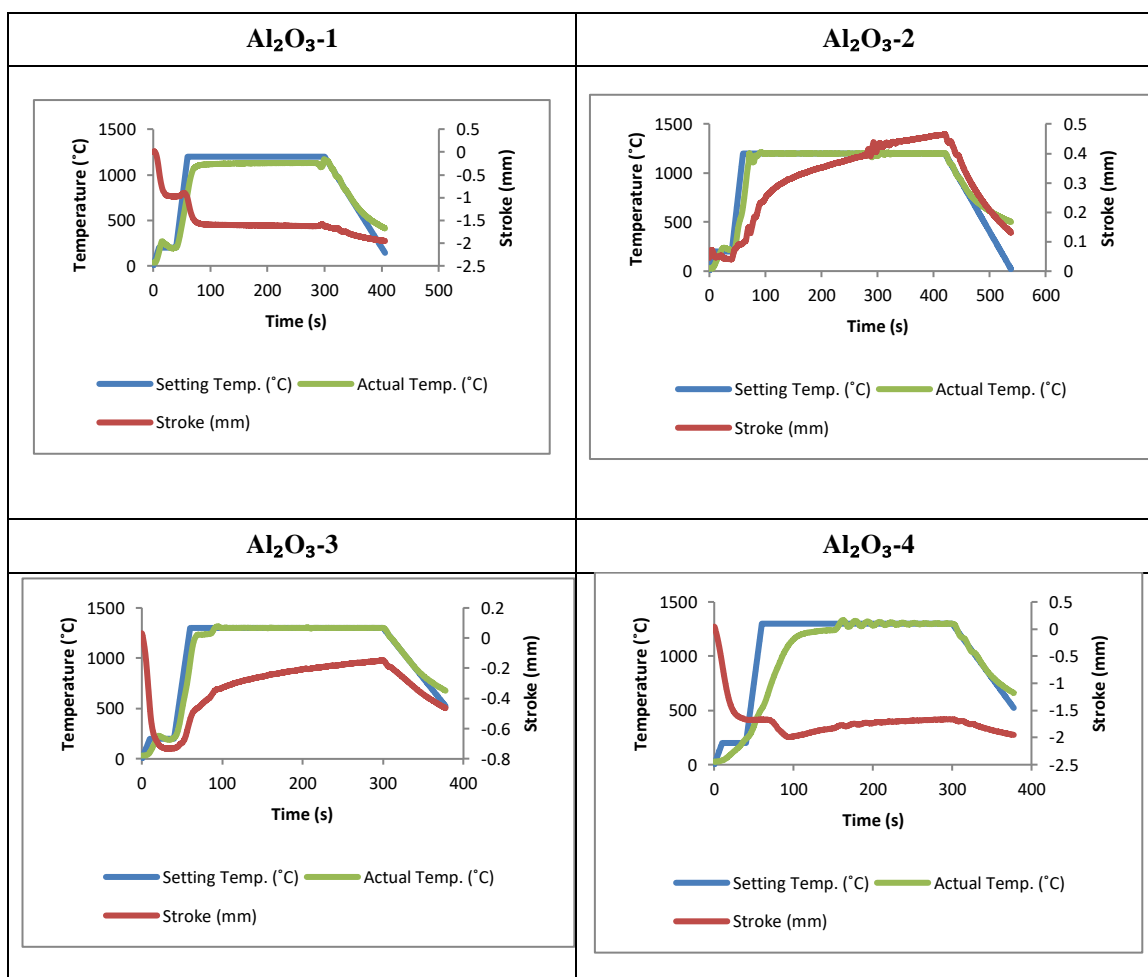


FIGURE 5-19: THE HEATING TEMPERATURE AND SHRINKAGE OF STROKE PUNCHES OF GLEEBLE® 3800 MACHINE FOR ALUMINA SAMPLES.

The first sample Al_2O_3 -1 has recorded 72.91% relative density and this has been increased in the Al_2O_3 -2 to 86.08%. This increase happens due to the increase in the holding time from 417 seconds to 537 seconds. Another attempt has been made for sample Al_2O_3 -3 with the same parameters as the Al_2O_3 -3, but with an increase in the sintering temperature. The sample has reported an improvement and reached 87.09%. This shows that the relative density is directly proportional to the heating temperature. In the last sample Al_2O_3 -4, the relative density was 92.68% after using the same parameters as Al_2O_3 -3, the applied pressure was increased to 125 MPa. It was obvious that increasing the applied pressure also played an important role in improving the relative density.

Figure 5-19 illustrates the actual temperature and the setting temperature that has been used in the software. The required temperature has been achieved for all samples as shown in the graphs. Moreover, in the same graphs the stroke of the punches for the Gleeble Machine have been shown. In the first graph for Al_2O_3 -1 the stroke started normally and decreased slightly to reach the -0.2 mm. The stroke in Al_2O_3 -2 started normally, but the reading increased to 5 mm which is high. The reason behind that could be the sticking of some carbon inside the die causing a jamming of the movement. In the third graph Al_2O_3 -3, the stroke started normally and decreased to nearly -0.8mm. Suddenly, the reading went up and kept increasing to reach above -.02 mm. After 300 seconds, this decreased again to reach nearly -0.5 mm. In the last graph Al_2O_3 -4, the stroke started normally and decreased to -2 mm and the line fluctuated between reading -1.5 in the period between 100 seconds and 400 seconds. This is due to the applied pressure of the last sample which is 125 MPa.

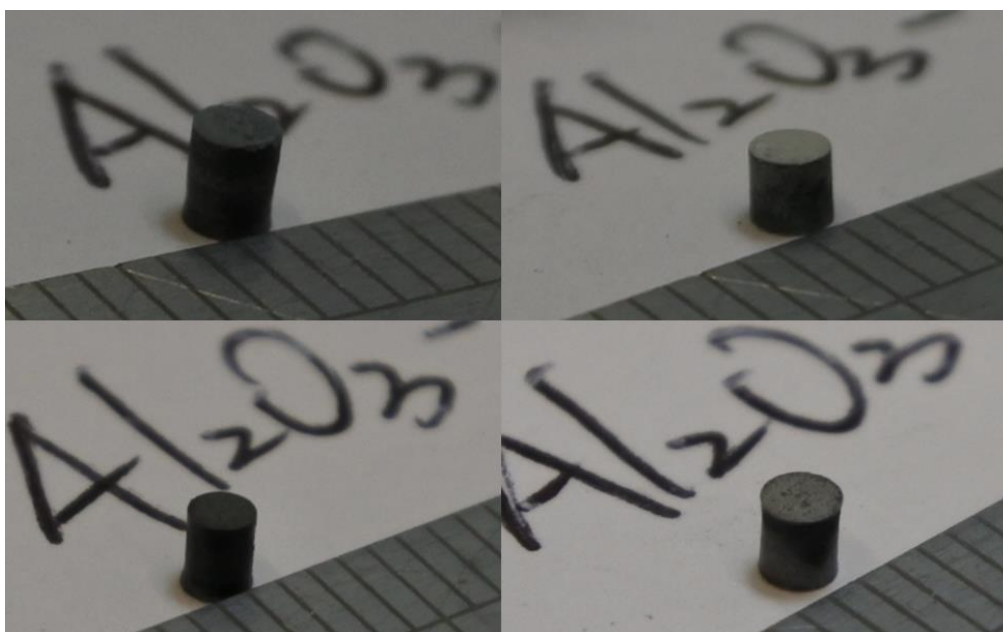


FIGURE 5-20: THE ALUMINA SAMPLES

The Al_2O_3 -4 reached the optimal parameter for the Micro-FAST process for Alumina powders. It is clear that the applied pressure, and second heating temperature and second holding time have a direct effect on the relative density of the samples. Figure 5-20 shows the formed sample after having been ejected from the die. Three samples have very good relative

density and have been produced in very good condition. The carbon from the die and the punch have affected the relative density of the samples. From the experiment results the Micro-FAST process has shown to have a very good potential for producing miniature parts from Alumina powder with less process time than previous experiments.

5.5.1.3 PIEZOCERAMIC (PZT)

In investigating the piezoceramic powder, two die sets (Die set B and Die set C) have been used. Table 5-13 shows the results of the Micro-FAST experiment for piezoceramic powders. The first two samples PZT-1 and PZT-2 have been tested using die set B, in which the samples are of 2x2 mm cylindrical shape. The PZT-3 and PZT-4 samples were formed by using the die set C, which were cuboid shapes. All samples reported no gap between the die and the punch and the heating distribution was uniform for each of the samples.

The PZT-1 and PZT-2 samples recorded 2.22 mm and 2.16 mm of height respectively. Meanwhile the diameter was 1.99 mm for PZT-1 and 2.02 mm for the PZT-2. The parameters that have been used for the first two samples were the same and only the temperature has been increased from 1000 °C to 1100 °C for sample PZT-2. The applied pressure was 125 MPa, the heating rate was 50 °C/s, and the holding time was 60s. The difference in sample weights before and after the cleaning process was 3.9% for PZT-1 and 2.45% for PZT-2. This indicates that there was amount of carbon sticking to the samples.

As seen in Table 5-13 and Figure 5-23, the PZT-1 has recorded a relative density of 72.87% and the PZT-2 has reached 82.49%. Based on these results, it can be shown that the heating temperature is directly proportional to relative density. The total process time for PZT-1 and PZT-2 were 213 and 225 seconds respectively.

TABLE 5-13: RESULTS OF THE DIMENSIONS, WEIGHT AND RELATIVE DENSITY FOR PIEZOCERAMIC SAMPLES USING THE DIE SET B AND C FOR THE MICRO-FAST PROCESS WHICH PERFORMED BY GLEEBLE® 3800 MACHINE

Parameters and Results	Units	PZT-1	PZT-2	PZT-3	PZT-4
Pressure	MPa	125	125	125	125
Second Heating Rate	°C/s	50	50	50	25
Second Heating Temp.	°C	1000	1100	1100	1100
Second Holding Time	s	60	60	60	60
Process Total Time	s	213.0	225.0	225.0	243.0
Gap Between Punches and Die		no	no	no	no
Die Set Heating Temp. Distribution		Uniform	Uniform	Uniform	Uniform
Dimensions of the Sample	mm	D=1.99, H=2.22	D=2.02, H=2.16	4.74x1.56x1.46	1.5x1.56x4.74
Sample Weight Before Cleaning (BC)	g	0.0384	0.0408	0.0687	0.0605
Sample Weight After Cleaning (AC)	g	0.0369	0.0398	0.0668	0.0592
Different Sample Weight (BC-AC)	g	0.0015	0.001	0.0019	0.0013
Relative Density	%	72.87%	82.49%	75.17%	81.66%

For the PZT-3, the parameters that have been used are the same as PZT-2. PZT-3 has been formed in cuboid shape with dimensions of 4.74x1.56x1.46 mm. The difference percentage of the sample weight before and after the cleaning process for the PZT-3 sample was 2.766%. Meanwhile, the PZT-4 has recorded dimensions of 4.74x1.5x1.56 mm and the difference percentage of the sample weight before and after the cleaning process was for PZT-4 2.15%. This is showed that there was amount of carbon sticking to the samples. The parameters that have been used in forming the PZT-4 sample were 125 MPa pressure, 25 °C/s heating rate, heating temperature 1100 °C and the holding time was 60 seconds. The PZT-3 has recorded a relative density of 75.17% and relative density of the PZT-4 has increased to 81.66%. These results show the incremental value of the relative density is directly proportional to the heating

rate. The total process time for the PZT-3 was 225 seconds and due to the decrease in the heating rate for the PZT-4 the total time increased to 243 seconds.

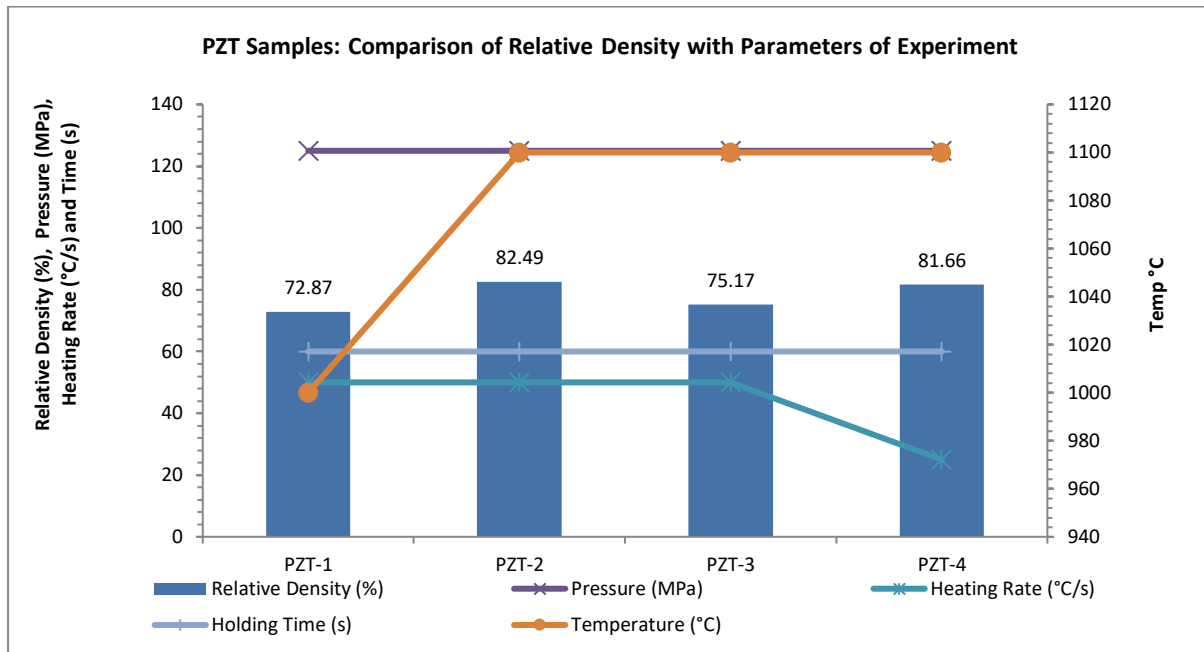


FIGURE 5-21: COMPARISON OF RELATIVE DENSITY WITH PARAMETERS OF EXPERIMENT FOR PZT SAMPLES

Figure 5-22 shows the actual temperature that has been measured using the thermocouple and the temperature that has been set up in the software. The required temperature has been achieved for all samples. The graphs show the stroke of the punches for the Gleeble Machine. When comparing the four samples PZT-1, PZT-2, PZT-3 and PZT-4, it can be seen that there are differences in the stroke distance due to the differences in the parameters and the used die set.

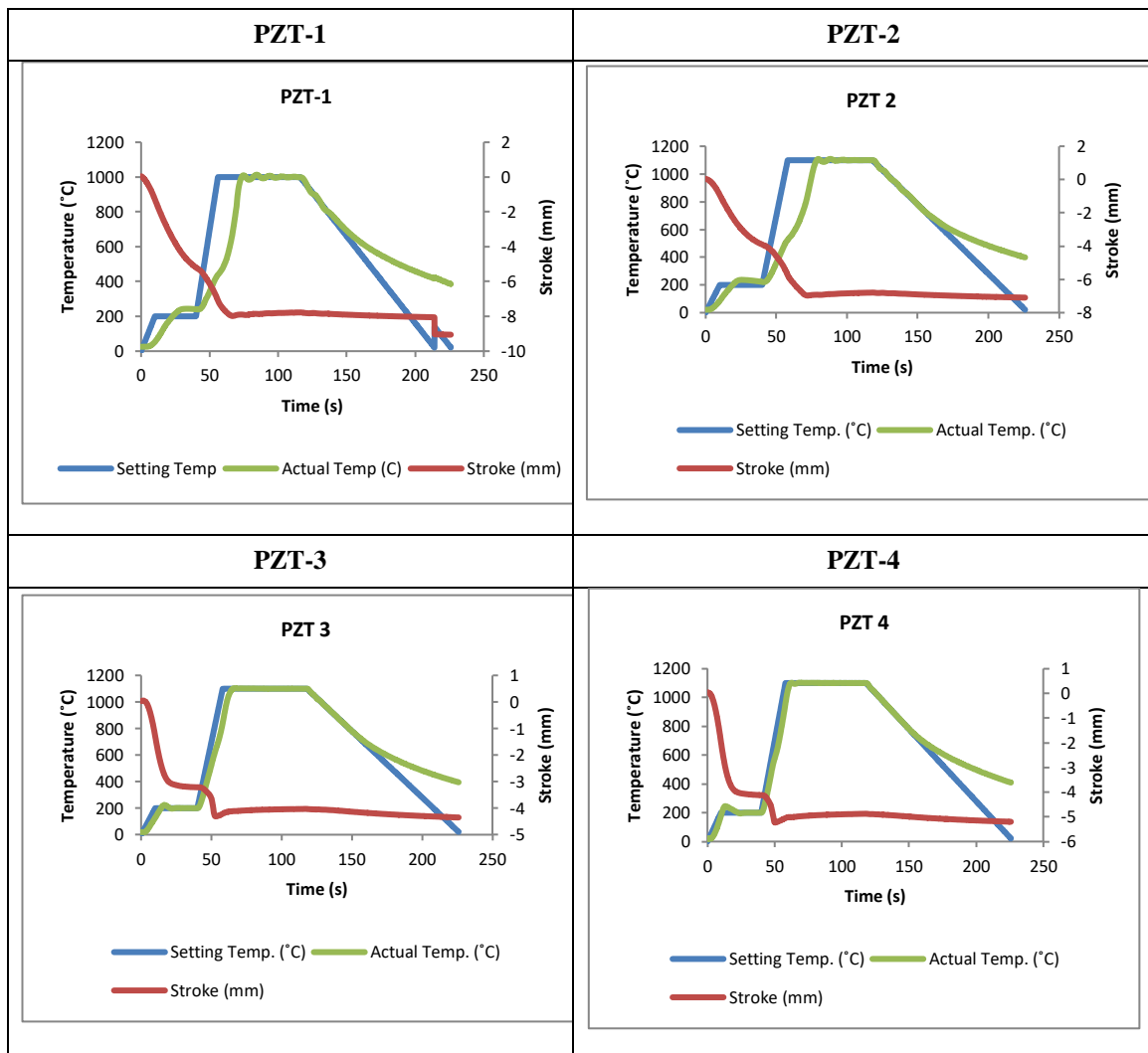


FIGURE 5-22: THE HEATING TEMPERATURE AND SHRINKAGE OF STROKE PUNCHES OF GLEEBLE® 3800 MACHINE FOR PZT SAMPLES.

The PZT-2 and PZT-4 have the best relative density in the Micro-FAST process. It is clear that the applied pressure, second heating rate, second heating temperature have a direct effect on the relative density of the samples. Figure 5-23 shows the produced samples after the ejection process. However, the samples did not have the expected relative density and have not been produced in very good condition. The reason behind that is the piezoceramic could need more holding time to reach the required relative density. Moreover, some of the formed samples have some cracks in the surface and the total finishing of the sample was not good as seen in Figure 5-23. Therefore, more experiments are required to identify the ideal parameters for the piezoceramic powders.

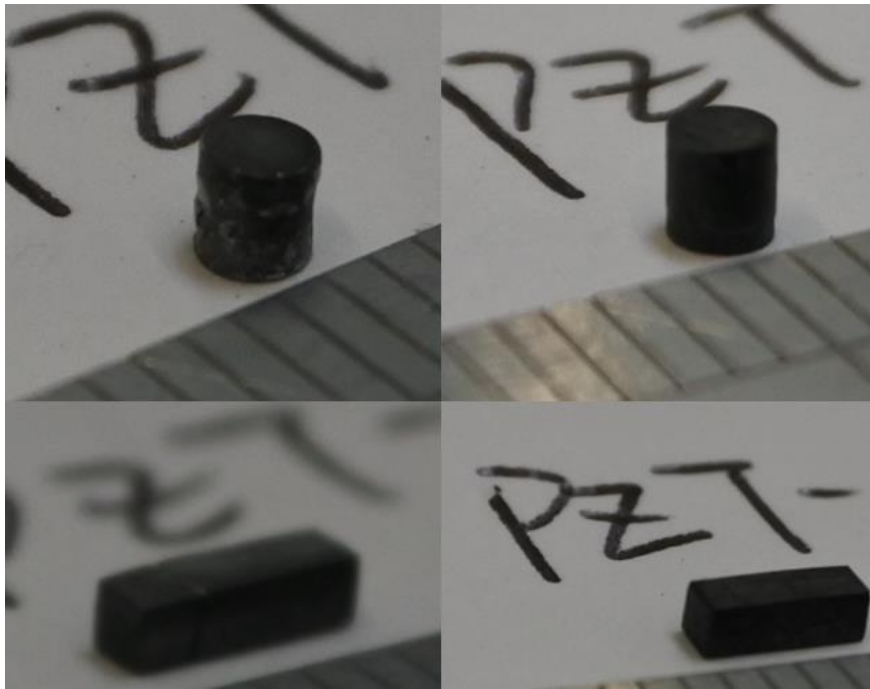


FIGURE 5-23: THE PIEZOCERAMIC SAMPLES

5.5.2 SAMPLES MICROSTRUCTURES

The description of the microstructure, particles, and chemical element weight percentage of carbon (wt%) is discussed for all samples from zirconia, alumina and piezoceramic.

5.5.2.1 ZIRCONIA

In this section, The description of the microstructure particles and chemical element weight percentage of carbon (wt%) has been discussed for three types of zirconia samples. The first one is Ytria Partially Stabilized Zirconia (3Y-ZrO₂). The second type of Zirconia is the Magnesia Partially Stabilized Zirconia (MSZ) The Third one is Magnesia Partially Stabilized Zirconia with with 5 wt% organic additives or organic binders MSZ(#).

5.5.2.1.1 3YZrO₂

Figure 5-24 and Figure 5-25 show the comparison of SEM for the position at the centre and the edge of 3YZrO₂ samples respectively. The 3YZrO₂-1 sample shows the most porous particle densification at the micrograph scale compared to the other samples at the position of centre and edge, where it shows the particle breakage and deformation during the applied constant pressure and high temperature. This phenomenon occurs in the other samples which indicates an increase of contact areas as the densification value increased. 3YZrO₂-2 shows that the pores of the particles melting were reduced as it continued at the positions of centre and edge. This was due to the heating temperature incrementing from 1200 to 1,300 °C. For sample 3YZrO₂-3 the pores of the particles melting were reduced due to the increase of the applied pressure from 75 to 125 MPa. This helps the deformation and crushing of particles which contributes to forcing the 3YZrO₂ particles to touch each other during the strengthened sintering process until the pores become smaller and disappear. In the last sample 3YZrO₂-4, there was a small amount of pores existing at the edge and the centre of the sample. The pores of the particles melting were reduced due to using 125 MPa applied pressure and by decreasing the heating rate causing an increase in the heating time.

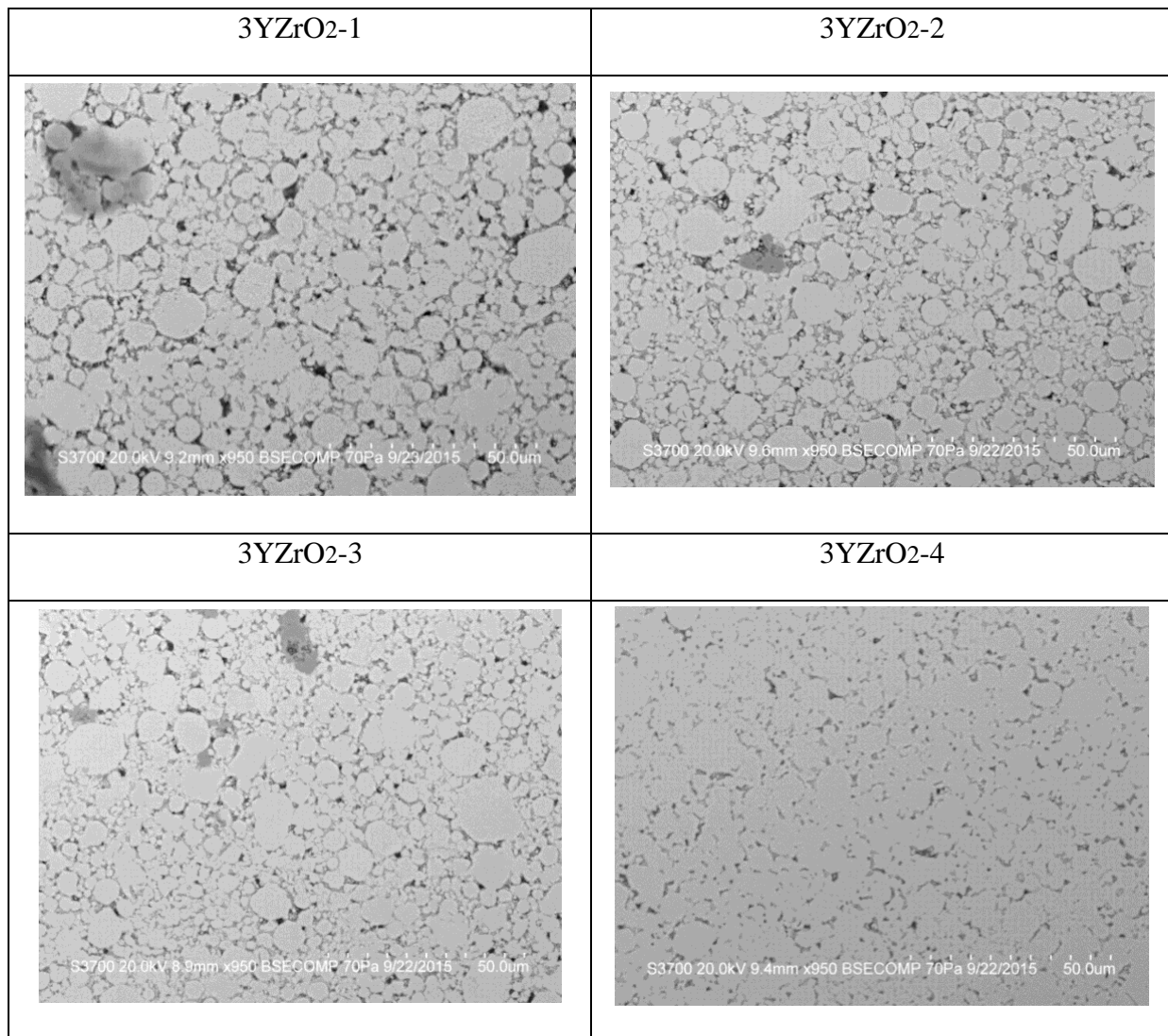


FIGURE 5-24: SEM MICROGRAPH FOR 3YZRO₂ SAMPLE AT CENTRE POSITION (MAGNIFICATION: 950 BSE)

However there were several limitations when using the die set made fully of graphite. With regard to durability, based on observation the punch nose was easily broken due to many cycles of the process. The resistance to impact from the higher forming pressure on the graphite die set was a key weakness due to low mechanical strength at the elevated temperature during the forming and sintering process. In addition the punch also needed to be cleaned after a number of cycles due to the used powder material melting and becoming stuck onto the punch and die surfaces.

TABLE 5-14: CHEMICAL ELEMENT WEIGHT PERCENTAGE OF CARBON (WT%) AT THE POSITIONS OF CENTRE AND EDGE OF 3YZrO₂ SAMPLES.

Positions of Inspections	Units	3YZrO₂-1	3YZrO₂-2	3YZrO₂-3	3YZrO₂-4
Centre of the Samples	wt.%	13.12	12.54	13.11	11.18
Edge of the Samples	wt.%	14.82	13.93	13.73	12.07

Regarding the presence of carbon at the centre and edge of 3YZrO₂ samples, Table 5-14 shows the high amount of carbon contaminate was in the range of 11.18 to 13.12 wt% for the centre position and 12.07 to 14.82 wt% for the edge location of the samples. This is a drawback when using a graphite die where the carbon element at the wall of the die can be mixed into the solidified 3YZrO₂ sample during the high temperature of the sintering process. Based on this disadvantage, it was hard to achieve a sample that was free from contamination such as carbon especially on the sample surfaces when a graphite die set was used.

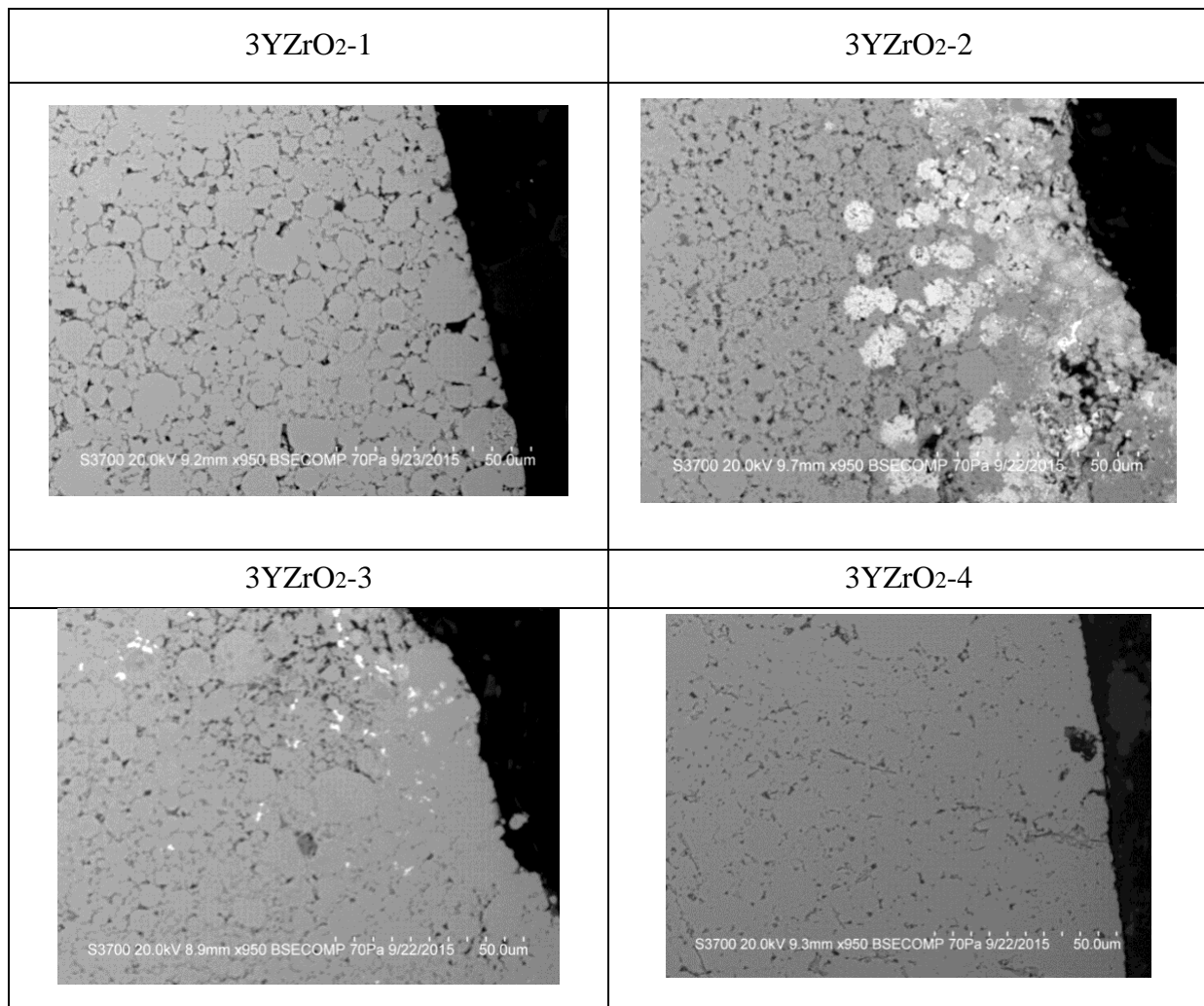


FIGURE 5-25: SEM MICROGRAPH FOR 3YZRO₂ SAMPLE AT EDGE POSITION (MAGNIFICATION: 950 BSE)

5.5.2.1.2 MSZ

Figure 5-26 and Figure 5-27 show the comparison of SEM for the position at the centre and the edge of the MSZ samples respectively. The MSZ-1 sample shows the most porous particle densification at micrograph scale among the other samples at the positions of centre and edge. Here it shows the particle breakage and deformation during the applied constant pressure and high temperature. The pores of the particles melting were reduced as the process continued at the positions of centre and edge in sample MSZ-2 due to the reduction in the heating rate from 100 °C/s to 25°C/s. In the MSZ-3 sample, the pores of the particles melting were reduced more after increasing the holding time and setting the heating rate at 50°C/s. In the last sample MSZ-4, there was not that much difference in the micrograph. The porosity of particle densification and particle breakage and deformation reduced and the surface improved.

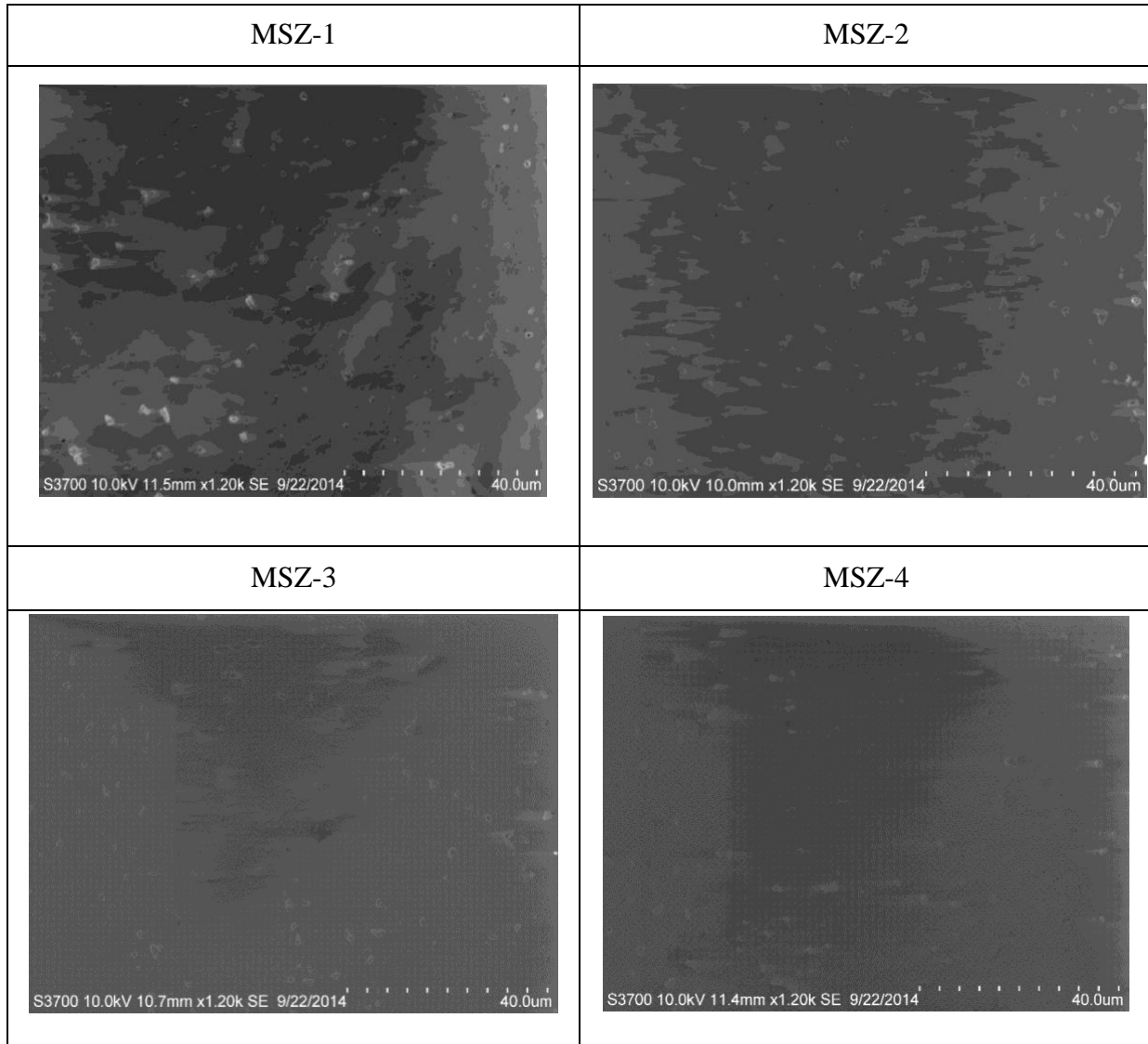


FIGURE 5-26: SEM MICROGRAPH FOR MSZ SAMPLE AT CENTRE POSITION (MAGNIFICATION: : 1.20 K SE)

However, using the die set made fully of graphite has limitations when using it in this process. The durability is an important matter as the die set could be broken and in particular the punch nose due to many cycles of the process. The resistance to impact from the higher pressure on the graphite die set was a key weakness due to low mechanical strength at Micro-

FAST. Moreover, the punch needed to be cleaned carefully because of using the other materials.

TABLE 5-15: CHEMICAL ELEMENT WEIGHT PERCENTAGE OF CARBON (WT%) AT THE POSITIONS OF CENTRE AND EDGE OF MSZ SAMPLES.

Positions of Inspections	Units	MSZ-1	MSZ-2	MSZ-3	MSZ-4
Centre of the Samples	wt.%	12.56	12.91	10.77	11.02
Edge of the Samples	wt.%	13.64	13.55	11.67	11.97

Using the graphite materials in the die set lead to a presence of carbon element at the centre and edge of MSZ samples. This is due to the drawback when using a graphite die where the carbon element at the die's wall can be mixed into the solidified MSZ samples during the high temperature of the sintering process. Table 5-15 shows the high amount of carbon contaminate was in the range of 10.77 to 12.91 wt% for the centre position and 11.67 to 13.64 wt% for the edge location of the samples. It was difficult to achieve a sample that was completely free from contamination such as carbon especially on the sample surfaces when a graphite die set was used.

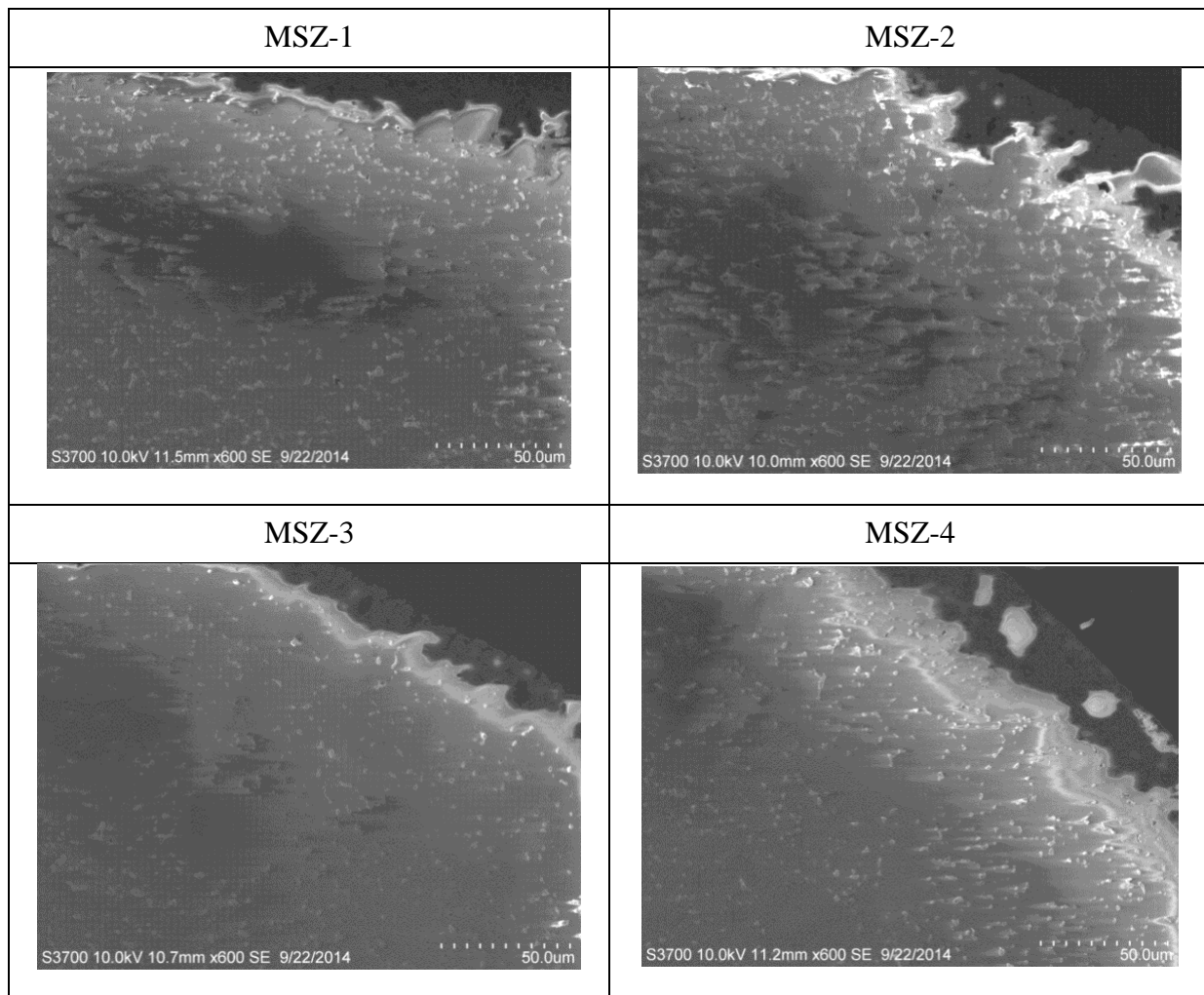


FIGURE 5-27: SEM MICROGRAPH FOR MSZ SAMPLE AT EDGE POSITION (MAGNIFICATION: : 600 SE)

5.5.2.1.3 MSZ(#)

Figure 5-28 and Figure 5-29 show the comparison of SEM for the position at the centre and the edge of MSZ(#) samples respectively. The MSZ(#)-1 sample shows the most porosity of particle densification at the micrograph scale among the other samples at the position of centre and edge where it shows particle breakage and deformation during the applied constant pressure and high temperature. In the MSZ(#)-2 sample, the pores of the particles melting were clearly reduced as they continued at the centre due to the increase in the holding time to 60 seconds. In the MSZ(#)-3 sample, the holding time and the heating rate have been increased to 120 seconds and 50°C/s respectively. In this sample, a better surface has been achieved and the pores of the particles melting were further reduced. In the sample MSZ-4, the porosity of

particle densification and particle breakage and deformation reduced and the surface improved. In addition to that, there are no coarsening of grains accompanying the process of part densification.

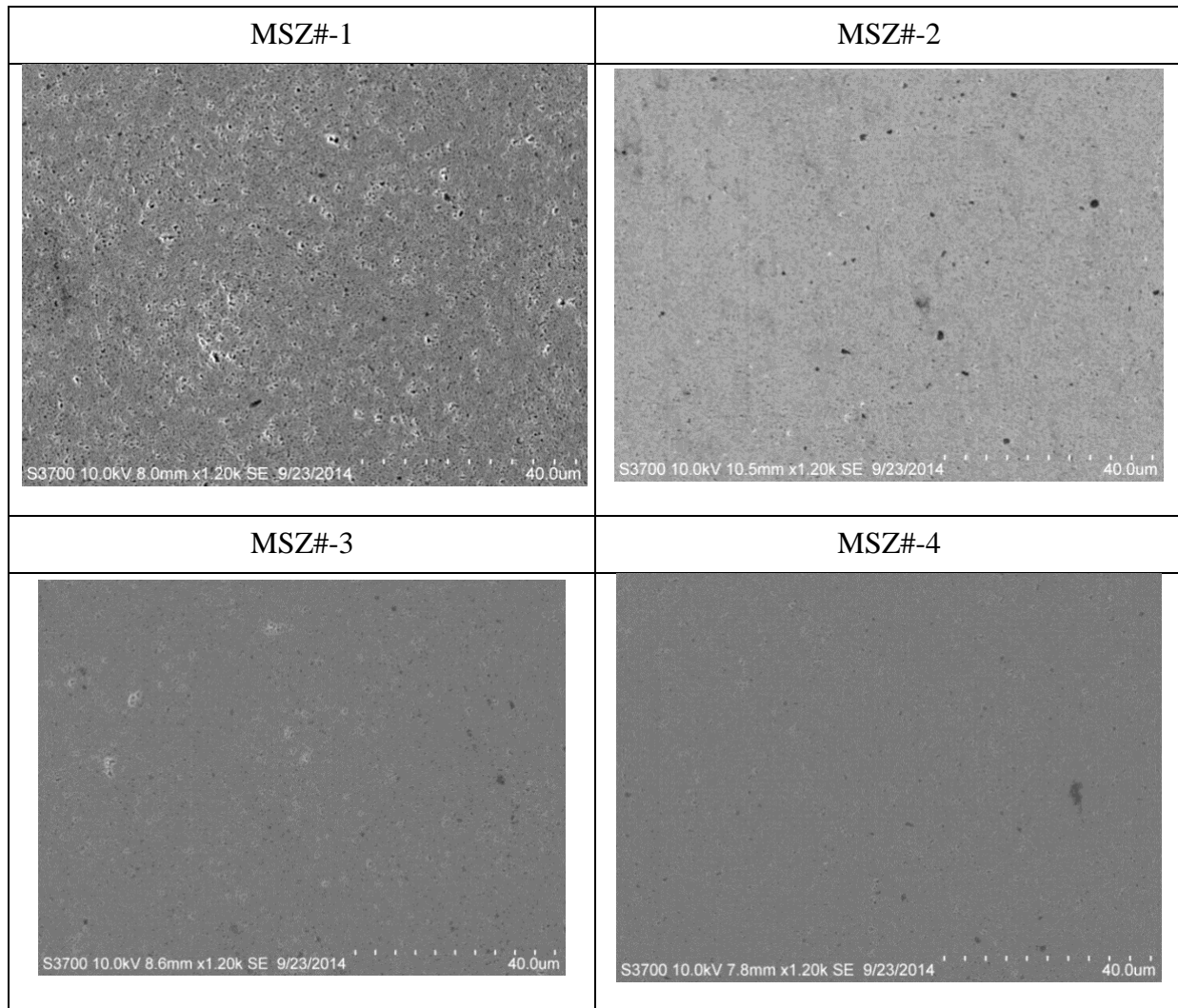


FIGURE 5-28: SEM MICROGRAPH FOR MSZ (#) SAMPLE AT CENTRE POSITION (MAGNIFICATION: : 1.20 K SE)

Table 5-16 shows the high amount of carbon contaminate was in the range of 0 to 2.79 wt% for the centre position and 0 to 3.47 wt% for the edge location of the samples. This shows an improvement since there were no carbon elements sticking in the last two samples MSZ(#)-3 and MSZ(#)-4.

TABLE 5-16: CHEMICAL ELEMENT WEIGHT PERCENTAGE OF CARBON (WT%) AT THE POSITIONS OF CENTRE AND EDGE OF MSZ (#) SAMPLES

Positions of Inspections	Units	MSZ#-1	MSZ#-2	MSZ#-3	MSZ#-4
Centre of the Samples	wt.%	2.79	0.54	0	0
Edge of the Samples	wt.%	3.47	0.89	0	0

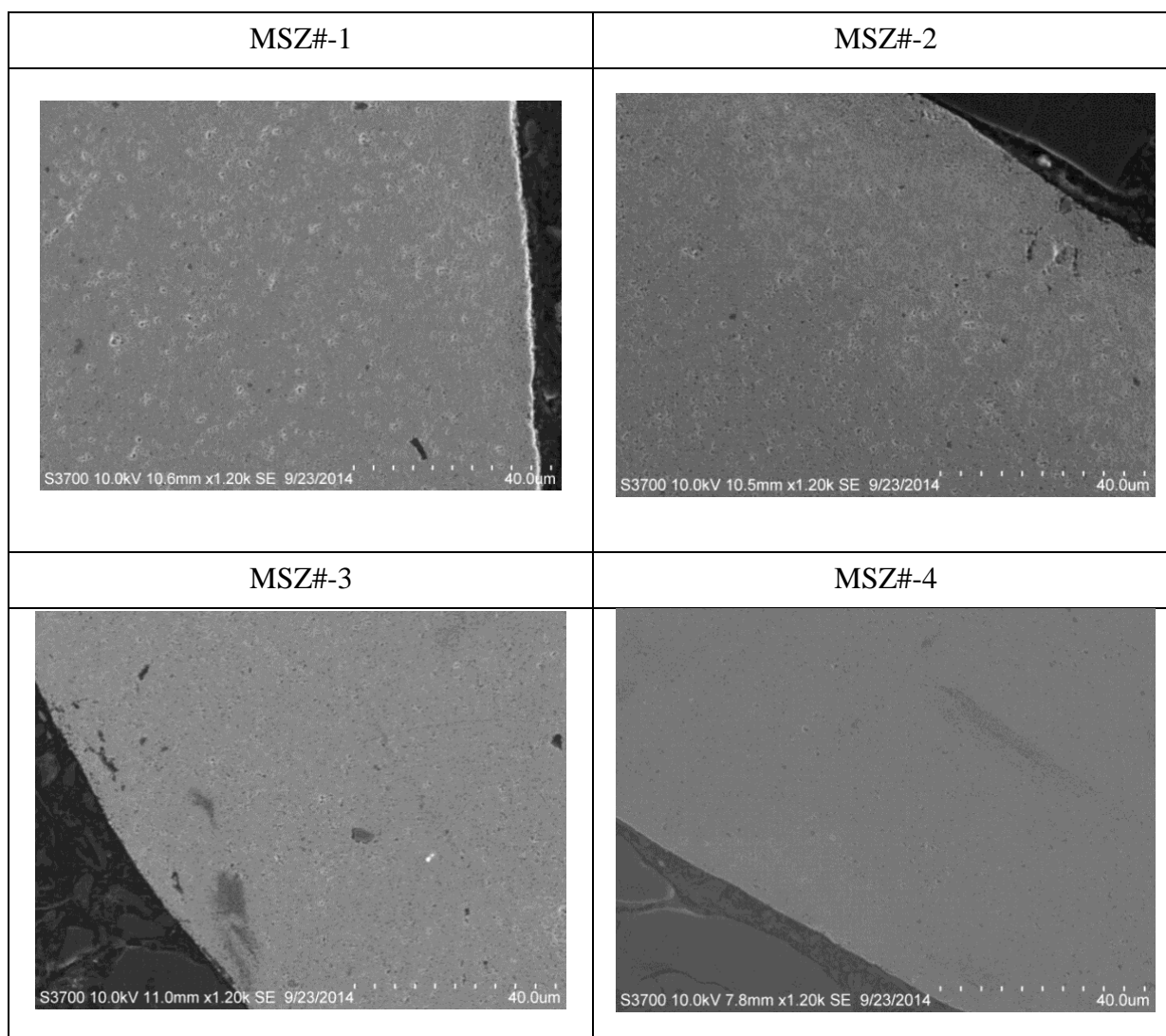


FIGURE 5-29: SEM MICROGRAPH FOR MSZ (#) SAMPLE AT EDGE (MAGNIFICATION: : 1.20 K SE)

5.5.2.2 ALUMINA

Figure 5-30 and Figure 5-31 show the comparison of SEM for the position at the centre and the edge of the Alumina samples respectively. The Al₂O₃-1 sample shows the most porosity

of particle densification at the micrograph scale among the others samples at the position of centre and edge where it shows the particle breakage and deformation during the applied constant pressure and high temperature. This process also occurs in the other samples which indicated an increase of contact area as the densification value increased. The pores of the particles melting were reduced as it continued to the samples Al_2O_3 -2 and Al_2O_3 -3 at the positions of centre and edge. In the Al_2O_3 -2, the pores of the particles melting were reduced as it continued at the positions of centre due to the incremental of holding time and the heating temperature. In the Al_2O_3 -2 sample, the holding time increased to 360 seconds and in Al_2O_3 -3 sample the holding time was 240 seconds and the heating temperature increased to 1300 °C. In the sample Al_2O_3 -4, there was a clear improvement. The porosity of particle densification and particle breakage and deformation reduced and the surface improved. This is because of the increase of the applied pressure from 75 to 125 MPa. This helps the deformation and crushing of particles which can contribute to forcing the Alumina particles to touch each other during the strengthened sintering process until the pores become smaller and disappear.

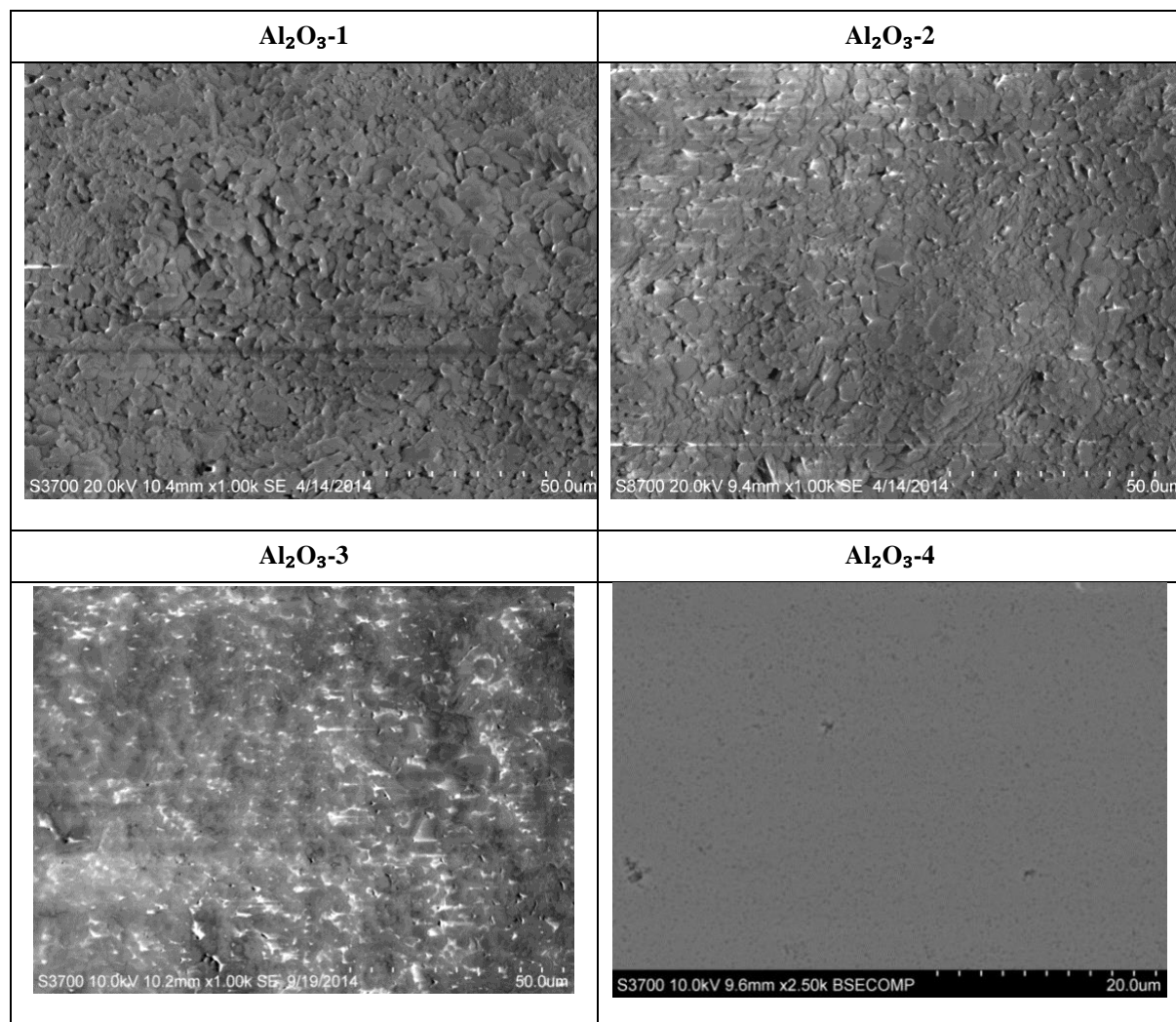


FIGURE 5-30: SEM MICROGRAPH FOR ALUMINA SAMPLE AT CENTRE POSITION

The chemical element weight percentage of carbon in the Alumina samples is shown in Table 5-17. The range was 3.43 to 7.04 wt% for the centre position and 4.82 to 8.49 wt% for the edge location. The results regarding the contamination of the carbon element for Alumina samples was better compared to some zirconia samples as shown previously.

TABLE 5-17: CHEMICAL ELEMENT WEIGHT PERCENTAGE OF CARBON (WT%) AT THE POSITIONS OF CENTRE AND EDGE OF ALUMINA SAMPLES

Positions of Inspections	Units	Al ₂ O ₃ -1	Al ₂ O ₃ -2	Al ₂ O ₃ -3	Al ₂ O ₃ -4
Centre of the Samples	wt. %	7.04	6.03	5.26	3.43
Edge of the Samples	wt. %	8.49	7.69	7.03	4.82

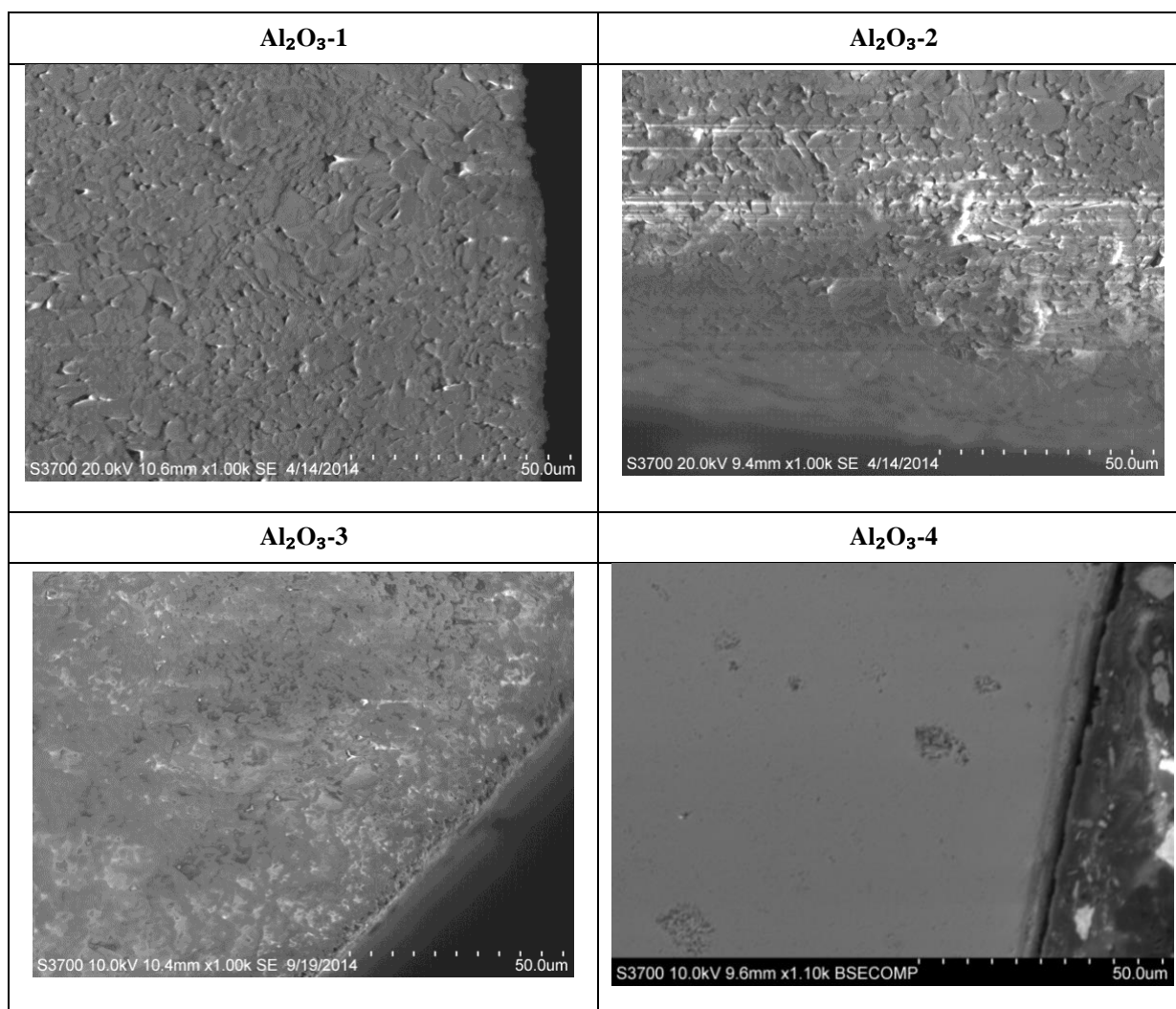


FIGURE 5-31: SEM MICROGRAPH FOR ALUMINA SAMPLE AT EDGE POSITION

5.5.2.3 PIEZOCERAMIC (PZT)

Figure 5-32 and Figure 5-33 show only two piezoceramic samples (PZT-2 and PZT-4) that SEM and the EDS investigated because the other samples were not formed enough and showed some large pores and cracks on the surface. The PZT-2 Sample shows some porosity of particle densification at the micrograph scale at the position of centre and edge where it shows particle breakage and deformation during the applied constant pressure and high temperature. In the sample PZT-4, the pores of the particles melting were reduced at the positions of centre and edge. The reason behind that is decreasing the heating rate to 25 °C/s. In the sample PZT-4, there was a clear improvement. The porosity of particle densification and particle breakage and deformation reduced and the surface improved. However, the PZT-4 sample showed a small crack in the edge of the surface regardless of the fine microstructure.

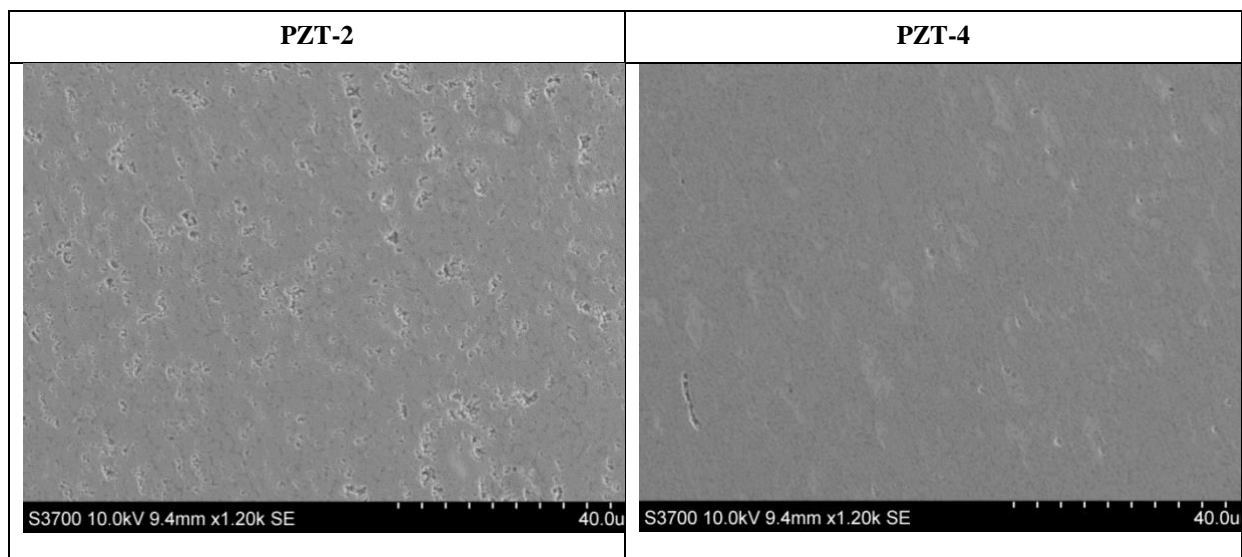


FIGURE 5-32: SEM MICROGRAPH FOR PIEZOCERAMIC SAMPLE AT CENTRE POSITION

The chemical element weight percentage carbon of piezoceramic samples is shown in Table 5-18. The PZT-2 indicated 9.04 wt% for the centre and 8.13 wt% for the edge. The PZT-4 indicated 8.13 wt% for the centre and 8.69 wt% for the edge.

TABLE 5-18: CHEMICAL ELEMENT WEIGHT PERCENTAGE OF CARBON (WT%) AT THE POSITIONS OF CENTRE AND EDGE OF PIEZOCERAMIC SAMPLES

Positions of Inspections	Units	PZT-2	PZT-4
Centre of the Samples	wt. %	9.04	8.13
Edge of the Samples	wt. %	10.49	8.69

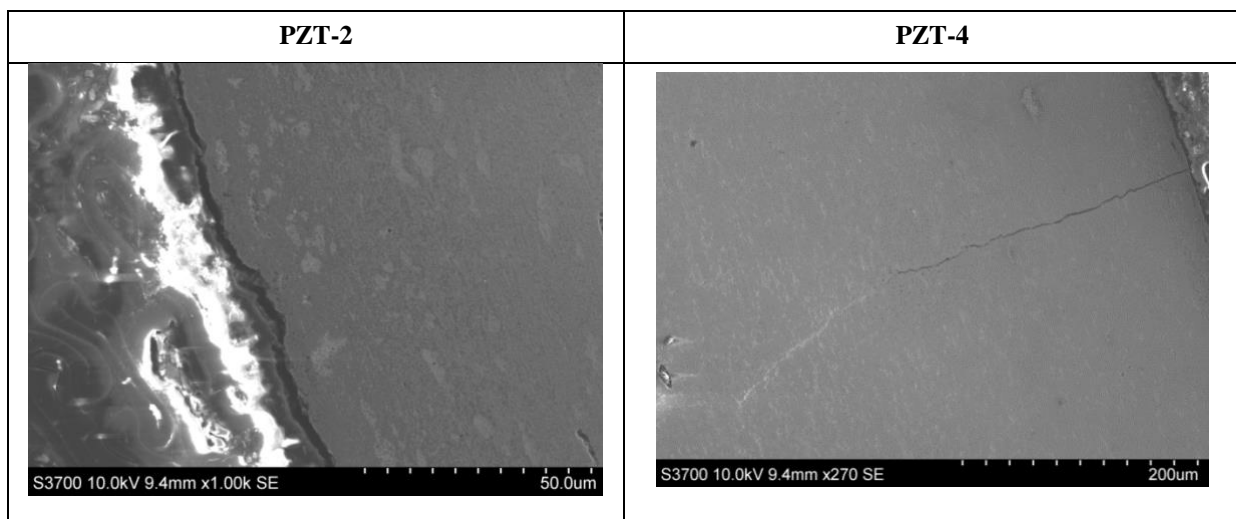


FIGURE 5-33: SEM MICROGRAPH FOR PZT SAMPLE AT EDGE POSITION

5.5.3 SAMPLES HARDNESS

Based on the relative density and microstructure of all samples, two materials have been chosen to conduct the samples hardness test. The Nano-hardness test (Nano-indentation) has been carried out for samples MSZ and MSZ(#)

5.5.3.1 MSZ

The Nano-hardness test has been done at the sample MSZ-3 by using the NanoTest Vantage hardness tester as shown in Figure 5-34 due to its high relative densification recorded which was 97.53%. Table 5-19 shows the average value for 100 indentations of nano-hardness test that have been made which indicated the reading for the nano-hardness and reduced Young Modulus (E_r) value was 13.76014 GPa and 209.0603 GPa respectively. Figure 5-36 shows the distribution of nano-hardness and reduced Young's modulus (E_r) value for the sample MSZ-3.

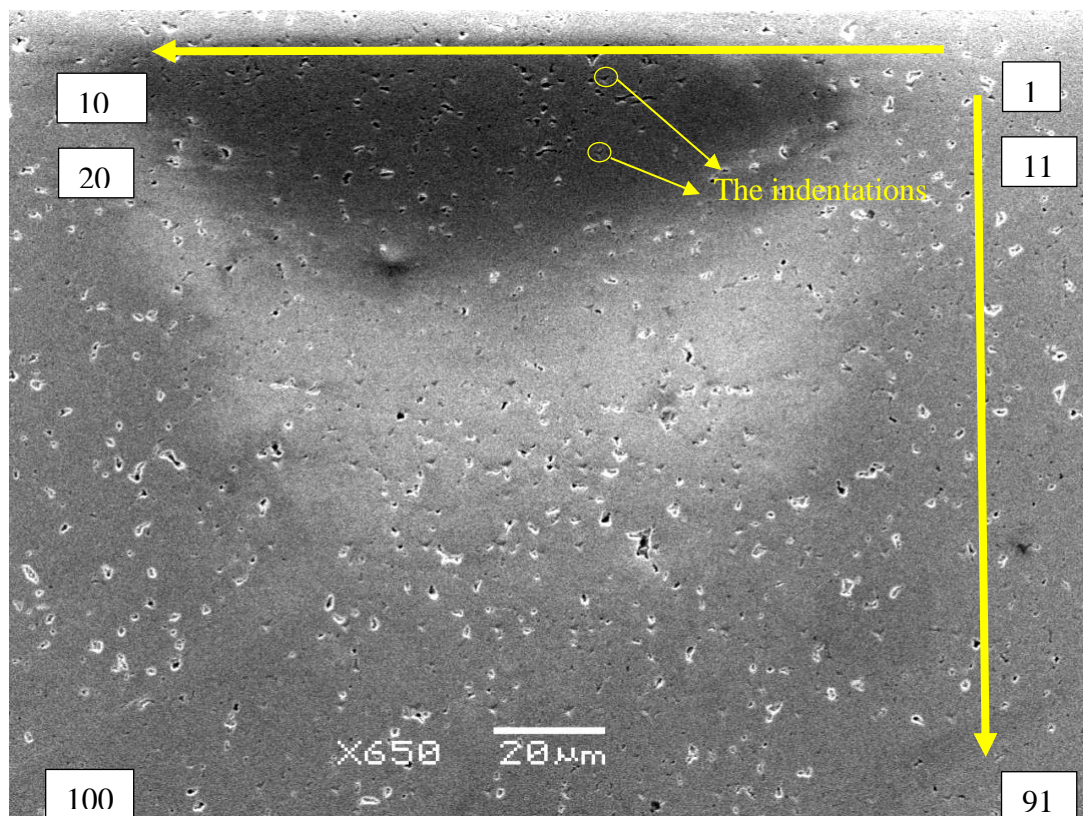


FIGURE 5-34: POSITIONS OF NANO-HARDNESS INDENTATION OF MSZ-3 SAMPLE BY USING NANOTEST VANTAGE HARDNESS TESTER.

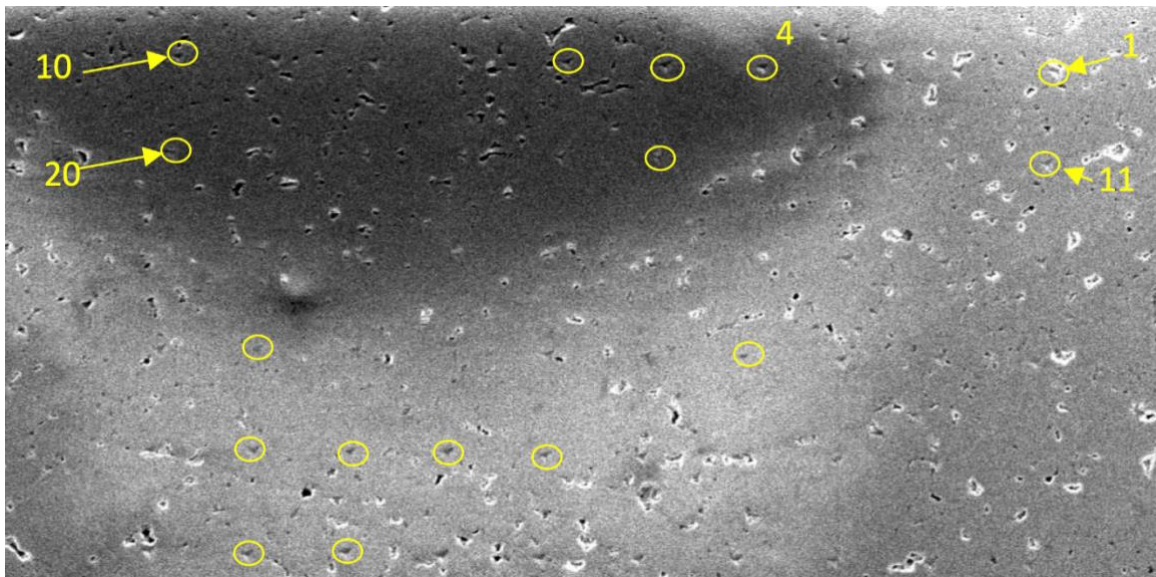


FIGURE 5-35: LARGE IMAGE FOR SOME POSITIONS OF NANO-HARDNESS INDENTATION OF MSZ-3 SAMPLE

However, due to similarity in the size of the pore, a zoomed picture has been illustrated as seen in Figure 5-35. Some of the indentations may locate near to or on the pore which leads to a low hardness such as point 1 as shown in Figure 5-35. These indentations on a solid place will have good measurements for the Nano-hardness and modulus of the materials. Therefore, selective points in good locations will be used to calculate the average Nano-hardness and a reduced elastic modulus. The chosen indentations are 4,8,9,12 and 16. The average Nano-hardness is about 14.44 GPa and reduced Young Modulus (E_r) is about 213.58 GPa.

TABLE 5-19: AVERAGE VALUES FOR NANO-HARDNESS TEST FOR MSZ-3 BY USING NANOTEST VANTAGE HARDNESS TESTER

Results	Units	Means	Errors
Max Depth	nm	373.3352	31.42479
Plastic Depth	nm	301.4467	33.32642
Maximum Load	mN	40.02	0.000001
Hardness	GPa	13.76014	2.329558
Reduced Young Modulus, E_r	GPa	209.0603	16.32858
Elastic Recovery Parameter, ERP		0.241675	0.030812
Contact Compliance	nm/mN	2.395085	0.115092
Plastic Work	nJ	3.2326	0.531406
Elastic Work	nJ	2.326256	0.080666

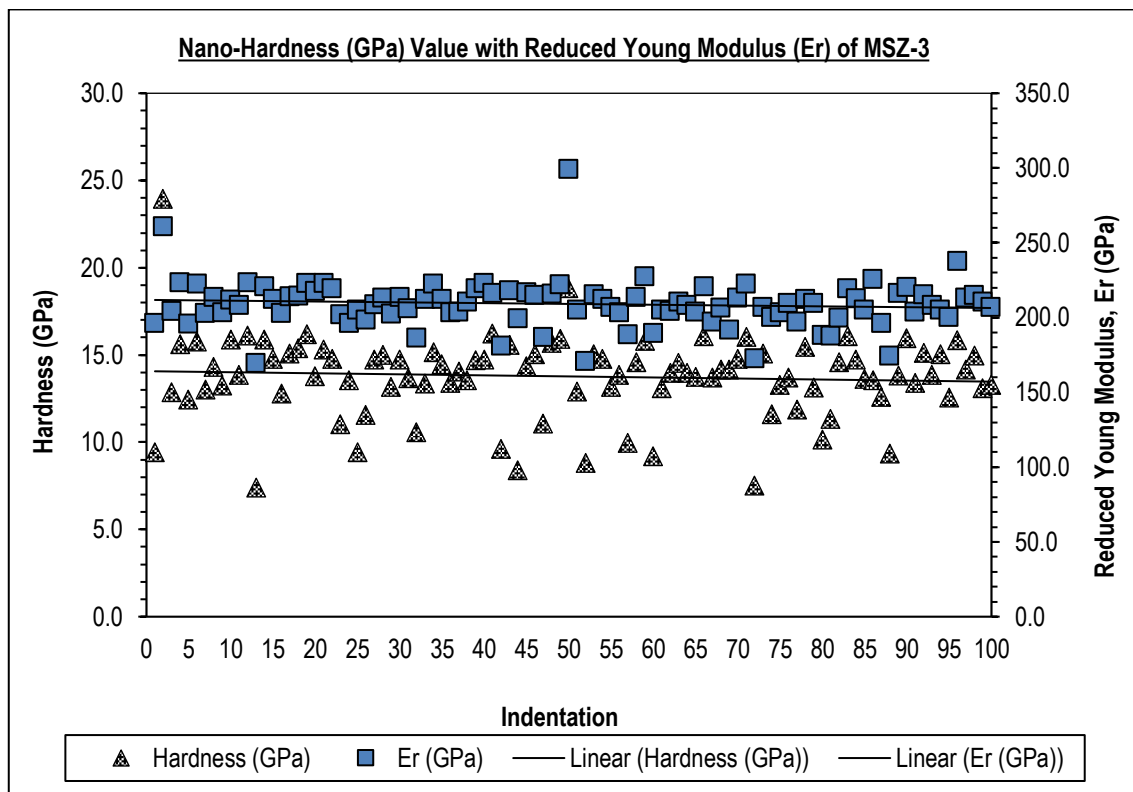


FIGURE 5-36 : DISTRIBUTION OF NANO-HARDNESS AND REDUCED YOUNG MODULUS (ER) VALUE FOR MSZ-3

5.5.3.2 MSZ(#)

Overall 100 points (10x10) of Nano-hardness test material has been done of the sample MSZ(#)-4 by using the NanoTest Vantage hardness tester as shown in Figure 5-37 due to the high relative densification recorded which was 97.45%. Meanwhile, Table 5-20 shows the average value for 100 indentations of Nano-hardness that have been made which indicated the reading for the Nano-hardness and reduced Young Modulus (Er) value was 4.564302 GPa and 107.9313 GPa respectively. Moreover, Figure 5-38 shows the distribution of nano-hardness and reduced Young's modulus (Er) value for the sample MSZ(#)-4.

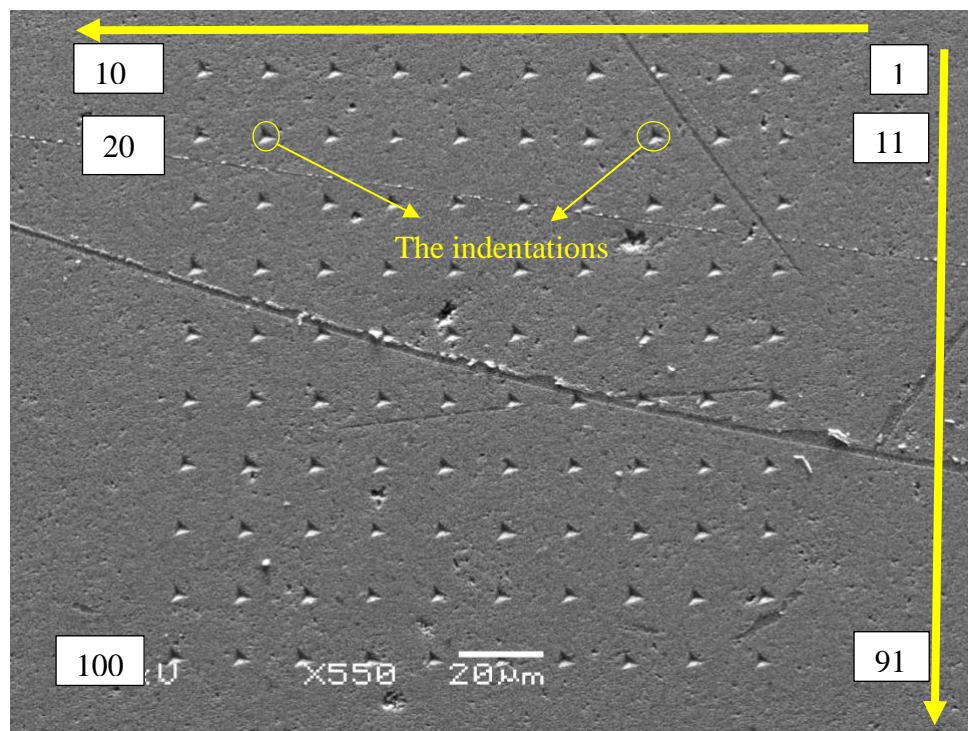


FIGURE 5-37: POSITIONS OF NANO-HARDNESS INDENTATION OF MSZ(#)-4 SAMPLE BY USING NANOTEST VANTAGE HARDNESS TESTER

By comparing the results of two materials, it can be shown that there are big differences in the hardness value due to the existence of the organic binders. The organic additive has low hardness and that affect the hardness of the magnesia stabilised zirconia.

TABLE 5-20: AVERAGE VALUES FOR NANO-HARDNESS TEST FOR MSZ(#)-4 BY USING NANOTEST VANTAGE HARDNESS TESTER

Results	Units	Means	Errors
Max Depth	nm	633.9504	41.09727
Plastic Depth	nm	553.643	42.17041
Maximum Load	mN	40.02	0
Hardness	GPa	4.564302	0.627345
Reduced Young Modulus, Er	GPa	107.9313	6.669121
Elastic Recovery Parameter, ERP		0.146013	0.013379
Contact Compliance	nm/mN	2.675574	0.083657
Plastic Work	nJ	6.804714	0.599118
Elastic Work	nJ	2.675279	0.079608

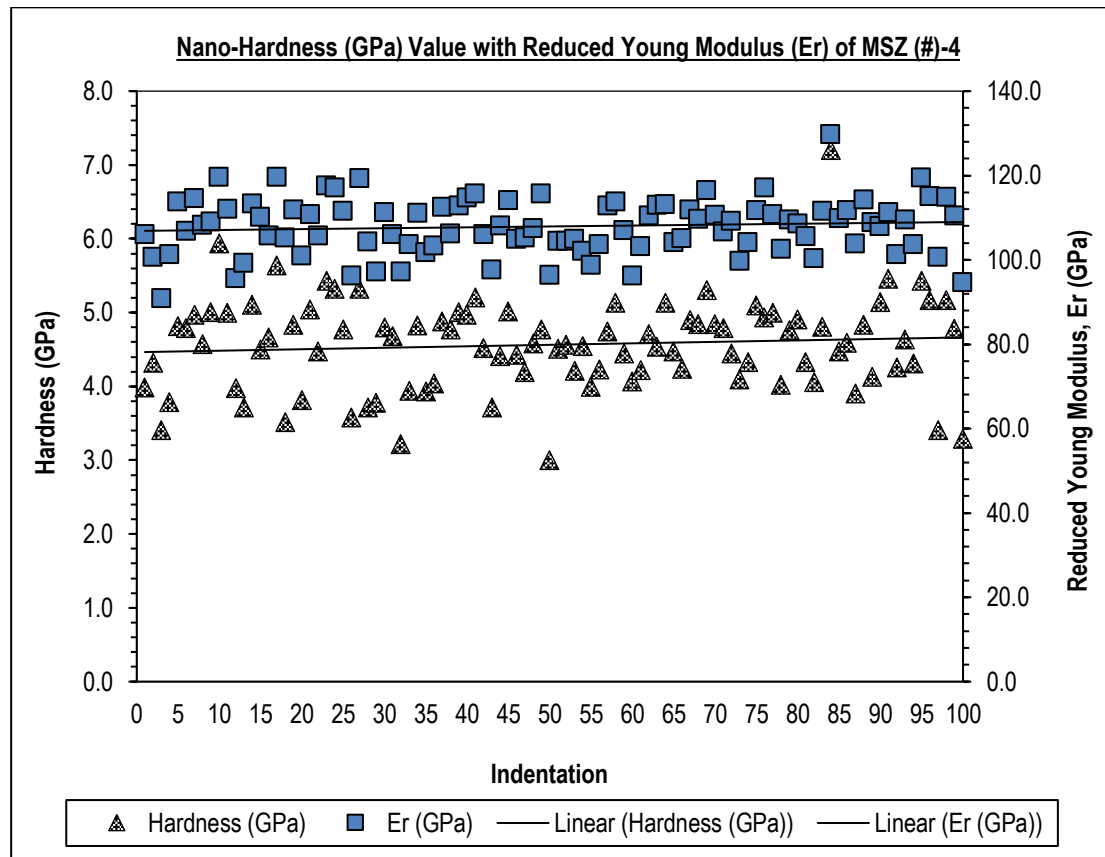


FIGURE 5-38: DISTRIBUTION OF NANO-HARDNESS AND REDUCED YOUNG MODULUS (ER) VALUE FOR MSZ(#)-4

5.6 SUMMARY OF THE CHAPTER

In this chapter, experiments using the Micro-FAST process have been conducted on three main powders (alumina, zirconia and piezoceramic) using the Gleeble[®] 3800 which is a thermal mechanical machine. Three types of zirconia have been tested. The first one is Ytria Partially Stabilized Zirconia ($ZrO_2 + 3 \text{ mol\% ytria}$) (**3Y-ZrO₂**) the average particle size of powder materials was $6.5 \mu\text{m}$ and it had 5.285 g/cm^3 for theoretical density. The other type of Zirconia is the Magnesia Partially Stabilized Zirconia (MSZ) and the starting partical size was below $5 \mu\text{m}$ with spray dried granulates that were sieved between $40\text{-}80 \mu\text{m}$ and a theoretical density of 5.82 g/cm^3 . The Third Zirconia powder was MSZ(#) with 5 wt% organic additives or organic binders to improve the forming process, and the theoretical density for this one was 5.72 g/cm . The starting partical size for MSZ(#) was below $2 \mu\text{m}$ with spray dried granulates that were sieved between $40\text{-}80 \mu\text{m}$. The organic materials burn out in two steps. Around 2.2 wt% organic material can be removed at 200°C and the other 2.6 wt% can be removed around

380°C. The Alumina powder material Al_2O_3 had an average particle size of 0.18 μm and purity of 99.9% and the theoretical bulk density for the used powder is 3.95 g/cm^3 . The piezoceramic used for this experiment has a particle size of 6.5 μm and the theoretical density for the used powder is 7.4 g/cm^3 . The parameters that have been used in the experiments, such as pressure, heating temperature, heating rate and holding time were controlled automatically using a computer-controlled system (QuickSimTM software). The electrical field produced by the Gleeble[®] 3800 machine has a high current (3000~30000 A) and low voltage (3~10 V). The die sets used in the experiment were of the optimised design shown in a previous chapter and the punches and dies were made from graphite. The selection of the graphite material was because the value of the thermal expansion coefficient of punches and die must be less than the powder material being tested. This will prevent any traps and sticking between the punches, die and samples during the ejection process. Moreover, by using graphite for the die set material, a higher sintering temperature can be utilised up to its maximum service temperature up to 2,700 °C.

After the powder material had been weighed, it was carefully poured into the die sets. Then, the die set with the powder material was placed into the chamber of the Gleeble[®] 3800 machine with the thermocouple as in Figure 5-1. After that, the die set with the powder material was heated promptly to a specific sintering temperature in the vacuum. The electrical current was passed through the die set with powder material inside it and at the same time a specific pressure was applied to the upper and lower die punches. Then, the sample was ejected out from the die set. Then, the formed samples from the experiments were analysed using several apparatus. For their relative density, a Sartorius YDK03 apparatus was used, and for the surface of microstructure of the sample the scanning electron microscope machine (SEM/EDS) was used. Also a chemical element weight percentage test has been performed at the centre and edge of the sample parts using an energy dispersive spectroscopy (EDS) facility. A nano-hardness (NanoTest Vantage) test was also done at the sintered neck of the zirconia sample.

Based on the work that has been made in this chapter, it can be shown that the die set showed good efficiency during the Micro-FAST process and plays a significant role in the sample size and its densification. It was important to have a fully closed die set during the experiment so that the electrical current can go through the overall die and the heat is generated

for the entire die set efficiently. The results that have been displayed in this experiment regarding the relative density indicates the efficiency of the Micro-FAST process.

For the zirconia (3YZrO_2) it shows that 3YZrO_2 -3 and 3YZrO_2 -4 have the highest relative density which are 97.31 and 99.47 % respectively. The holding time for these samples was 120 seconds which is half of the previous time compared to 3YZrO_2 -1 and 3YZrO_2 -2. By using this Micro-FAST process, it has the potential to save time compared to the conventional electrical field sintering process. For 3YZrO_2 -4 sample, the optimum parameters of 125 MPa for the applied pressure, 1,300 °C for the second heating temperature and 25 °C/s for the second heating rate were used. The 3YZrO_2 -3 sample used the optimum parameters of 125 MPa for the applied pressure, 1,300 °C for the second heating temperature and 50 °C/s for the second heating rate.

The zirconia (MSZ), the MSZ-3 sample recorded a 97.53% relative density and the total process time was 391.0 seconds. The parameters that have been used are 125 MPa applied pressure, 1300 °C sintering temperature, 50 °C/s heating rate and the holding time was 180 seconds., which is good compared to the conventional sintering process. For sample MSZ-4, the applied pressure maintained the same (125 MPa), but the sintering temperature was increased to 1400 °C. Compared to MSZ-3, the heating rate and holding time increased for the MSZ-4 sample to 25 °C/s and 90 seconds respectively. The MSZ-4 sample reached a 99.49% relative density.

For the zirconia (MSZ#) samples. The MSZ(#)-3, sintering temperature was 1300 °C , the holding was 120 seconds and the heating rate was 50 °C/s. The MSZ(#)-3 sample has achieved 95.51% but the total process time increased to 484.4 seconds. In the last sample MSZ(#)-4, the holding time and the heating temperature was the same as MSZ(#)-3 which is 120 seconds and 1300, but the heating rate was increased to reduce the total time process. The relative density for the MSZ(#)-4 sample was 97.45% with a total process time of 475.2 seconds.

For Alumina, Al_2O_3 -3 and Al_2O_3 -4 have recorded 87.09 and 92.68 % density respectively. The holding time for these samples was 240 s and the heating temperature was 1300 C. The applied pressure for Al_2O_3 -3 sample was 75 MPa and for Al_2O_3 -4 was 125 MPa. It is shown

that in this case the pressure played an important role in increasing the relative density of the Al_2O_3 -4.

Regarding the presence of carbon elements contamination at the centre and edge of all samples. This is due to the drawback when using graphite material for punches or dies where the carbon can be mixed into the solidified sample during the high-temperature sintering process.

Two materials have been chosen to conduct the samples hardness test. The Nano-hardness test (Nano-indentation) has been carried out for samples MSZ-3 and MSZ(#)-4, it has been chosen for the testing of micro- and nano-hardness and has been applied with 100 indentations which shows the hardness value of 13.76014GPa and 4.564302 GPa value respectively. The two materials have big differences in the hardness value due to the existence of the organic binders. The organic additive has low hardness and that affect the hardness of the magnesia stabilised zirconia MSZ(#)-4.

6

NEW TOOLING CONCEPT FOR MICRO-FAST OF CERAMIC COMPONENTS

6.1 TOOL CONCEPT AND DETAIL DESIGN

Finite element analysis has been carried out and experiments have been made using the Gleeble[®] 3800 machine. Guideline values of the optimum parameters have been obtained for producing high densification components. However several problems were encountered in the experiment which could prevent eventual applications of the technology. Therefore, a new tool concept is proposed which could potentially be used in production to produce miniature ceramic components. The new alternative design is going to be validated and examined using Finite Element (FE) analysis using ABAQUS/CAE software (Abaqus version 6.14).

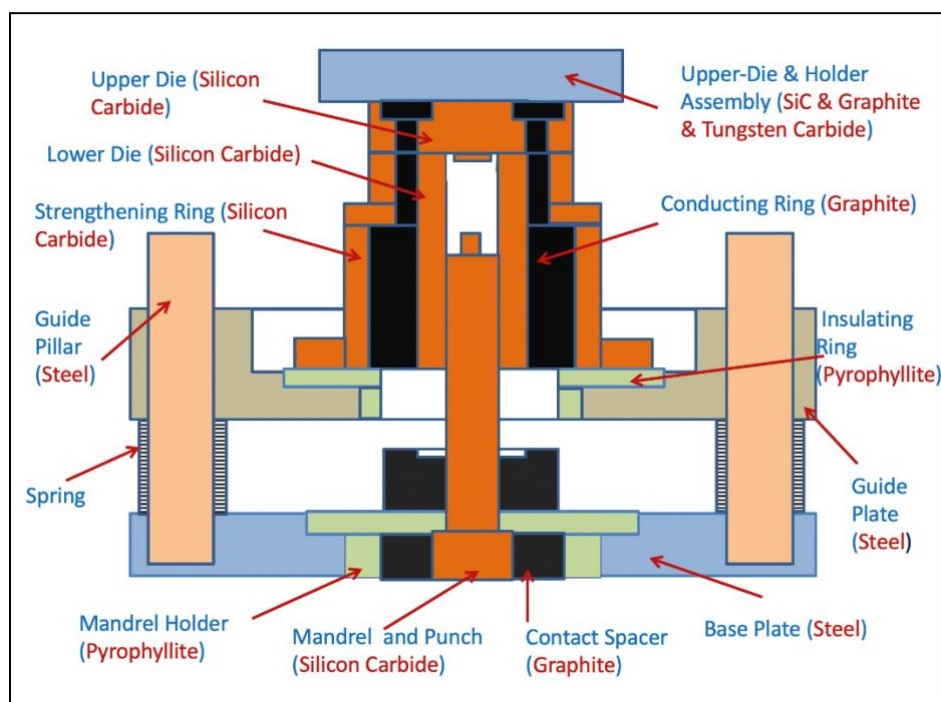


FIGURE 6-1: THE INITIAL DESIGN FOR THE ALTERNATIVE TOOL FOR MICRO-FAST PROCESS

Figure 6-1 shows the tooling concept that has been suggested for the Micro-FAST process. The idea of the new design is to develop the potential for mass production with quality and productivity. Currently, in the mass production industry, products must be designed and manufactured with the following opposing goals: decreasing time and cost; improving quality and flexibility. However, there are many challenges and issues that need to be considered for new tool design. These challenges are the filling process of the powder, difficulty to control the volume of the powder feeding, difficulty to handle the die during the operation, difficulty to eject the component outside the die, and die-life is too short due to small sizes having fragility. The design has gone through several stages because of these challenges and other features that have been considered during the design process. Figure 6-2 shows the first two stages of the new tool design for the Micro-FAST process. The first two designs had some issues with the size of the parts and the shape of the formed sample. Moreover, the ways of attaching the parts together has been considered and resolved in the final design as seen in Figure 6-3 and Figure 6-4.

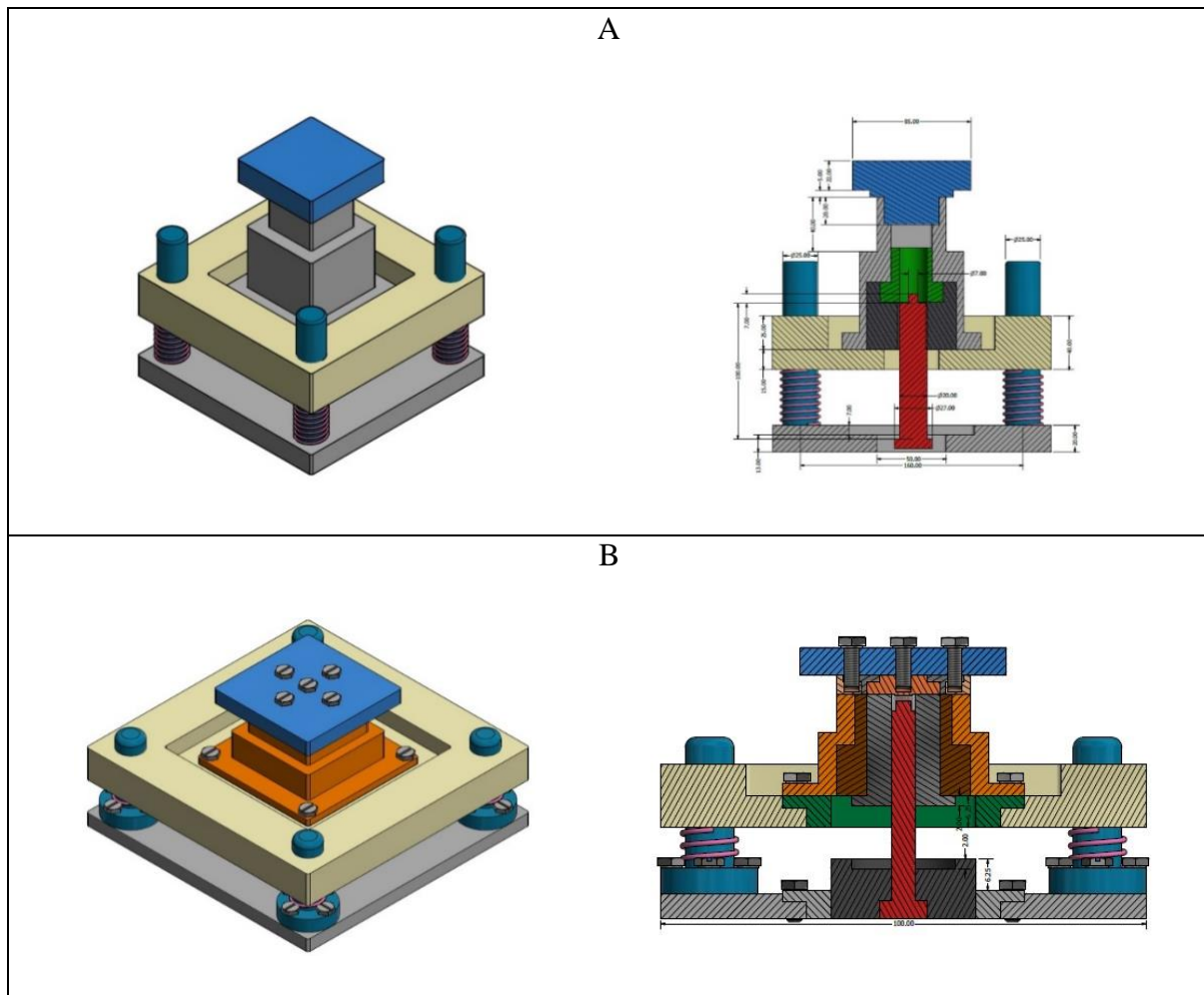


FIGURE 6-2: THE FIRST TWO DESIGN OF THE ALTERNATIVE TOOLS FOR MICRO-FAST

In previous experiments, when filling the powder inside the die some powder could be dropped outside the die because human error. The amount of the powder is calculated and then filled inside the die and the upper and the lower punches have to be placed inside the Gleeble machine. The process of balancing the die is done manually which could affect the filling process by dropping some amount of the powder that could affect the densification of the materials.

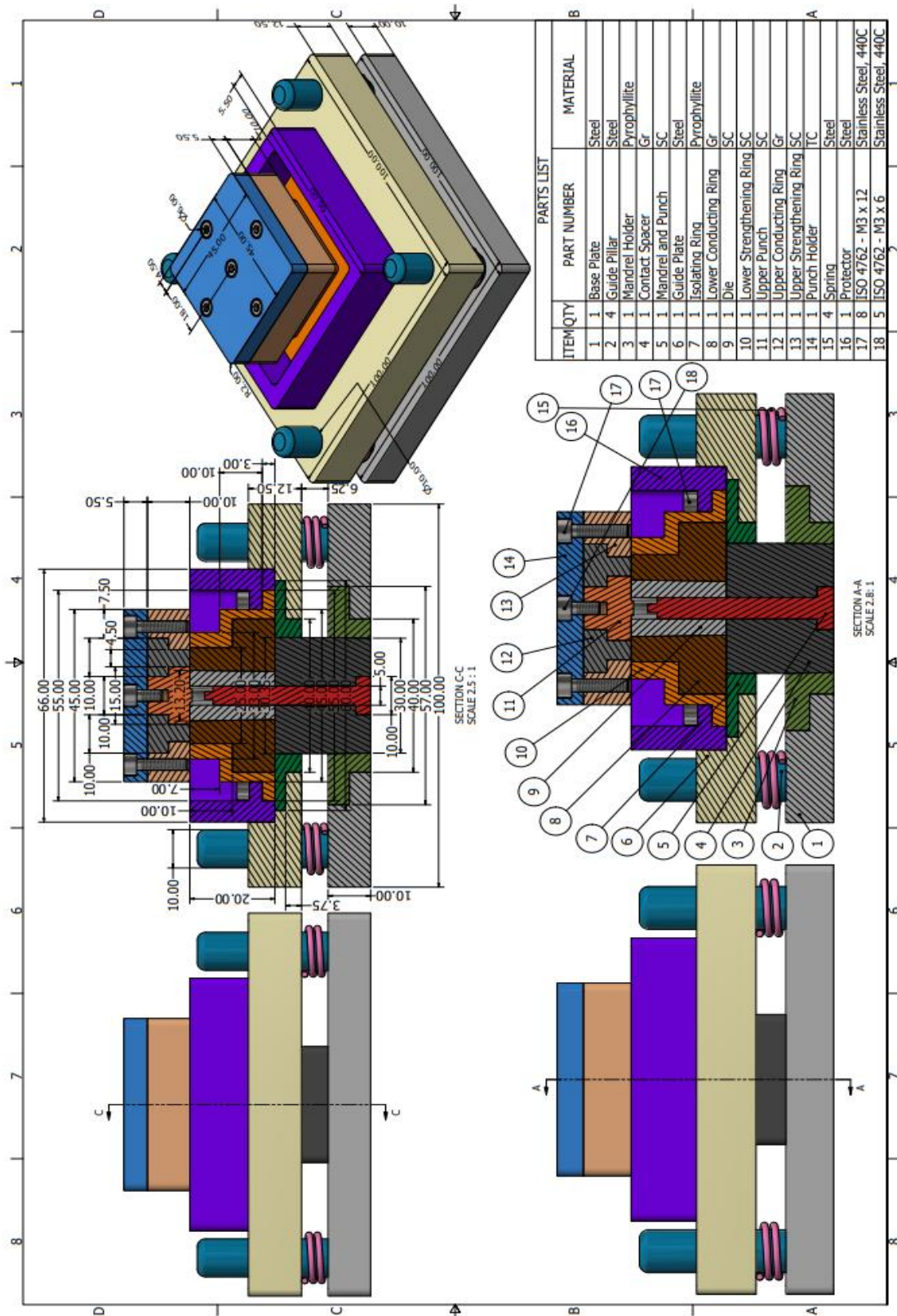


FIGURE 6-3: THE NEW TOOL DESIGN FOR MICRO-FAST PROCESS WITH FULL DETAILS

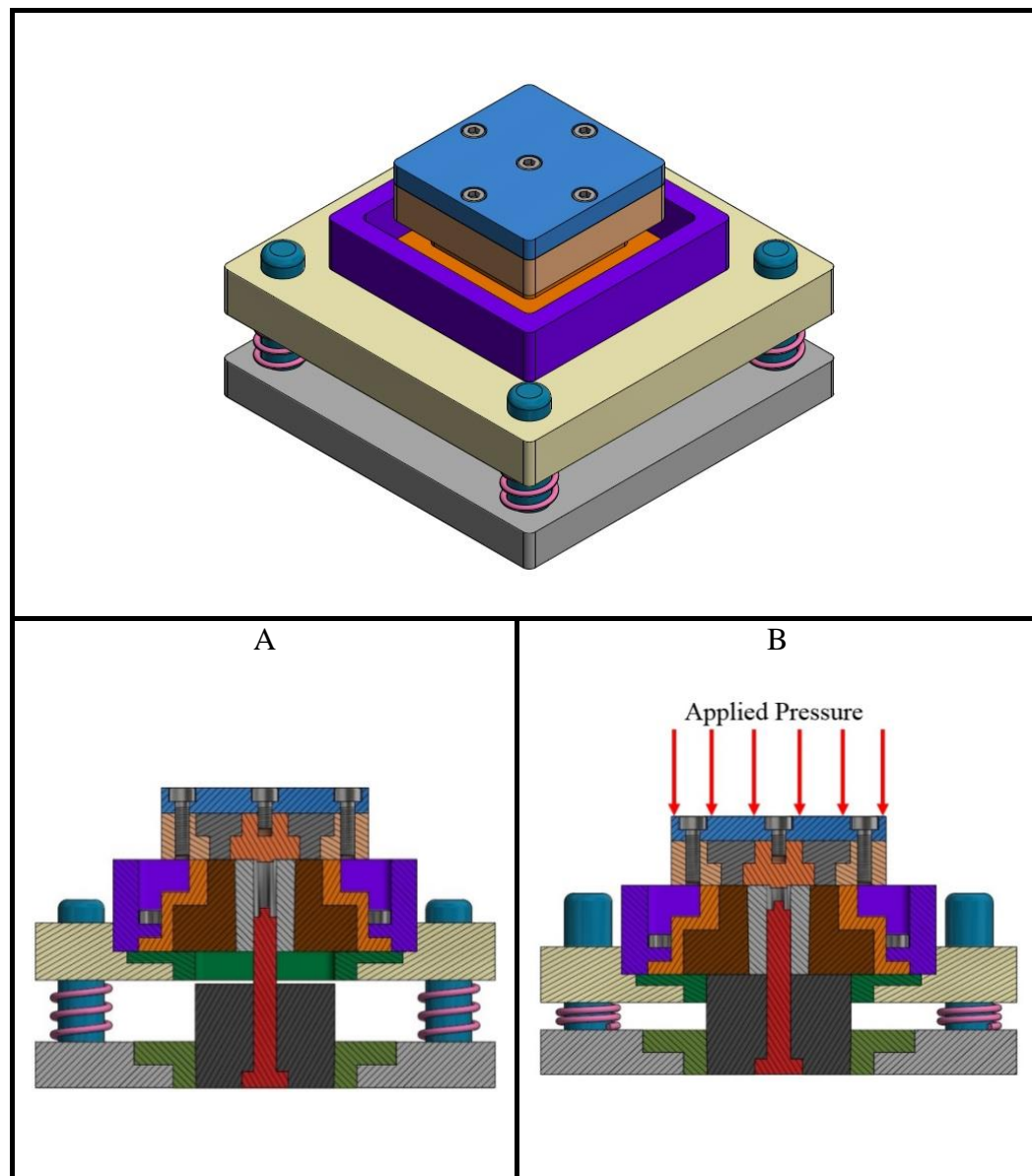


FIGURE 6-4: NEW TOOL DESIGN FOR MICRO-FAST PROCESS (A) WITHOUT THE APPLIED PRESSURE (B) WITH THE APPLIED PRESSURE

Additionally, this operation will lead to difficulty in controlling the feeding of the powder when the amount of powder may be different for different volumes of the components to be formed or the amount of powder varies due to weighting accuracy and losses during handling.. Figure 6-5 shows the tool design without the upper part and how the powder is going to be fed during the filling process. The new tool design will make the filling process easier and more consistent during the Micro-FAST process. Filling the calculated amount of powder inside the die will help obtaining fine products without porosity.

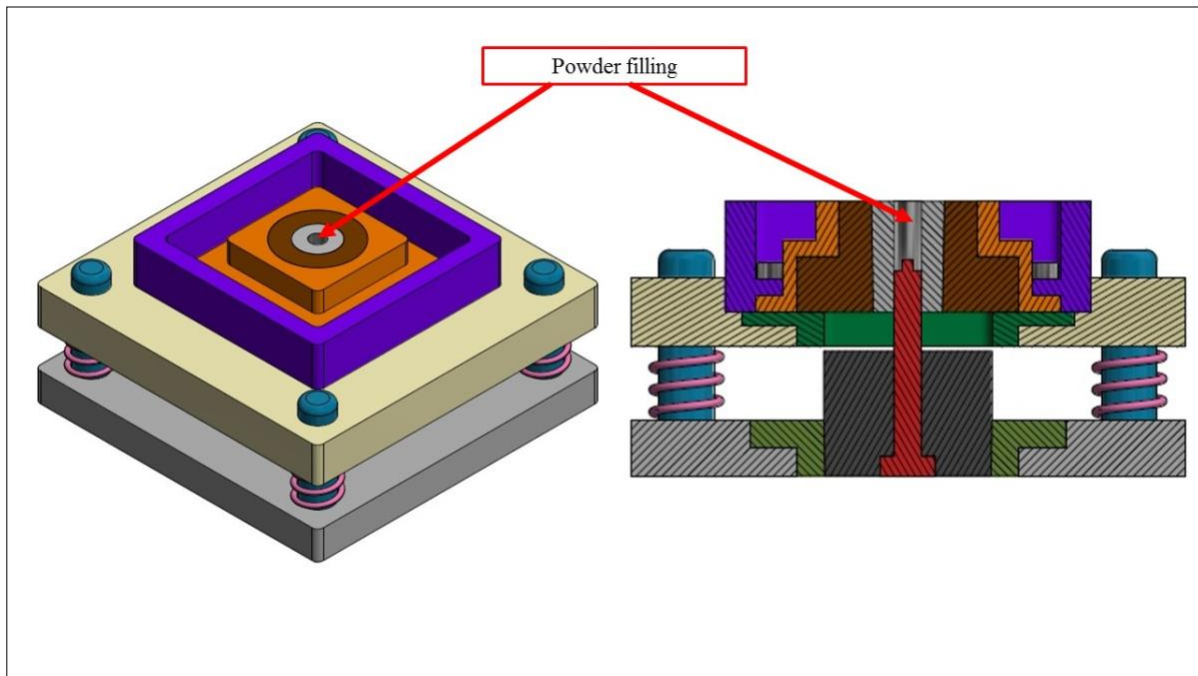


FIGURE 6-5: THE LOWER PARTS OF THE NEW TOOL DESIGN AND WHERE THE POWDER GOING TO BE FILLED

After the heating and sintering/forming in the Micro-FAST process, the new tool set should be cooled until room temperature. The upper and lower part opened, and the formed sample can be easily removed from the die. In the previous experiment the die set was placed above the die ring and using an ejector and hammer the sample was carefully knocked out. This action was made to prevent the sample from damaged. When comparing this method with the previous one, the new tools will make it easier to eject the sample and will protect the sample from being damaged.

As mentioned before, most conventional electrical sintering applications used graphite as die set material, which shows an excellent choice concerning its capability working at high temperatures up to 2,700 °C [118, 120]. However, the graphite has a lower compressin stress than other materials, such as silicon carbide and tungsten carbide. Therefore, due to the small size of tools, the life of a graphite die could be an issue and the die might be fragile during the

Micro-FAST process. In the new tool design, silicon carbide has been suggested for the die due to its properties. Silicon carbide has excellent thermal conductivity, high melting temperature (>2000 °C), interesting electrical properties due to its semiconductor characteristics. In addition, SiC has high hardness and corrosion resistance [120, 135]. Considering the non-conductive ceramic powder itself is not conductive electrically, heating could be mostly facilitated by heat transfer from the heating element (graphite), through the SiC die-insert. From this point of view, selecting highly thermally conductive SiC as die-insert material can be justified.

In addition, using the potential tool design for the micro-FAST process will make it easier in handling the process due to size issues. The new tool design will offer more flexibility in controlling and managing the experiment. Each part of the new tool design has been explained and justified in details in the appendices.

6.2 THERMAL-ELECTRICAL FINITE ELEMENT ANALYSIS OF THE TOOL

The Finite Element (FE) analysis of the effect of coupled thermal-electrical characteristics of the new tool design during the heating and cooling process was examined by using ABAQUS/CAE software (Abaqus version 6.14). The information collected from the FE simulation is going to be useful in the future for the experimental process in order to gain information on how the heating distribution occurs in the tool that is going to be used in the Micro-FAST process. The first step of the analysis was to include the electrical potential being exposed to the die set, this was calculated by using electrical boundary conditions. In the second step transient heat transfer analysis was conducted by the application of Joule heat generation to each finite element under a given thermal boundary condition. The temperature dependency of the electrical conductivity was used for the analysis where the electrical and thermal analyses are fully coupled.

6.3 ANALYSIS PROCEDURE

In the coupled thermal-electrical analysis, both transient responses have been applied for electrical analysis in the first step and thermal analysis in the second one where they are sequentially conducted in each time increment. Therefore, the temperature at integration points of each of the tool sets can be gained dependent on the step time to complete the process. The sample material used in the simulation was Alumina. The simulation analysis was mainly concentrated on the heating distribution process on the alternative tool design. Figure 6-23 shows the simplified parts used in the new tool design for thermal-electrical analysis.

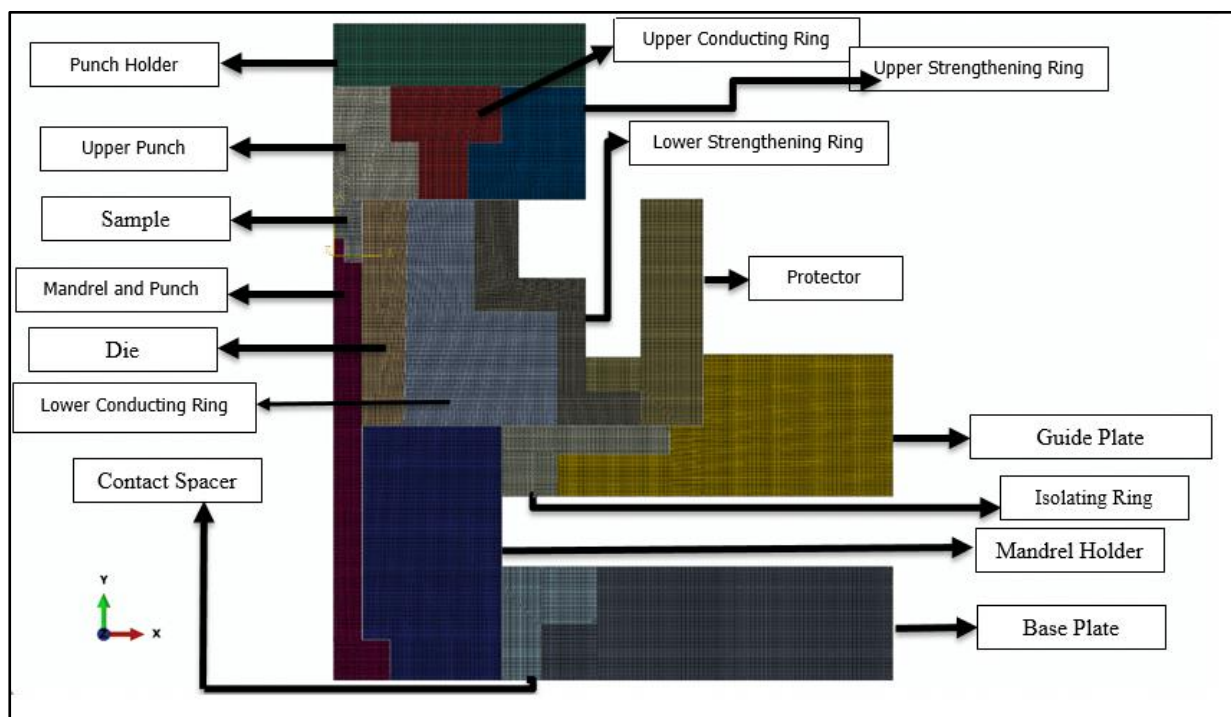


FIGURE 6-6: SIMPLIFIED PARTS OF THE NEW TOOL DESIGN USED IN THE SIMULATION OF COUPLED THERMAL-ELECTRICAL ANALYSIS

Table 6-1 shows the physical, thermal and electrical properties of materials used in the new tool design used to evaluate the coupled thermal-electrical analysis for the Micro-FAST process. Regarding the boundary conditions, the electrical potential at the top of the tool design was set to 0.5 V and at the bottom in the base plate was assumed to be zero because it was

electrically grounded as seen in Figure 6-23. Regarding the emissivity and the film coefficient used were 0.8 and 10 respectively, meanwhile the ambient temperature was set to 30 °C. The initial time increment was 1×10^{-5} s and the automatic time increments function provided from Abaqus software were used. After the first step of the electrical and thermal analysis, no electrical load existed. Therefore, general transient heat transfer analysis was conducted to save calculation time in the second step.

TABLE 6-1: PROPERTIES OF PART MATERIALS USED IN THE THERMAL-ELECTRICAL ANALYSIS FOR THE NEW TOOL DESIGN [120]

Part Name	Materials	Density	Specific Heat	Thermal Conductivity	Electric Conductivity
		(kg/m ³)	(J/kg)	(W/m.K)	(S/m)
Base plate	Steel	8050	500	21.4	14.5×10^6
Upper Conducting Ring	Graphite	1,860	771	81	9.1×10^6
Samples	Alumina	3900	850	18	1×10^{-8}
Mandrel Holder	Pyrophyllite	2400	920	1.9	1×10^{-6}
Contact spacer	Graphite	1,860	771	81	9.1×10^6
Mandrel	Silicon Carbide	3200	670	60	1×10^{-6}
Guide Plate	steel	8050	500	21.4	14.5×10^6
Isolating Ring	Pyrophyllite	2400	920	1.9	1×10^{-6}
Lower conducting ring	Graphite	1,860	771	81	9.1×10^6
die	Silicon Carbide	3200	670	60	1×10^{-6}
Lower Strengthen Ring	Silicon Carbide	3200	670	60	1×10^{-6}
Upper Punch	Silicon Carbide	3200	670	60	1×10^{-6}
Upper Strengthen Ring	Silicon Carbide	3200	670	60	1×10^{-6}
Punch Holder	Tungsten Carbide	15,580	292	88	1×10^6
Protector	steel	8050	500	21.4	14.5×10^6

Table 4-2 shows, the number of the mesh (nodes and elements) for each part. The global size of the parts that has been used in the simulation of electrical-heat analysis for meshing is 0.2. Meanwhile, the thermal electric element type has been assigned for all the parts. The total number of nodes for the meshing of all parts is 50476 and the total number of elements for the meshing is 48348. The process has been set for 20 seconds for thermal and electrical analysis. The process has been heated for the first 10 seconds, then followed by 2 seconds cooling and 2 seconds heating repeatedly until reaching a total time of 20 seconds for thermal and electrical analysis. The reason for the 2 seconds cooling and 2 seconds heating repeatedly is to make sure the electrical transit and heat distribute properly. After the 20 seconds, the second step starts which is the cooling process.

TABLE 6-2: THE NUMBER OF THE MESH (NODES AND ELEMENTS) FOR EACH PART IN NEW TOOL DESIGN

Part Name	Mesh (No of elements)	Mesh (No of nodes)
Base plate	7275	7484
Upper Conducting Ring	1850	1952
Samples	290	332
Mandrel Holder	6885	7062
Contact spacer	1525	1619
Mandrel	2702	2925
Guide Plate	6785	6999
Isolating Ring	1450	1558
Lower conducting ring	4900	5069
die	1951	2071
Lower Strengthen Ring	2522	2700
Upper Punch	1599	1691
Upper Strengthen Ring	2275	2379
Punch Holder	3164	3306
Protector	3175	3329

6.4 RESULTS AND DISCUSSION

Figure 6-23 shows the heating temperature distribution of the new tool design of the die, punch and Alumina sample for the first step (electrical and thermal analysis) and step 2 for heat transfer analysis after the current is off. The materials that have been selected for the die and the punch is silicon carbide due to its excellent thermal conductivity and low thermal expansion. The sample material is Alumina and the reason for choosing Alumina is that it has better thermal conductivity than some other ceramic materials.

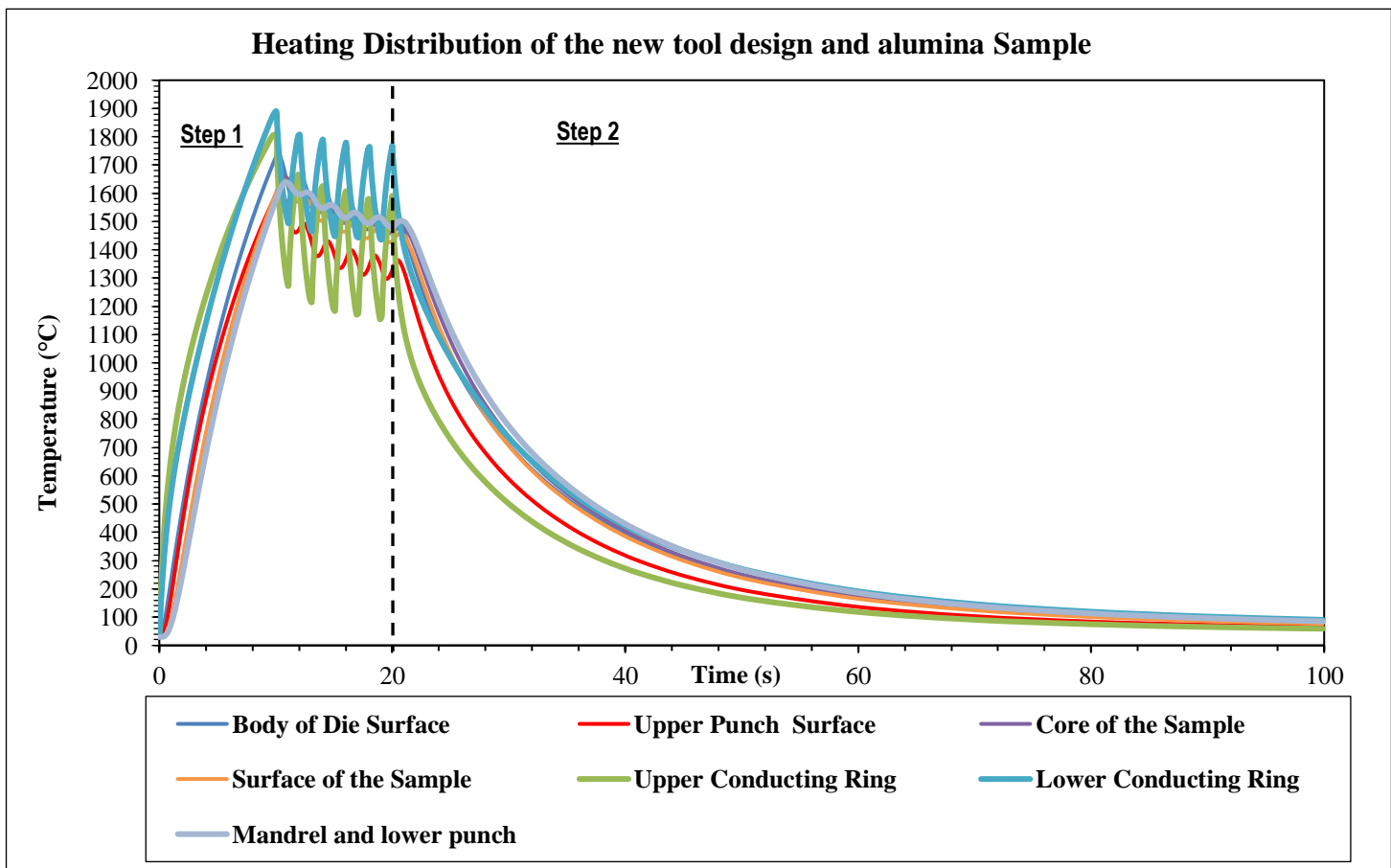


FIGURE 6-7: HEATING TEMPERATURE DISTRIBUTION OF NEW TOOL DESIGN AND ALUMINA SAMPLE FOR STEP ONE: ELECTRICAL AND THERMAL ANALYSIS AND STEP TWO: HEAT TRANSFER ANALYSIS AFTER THE CURRENT IS OFF

In Table 6-4 the figures of the new tool design of the die, punch and Alumina sample for heating temperature distribution at integration points of step one: electrical and thermal

analysis are shown. From Figure 1 to Figure 4 the rapid increase in the temperature at the core of the new tool design in the lower and upper conducting ring can be seen. The material in the lower and upper conducting ring is graphite to allow the heat and the electricity to transit through the die, the contact spacer and then to the mandrel. The reason for using graphite for the conducting ring is due its high thermal and electrical conductivity.

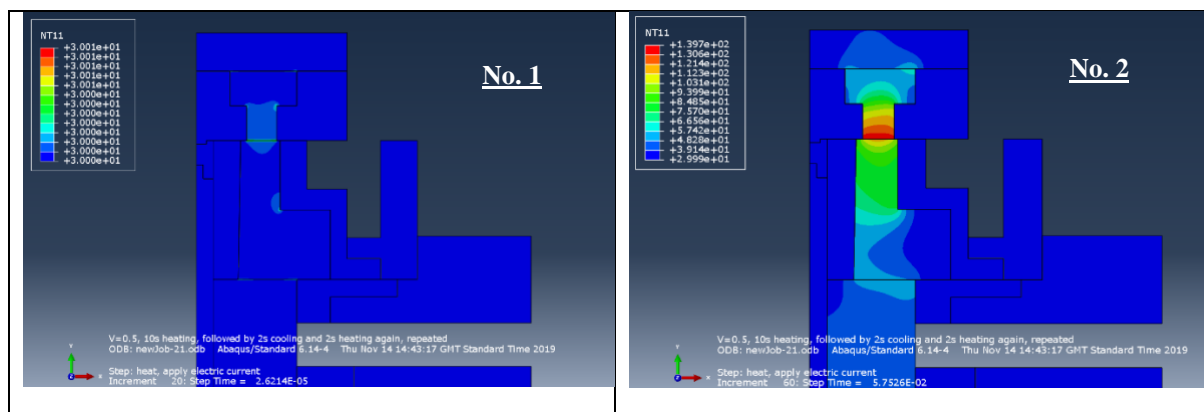
TABLE 6-3: TEMPERATURE AND TIME DATA FOR CONTOUR OF THE NEW TOOL DESIGN AND ALUMINA SAMPLE FOR STEP ONE: ELECTRICAL AND THERMAL ANALYSIS

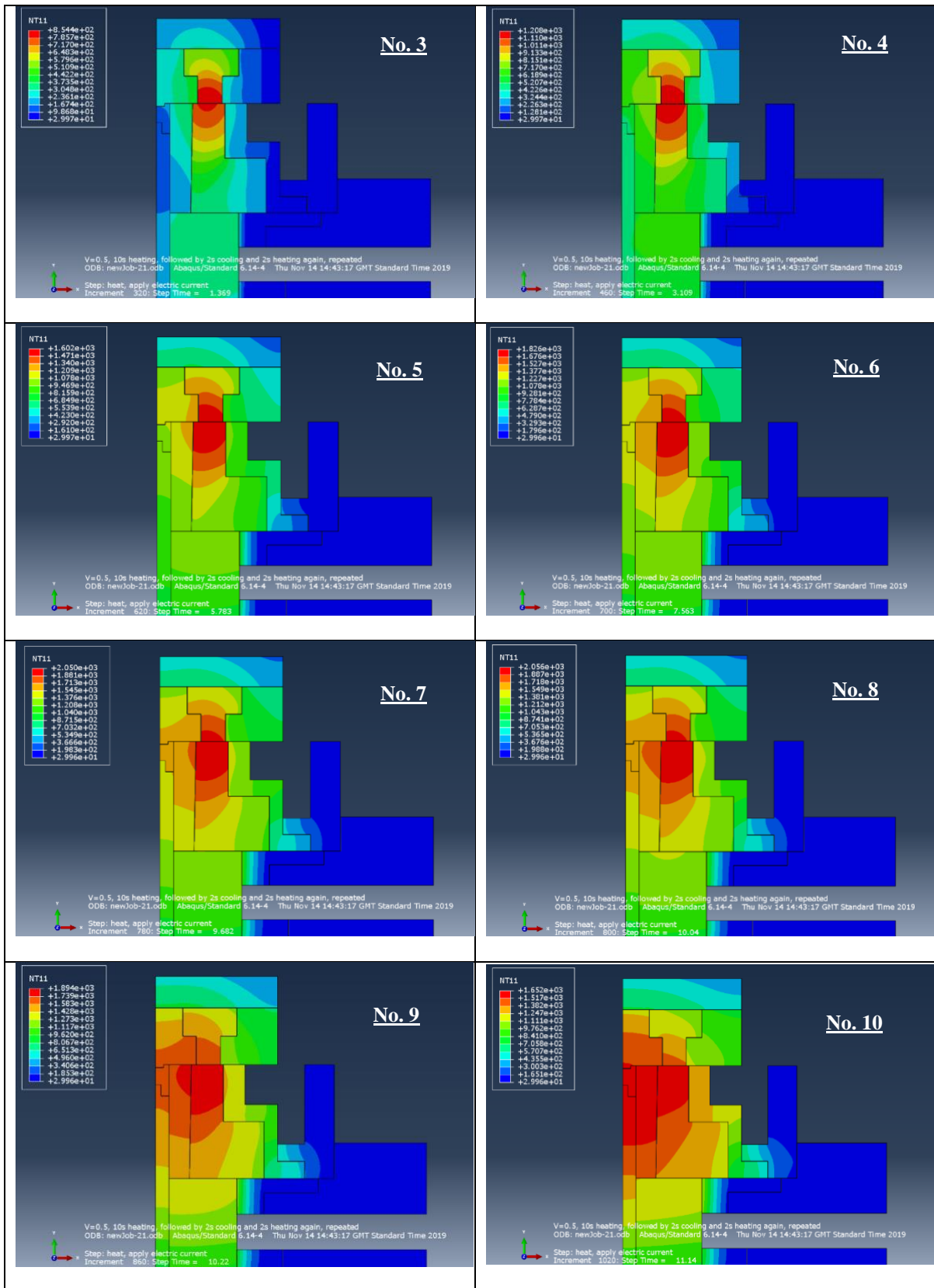
Contour No.	Step Time (s)	Body of Die Surface (°C)	Upper Punch Surface (°C)	Core of the Samples (°C)	Surface of the Sample (°C)	Upper Conducting Ring (°C)	Lower Conducting Ring (°C)	Mandrel and lower punch (°C)
1	0.021	30.016	30	30	30	61.2385	49.1957	30
2	0.058	30.489	30.001	30	30	110.806	80.6737	30
3	1.369	329.472	270.926	142.319	165.853	770.332	637.27	130.086
4	3.109	742.197	698.068	531.824	566.576	1108.92	990.937	494.906
5	5.783	1213.370	1142.940	1045.010	1067.200	1453.17	1408.96	1005.27
6	7.563	1457.040	1358.900	1307.900	1320.450	1629.79	1638.67	1274.28
7	9.682	1696.730	1566.810	1564.270	1566.690	1801.97	1869.58	1538.97
8	10.044	1732.980	1598.040	1603.010	1603.860	1804.38	1890.26	1579.1
9	10.221	1740.080	1611.780	1621.470	1621.480	1622.06	1773.46	1598.23
10	11.136	1609.190	1517.320	1646.470	1624.970	1330.06	1527.99	1634.04
11	11.535	1597.220	1464.400	1615.150	1586.700	1562.04	1706.98	1611.03
12	13.194	1534.200	1408.210	1578.290	1546.240	1320.93	1530.86	1585.77
13	15.4265	1495.59	1337.850	1515.210	1479.870	1436.33	1625.22	1531.51
14	17.0989	1485.29	1347.350	1509.560	1478.220	1176.69	1443.3	1525.54
15	18.0549	1545.1	1347.830	1473.960	1445.900	1578.56	1763.95	1494.14
16	18.561	1540.92	1379.040	1494.860	1471.100	1261.42	1532.01	1511.72
17	19.344	1459.39	1303.540	1479.550	1444.710	1363.93	1573.66	1499.03
18	20	1526.6	1328.520	1459.490	1430.410	1591.15	1769.6	1481.21

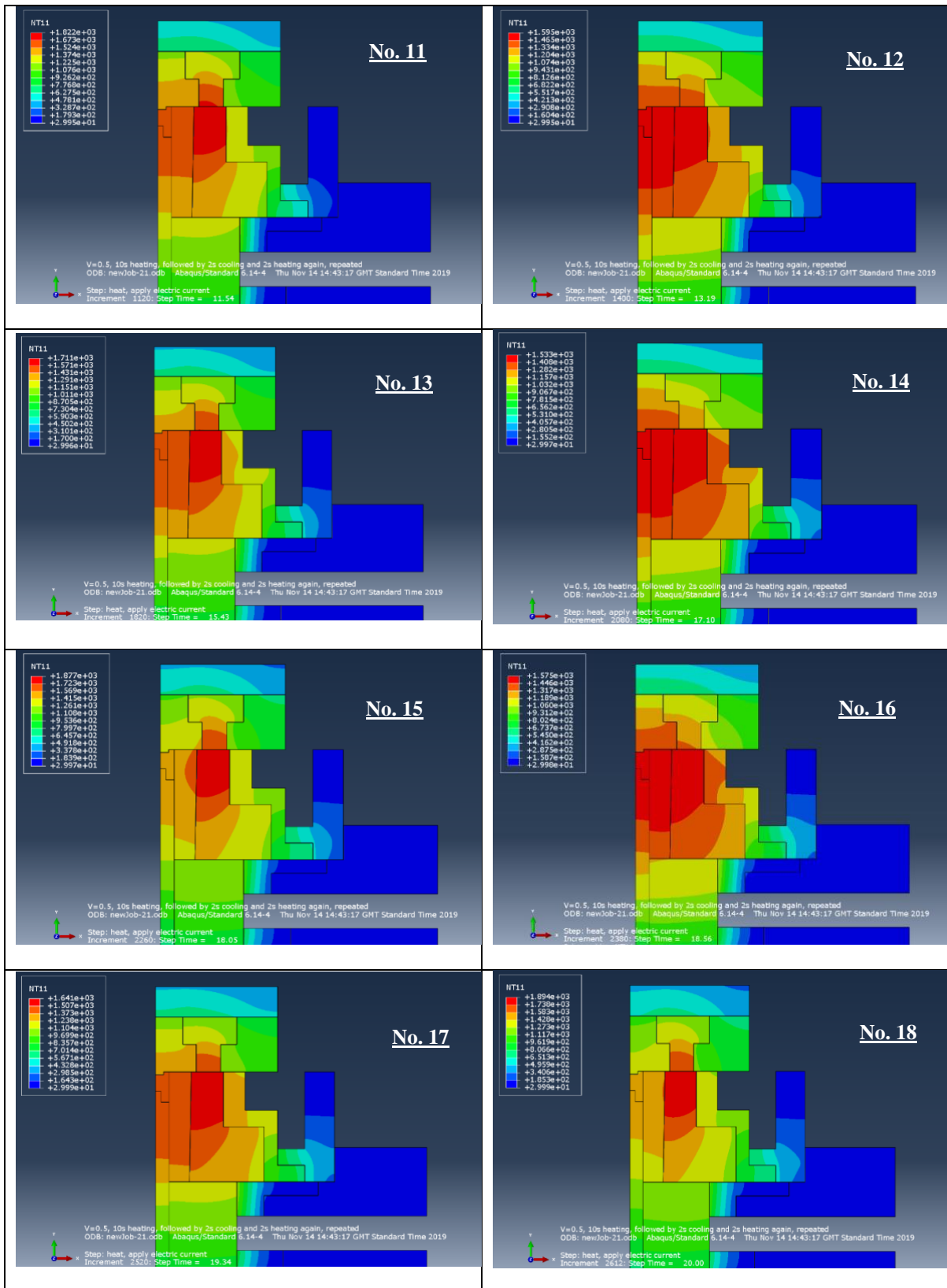
The heat begins from the top and then is transmitted to the upper and the lower conducting ring and then reaches the die, the upper punch, the sample and the mandrel and lower punch as seen in the figures illustrated in Table 6-4. The temperature of the lower and upper conducting ring could reach the 1000 °C barrier within approximately 3 seconds. While the die might reach 742.197 °C and the core of the sample and the surface have recorded 531.824 °C and 566.576°C respectively. By increasing the step time to 10 seconds, then the heating temperature rises to reach 1600 °C for the sample.

After 10 seconds, it can be seen in the Figure 6-23 that there are fluctuations in the temperature lines due to the 2 seconds cooling and 2 seconds heating repeatedly until the process reaches the step time of 20 seconds. The reason is to be sure that the electric current and heat distribute properly. After reaching the step time of 20 seconds, the die will record an average temperature of 1526.6 °C. Moreover, the sample surface and core have achieved heating temperature of 1459.490°C and 1430.410°C respectively. In practice, the applied electrical potential in this exercise may be too high for the die-materials simulated, considering their reliable working temperatures that should be used in engineering environment. Nevertheless, this simulation demonstrates feasibility of heating the sintering material rapidly by this design concept.

TABLE 6-4: THE FIGURES OF THE NEW TOOL DESIGN AND ALUMINA SAMPLE FOR HEATING TEMPERATURE DISTRIBUTION AT INTEGRATION POINTS OF STEP ONE : ELECTRICAL AND THERMAL ANALYSIS





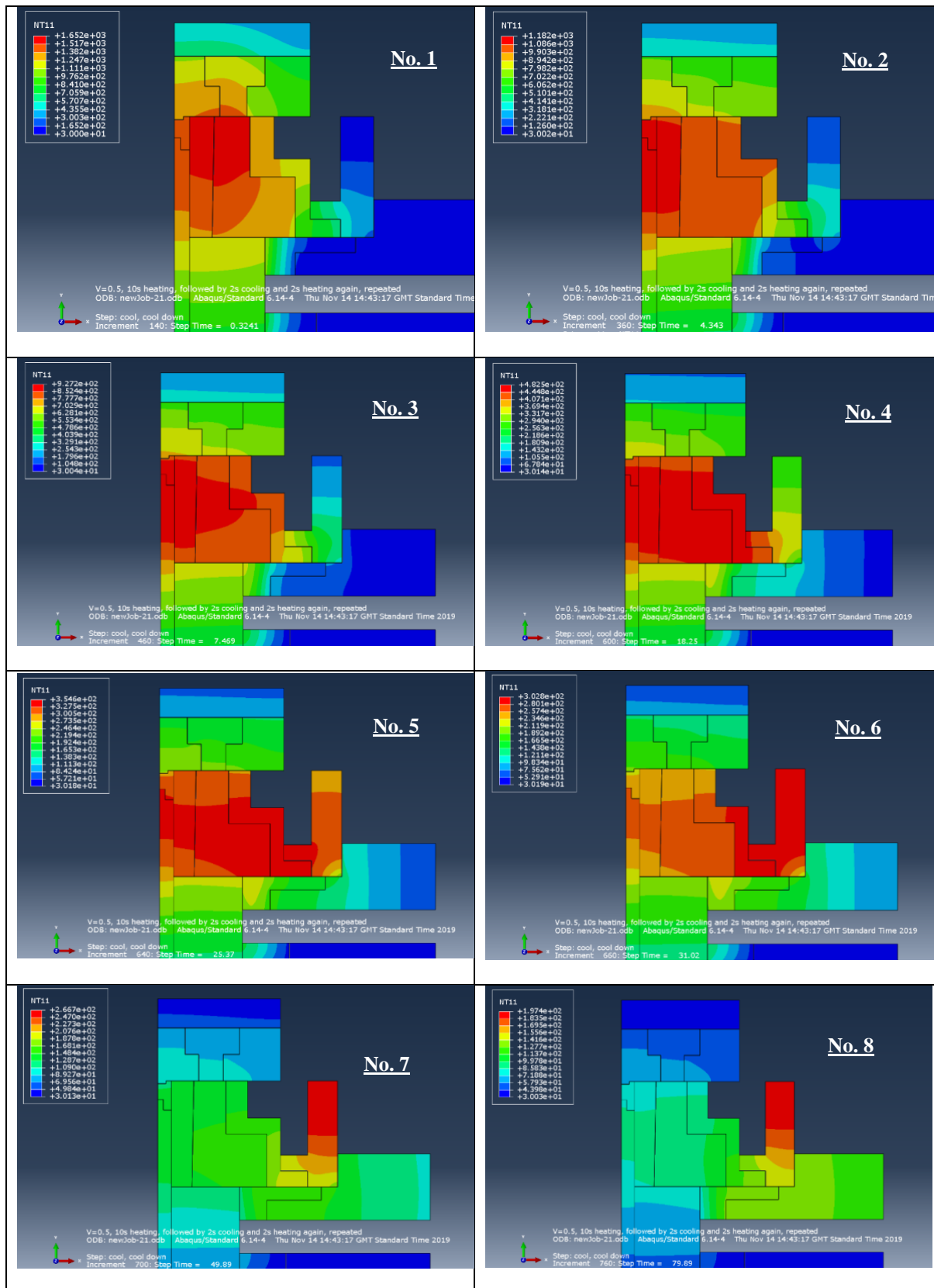


After the end of step one the rapid cooling due to the heat transfer for the new tool design can be seen. The temperature decreased from an average of 1234.85 °C at a step time of 20.32 seconds to reach an average temperature of 77 °C at a total time of 100 seconds as seen in Table 6-5. The illustration figures of heat transfer analysis of the new tool design for step two can be shown in Table 6-6.

TABLE 6-5: TEMPERATURE AND TIME DATA FOR CONTOUR OF THE NEW TOOL DESIGN AND ALUMINA SAMPLE FOR STEP TWO: HEAT TRANSFER ANALYSIS AFTER THE CURRENT IS OFF

Contour No.	Step Time (s)	Body of Die Set Surface (°C)	Punches of Die Set Surface (°C)	Core of the Samples (°C)	Surface of the Sample (°C)	Upper Conducting Ring (°C)	Lower Conducting Ring (°C)	Mandrel and lower punch (°C)
1	20.3241	1541.51	1360.880	1471.530	1447.260	1331.5	1594.09	1491.26
2	24.343	1075.89	924.271	1140.200	1094.800	770.384	1065.21	1181.93
3	27.4688	844.363	708.856	885.122	847.416	601.003	861.6	926.193
4	38.2455	432.03	350.735	445.561	424.894	299.889	462.352	472.732
5	45.3721	301.811	242.238	309.250	294.537	207.812	329.106	329.932
6	51.0222	236.242	188.646	240.969	229.427	162.495	260.619	257.872
7	69.8884	129.705	103.597	130.702	124.654	90.9703	146.539	140.445
8	99.8884	79.703	65.2919	79.5738	76.3572	59.0343	90.5032	85.1462

TABLE 6-6: THE FIGURES OF THE NEW TOOL DESIGN OF THE DIE, PUNCH AND ALUMINA SAMPLE FOR HEATING TEMPERATURE DISTRIBUTION AT INTEGRATION POINTS OF STEP TWO: HEAT TRANSFER ANALYSIS AFTER THE CURRENT IS OFF



6.5 SUMMARY OF THE CHAPTER

Based on the finite element analysis and experiments that have been made using the Gleeble[®] 3800 machine and after obtaining the guideline values of the optimum parameters to produce high densification components, several problems could be identified in the experiment which could prevent eventual applications of the technology. These are difficulty to fill the powder, difficulty to control the volume of the powder feeding, difficulty to handle the die during the operation, difficulty to eject the component outside the die, and die-life is too short due to small sizes having fragility. Therefore, a development of an alternative new concept tool design has been presented which could potentially be used for mass production that meets quality and productivity target for producing miniature ceramic components. Currently, in the mass production industry, products must be designed and manufactured with the following opposing goals: decreasing time and cost; improving quality and flexibility. However, there are many challenges and issues that need to be considered , as indicated above.

An initial design has been suggested for the Micro-FAST process and followed with several stages and modifications with the consideration of all challenges and issues. After several design changes and taking into the account the issues and the materials required for the part, a final concept of tool design has been introduced. The new potential tool design for the Micro-FAST process will make it easier in handling the process due to size issues. The new tool design will offer more flexibility in controlling and managing the experiment.

The new alternative design has been validated and examined using the Finite Element (FE) analysis. The effect of coupled thermal-electrical characteristics during the heating and cooling process was examined using ABAQUS/CAE. The information collected from the FE simulation is going to be useful in the future for the experimental processto further validate this design concept. .

7

CONCLUSIONS AND RECOMMENDATIONS

7.1 CONCLUSIONS

- Based on the research of the Micro-FAST process, improvements have been shown regarding process time for the manufacture of miniature components with a variety of ceramic powder material which show less time to fabricate miniature components. The main differences between the Micro-FAST process and the other processes was the better efficiency of the current flow to heat the particles of the powder, the high heating rate during the experiment to speed up the process, the densification of the samples dependent on the pressure, and a simplified process setup and control. Moreover, most of the conventional processes produce macro size parts using ceramic powder.
- By considering all previous studies, it can be seen that compared to the Micro-FAST offers good potential compared to the existing conventional processes. It can be summed up by saying that the Micro-FAST process is faster than conventional processes for producing miniature ceramics components and it will reduce the influence of the issue of the size effect in the forming process of micro parts. It has short manufacturing cycles and it is easy to control the microstructure of the fabricated part. In addition, the Micro-FAST has the flexibility to use different materials and it has the potential for forming structurally and functionally graded parts. It has the ability to form 3D shaped micro parts with the dedicated micro tool design and control and also miniature components with high strength materials. The feeding of the loose powders in the die for the Micro-FAST process into is done without the need to prepare a green compact and therefore small size components could be made based on the design of the die set used.

-
- By using Finite Element (FE) analysis the effect of coupled thermal-electrical characteristics of the die sets of the Micro-FAST process was examined during the heating and cooling process by using ABAQUS/CAE software. This showed the feasibility of the Micro-FAST process to do the experimental procedure and the design of die plays a significant role to ensure the high efficiency of heating during the Micro-FAST process for powder material.
 - Experimental work using the Micro-FAST process was conducted to validate the results from the Finite Element analysis. The experiment was conducted with three kinds of raw material powder which were alumina, zirconia and piezoceramic. The experiment for the three materials using Micro-FAST process has produced good solid miniature parts.
 - In terms of the new alternative tool design, the concept design has been analysed and examined by Finite Element Analysis to see the effect of the coupled thermal-electrical characteristics of the new tool design during the heating and cooling process. The results showed from the FE simulation was very promising and it showed the feasibility of the new tool design for future applications.
 - New experiences gained from Micro-FAST experiment on ceramic materials. Experiments. The die set design and the tools used for the experiment showed higher durability and efficiency of transferring the heating to produce the samples and there were no issues during the ejection process of the samples. The efficiency of using the Micro-FAST process provides significant contributions towards the sample size and its densification. It was an ideal condition to have a fully closed die set during the experimental work as the current could pass through the die and generate heat to produce a more efficient process and high quality samples. Therefore the Micro-FAST is a suitable process to produce solid miniature ceramics components in faster time, with high quality and low cost.

7.2 CONTRIBUTIONS TO KNOWLEDGE

The contributions of this work can be stated in several points below:

- New knowledge about forming of ceramic parts with Micro-FAST –. The Micro-FAST process has been developed to save time compared to the conventional Electric Field Assisted Sintering Technology process. The concept comprises applying external electrical-field currents alongside the high applied pressure simultaneously to the die set and material particles of the samples. There are 4 stages involved in the densification mechanism of The Micro-FAST process which can be classified as preheating period, high-temperature pressing, sintering period and cooling period. Micro-forming is one of the common micro-manufacturing processes that could meet the demands of mass production along with enhancing the product performance with minimal waste. It can handle complex geometries and features that are costly for conventional micro-manufacturing processes. However, it was not an easy task to achieve the desired micro shape of a product. Therefore, the concept and the results from this Micro-FAST research can be used in the future for further investigations. It can, nevertheless, be concluded that the densification of the ceramic components by using the Micro-FAST process can achieve good quality and could be completed within a short time due to it being a continuously coupled process of the electrical-field which generated the high pressure and Joule heat.
- Sintering die designs and selection of the tool materials for the die sets. There are several designs of the die sets that have been used for the Micro-FAST process. The final output samples were of cylindrical and cuboid shape. The main aim for the design of the three die sets was to reduce the thermal stress concentration in the punches. The punch shape was the positive effect of the concentrated heating at the punch nose, as more uniform temperature distributions in the middle section of the die occurred which could help to optimise the process of sintering. Based on the guidelines, the material used for the die set is graphite. The graphite material was used for the die set by using guidelines and standards

(comparing the compressive strength, thermal expansion coefficient and maximum service temperature of the selected material) to avoid trapping between the punches and the sample inside the die during the ejection process.

- Investigation and understanding of the effect of the heating distributions during the heating and the cooling in Micro-FAST. In the first step the electrical analysis involving the electrical potential, the die set design has shown good and rapid heating temperature distribution. In step two of the thermal analysis this involved the transient heat transfers and rapid cooling. The information collected from the FE simulation was used for the experimental process in order to have the proper information on how the heating distribution happened in the die sets used in the Micro-FAST process and to determine suitable parameters for the experiments.
- A new tool concept that could potentially be used for mass production to produce miniature ceramic components. The effect of coupled thermal-electrical characteristics during the heating and cooling process was examined using Finite Element Analysis. The results showed very good potential for future applications. The results also showed that the new tool design for the Micro-FAST process could make it easier in handling the process due to size issues. It will also offer more flexibility in controlling and managing the experiment.

7.3 RECOMMENDATION AND FUTURE WORK

The recommendations for future works on this research are described as below.

- Use different thermocouples for the measurement of the temperature where it can work at high temperatures that exceed 1,400 °C during the Micro-FAST process. Although

existing thermocouples were suitable for most of the experiments which used the ceramic and composite powder material, some other ceramic powders need the temperature of the process to be above 1,300 °C to achieve the excellent result of the relative density samples.

- The analysis of the quality of the sample was focusing on the relative density the micro-structure, but the mechanical properties and dimensional accuracy of the formed samples need to be considered.
- New mechanical testing methods/devices on the micro-samples are needed as the current options are designed mostly for macro-size components. Also new standards of the procedure for testing also need to be established.
- The coupled Finite Element thermal-electrical analysis in this study was focused on the heat transfer and heating distributions during the heating and cooling, but in the future a potential study of powder behaviours and interactions, such as deformations and diffusion bonding, should be considered.
- The alternative new tool design for the Micro-FAST process has been proposed for manufacturing miniature ceramic parts. Next step will be conducting experiment to validate this design concept.

REFERENCES

1. Qin, Y., *Micromanufacturing engineering and technology*. 2010, Norwich, N.Y.: William Andrew.
2. Qin, Y., *Micromanufacturing engineering and technology* 2nd ed. 2015, Oxford: Elsevier.
3. Zulkipli, M.B., *Electrical-Field Activated Sintering and Forming of Micro-Components*. 2017, University of Strathclyde.
4. Malek, C.K. and V. Saile, *Applications of LIGA technology to precision manufacturing of high-aspect-ratio micro-components and-systems: a review*. *Microelectronics journal*, 2004. **35**(2): p. 131-143.
5. Qin, Y., *Overview of Micro-manufacturing*. 2015: p. 1-33.
6. Qin, Y., et al., *Micro-manufacturing: research, technology outcomes and development issues*. *The International Journal of Advanced Manufacturing Technology*, 2010. **47**(9-12): p. 821-837.
7. Ruprecht, R., et al., *Various replication techniques for manufacturing three-dimensional metal microstructures*. *Microsystem technologies*, 1997. **4**(1): p. 28-31.
8. Thian, S., et al., *Micro-rapid-prototyping via multi-layered photo-lithography*. *The International Journal of Advanced Manufacturing Technology*, 2006. **29**(9-10): p. 1026-1032.
9. Qin, Y., *Micro-forming and miniature manufacturing systems — development needs and perspectives*. *Journal of Materials Processing Technology*, 2006. **177**(1-3): p. 8-18.
10. Vollertsen, F., et al., *State of the art in micro forming and investigations into micro deep drawing*. *Journal of Materials Processing Technology*, 2004. **151**(1-3): p. 70-79.
11. Engel, U., et al., *Microforming and nanomaterials*, in *Advances in material forming*. 2007, Springer. p. 99-124.
12. Chan, W.L., M. Fu, and J. Lu, *The size effect on micro deformation behaviour in micro-scale plastic deformation*. *Materials & Design*, 2011. **32**(1): p. 198-206.
13. Armstrong, R., *On size effects in polycrystal plasticity*. *Journal of the Mechanics and Physics of Solids*, 1961. **9**(3): p. 196-199.

14. Tiesler, N., *Microforming-effects of miniaturization*. Proc. Metalforming, 2000: p. 355-360.
15. Uhlmann, E., et al., *Micro-electrical Discharge Machining*. 2015: p. 81-105.
16. Uhlmann, E., S. Piltz, and U. Doll, *Machining of micro/miniature dies and moulds by electrical discharge machining—recent development*. Journal of Materials Processing Technology, 2005. **167**(2-3): p. 488-493.
17. Li, D., et al., *Dense and strong ZrO₂ ceramics fully densified in < 15 min*. Advances in Applied Ceramics, 2019. **118**(1-2): p. 23-29.
18. Orru, R., et al., *Consolidation/synthesis of materials by electric current activated/assisted sintering*. Materials Science and Engineering: R: Reports, 2009. **63**(4): p. 127-287.
19. Lange, F., *Densification of powder compacts: An unfinished story*. Journal of the European Ceramic Society, 2008. **28**(7): p. 1509-1516.
20. Zadra, M., et al., *Spark plasma sintering of pure aluminium powder: mechanical properties and fracture analysis*. Powder Metallurgy, 2007. **50**(1): p. 40-45.
21. Jeswiet, J., et al., *Metal forming progress since 2000*. CIRP Journal of Manufacturing Science and Technology, 2008. **1**(1): p. 2-17.
22. Mahalik, N.P., S. Iyuke, and B. Ahn, *Principles of MEMS and MOEMS*, in *Micromanufacturing and Nanotechnology*. 2006, Springer. p. 19-44.
23. Dimov, S., et al., *Micro-and nano-manufacturing: Challenges and opportunities*. Proceedings of the Institution of Mechanical Engineers, Part C: Journal of Mechanical Engineering Science, 2012. **226**(1): p. 3-15.
24. Akhtar Razul, R. and Q. Yi, *A review on micro-manufacturing, micro-forming and their key issues*. 2012.
25. Okazaki, Y., N. Mishima, and K. Ashida, *Microfactory—concept, history, and developments*. Journal of Manufacturing Science and Engineering, 2004. **126**(4): p. 837-844.
26. Qin, Y., *Micro-forming and miniature manufacturing systems—development needs and perspectives*. Journal of Materials Processing Technology, 2006. **177**(1): p. 8-18.
27. Koç, M. and T. Özel, *Micro-manufacturing: Design and Manufacturing of Micro-products*. 2011: John Wiley & Sons.

28. Saotome, Y. and H. Iwazaki, *Superplastic backward microextrusion of microparts for micro-electro-mechanical systems*. Journal of Materials Processing Technology, 2001. **119**(1): p. 307-311.
29. Krishnan, N., *Microforming: Experimental Investigation of Size Effects in the Extrusion of Micropins*. 2006: ProQuest.
30. Engel, U. and R. Eckstein, *Microforming—from basic research to its realization*. Journal of Materials Processing Technology, 2002. **125**: p. 35-44.
31. Koç, M. and T. Özel, *Micro-manufacturing: design and manufacturing of micro-products*. 2011: John Wiley & Sons.
32. Renn, J.-C. and G.-L. Chern, *Development of a novel micro-punching machine using proportional solenoid*. JOURNAL-CHINESE SOCIETY OF MECHANICAL ENGINEERS, 2004. **25**(1): p. 89-93.
33. Razali, A.R., *High-precision, high speed strip feeding in micro-forming*. 2010, The University of Strathclyde.
34. Tomas, J., *Adhesion of ultrafine particles—a micromechanical approach*. Chemical Engineering Science, 2007. **62**(7): p. 1997-2010.
35. Feddema, J.T., P. Xavier, and R. Brown. *Micro-assembly planning with van der Waals force*. in *Proceedings of the 1999 IEEE International Symposium on Assembly and Task Planning (ISATP'99)*(Cat. No. 99TH8470). 1999. IEEE.
36. Rougeot, P., S. Regnier, and N. Chaillet. *Forces analysis for micro-manipulation*. in *2005 International Symposium on Computational Intelligence in Robotics and Automation*. 2005. IEEE.
37. Bowling, R.A., *A theoretical review of particle adhesion*, in *Particles on Surfaces 1*. 1988, Springer. p. 129-142.
38. Arai, F., et al. *Micro manipulation based on micro physics-strategy based on attractive force reduction and stress measurement*. in *Proceedings 1995 IEEE/RSJ International Conference on Intelligent Robots and Systems. Human Robot Interaction and Cooperative Robots*. 1995. IEEE.
39. Arai, F. and T. Fukuda. *A new pick up and release method by heating for micromanipulation*. in *Proceedings IEEE The Tenth Annual International Workshop on Micro Electro Mechanical Systems. An Investigation of Micro Structures, Sensors, Actuators, Machines and Robots*. 1997. IEEE.

40. Aronson, R.B., *The new world of micromanufacturing*. Manufacturing Engineering, 2003. **130**(4): p. 81-81.
41. Aronson, R.B., *Micromanufacturing Is Growing*. Manufacturing Engineering, 2004. **132**(4).
42. Kibe, Y., Y. Okada, and K. Mitsui, *Machining accuracy for shearing process of thin-sheet metals—Development of initial tool position adjustment system*. International Journal of Machine Tools and Manufacture, 2007. **47**(11): p. 1728-1737.
43. Geiger, M., et al., *Microforming*. CIRP Annals, 2001. **50**(2): p. 445-462.
44. Joo, B.-Y., S.-H. Rhim, and S.-I. Oh, *Micro-hole fabrication by mechanical punching process*. Journal of Materials Processing Technology, 2005. **170**(3): p. 593-601.
45. Chern, G.-L. and Y. Chuang, *Study on vibration-EDM and mass punching of micro-holes*. Journal of Materials Processing Technology, 2006. **180**(1-3): p. 151-160.
46. Jiang, Z., J. Zhao, and H. Xie, *Microforming technology: theory, simulation and practice*. 2017: Academic Press.
47. Paldan, N.A., M. Arentoft, and R.S. Eriksen. *Production equipment and processes for bulk formed micro components*. in *10th ESAFORM Conference on Material Forming*. 2007. AIP Publishing.
48. Qin, Y., et al., *Development of a new machine system for the forming of micro-sheet-products*. International Journal of Material Forming, 2008. **1**(1): p. 475-478.
49. Hartl, C., et al. *Micro hydroforming process and machine system for miniature/micro products*. in *Proc. of Int. Conf 7th euspen, Bremen*. 2007.
50. Koç, M. and S. Mahabunphachai, *Feasibility investigations on a novel micro-manufacturing process for fabrication of fuel cell bipolar plates: Internal pressure-assisted embossing of micro-channels with in-die mechanical bonding*. Journal of Power Sources, 2007. **172**(2): p. 725-733.
51. Kals, T. and R. Eckstein, *Miniaturization in sheet metal working*. Journal of Materials Processing Technology, 2000. **103**(1): p. 95-101.
52. Li, J., et al., *Nanoscale stacking fault–assisted room temperature plasticity in flash-sintered TiO₂*. Science Advances, 2019. **5**(9): p. eaaw5519.
53. Kang, S.-J.L., *Sintering: densification, grain growth and microstructure*. 2004: Butterworth-Heinemann.

54. German, R.M., *Sintering theory and practice*. Sintering Theory and Practice, by Randall M. German, pp. 568. ISBN 0-471-05786-X. Wiley-VCH, January 1996., 1996. **1**.
55. German, R., *Sintering: from empirical observations to scientific principles*. 2014: Butterworth-Heinemann.
56. Lakshmanan, A., *Sintering of ceramics: new emerging techniques*. 2012: BoD–Books on Demand.
57. Kraft, T. and H. Riedel, *Numerical simulation of solid state sintering; model and application*. Journal of the European Ceramic Society, 2004. **24**(2): p. 345-361.
58. Lee, H., C.-Y. Huang, and C. Wang, *Forming and sintering behaviors of commercial α -Al₂O₃ powders with different particle size distribution and agglomeration*. Journal of materials processing technology, 2009. **209**(2): p. 714-722.
59. Chang, Q., et al., *Effect of particle size distribution of raw powders on pore size distribution and bending strength of Al₂O₃ microfiltration membrane supports*. Journal of the European Ceramic Society, 2014. **34**(15): p. 3819-3825.
60. Kumar, V., *Simulations and modeling of unequal sized particles sintering*. 2011: The University of Utah.
61. Parhami, F., et al., *A model for the sintering and coarsening of rows of spherical particles*. Mechanics of Materials, 1999. **31**(1): p. 43-61.
62. Cinert, J., *Study of mechanisms of the Spark Plasma Sintering technique*. 2018.
63. Takagi, K., et al., *Preparation of monosized copper micro particles by pulsated orifice ejection method*. Materials transactions, 2006. **47**(5): p. 1380-1385.
64. Van Nguyen, C., et al., *A comparative study of different sintering models for Al₂O₃*. Journal of the Ceramic Society of Japan, 2016. **124**(4): p. 301-312.
65. Grigoriev, S.N., S.V. Fedorov, and K. Hamdy, *Materials, properties, manufacturing methods and cutting performance of innovative ceramic cutting tools– a review*. Manufacturing Review, 2019. **6**: p. 19.
66. Rahaman, M.N., *Ceramic processing and sintering*. 2017: CRC press.
67. Li, D., *Rapid sintering of ceramics by intense thermal radiation*. 2016, Department of Materials and Environmental Chemistry (MMK), Stockholm University.

68. Li, D. and Z. Shen, *Rapid sintering of ceramics with gradient porous structure by asymmetric thermal radiation*. Journal of the American Ceramic Society, 2015. **98**(12): p. 3631-3634.
69. Naterer, G.F., *Advanced heat transfer*. 2018: CRC Press.
70. Faghri, A., Y. Zhang, and J.R. Howell, *Advanced heat and mass transfer*. 2010: Global Digital Press.
71. Sparrow, E.M., *Radiation heat transfer*. 2018: Routledge.
72. Hijji, H., et al. *Fabrication of micro components with MSZ material using electrical-field activated powder sintering technology*. in *Advances in Manufacturing Technology XXX: Proceedings of the 14th International Conference on Manufacturing Research, Incorporating the 31st National Conference on Manufacturing Research, September 6–8, 2016, Loughborough University, UK*. 2016. IOS Press.
73. Zhao, J., et al. *Forming of micro-components by electrical-field activated sintering*. in *MATEC Web of Conferences*. 2015. EDP Sciences.
74. Hijji, H., et al. *Forming alumina (Al₂O₃) by micro-FAST*. in *Proc. of the 14th Int. Conf. on Manufacturing Research, Loughborough*. 2016.
75. Hijji, H., et al. *Fabrication of Miniature Components from ZrO₂ Powder by Combining Electrical-field Activated Sintering Technique and Micro-forming*. in *MATEC Web of Conferences*. 2018. EDP Sciences.
76. Grasso, S., Y. Sakka, and G. Maizza, *Electric current activated/assisted sintering (ECAS): a review of patents 1906–2008*. Science and Technology of Advanced Materials, 2009. **10**(5): p. 053001.
77. Castro, R. and K. Van Benthem, *Sintering: mechanisms of convention nanodensification and field assisted processes*. Vol. 35. 2012: Springer Science & Business Media.
78. Guillon, O., et al., *Field-Assisted Sintering Technology/Spark Plasma Sintering: Mechanisms, Materials, and Technology Developments*. Advanced Engineering Materials, 2014.
79. Olevsky, E.A., S. Kandukuri, and L. Froyen, *Consolidation enhancement in spark-plasma sintering: Impact of high heating rates*. Journal of Applied Physics, 2007. **102**(11): p. 114913.
80. Luitjohan, K.E., *The effects of an electric field on the sintering of ceramics*. 2015.

81. Lubliner, J., *Plasticity theory*. 2008: Courier Corporation.
82. Tokita, M., *Trends in advanced SPS spark plasma sintering systems and technology*. Journal of the Society of Powder Technology, Japan, 1993. **30**(11): p. 790-804.
83. Kir'yanchev, N., O. Troitskii, and S. Klevtsur, *Electroplastic deformation of metals*. Strength of Materials, 1983. **15**(5): p. 709-715.
84. Tang, G., et al., *Experimental study of electroplastic effect on stainless steel wire 304L*. Materials Science and Engineering: A, 2000. **281**(1-2): p. 263-267.
85. Tang, G., et al., *The application of the electro-plastic technique in the cold-drawing of steel wires*. Journal of Materials processing technology, 1998. **84**(1-3): p. 268-270.
86. Conrad, H., *Electroplasticity in metals and ceramics*. Materials Science and Engineering: A, 2000. **287**(2): p. 276-287.
87. Breda, M., et al. *Experimental study on electroplastic effect in AISI 316L austenitic stainless steel*. in *Applied Mechanics and Materials*. 2015. Trans Tech Publ.
88. Siopis, M.S., *Investigation of electrical-assisted forming at the microscale*. 2009.
89. Mai, J., et al., *Electrical-assisted embossing process for fabrication of micro-channels on 316L stainless steel plate*. Journal of Materials Processing Technology, 2013. **213**(2): p. 314-321.
90. Campbell, J., Y. Fahmy, and H. Conrad, *Influence of an electric field on the plastic deformation of fine-grained Al₂O₃*. Metallurgical and Materials Transactions A, 1999. **30**(11): p. 2817-2823.
91. Galligan, J., T. McKrell, and M. Robson, *Dislocation drag processes*. Materials Science and Engineering: A, 2000. **287**(2): p. 259-264.
92. Ross, C. and J.T. Roth. *The effects of DC current on the tensile properties of metals*. in *ASME 2005 International Mechanical Engineering Congress and Exposition*. 2005. American Society of Mechanical Engineers.
93. Perkins, T.A., T.J. Kronenberger, and J.T. Roth, *Metallic forging using electrical flow as an alternative to warm/hot working*. Journal of manufacturing science and engineering, 2007. **129**(1): p. 84-94.
94. Yao, L., et al., *Effect of electric current pulse on superplasticity of aluminium alloy 7475*. Transactions of Nonferrous Metals Society of China, 1996. **6**(1): p. 77-&.

95. Munir, Z.A., U. Anselmi-Tamburini, and M. Ohyanagi, *The effect of electric field and pressure on the synthesis and consolidation of materials: A review of the spark plasma sintering method*. Journal of Materials Science, 2006. **41**(3): p. 763-777.
96. Garay, J., *Current-activated, pressure-assisted densification of materials*. Annual review of materials research, 2010. **40**: p. 445-468.
97. Chen, X., et al., *Preparation yttria-stabilized zirconia electrolyte by spark-plasma sintering*. Materials Science and Engineering: A, 2003. **341**(1-2): p. 43-48.
98. Bernard-Granger, G. and C. Guizard, *Spark plasma sintering of a commercially available granulated zirconia powder: I. Sintering path and hypotheses about the mechanism (s) controlling densification*. Acta Materialia, 2007. **55**(10): p. 3493-3504.
99. Li, W. and L. Gao, *Rapid sintering of nanocrystalline ZrO₂ (3Y) by spark plasma sintering*. Journal of the European Ceramic Society, 2000. **20**(14-15): p. 2441-2445.
100. Hulbert, D.M., et al., *A low-temperature high-strain-rate formable nanocrystalline superplastic ceramic*. Scripta materialia, 2007. **56**(12): p. 1103-1106.
101. Dini, F., et al., *A review of binder jet process parameters; powder, binder, printing and sintering condition*. Metal Powder Report, 2019.
102. Ozkan, N., *Compaction and sintering of ceramic powders*. 1994.
103. Wang, J., S. Li, and R. Stevens, *Effects of organic binders on the sintering of isostatically compacted zirconia powders*. Journal of materials science, 1992. **27**(1): p. 63-67.
104. Gao, L., et al., *Bending strength and microstructure of Al₂O₃ ceramics densified by spark plasma sintering*. Journal of the European Ceramic Society, 2000. **20**(12): p. 2149-2152.
105. Wang, S., L. Chen, and T. Hirai, *Densification of Al₂O₃ powder using spark plasma sintering*. Journal of materials research, 2000. **15**(4): p. 982-987.
106. Jayaseelan, D.D., et al., *Thermo-mechanical stability of porous alumina: effect of sintering parameters*. Science and Technology of Advanced Materials, 2004. **5**(4): p. 387.
107. Shen, Z., et al., *Spark plasma sintering of alumina*. Journal of the American Ceramic Society, 2002. **85**(8): p. 1921-1927.
108. Zhou, Y., et al., *Densification and grain growth in pulse electric current sintering of alumina*. Journal of the European Ceramic Society, 2004. **24**(12): p. 3465-3470.

109. Hong, C.-H., et al., *Lead-free piezoceramics—Where to move on?* Journal of Materiomics, 2016. **2**(1): p. 1-24.
110. Makhlof, A.S.H. and D. Scharnweber, *Handbook of nanoceramic and nanocomposite coatings and materials*. 2015: Butterworth-Heinemann.
111. Chinen, F.K., et al. *PZT consolidation by Spark Plasma Sintering (SPS)*. in *Proceedings of COBEM 2011 21st International Congress of Mechanical Engineering*. 2011.
112. Su, X., et al., *Flash sintering of lead zirconate titanate (PZT) ceramics: Influence of electrical field and current limit on densification and grain growth*. Journal of the European Ceramic Society, 2018. **38**(10): p. 3489-3497.
113. Qin, Y., et al., *Forming of Miniature Components from Powders by Combining Field-activated Sintering and Micro-Forming*. Procedia Engineering, 2017. **207**: p. 1212-1217.
114. Lu, D., et al., *Forming microgears by micro-fast technology*. Microelectromechanical Systems, Journal of, 2013. **22**(3): p. 708-715.
115. Harmer, M. and R. Brook, *FAST FIRING- MICROSTRUCTURAL BENEFITS*. Trans. J. Br. Ceram. Soc., 1981. **80**(5): p. 147.
116. Lu, D., et al., *Effect of particle size and sintering temperature on densification during coupled multifield-activated microforming*. Journal of Materials Research, 2012. **27**(20): p. 2579-2586.
117. Huang, K., et al., *316 L Stainless Steel Powder Densification during the Coupled Multi-Fields Activated Micro-Forming*. Materials and Manufacturing Processes, 2013. **28**(2): p. 183-188.
118. Hillery, M.T. and V.J. McCabe, *Wire drawing at elevated temperatures using different die materials and lubricants*. Journal of materials processing technology, 1995. **55**(2): p. 53-57.
119. Sun, F., X. Chen, and Z. Zhao, *Synthesis of monocrystalline tungsten carbide powder in carbon saturated cobalt melt*. Ceramics International, 2018. **44**(7): p. 8716-8719.
120. AZoM. *AZoMaterials*. [cited 2018; AZoM is the leading online publication for the Materials Science community]. Available from: <https://www.azom.com/>.
121. Eriksson, M., Z. Shen, and M. Nygren, *Fast densification and deformation of titanium powder*. Powder metallurgy, 2005. **48**(3): p. 231-236.

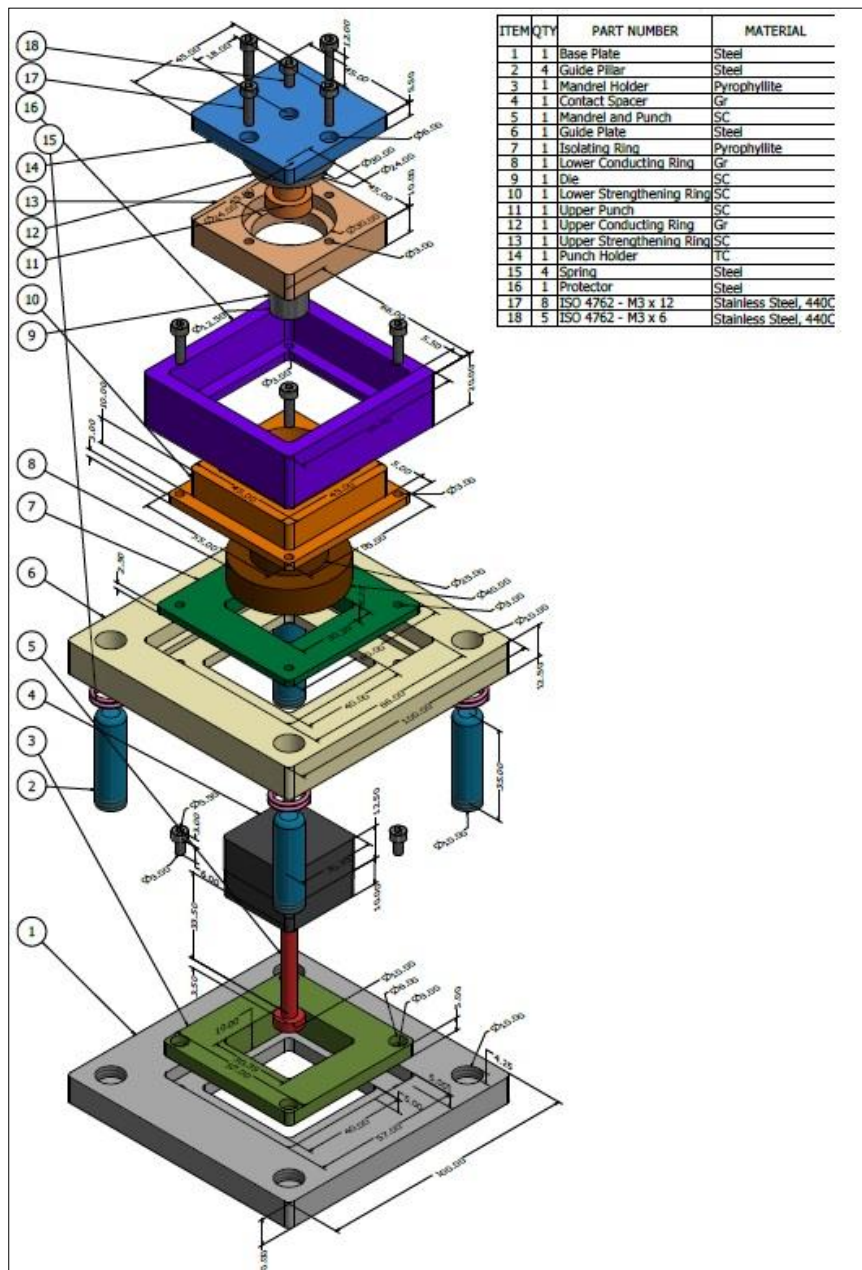
122. Kumagai, T., *Rapid Densification of Yttria-Stabilized Tetragonal Zirconia by Electric Current-Activated/Assisted Sintering Technique*. Journal of the American Ceramic Society, 2011. **94**(4): p. 1215-1223.
123. Yang, Y., et al., *Comparison of spark plasma sintering of elemental and master alloy powder mixes and prealloyed Ti-6Al-4V powder*. International Journal of Powder Metallurgy, 2014. **50**(1): p. 41-47.
124. Blundell, S.J. and K.M. Blundell, *Concepts in thermal physics*. 2009: OUP Oxford.
125. Welty, J., G.L. Rorrer, and D.G. Foster, *Fundamentals of momentum, heat, and mass transfer*. 2014: John Wiley & Sons.
126. Suarez, M., et al., *Challenges and Opportunities for Spark Plasma Sintering: A Key Technology for a New Generation of Materials*. 2013.
127. Zapata-Solvas, E., et al., *Ultra-fast and energy-efficient sintering of ceramics by electric current concentration*. Sci Rep, 2015. **5**: p. 8513.
128. Barsoum, M. and M. Barsoum, *Fundamentals of ceramics*. 2002: CRC press.
129. *Abaqus Theory Manual :6.7.2 Coupled Thermal-Electrical Analysis,* Dassault System Simulia. . 2010.
130. Gao, T., L. Ma, and X.-G. Peng, *Study on Temperature Distribution of Specimens Tested on the Gleeble 3800 at Hot Forming Conditions*. Journal of Electronic Science and Technology, 2014. **12**(4): p. 419-423.
131. Ogasawara, T., Y. Hirano, and A. Yoshimura, *Coupled thermal–electrical analysis for carbon fiber/epoxy composites exposed to simulated lightning current*. Composites Part A: Applied Science and Manufacturing, 2010. **41**(8): p. 973-981.
132. Gleeble. *GLEEBLE 3800, Dynamic Systems Inc*. 2019; Available from: <https://www.leeble.com/products/leeble-systems/leeble-3800.html>.
133. HITACHI. *Scanning Electron Microscope S-3700N*. 2019; Available from: https://www.hitachi-hightech.com/global/product_detail/?pn=em-s3700n.
134. Micro-Materials. *NanoTest Vantage*. 2019; Available from: <https://www.micromaterials.co.uk/products/nanotest-vantage/>.
135. Harris, G.L., *Properties of silicon carbide*. 1995: Iet.
136. Verhoeven, J.D., *Steel metallurgy for the non-metallurgist*. 2007: ASM International.
137. Roberts, G.A., R. Kennedy, and G. Krauss, *Tool steels*. 1998: ASM international.

138. Wypych, G. and G. Wypych, *2-Fillers-origin, Chemical Composition, Properties, and Morphology*. Handbook of Fillers (Fourth Edition), Chem Tec Publishing, 2016: p. 13-266.
139. Dante, R.C., *Handbook of friction materials and their applications*. 2015: Woodhead Publishing.
140. Chen, L.-Y., G.W. Hunter, and P.G. Neudeck, *Silicon carbide die attach scheme for 500 C operation*. MRS Online Proceedings Library Archive, 2000. **622**.

APPENDICES

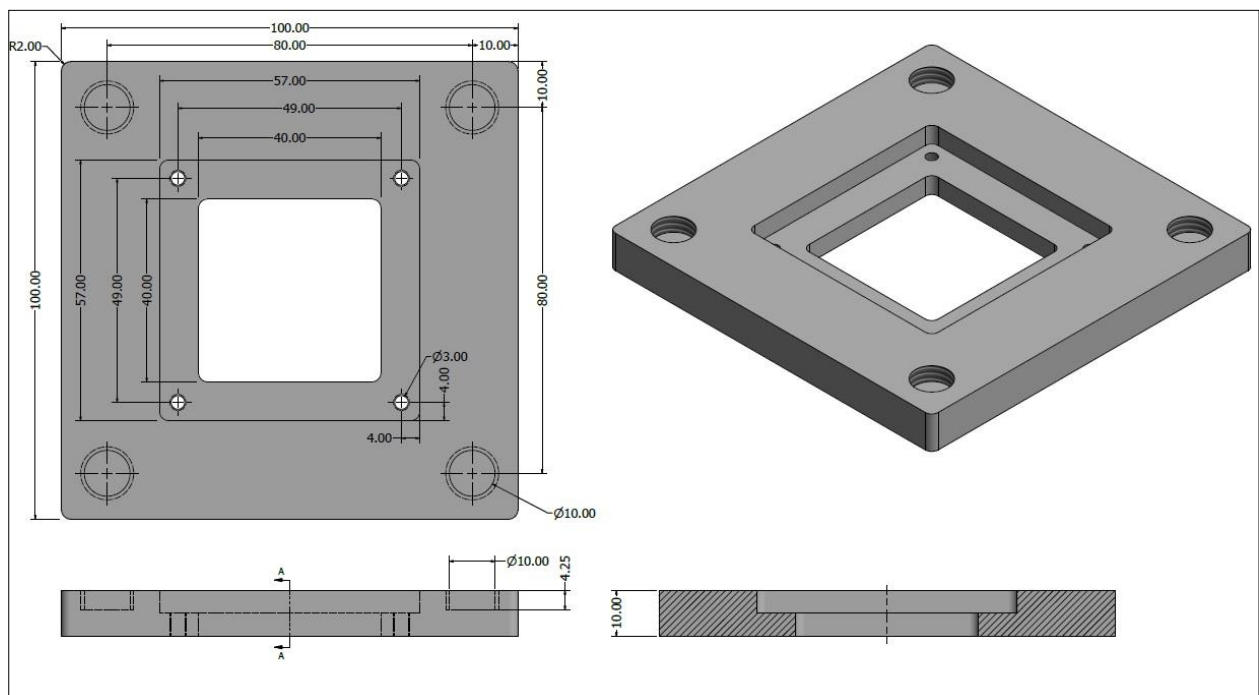
APPENDIX 1: NEW TOOL DESIGN FOR MICRO-FAST PROCESS WITH FULL DETAILS

The figure below shows the full details for the new concept design with the dimensions



APPENDIX 2: BASE PLATE

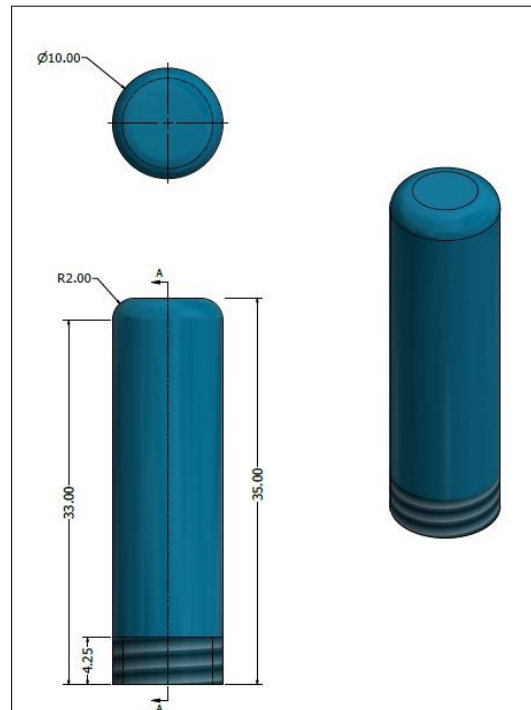
The base plate is the plate where all parts are placed. The material that has been suggested for the plate is steel. Steel is the most common material used for most bases due to its hardness. Steel is iron mixed with carbon and perhaps other metals. However, steel is harder and stronger than iron. The steel that has been chose here is the tool steel. Tool steels are hard and heat and scrape-resistant. Tool steel is made up of vanadium, cobalt, molybdenum, and tungsten in different amounts, which improve its durability and heat resistance property [120, 136, 137]. The 4 guide pillars are going to be attached to the base plate and the mandrel holder is going to be placed in the centre of the plate.



The dimensions of the base plate are 100x100 mm. The thickness of the plate is 10 mm and it has been extruded from centre to fit the mandrel holder and the contact spacer. The plate has 4 threaded holes to attach the guide pillars.

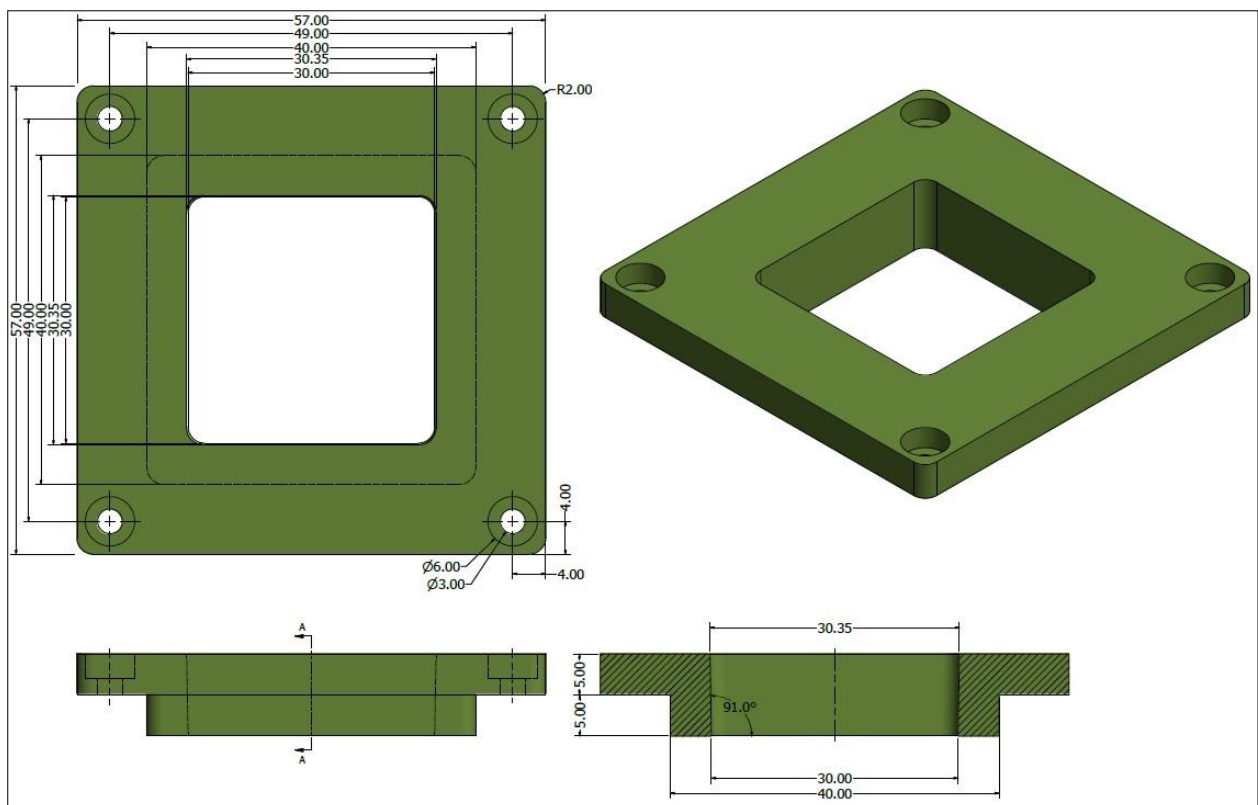
APPENDIX 3: GUIDE PILLAR

The guide pillars are used to hold and control the movement of the guide plate. The pillars are threaded from the edges to be attached in the 4 corners of the base plate. The material that has been chosen for the pillars is steel. The diameter of the pillar is 10 mm and the length is 35 mm



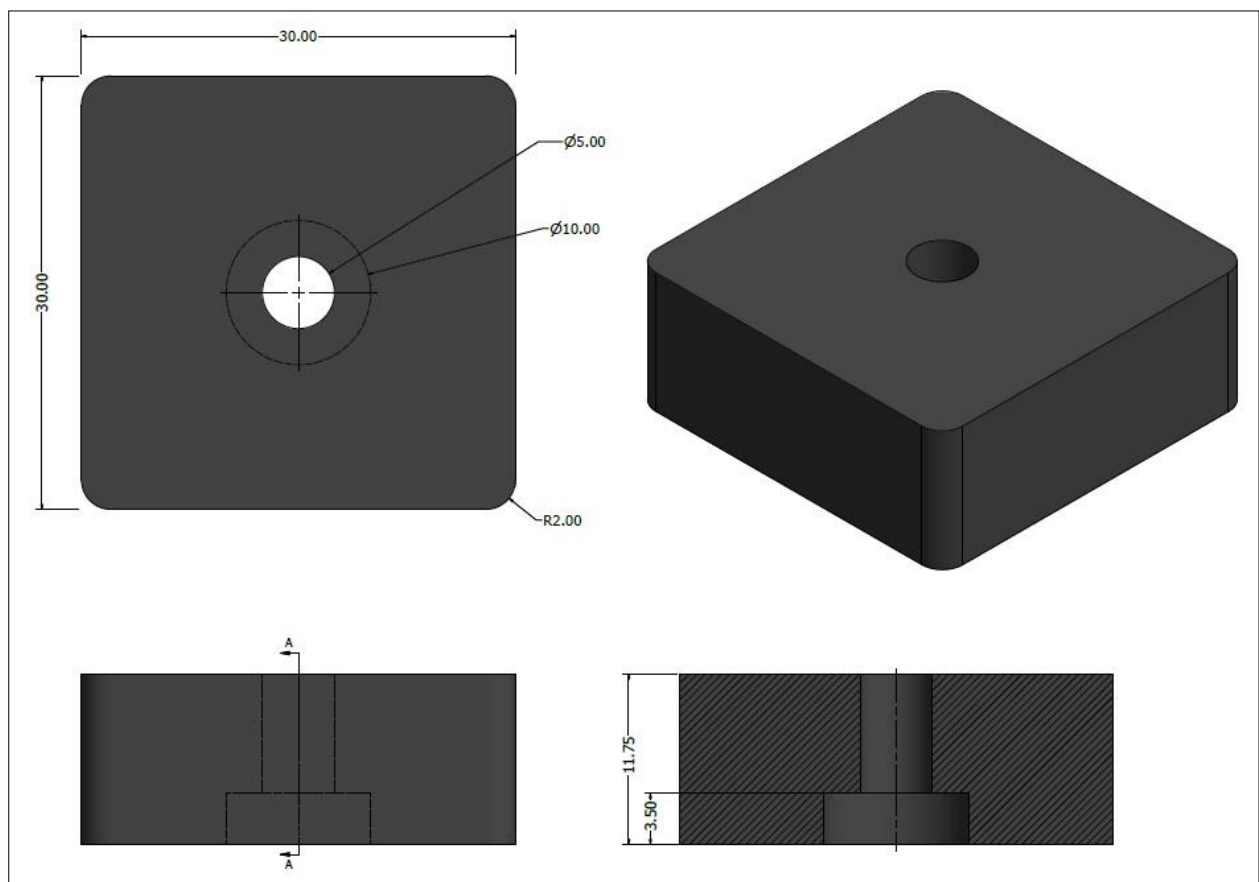
APPENDIX 4: MANDREL HOLDER

This part is going to be used to hold the mandrel and the contact spacer. The material that has been chosen for the mandrel holder is pyrophyllite plastic to isolate the heat and the electricity that goes through the contact spacer and the mandrel from contacting the base plate. The pyrophyllite is thermally stable and Heat and Electrical insulation. Moreover, it has high resistance for thermal shocks and Resists deformation at loads and creep. The pyrophyllite has High melting point and medium hardness [120, 138-140]. The dimensions of the upper part of mandrel holder are 57x 57 mm, and the lower and extended part dimension is 40x40 mm. The mandrel holder has 4 holes in the corners and going to be fitted to the base plate with bolts. The hole where the contact spacer going to be fit has a dimension of 30x30 mm from the bottom and 30.35 x 30.35 mm from the top because of the extruded part of the spacer.



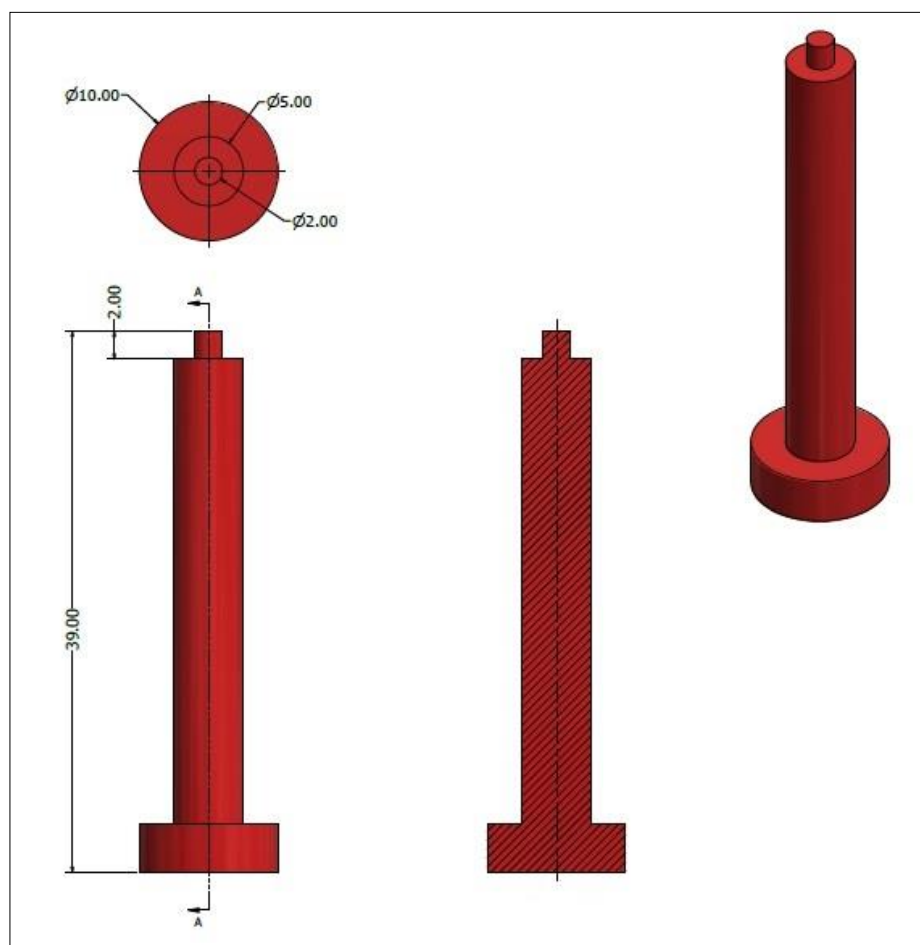
APPENDIX 5: CONTACT SPACER

The location of the contact spacer is in the centre of the mandrel holder. The mandrel goes inside the spacer and the material that has been chosen for the spacer is the graphite, to make sure that the heat and the electricity transit in efficient way. The dimension of 30x30 mm from the bottom and 30.35 x 30.35 mm from the top part so the contact spacer can fit well in the isolating ring.



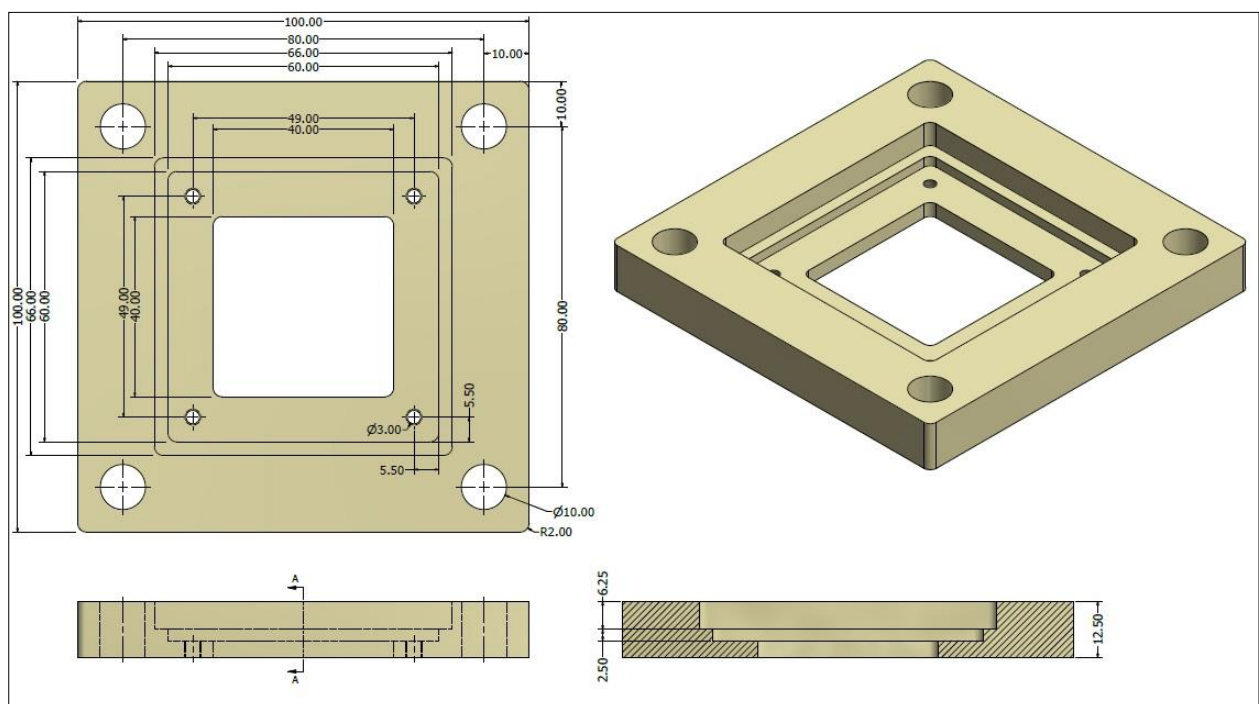
APPENDIX 6: MANDREL

The mandrel is a cylindrical rod with tapered end to shape and form the workpiece from the powder. This mandrel has ability to change shape and be easily extracted and in this condition, it can be considered as lower punch for the die. The materials that has been chosen for the mandrel is the Silicon Carbide (SiC). The SiC are extremely high thermal conductivity and has good electrical properties and it keeps its strength property even at temperatures up to 1400°C [120, 135]. The total length of the mandrel is 39 mm and that is including the 2 mm nose part. The diameter of the base of the mandrel is 10 mm and the body of the mandrel is 5 mm. The diameter of the nose which is going to be used to fabricate the formed part is 2 mm.



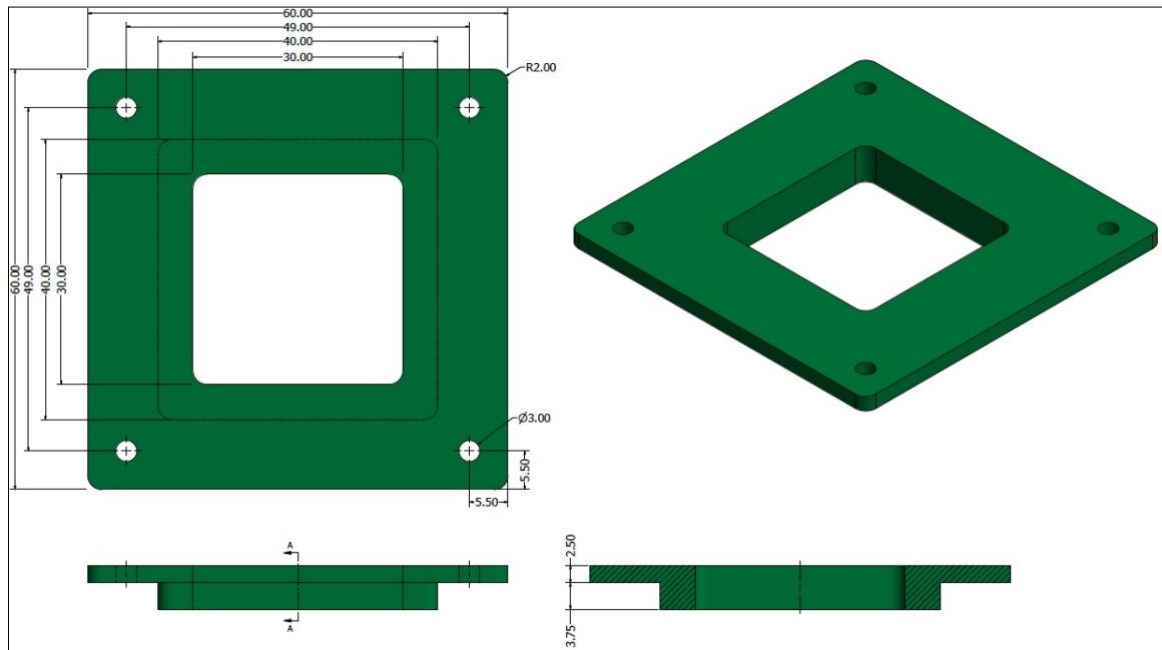
APPENDIX 7: GUIDE PLATE

In This plate, the rest and most of the parts are going to be attached. The isolating ring is going to be located in the centre of the plate. Then the contact spacer will be attached from the top with the isolating ring. The protector and the lower strengthen ring will be attached to the plate and the isolating ring using screws as seen in Figure 6-3. The guide plate will be fitted in the guide pillars to move up and down depending on the pressure. The material that has been chosen for this plate is the tool steel.



APPENDIX 8: ISOLATING RING

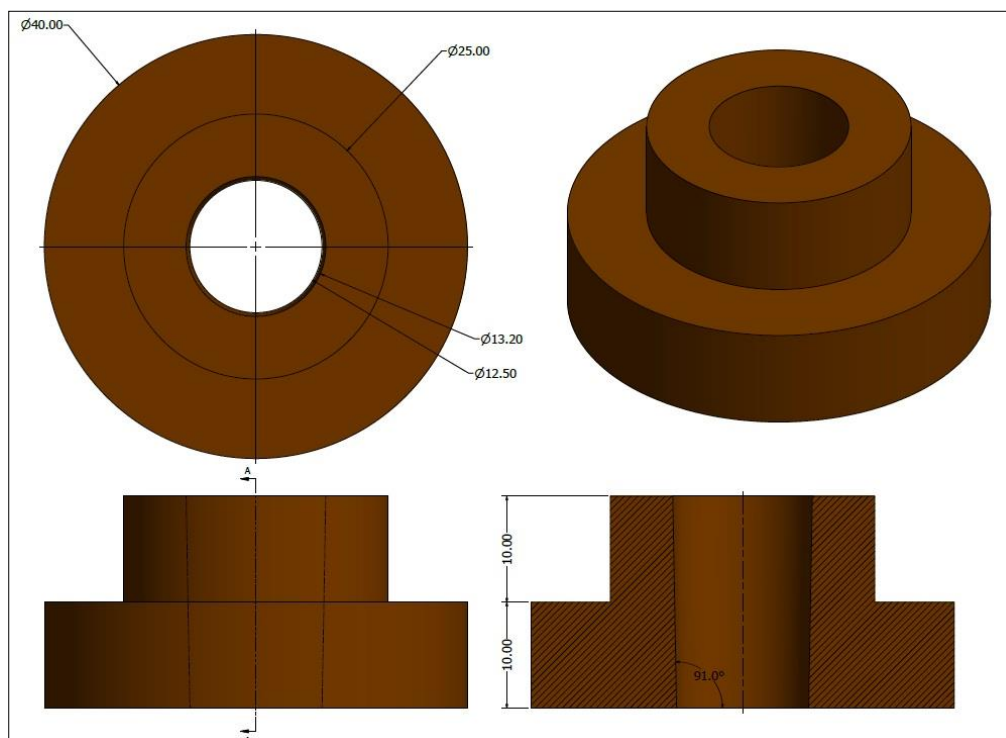
The isolating ring is going to be used to isolate the heat and the electricity from the plate. The material that has been chosen for the mandrel holder is pyrophyllite plastic.



The dimension of the upper part of isolating ring is 60 x 60 mm, and the lower and extruded part dimension is 49x49 mm.

APPENDIX 9: LOWER CONDUCTING RING

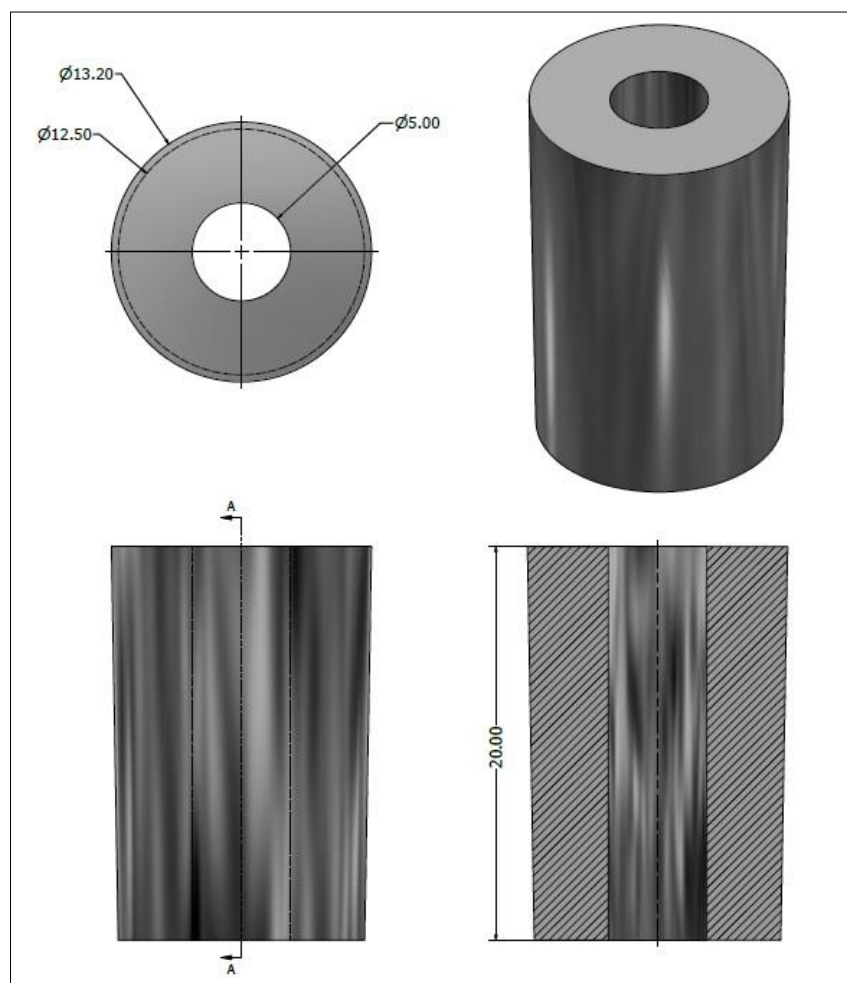
The purpose of this ring is to allow the heat and the electricity transit through the die, the contact spacer and then to the mandrel. The materials that going to be used for the conducting ring is the graphite due its high thermal and electrical conductivity.



The total length of the part is 20 mm. The upper part is 10 mm and the lower section is 10 mm. The hole where the die going to be fitted is 12.5 mm diameter from the top and the diameter increased by 1 degree to be 13.2 mm diameter at the end of the hole to make sure that the die fit and will not fill from inside the ring.

APPENDIX 10: THE DIE

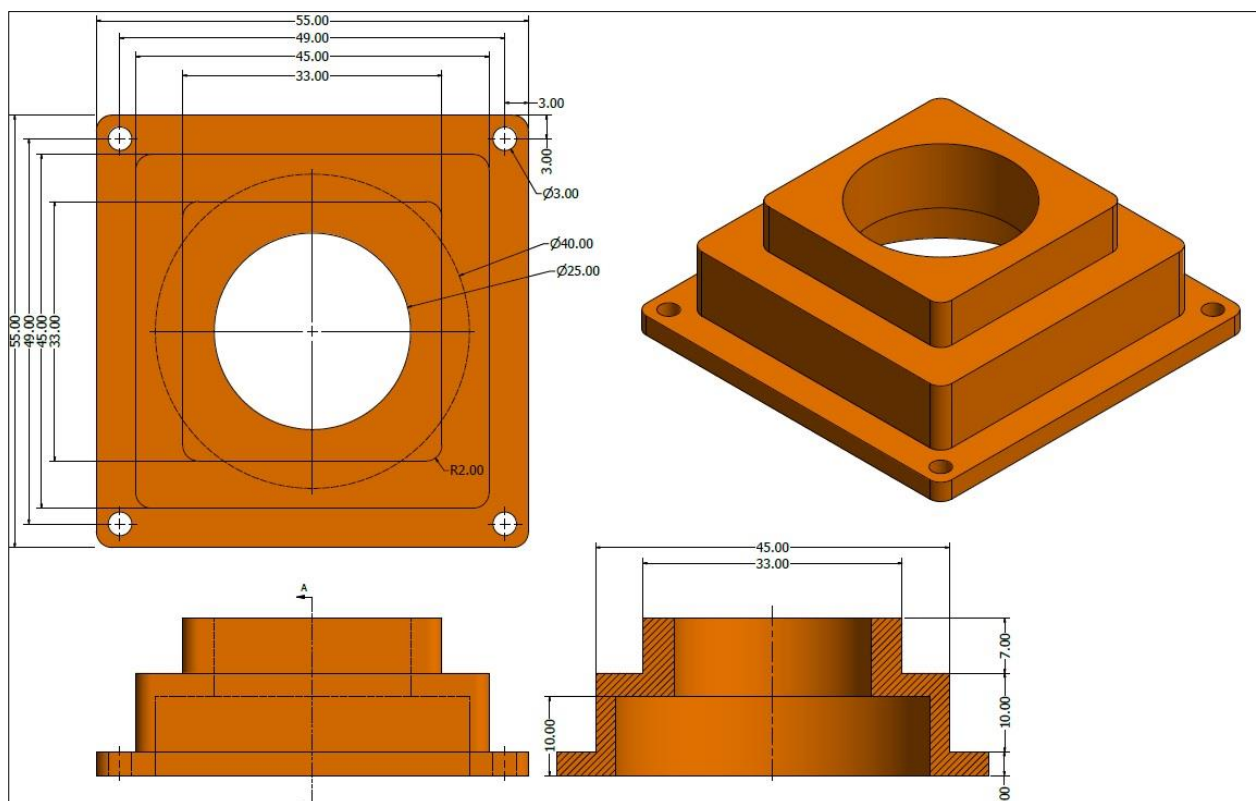
The die is going to be used to shape the powder into a solid part. The materials that has been chosen to manufacture the die is the Silicon Carbide (SiC). As mentioned before, the Silicon Carbide has excellent thermal conductivity and low thermal expansion, therefore it shows good thermal shock resistance. Moreover, the SiC has high melting temperature (more thab 1700 °C). Furthermore, the SiC has interesting electrical properties due to its semiconductor characteristics. In addition, the SiC has high hardness and corrosion resistance.



The diameter of the hole inside the die is 5 mm. The height of the die is 20 mm and the diameter of the die is 12.5 mm from the top and 13.2 from the other side so the die can fit inside the lower conducting ring.

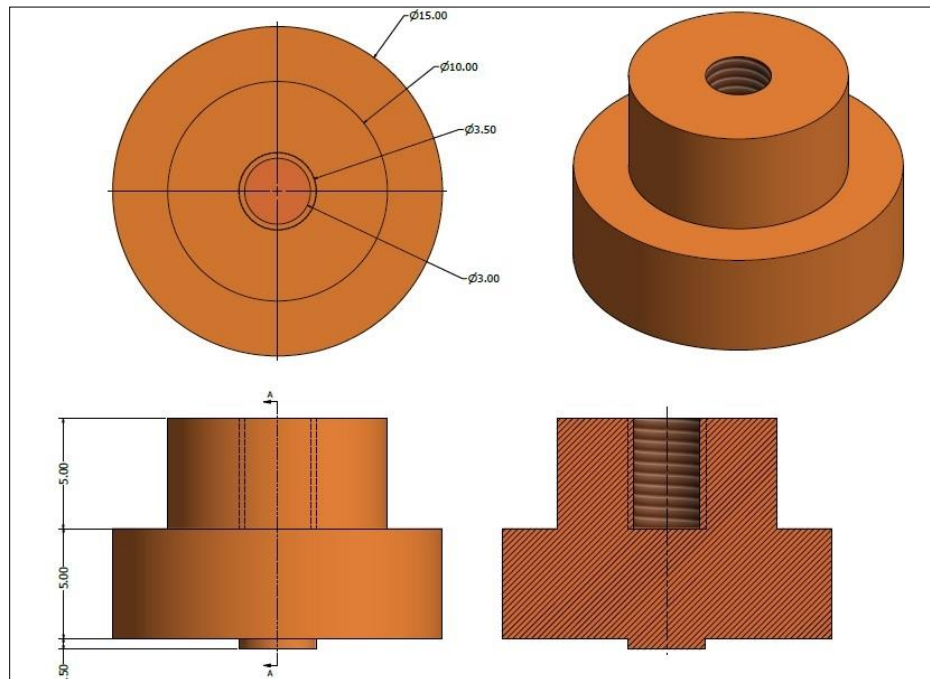
APPENDIX 11: LOWER STRENGTHEN RING

The lower strengthen ring is going to be used to protect the conducting ring and preventing it from any fragile and allow the heat and the electricity to go through to the conducting ring and the die. The material that has been used for this part is the SiC due its thermal and electrical conductivity and the most thing it has high hardness ability.



APPENDIX 12: UPPER PUNCH

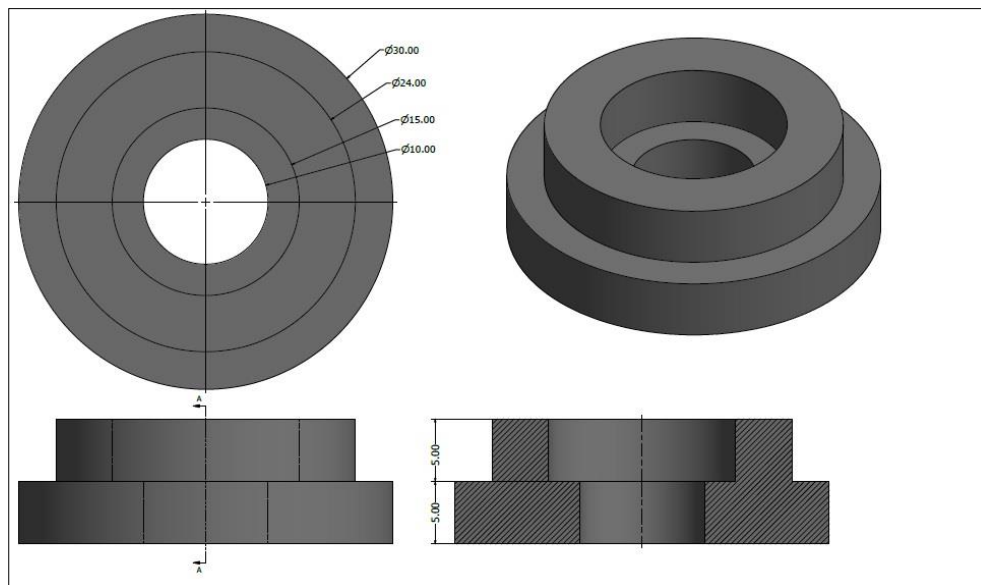
The upper punch is used to form the powder to shaped part during the sintering process. The material that is going to be used in the punch is SiC due its excellent properties.



It can be seen that the upper punch is cylindrical shape. The punch is one part with three sections. The punch has a threaded hole in the middle so it can be attached to the punch holder with bolt.

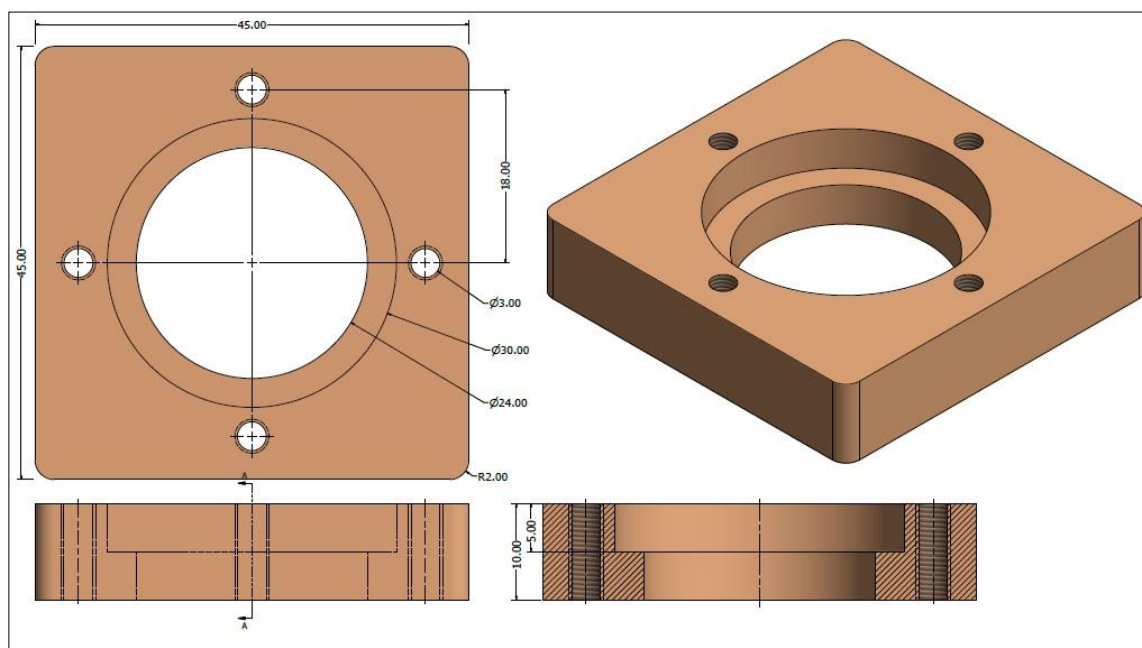
APPENDIX 13: UPPER CONDUCTING RING

The purpose of this ring is to allow the heat and the electricity transit through the upper punch and then to the die. The materials that going to be used for the conducting ring is the graphite due its thermal and electrical conductivity. The upper punch going to be inserted inside the ring.



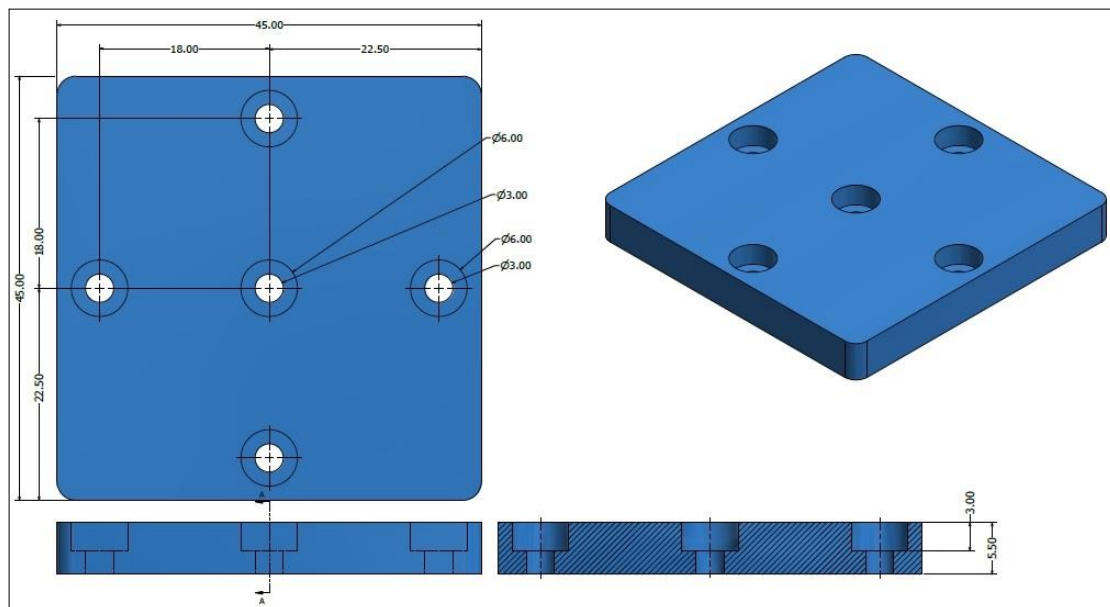
APPENDIX 14: UPPER STRENGTHEN RING

The upper strengthen ring is going to be used to protect the conducting ring and preventing it from any fragility and allow the heat and the electricity to go through to the conducting ring and the die. The material that has been used for this part is the SiC due its thermal and electrical conductivity and the most thing it has high hardness ability. The upper conducting ring going to be placed inside the upper strengthen ring. The ring has 4 threaded holes so it can be attached to the punch holder by 4 bolts.



APPENDIX 15: PUNCH HOLDER

The punch holder is the plate that is going to hold the upper strengthen ring, the upper conducting ring and the upper punch. The material that going to be used for the punch holder is tungsten carbide due its mechanical properties. Tungsten carbide has excellent compressive strength compared to other materials which would make the part more robust when dealing with the high pressure and temperature environment during the Micro-FAST process[120]. The punch holder has 5 holes as seen in figure below to attach the upper punch and the upper strengthen ring. The dimension of this plate is 45 x 45 mm with thickness of 5.5 mm.



APPENDIX 16: SPRING

Spring is a mechanical elastic device that obtain a weight or force from one object to absorb the energy and to prevent the part from being damaged. There are going to be 4 springs and it will be put inside the four guide pillars. When the spring is compressed or stretched from its resting position, it exerts an opposing force approximately proportional to its change in length. The material that has been chosen for this spring is steel.



APPENDIX 17: PROTECTOR

The protector is going to be used as shield to protect the upper part of the tool during the Micro-FAST process.

